UNIVERSITY OF NATAL

ESTIMATION OF REFERENCE EVAPORATION AND COMPARISON WITH ET-GAGE EVAPORIMETER

by

Tekeste Weldegabrial Abezghi

B.ScAgric. (Soil and Water Conservation), University of Asmara

Submitted in partial

fulfilment of the requirement

for degree of

MASTER OF SCIENCE IN AGRICULTURE
(Agricultural and Environmental Instrumentation)

in Agrometeorology, SPACRU, School of Applied Environmental Sciences

Faculty of Science and Agriculture

University of Natal

Pietermaritzburg

South Africa

2003

DECLARATION

I hear by certify that the research results reported in this thesis are my own original investigation except where acknowledged.

T.W. Abezghi.....

Supervisor M.J Savage .....

Date: 14 July 2003

ACKNOWLEDGMENTS

I would like to acknowledge the generous support of the following people:

my supervisor,

Professor M.J. Savage, Agrometeorology Discipline, School of Applied and Environmental Sciences, Faculty of Science and Agriculture for his great supervision and support in every aspect of the work throughout the MScAgric program and for his patience;

my co-supervisors

Professor M.A. Johnson, Soil Science Discipline, School of Applied and Environment Sciences, Faculty of Science and Agriculture who passed away in the progress of the work and may God rest his soul in eternal peace

Dr C.S. Everson of the CSIR for his co-supervision;

Ms J. Moodley and Mr P. Dovey, staff of Agrometeorology section and my colleagues and friend G. Odhiambo, M. Abraha, M. Gebregiorgis, M. Mengistu and T. Ghebreab and Mrs M.A. Savage for their support in various ways;

staff of the Life Science library and Soil Science laboratory technicians for providing a good working atmosphere for reading and work;

the Water Research Commission and the National Research Foundation for previously funding the equipment used in this research;

The World Bank in agreement with Human Resource Development Foundation of the University Asmara, Eritrea funded the research and support is greatly acknowledged;

and my girl friend F. Tekle and my family for the patience and moral support they showed me throughout my school life;

and at last but not least thanks almighty God who helps me in every aspect of my life.

ABSTRACT

Accurate estimation of reference evaporation is necessary for the estimation of actual evaporation for irrigation and water resource management purposes. Estimation of reference evaporation using the Penman-Monteith method using automatic weather station (AWS) measurements requires the available energy to be accurately estimated. The available energy of short grass of 0.12 m was measured using a component net radiometer and soil heat flux plate measurements at the Faculty of Sciences and Agricultural (Agrometeorological station, University of Natal, Pietermaritzburg, latitude ≈ 29.79 °S, longitude ≈ 30.95 °E, altitude ≈ 650 m). In an attempt to evaluate the accuracy of commonly used procedures of estimating available energy, estimates of net irradiance (from net long wave irradiance and reflection coefficient estimate) and soil heat flux density were compared to the actual measurements. The linear approximation of atmosphere minus crop surface emittance based on air temperature was compared with measured net long wave irradiance and similar empirical formulations. The underestimation of the measured net long wave irradiance was observed using the linear approach. Furthermore, a plot of measured clear sky net long wave irradiance and air temperature showed a logarithmic relation. The estimated reflected solar irradiance was overestimated for the reference crop. The measured soil heat flux density was observed to vary not only with net irradiance but also with cloudiness, wind speed and soil water content. The soil heat flux density measured with plates was noticed to follow the measured net irradiance. The sensitivity of Penman-Monteith latent heat estimate was investigated for the use of estimated reflection coefficient and soil heat flux density as well as ignored soil heat flux density. Results showed the latent heat estimate to be greater when soil heat flux density was ignored.

Reduced set assumptions of Penman-Monteith were assessed using the microclimatic measurements. The grass reference evaporation estimate using estimated water vapour pressure from the pervious day minimum air temperature and approximated wind speed were found to be seasonal and procedure dependent. The hourly-reduced set estimate of reference evaporation was in good agreement with the grass Penman-Monteith estimate. The estimated daily water vapour pressure underestimated the daily grass Penman-Monteith estimate. The sensitivity of the reduced set reference evaporation estimate was compared for the two values of approximated wind speeds. The assumption of 2 m s^{-1} wind speed gave a relatively better result.

The sensitivity of the surface temperature energy balance (STEB) estimate of reference evaporation was investigated using two different atmospheric stability procedures. The evaporation estimate agreement and performance of the technique were found to vary depending on the stability correction procedure. The Monteith (1973) correction procedure was observed to be more sensitive to a higher surface-air temperature difference. The Monteith (1973) procedure was found to underestimate the reference evaporation and this resulted in a lower correlation coefficient. The uncorrected and Campbell and Norman (1998) stability corrected procedure of STEB estimate overestimated the reference evaporation but resulted in good agreement with actual reference evaporation. The use of estimated available energy using the STEB method resulted in a 7 % overestimate of measured available energy.

Different designs of atmometers have been used to measure evaporation. The less expensive and simple ET-gage^{R} (Model A and E) atmometer for daily evaporation measures were compared to grass-based and alfalfa-based Penman-Monteith and STEB estimate of reference evaporation. Two different evaporation surface covers used with the device allowed for the comparison to be made. Measurements using the canvas 30 ET-gage cover for grass reference evaporation were compared to grass based Penman-Monteith and STEB reference evaporation estimates. Correlation between the canvas 30 measures and Penman-Monteith estimates were good compared to the STEB estimate. The ET-gage canvas 54 measures were in a good agreement with alfalfa based Penman-Monteith reference evaporation estimate. There was, however, a slight time lag in ET-gage evaporation with ET-gage evaporation continuing accumulation when the reference evaporation was zero. The sensitivity of the ET-gage for microclimate variation was tested using the measurements made for two levels and three different microclimates. A shade measurement of reference evaporation was overestimated. The response of the ET-gage to one and two meter microclimate measures was similar to the short grass measurement. Furthermore, the ET-gage surface evaporation estimate using the STEB method showed equal response to the ET-gage surface for the microclimate measure and explained the possible cause of the lag of the ET-gage response.

Accurate microclimate measurements is a requirement for the performance of the Penman-Monteith approach for the estimation of reference evaporation. The investment cost required for an AWS set up is high. Alternative options for gathering information of the microclimate measurements required for calculating reference evaporation were assessed in terms of cost saving, accuracy and other advantages. A weather station system using a Hobo H8 logger (internal relative humidity and air temperature sensor and two external channels, one which was used for solar

irradiance measurements) was found to be a cost-effective method for calculating the necessary microclimatic information for calculating reference evaporation. With this system reference evaporation was estimated with reasonable accuracy, at 16 % of the cost of normal AWS system. The use of an Event Hobo logger and an ET-gage was found to provide a reasonable estimate of reference evaporation. The use of the reduced set evaporation weather station was found to be unreasonable in terms of cost and accuracy.

Air temperature and relative humidity were measured from different design of radiation shields and Stevenson screens. The use of home-made seven-plate plastic radiation shields provided a similar shield to radiation and ventilation compared to manufactured shields. At a low solar angle when wind speed was very low, all the radiation shields including the small Stevenson screens showed a higher air temperature difference relative to the standard Stevenson screen. The highest average difference of air temperature measurement was measured within the small Stevenson screen and metal-radiation shield. The home-made plastic radiation shield showed similar averages of air temperature and water vapour pressure difference compared to the six- and twelve-plate Gill radiation shields. The home-made metal radiation shield showed relatively higher deviation from the mean being cold at night time and hot during the day.

More research is needed to explore the efficiency of the ET-gage evaporation from variety of microclimates to establish the cause of the overestimate under shade, to develop better relation of clear day net long wave irradiance and air temperature and the use of a wind speed sensor with Hobo H8 weather station system.

TABLE OF CONTENTS

LIST OF FIGURES

LIST OF TABLES

Page

LIST OF APPENDICES

LIST OF SYMBOLS AND ABBREVIATIONS

A	Advection flux density	$W\ m^{-2}$
A	Area	m^2
ALPM	Alfalfa based Penman-Monteith	mm
AWS	Automatic weather station	
c	Cloudiness	
c_c	Specific heat capacity of ceramic (porcelain = 1085 $J\ kg^{-1}\ K^{-1}$)	$J\ kg^{-1}\ K^{-1}$
c_{dsoil}	Specific heat capacity of dry soil (= 837 $J\ kg^{-1}\ K^{-1}$)	$J\ kg^{-1}\ K^{-1}$
c_p	Specific heat capacity of air	$J\ kg^{-1}\ K^{-1}$
c_s	Specific heat capacity of evaporation surface (ceramic, porcelain = 1085 $J\ kg^{-1}K^{-1}$) plus water (= 4190 $J\ kg^{-1}K^{-1}$) with in the surface	$J\ kg^{-1}K^{-1}$
c_{soil}	Specific heat capacity of soil	$J\ kg^{-1}\ K^{-1}$
C_v	Volumetric soil heat capacity	$MJ\ m^{-3}\ ^oK^{-1}$
c_w	Specific heat capacity of water (= 4190 $J\ kg^{-1}\ K^{-1}$)	$J\ kg\ K^{-1}$
d	Zero-plane displacement height (= 0.67 h_c) of the crop height	m
d	Diameter	m
dT_{soil}	Change in soil temperature as function of measurement interval	^oC
dt	Measurement time interval	s
e	Water vapour pressure	hPa or mb
e	Natural logarithm	
e_o	Water vapour pressure at the surface	KPa
$e(T_{p\ min})$	Water vapour pressure from previous day minimum air temperature of day	kPa
e_{09}	Water vapour pressure measured at mid-morning	mb
e_a	Water vapour pressure at 2 meter	KPa or mb
E_a	Aerodynamic evaporation	mm
$e_a - e_z$	Water vapour pressure deficit	kPa
E_p	Pan evaporation	mm
E_{pi}	Piche evaporation	mm
e_s	Saturation water vapour pressure	KPa or mb
$e_s(T_{max})$	Saturation water vapour pressure at maximum air temperature of day	kPa
$e_s(T_{min})$	Saturation water vapour pressure at minimum air temperature of day	kPa
$e_s(T_o)$	Saturation water vapour pressure at surface temperature	kPa
$e_s(T_z)$	Saturation water vapour pressure at temperature z height above surface	kPa
$e_s - e_a$	Water vapour pressure deficit at 2 meter	kPa
ET	Evaporation	mm
ET_{crop}	Actual crop evaporation	mm
ET_o	Reference evaporation	mm
e_z	Water vapour pressure at height z	kPa
f	Function	
F	View factor	
F_h	Sensible heat flux density	$W\ m^{-2}$

F_s	Soil heat flux density measured with soil heat flux plate at 80 mm	$W\ m^{-2}$
F_{stored}	Stored soil heat flux density calculated from the soil temperature and soil water content	$W\ m^{-2}$
G	Soil heat flux density	$W\ m^{-2}$
g	Gravitational acceleration (= 9.8 $m\ s^{-1}$)	$m\ s^{-1}$
GPM	Grass based Penman-Monteith	mm
h_1	Water potential at lower part of evaporation surface of ceramic cup	m
h_2	Water potential at upper part of evaporation surface of ceramic cup	m
h_c	Crop height	m
I_a	Clear sky solar irradiance	$W\ m^{-2}$
I_{net}	Net irradiance	$W\ m^{-2}$
I_{net} - G	Available energy flux density	$W\ m^{-2}$
I_o	Extraterrestrial solar irradiance	$W\ m^{-2}$
rI_s	Reflected solar irradiance	$W\ m^{-2}$
IRT	Infrared thermometer	
I_s	Solar irradiance	$W\ m^{-2}$
k	von Karman's constant (= 0.41)	
K_c	Crop coefficient	
K_h	Hydraulic conductivity	$m\ s^{-1}$
k_p	Pan coefficient	
K_T	Thermal conductivity	$J\ m^{-2}s^{-1}K^{-1}$
L	Long wave irradiance	$W\ m^{-2}$
LAI	Leaf area index	
L_d	Incoming long wave irradiance	$W\ m^{-2}$
L_d - L_u	Net long wave irradiance	$W\ m^{-2}$
L_{net}	Net long wave irradiance	$W\ m^{-2}$
L_u	Upward long wave irradiance	$W\ m^{-2}$
$L_v F_w$	Latent heat flux density	$W\ m^{-2}$
m	Aerodynamic factor	
M_w	Molecular mass of water (= 0.018 $kg\ mol^{-1}$)	$Kg\ mol^{-1}$
n	Sunshine hours	hour
N	Potential sun shine hours	hour
PTFE	Poly-tetra-fluoro-ethylene	
n_1	Stomatal factor	
q	Flow rate	$m\ s^{-1}$
r	Reflection coefficient	
R	Gas constant (= 8.3143 $J\ K^{-1}\ mol^{-1}$)	$J\ K^{-1}\ mol^{-1}$
r_a	Aerodynamic resistance	$s\ m^{-1}$
r_{av}	Aerodynamic resistance of latent heat	$s\ m^{-1}$
r_{ah}	Aerodynamic resistance for sensible heat	$s\ m^{-1}$
r_{am}	Monteith (1973) stability corrected aerodynamic resistance	$s\ m^{-1}$
r_b	Cuticular resistance	$s\ m^{-1}$
r_c	Canopy resistance	$s\ m^{-1}$
r_H	Aerodynamic resistance to transfer of sensible heat	$s\ m^{-1}$
RH	Relative humidity	%
$R^{H,A}$	Boundary layer resistance for sensible heat flux density	$s\ m^{-1}$
r_i	Single stomatal resistance	$s\ m^{-1}$

RPM	Reduced set Penman-Monteith evaporation	mm
r_s	Equivalent surface resistance	s m^{-1}
r_s	Stomatal resistance	s m^{-1}
r_{sD}	Surface resistance under totally dry condition	s m^{-1}
r_{st}	Bulk stomatal resistance	s m^{-1}
r_{STO}	Stomatal resistance	s m^{-1}
RTD	Resistance thermometer detector	s m^{-1}
r_v	Canopy plus boundary layer resistance	s m^{-1}
$R^{V,A}$	Boundary layer resistance for latent heat flux	W m^{-2}
S	Total energy flux density between net radiometer and plates	W m^{-2}
STEB	Surface temperature energy balance latent heat flux density	W m^{-2}
STEB	Surface temperature energy balance evaporation	mm
STEB (I_{net} - G)	Surface temperature energy balance reference evaporation estimate using estimated available energy	mm
$STEB_{CC}$	Surface temperature energy balance reference evaporation estimate with Campbell and Norman (1998) procedure corrected aerodynamic resistance	mm
$STEB_{MC}$	Surface temperature energy balance reference evaporation estimate with Monteith (1973) corrected aerodynamic resistance	mm
$STEB_{UN}$	Surface temperature energy balance reference evaporation estimate with uncorrected aerodynamic resistance	mm
T_a	Air temperature	°C
T	Air temperature	K or °C
T	Air temperature	K
T_b	ET-gage body temperature measured with thermocouple	°C
T_c	Surface temperature of ceramic plate measured with thermocouple E	°C
T_{dp}	Dew point temperature	°C
T_i	Air temperature at time i	°C
T_{i+1}	Air temperature at time i+1	°C
T_{max}	Daily maximum temperature	°C
T_{min}	Daily minimum temperature	°C
T_o	Surface temperature	°C
$T_{p\ min}$	Previous day minimum air temperature	°C
T_s	Surface temperature	K
T_s - T_a	Surface-air temperature difference	°C
T_z	Air temperature at height z	°C
U	Wind run	Miles day^{-1} or km day^{-1}
u	Wind speed	m s^{-1}
U_*	Frictional velocity due to roughness	m s^{-1}
U_2	Wind speed at two meter	m s^{-1}
V	Water potential molar volume (=18 m^{-3} mol^{-1})	m^{-3} mol^{-1}
VPD	Water vapour pressure deficit	kPa
Z_h	Air temperature and water vapour pressure measurement height	m

Z_H	Surface roughness for sensible and water vapour pressure (= 0.01 Z_m)	m
Z_m	Wind speed measurement height	m
Z_M	Surface roughness for momentum (= 0.12 h_c)	m
o	Symbolize the surface condition	
z	Symbolize the atmosphere above surface of z condition	
Θ	Gravimetric soil water contents	
γ	Psychrometric constant	Pa °C
Δ	Slope of saturation water vapour pressure *vs* temperature relationship	Pa °C
ρ	Density of air	kg m^{-3}
ρ_w	Density of water	kg m^{-3}
λ	Specific Latent heat of evaporation (= 2450 kJ kg^{-1})	J kg^{-1}
σ	Stefan-Boltzmann constant (= 5.673×10^{-8} W m^{-2} K^{-4})	W m^{-2} K^{-4}
δt	Change in measurement time	s
Θ	Kelvin temperature (= 293 K)	K
Φ	Solar altitude	Degrees
γ^*	Apparent psychrometric constant	Pa °C
ε_a	Clear sky emissivity	
ρ_c	Density of ceramic (porcelain = 2450 kg m^{-3})	kg m^{-3}
Δh	Difference in pressure head	m
Ψ_H	Stability factor of sensible heat	
Ψ_M	Stability factor of momentum	
ε_s	Surface emissivity	
ρ_{soil}	Bulk density of dry soil (= 1200 kg m^{-3})	kg m^{-3}
$\delta T/\delta Z$	Change in soil temperature as a function of soil depth	°C m^{-1}
ξ	Monin-Obukhov stability parameter	m
Δt	Change in time	s
Δx	Thickness of cup	m
Δz_{soil}	Depth of soil heat flux plate (= 80 mm)	m
ΔZ	Thickness of ceramic evaporation surface (= 3 mm)	m
ΔZ	Depth of measurements	m

CHAPTER 1

INTRODUCTION

1.1 BACKGROUND

Accurate measurement of evaporation is crucial in agricultural and water resources management although direct measurement of evaporation is usually not feasible for practical, theoretical and financial reasons. The direct approach of measuring evaporation using a lysimeter is expensive, cumbersome (Giambelluca 1992) and destructive (Savage *et al.* 1997). According to Savage *et al.* (1997) meteorological methods are still expensive but non-destructive, continuous and mobile when compared to lysimetry and less dependent on empirical factors. They also indicate the possible use of methods for collecting more reliable and worthwhile data within time periods as short as 12 minutes from fields and sub-regional scale.

Most of the micro-meteorological methods of measuring evaporation (like Bowen ratio and infrared techniques) require measurements at two levels in the atmosphere. However the Penman-Monteith method is a micrometeorological method for measuring evaporation that requires single level measurements of the microclimate. Using measured surface temperature, calculating evaporation from residual of the STEB is a relatively simple micrometeorological method. However, the amount of information required for the continuous application of the Penman-Monteith and STEB evaporation methods is difficult for implementation since some parameters are very difficult to measure continuously.

To solve the problems with direct measurement of evaporation, two alternative strategies have been used: 1. evaporation may be measured from an evaporimeter full of water as an index of evaporation from a reference surface; 2. evaporation from a crop reference surface is estimated using physically-empirically-derived equations involving single level measurements of the microclimates. The actual amount of evaporation is then calculated using the crop factor.

The measurement of evaporation from a specific crop is referred to as reference evaporation. Reference evaporation is defined as the rate at which the available water would be removed from the soil for a canopy that fully covers the soil and is not deficient of water and

nutrients (Doorenbos and Pruitt 1977). Doorenbos and Pruitt (1977) used short grass of height 80 to 150 mm and Allen *et al.* (1989, 1994*a*, 1998) and Jensen *et al.* (1990) used a short grass height of 120 mm and alfalfa of height 500 mm for determining reference evaporation. The reference evaporation is related to the actual evaporation of the crop at different stages using a crop coefficient (K_c):

$$ET_{crop} = K_c ET_o \qquad 1.1$$

where ET_{crop} is the actual crop evaporation in mm day^{-1}, K_c is the crop coefficient developed under extensive study of crops with lysimeter measurement under different growth stage and climatic conditions and ET_o is the reference evaporation in mm day^{-1} (Doorenbos and Pruitt 1977).

The accuracy of using Eq. 1.1 strongly depends on the estimation accuracy of reference evaporation (ET_o). Many research studies have shown the outstanding performance of grass-based Penman-Monteith reference evaporation estimate compared to the other methods, even though more detailed measurement of weather variables is required for accurate estimation (Allen *et al.*1989; Jensen *et al.* 1990; Allen *et al.* 1994*a*, 1994*b*, 1998; De Bruin and Striker 2000). Specifically, the Penman-Monteith approach includes many more factors that influence crop water use compared to most other measurement methods (Savage 2001*a*). The requirement of detailed weather variables, sensors and the difficulty of accessing them often limit the use of the method in various parts of the world. As an alternative, a wide range of empirical methods and devices are also used. The empirical correlations of estimating reference evaporation lack generality and are limited to a daily time step and as such the use of those do may need careful consideration, possibly as a last option because of their locally specific character.

Most micrometeorological techniques of measuring evaporation involve assumptions to ensure that only routine AWS measurements are required. The grass and alfalfa based Penman-Monteith approach of estimating reference evaporation strongly depends on the estimation of the radiative term of the equation. Normally net irradiance and soil heat flux density are not part of standard AWS measurements. The estimation of net irradiance and soil heat flux density is therefore preferred compared to the direct measurement with net radiometer and soil heat flux plates. Sensor cost and maintenance requirement for certain long-term applications, such as reference evaporation estimation for irrigation scheduling, often preclude the measurement of net irradiance and soil heat flux density (Hatfield and Fuchs 1990). The Penman-Monteith approach of estimating reference evaporation greatly depends on the accuracy of net irradiance estimation (Liasat and Snyder 1998). The performance of the different procedures for

calculating reference evaporation needs investigation especially for those procedures that have site specific (empirical) inputs.

The linear approximation of clear sky net long wave irradiance from air temperature avoids the need for measuring water vapour pressure (Monteith and Unsworth 1990). Monteith and Unsworth (1990) recommended the use of this relationship for daily and greater time steps of the radiation balance but not micrometeorological analysis over a period of a few hours. In the unpublished and undated Campbell Scientific Inc application note, the approximation is recommended for online calculation of hourly reference evaporation using data loggers and computers. The sensitivity of the approximation needs more attention since the approximation is for a limited range of air temperatures. In the Campbell Scientific Inc (undated) application note, soil heat flux density and reflected solar irradiance of the reference crop are also approximated from the net irradiance and the incoming solar irradiance. Comparison of the approximation and comparison with measured values would indicate the accuracy of the approximation. Site-specific evaluation of this estimate may further improve the accuracy of the reference evaporation estimate.

The STEB estimate of reference evaporation requires accurately measured available energy flux density (I_{net} - G) and sensible heat flux density (F_h). Sensible heat flux density can be directly measured using eddy correlation techniques (Monteith and Unsworth 1990; Savage *et al.* 1997). The resistance law estimate of sensible heat based on the canopy to air temperature difference and wind speed may affect the evaporation estimate using the STEB method. The surface-air temperature difference can be calculated using infrared thermometer (IRT) measurements of the canopy surface and air temperature measured at 2 meters height. However, the aerodynamic resistance is difficult to measure. It is estimated using the momentum theory and depends on atmospheric stability. The procedures developed for stability correction of the estimated aerodynamic resistance of a neutral atmosphere may result and shows a different response depending on the roughness of crop surface. Investigating the possible error of using different correction procedures and their potential of improving accuracy of sensible heat and latent heat flux densities under unstable and stable atmospheric conditions may improve the practical use of the techniques. Kjelgaard *et al.* (1996) reported the insignificance of aerodynamic correction, using the technique on maize and potato crops. The absence of direct measurements methods of available energy flux density (I_{net} - G) using an AWS and considering the additional benefit of including the IRT as part of an AWS, the estimation of the available energy flux density needs further investigation, considering its importance in estimating reference evaporation.

The online application of the full set Penman-Monteith approach requires the use of an AWS (sensors, data loggers, communication system and peripheral equipment). The options of communication systems for this application, includes radio frequency, telephone line and satellite. Accessing an AWS is expensive at a farm level or in developing countries. In the unpublished Campbell Scientific Inc (1998) application note a reduced set evaporation weather station is recommended for the reference evaporation estimate using the Penman-Monteith approach. The system allows the use of surrogate wind speed and water vapour pressure data. The main difference of AWS and reduced set evaporation weather station is the absence of a wind speed and relative humidity sensor in the reduced set evaporation weather station. However, the major cost of the AWS lies with data logging and communication system. The use of an inexpensive weather station system to achieve the same aim of determing reference evaporation that may in fact be complimentary to the standard weather station system requires investigation. An analysis of the accuracy (and cost saving) of complimentary inexpensive systems for monitoring the microclimate and for calculating reference evaporation is required.

As an alternative to an AWS (or inexpensive alternative to an AWS), atmometers and evaporation pans have been used as an index of actual evaporation from vegetation. The atmometers appear to be more flexible, low cost and easy to maintain and operate compared to the evaporation pan (Messing 1998). The ET-gage atmometer (Altenhofen 1985; Broner and Law 1991; Fontaine and Todd 1993; Parchomchuk *et al.* 2000; Alam and Trooien 2001) can be a valuable tool for water resource management. The ET-gage can be a useful device for estimating reference evaporation, especially in remote areas where there is only one AWS some distance away. An ET-gage connected to a data logger and a time controlling mechanism of irrigation was reported to provide 70 % saving of water of vineyard over a season (Parchomchuk *et al.* 2000). As Savage *et al.* (1998) showed, the short time (hourly) reference evaporation measurements better describe the microclimate. The efficiency of the electronic ET-gage (Model E) needs to be investigated for use as a daily measure in comparison with the sum of hourly grass and alfalfa Penman-Monteith, daily Penman-Monteith and STEB estimate of reference evaporation.

Air temperature and relative humidity affect the evaporation estimate of the Penman-Monteith approach. Air temperature and relative humidity from AWS is often measured using naturally ventilated radiation shields. The 8 % bias in daily air temperature measurement using a radiation shield is reported to result in an average increase of 11 % in calculating reference evaporation (Dusek and Howell 1996). Alternatives to the six- and twelve-multi-plate Gill radiation shields that are simple in design and inexpensive requires investigation.

1.2 MOTIVATION

This investigation was motivated by a desire of arriving at a very simple, economically feasible and practical but accurate method and device for gathering information of the dynamic soil-plant-environment continuum. Such methods, if proved adequate could be complimentary to or alternatives to standard AWS systems used. The methods also allow for the estimation of grass reference evaporation. It is, however, recognized that many methods exist to determine reference evaporation. However, the application of methods can only be feasible when the performance is tested for a wider range of microclimates and yet are not economically affordable. The need for the proper management of unevenly distributed water resources and economic constraints is the main concern for the consideration of alternative options for the expensive but most accurate evaporation measuring techniques.

1.3 AIM

Thus the objectives of this research are:

- To assess the assumptions and approximations of the available energy estimated using the Penman-Monteith reference evaporation method
- Compare the daily ET-gage evaporation estimates with grass-based and alfalfa-based Penman-Monteith reference estimates
- To assess the improvement of STEB estimate of reference evaporation by correcting for atmospheric stability and its estimate of available energy
- To evaluate the use and investment cost of the ET-gage evaporimeter, reduced set evaporation weather station systems and inexpensive weather station systems for estimating reference evaporation
- To assess the feasibility of using home-made radiation shields for housing the air temperature and relative humidity sensors, thereby reducing costs.

1.4 THESIS ROADMAP

The various methods for estimating reference evaporation are discussed in Chapters 2 and 3 with assumptions of Penman-Monteith approach discussed in Chapter 4. Measured data are used to test the assumptions of the Penman-Monteith approach (Chapter 6) and the performance of ET-gage evaporimeter and the micrometeorological techniques for measuring evaporation is investigated in Chapter 7. The cost and accuracy consideration of the various methods for estimating evaporation are dealt within Chapter 8.

CHAPTER 2

METHODS FOR ESTIMATING REFERENCE EVAPORATION

2.1 INTRODUCTION

Accurate hourly absolute estimation of water loss by evaporation is required in both irrigated agricultural areas and natural ecosystems for irrigation scheduling and hydrological monitoring respectively (Savage *et al.* 1997). Actual crop evaporation is traditionally estimated using Eq. 1.1. In that sense, selecting the best methodologies of estimating reference crop evaporation is critical. Appropriate measuring devices and the nature of formulation of methods are major limitations in computing reference evaporation. Most studies showed that the combination method based on the Penman (1948) formulation, yields a reliable estimate of actual evaporation from a short reference crop. On the other hand in the absence of meteorological data or reliable data, it has also been found that a much simpler approach, involving empirical and semi-empirical methods are in use to estimate actual evaporation of short grass or alfalfa.

The combination approach is physically realistic (accurate) but also complex, requiring far more measurements or estimates of parameters (variables) than routinely available at a meteorological station (Stewart 1983). The original Penman (1948) equation is developed to estimate the atmospheric evaporative demand from a saturated water surface. It is empirically modified to estimate reference evaporation of short grass (Doorenbos and Pruitt 1977). Furthermore, it is related to the physiology of a plant based on the analog of the electrical law of resistance (Monteith 1965), which reduces the complexity. The Penman approach of Doorenbos and Pruitt (1977) is referred to as the FAO Modified Penman approach while the Monteith (1965) modification is referred to as the Penman-Monteith approach. The evaporation is estimated from single level measurements. This makes the Penman (1948) and Penman-Monteith (1965) approach more practical than other micrometeorological methods.

Alternative methods of estimating reference evaporation from single-level measurements include the empirical temperature, radiation, semi-combination, reduced set of combination methods and evaporation devices. The application of the empirical approach is generally limited in estimation accuracy due to their empirical nature of formulation of the relation and their site-specific characters and conditions. Recently Allen *et al.* (1998) and unpublished Campbell

Scientific Inc. (1998) application notes report on the use of Penman-Monteith approach with surrogate data. The evaporation devices that are related to evaporation measured from a reference crop are evaporation pans and atmometers. Thus the objective is to review the theoretical background, time of application and data requirement of the combination approach and alternative reference evaporation estimating methods. The discussion of the use of evaporimeters for the measurement of reference evaporation, however, is deferred to Chapter 3. The estimation of reference evaporation using the Penman-Monteith approach is reviewed in Chapter 4.

2.2 METEOROLOGICAL METHODS

2.2.1 Empirical Methods

Empirical methods for estimating reference evaporation are regression equations developed from correlation between measured evaporation and meteorological variables where measured variables are normally conducted using lysimeters (Burman *et al.* 1980). Lysimeters are considered as the standard against which other methods are calibrated. Empirical models recommended for the estimation of reference evaporation (Appendix 1) have been grouped based on the requirements of the data and mode of derivation. The application of the method is dictated by the availability of meteorological data (Stewart 1983) and their main attraction is that they permit estimation of reference evaporation where meteorological records are limited (Sharma 1985).

2.2.1.1 Temperature method

The methods of estimating reference evaporation based on temperature methods are basically empirical. The methods depend on air temperature as a surrogate for the amount of energy that is available to the reference crop for evaporation. Air temperature is most readily available (Hatfield and Fuchs 1990; Thornton and Running 1999). The most common methods are given in Appendix 1.1. The FAO Blaney-Criddle (1977) method is a much more studied method for monthly grass reference evaporation. It has also been calibrated for daily reference evaporation (Allen and Pruitt 1986). The empirical nature of the temperature methods is their main limitation. But if estimation is made for periods of several weeks or months reasonable approximations are possible even with the defects inherent in these models (Hashim and Habibian 1979). According to Hatfield and Fuchs (1990), the Thornthwaite and Blaney-Criddle methods are better suited for climatologically or seasonal patterns rather than daily reference evaporation values needed for irrigation management.

2.2.1.2 Radiation method

The physical process of evaporation is controlled by the available energy and the ability of evaporated water to be transferred from the surface to the atmosphere. This transfer process of water vapour is a function of wind speed and amount of water vapour in the air close to the surface and air temperature. Under non-advective conditions the role of available energy is clear from the studies of Priestley and Taylor (1972) and evaluation of the method from an unstressed short grass surface (De Bruin and Stricker 2000).

The radiation method uses a measure of solar irradiance together with air temperature to calculate reference evaporation, depending on the approach followed in the derivation of the method (Appendix 1.2). Jensen (1966) presented two forms, which are common to most of the methods developed from the net irradiance or solar irradiance approximation of energy balance:

$$ET = K_c \Phi_1 I_{net} \qquad 2.1a$$

$$ET = K_c \Phi_2 I_s \qquad 2.1b$$

where $\Phi_1 = 1 - (F_h - G)/I_{net}$, $\Phi_2 = 1 - r\,(L_{net}/I_s) - (F_h - G)/I_s$, K_c is crop coefficient, F_h is sensible heat flux density (W m^{-2}), G is soil heat flux density (W m^{-2}), I_s is the solar irradiance (W m^{-2}), I_{net} is the net irradiance (W m^{-2}) and r is the reflection coefficient. The FAO radiation methods, developed from the Makkink (1957) and Hargreaves method (1982, 1985) are the two methods globally recommended for grass related reference evaporation (Doorenbos and Pruitt 1977; Jensen *et al.* 1990; Allen *et al.* 1998). The solar irradiance may be used directly to estimate evaporation or indirectly to provide a measure of net irradiance. Most research studies indicated the approach as a better method than the temperature method (Doorenbos and Pruitt 1977; Hatfield and Fuchs 1990; Jensen *et al.* 1990; Allen *et al.* 1998) and recommended its use as an alternative to the FAO Modified Penman and Penman-Monteith approach of estimating reference evaporation in the absence of reliable data. However, the accuracy of the method is limited in the presence of advection.

2.2.2 Combination Methods

The combination method of estimating reference evaporation is based on the original Penman (1948) equation that consists of the simplified energy balance, an aerodynamic Dalton type and psychrometric constant equations of the water surface. The equation is modified to simulate the evaporation from vegetation in several studies. According to Stewart (1983) the different forms of

the combination equation arise from the different assumptions used in each derivation and these determine the degree of physical reality of each approach and define the input data required to use the approach (see Table 2.1).

2.3 PENMAN-MONTEITH THEORY

2.3.1 Penman Equation

Penman (1948) attempted to estimate sensible heat flux density of the simplified energy balance equation (cited by Penman, 1956). The fundamental basis of the equation is that evaporation from the surface of pure water depends on: water vapour pressure e_o (Pa) of air in contact with the surface; water vapour pressure e_z (Pa) of air at height z; and turbulence specified by an exchange coefficient which is a function wind speed, normally written as $f(u)$. Penman (1948) assumed that the transport of latent heat flux density (L_vF_w) is governed by the water vapour pressure difference according to the relation:

$$L_vF_w = f(u)(e_o - e_z) \qquad 2.2$$

In the same way the transport of sensible heat flux density is governed by a temperature difference:

$$F_h = \gamma f(u)(T_o - T_Z) \qquad 2.3$$

where T_o is water surface temperature (°C), T_z is the air temperature (°C) at height z above water surface and γ is psychrometric constant (Pa K^{-1}) (Appendix 2). Assuming that $e_o = e_s(T_o)$ where $e_s(T_o)$ is the saturated water vapour pressure at surface temperature (T_o), the slope in the saturation water vapour pressure *vs* temperature can be defined as:

$$\Delta = [e_s(T_o) - e_s(T_z)]/(T_o - T_z). \qquad 2.4$$

The energy balance of the water surface is given by:

$$I_{net} - L_vF_w - F_h - G - A = 0 \qquad 2.5$$

where A is the advection flux density (W m^{-2}) and G is stored heat flux density (W m^{-2}). Neglecting the advection heat flux densities, Eq. 2.5 can be written as:

$$I_{net} - L_vF_w - F_h - G = 0. \qquad 2.6$$

These expressions were combined to avoid the need for measuring surface temperature (T_o) and surface water vapour pressure (e_o). Systematic mathematical combination of Eqs 2.2, 2.3, 2.4 and 2.6 eliminates surface water vapour pressure (e_o) and the surface temperature (T_o). This yields the Penman (1948) equation:

$$L_vF_w = \frac{\Delta}{\gamma + \Delta}(I_{net} - G) + \frac{\gamma}{\gamma + \Delta} f(u)[e_s(T_z) - e_z]. \qquad 2.7$$

Table 2.1 The main forms of the combination equation for estimating evaporation, with their assumptions and data requirements (Stewart 1983)

Author	Estimation of	Type of model	Assumptions	Data requirements	
				Variables	Averaged over
Penman (1948)	Potential, weekly or monthly	One-level	Extensive uniform surface, same height for both sources–sinks, aerodynamically smooth, zero surface resistance, empirical relationships for I_{net}, and r_a	n, T_{max}, T_{min}, e_{09}, U	Day, month
Monteith (1965)	Actual hourly	One-level	Extensive uniform surface, steady state conditions, mean source–sinks of sensible heat and water vapour at same height as sinks of momentum	I_{net}, S, G, T, e, r_s, r_a	Hour
Thom	Actual hourly	Two-level	Extensive uniform surface steady state conditions, single source-sink of sensible heat and another of water vapour	I_{net}, S, G, T, e, r_{ST}, r_H, r_v	Hour
Priestley and Taylor (1972)	Potential, weekly or monthly	One-level	Extensive uniform surface, same height for both sources–sinks, zero surface resistance, constant relationships between water vapour pressure deficit and radiation	I_{net}, G, T	Day, month
Shuttleworth	Actual, hourly	Analytical (many levels)	Extensive uniform surface, steady state conditions	I_{net}, S, G, T, e, r_{STO}, r_H, r_V, $R^{H,A}$, $R^{v,A}$	Hour
Thom and Oliver (1977)	Actual monthly annually	One-level	Extensive uniform surface, same height for both sources–sinks, empirical relations for r_{sD}, r_s and r_a	I_{net}, G, T, m, n_1	Day, month, year

I_{net} = net irradiance (W m^{-2}), S = total flux density of energy into storage between levels of net radiometer and soil heat flux plates (W m^{-2}), G = soil heat flux density (W m^{-2}), T = air temperature (°C), e = water vapour pressure (mb), r_{STO} = stomatal resistance (s m^{-1}), r_H = aerodynamic resistance of sensible heat (s m^{-1}), r_V = aerodynamic resistance to water vapour pressure (s m^{-1}), $R^{v,A}$ = boundary-layer resistance for latent heat flux (s m^{-1}), $R^{H,A}$ = boundary layer resistance for sensible heat flux (s m^{-1}), r_s= surface resistance (s m^{-1}), r_a= aerodynamic resistance (s m^{-1}), r_{ST} = bulk stomatal resistance (s m^{-1}), m = aerodynamic factor, n_1 = stomatal factor, n = number of sunshine hours (h), T_{max}= mean daily maximum air temperature (°C), T_{min} = mean daily minimum air temperature (°C), e_{09} = water vapour pressure measured at mid-morning (mb), u = wind run (miles day^{-1}), r_{sD} = surface resistance under totally dry conditions (s m^{-1})

The Penman equation (Eq. 2.7) was further studied and related to the evaporation from a standard transpiring short grass or alfalfa surface. Procedures of estimation and measurement of each parameter are also reported in those studies. Doorenbos and Pruitt (1977) revised the method and empirically modified it to estimate reference evaporation from a short grass. The modifications includes the wind function $f(u)$, an adjustment factor to account for local condition (c) and an assumption that the daily average soil heat flux density is zero. The equation is referred to as the FAO Penman equation:

$$ET_o = c[WI_{net} + (1-W)f(u)(e_s - e_a)] \qquad 2.8$$

where $W=\Delta/\Delta+\gamma$, e_a is actual water vapour pressure (mb) and e_s is saturation water vapour pressure (mb). In a similar manner Wright (1982) related Eq. 2.7 to alfalfa reference crop and gave a different procedure for estimating the parameters. Jensen *et al.* (1990) discussed the procedures used to estimate parameters and found that the empirically derived wind function term $f(u)=a+bu$ as most variable among researchers. Unlike others, Wright (1982) presented a variable wind function, which is a function of day of year for calculating the coefficients. The coefficients and reference crops used with some of the wind function equations applied to the Penman approaches are shown in Table 2.2.

2.3.2 Penman-Monteith

In an attempt to better characterize water loss by plants, Monteith (1965) introduced a modification to the Penman (1948) equation (Eq. 2.7), resulting in the well-known Penman-Monteith equation (Alves and Pereira 2000). Monteith (1965) incorporated the biological based canopy and physically based aerodynamic resistance terms into the wind function (Steiner *et al.* 1991).

Table 2.2 Coefficients of the wind function $f(u)=a(1+bu)$, for various reference crops as used in the Penman approach (Hatfield and Fuchs 1990)

Reference crop	a	b	Source
Short grass	2.63	0.53	Penman (1948)
Clipped grass	2.63	0.55	Penman (1956)
Alfalfa	1.97	1.32	Wright and Jensen (1972)[1]
Alfalfa	2.89	0.83	Kincaid and Herman (1974)[1]
Grass	2.7	0.86	Doorenbos and Pruitt (1977)
Grass	3.7	0.54	Stigter (1981)[1]

[1]cisted by Hatfield and Fuchs (1990)

A schematic illustration of the resistance model is shown in Fig. 2.1. Monteith (1965) assumed the surface of vegetation canopy as a uniform and homogeneous big leaf and used Ohm's law of electrical resistance to define sensible heat energy from the canopy to the atmosphere using aerodynamic resistance r_{ah} and the canopy temperature T_o as:

$$r_{ah} = \rho c_p (T_o - T_z)/F_h \qquad 2.9$$

where ρ is the density of air (kg m^{-3}) and c_p the specific heat capacity of dry air at constant pressure (J kg^{-1} K^{-1}). According to Monteith and Unsworth (1990), taking the myriads of inter-cellular space of leaf as the source of water vapour pressure, where water vapour pressure $e_s(T_o)$ is in saturation state, the latent heat flux density will encounter the stomatal resistance r_s, the cuticle resistance r_b and aerodynamic resistance r_{av} in its way to the atmosphere. Assuming a very large cuticle resistance r_b and applying Ohm's law of electrical resistance, the latent heat of evaporation is:

$$r_s = \rho c_p (e_s(T_o) - e_o)/\gamma L_v F_w \qquad 2.10$$

for the stomatal resistance (also referred to as the bulk stomatal resistance) and for aerodynamic resistance:

$$r_{av} = \rho c_p (e_o - e_z)/\gamma L_v F_w \qquad 2.11$$

where index $_o$ symbolizes surface condition under the surrounding atmosphere condition and $_z$ the surrounding atmosphere. In addition to the above relations, the slope of plot of saturation water vapor pressure versus air temperature (Eq. 2.4) and the energy balance equation (Eq. 2.6) were used by Monteith (1965) to compute the evaporation.

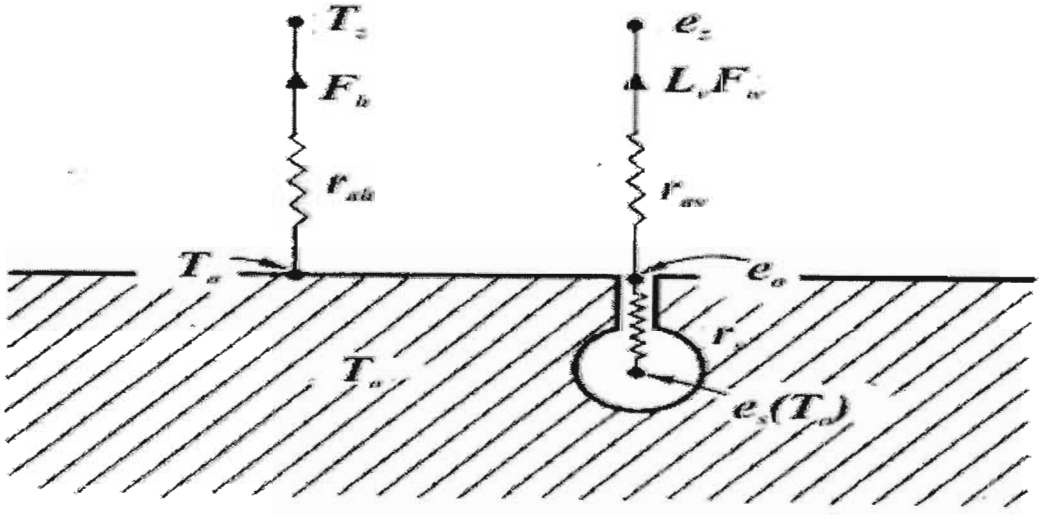

Fig. 2.1 Schematic representation of a vegetation surface at uniform temperature (from Thom 1975)

In a similar manner to Penman (1948), these relationships are combined mathematically to avoid measurement of the "unknown" surface values of water vapour pressure (e_o) and of temperature (T_o). The Penman-Monteith approach which includes the aerodynamic resistance (r_a) and stomatal resistance (r_s) is given as:

$$L_v F_w = [\Delta(I_{net} - G) + \rho c_p (e_s(T_z) - e_z)/r_a]/[\Delta r_a + \gamma(1 + r_s/r_a)] \quad 2.12$$

Thom (1975).

Although there are difficulties in measuring r_a and r_s, using an estimated value, a good agreement was reported between evaporation of short grass determined from the Penman-Monteith approach (Eq. 2.12) and measurement from lysimeter (Allen *et al.* 1989; Jensen *et al.* 1990; Steiner *et al.* 1991; Allen *et al.* 1994*b*). Recently, Allen *et al.* (1994*a*) discussed some studies to estimate I_{net}, G, r_a and r_s and reported an updated definition of reference evaporation. Procedures were also given for calculating reference evaporation considering a fixed grass canopy height of 0.12 m to compute the r_a term. He also assumed a constant daytime r_c term equal to 70 s m^{-1}, based on the results obtained by Allen *et al.* (1989) and Jensen *et al.* (1990). The equation is referred to as FAO Penman-Monteith by Allen *et al.* (1998):

$$ET_o = \frac{0.480(I_{net} - G) + \gamma(900/(273 + T_a)U_2(e_s - e_a)}{\Delta + \gamma(1 + 0.34U_2)} \quad 2.13$$

where I_{net} and G are expressed in MJ m^{-2}, T_a is air temperature at 2 m height (°C), U_2 is wind speed at a height of 2 meter (m s^{-1}), e_s is saturation water vapour pressure (kPa) at air temperature T_a, e_a is actual water vapour pressure (kPa) and γ and Δ are in kPa $°C^{-1}$. In the absence of reliable data, the approach using Eq. 2.13 is further recommended using surrogate data (Allen *et al.* 1998).

2.4 EVAPORATION MEASURING DEVICES

2.4.1 Evaporation Pan Method

The evaporation rate from a pan filled with water is measured with a micrometer hook gauge and the decrease in water depth per unit time is related to the amount of water evaporated from the surrounding plant surface (Doorenbos 1976). Evaporation pans provide a measurement of the integrated effect of solar irradiance, wind speed, air temperature and humidity on evaporation from a specific open water surface (Doorenbos and Pruitt 1977; Allen *et al.* 1998). Although the energy exchanges of pans are different from vegetation, the method is described as a relatively easy and reliable method if the evaporation site is maintained in a suitable and consistent manner (Al-Ghobari 2000). Estimates are reasonable over periods of ten days or longer (Allen *et al.* 1998).

According to descriptions by Doorenbos (1976) and Guyot (1997) there are two main types of evaporation pans: a pan set into the ground referred to as a sunken pan and a pan placed on the soil surface with evaporating surface and reservoir above ground level. Doorenbos and Pruitt (1977) presented the USA class-A pan (Fig. 2.2*a*) with 1.21 m diameter and Colorado sunken pan (Fig. 2.2*b*) and empirically related measured pan evaporation to reference evaporation of short grass:

$$ET_o = k_p E_p \qquad 2.14$$

where ET_o is the crop reference evaporation (mm day^{-1}), k_p the pan coefficient and E_p the evaporation from the pan (mm day^{-1}). They also recommended the use of those pans for the calibration of other pans. The pan coefficient is pan specific (Allen *et al.* 1998) and derived from the ratio of evaporation measured with lysimeter and that using an evaporation pan. The pan coefficient is a character of pan environment, growth season and farm practices (Brutsaert 1982) and depends on pan type and size, ground cover, use of screen, sitting of pan, pan environment, fetch distance, wind and humidity conditions (Doorenbos and Pruitt 1977; Jensen *et al.* 1990; Allen *et al.* 1998). Instead of pan coefficient, Christen (1968) and Christen and Hargreaves (1969) developed an empirical equation for estimating reference crop evaporation from USWB class-A pan evaporation and several weather parameters (cited from Jensen *et al.* 1990) (Appendix 4). Similarly, Allen *et al.* (1998) presented regression equations for a pan coefficient derived from a table of pan coefficients given for class-A pan and Colorado sunken pan in Doorenbos and Pruitt (1977).

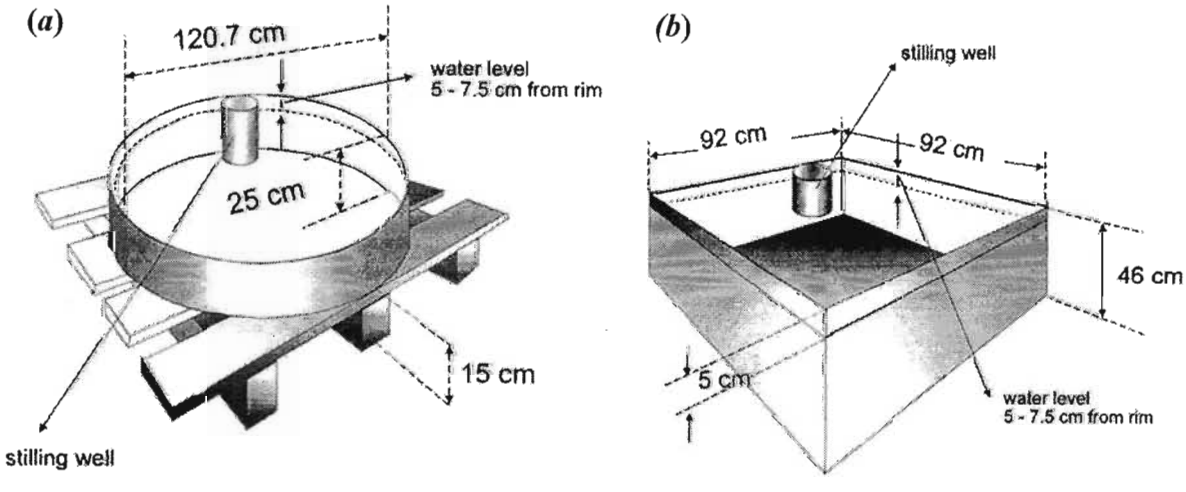

Fig. 2.2 Pan evaporation: (*a*) Class-A pan (*b*) Colorado sunken pan (Allen *et al.* 1998)

CHAPTER 3

ATMOMETERS

3.1 INTRODUCTION

Instruments for measuring evaporation are of two basic designs: open water evaporation pans, (discussed in Chapter 2) and porous surface type of atmometers (Chang 1968). Evaporation pans and atmometers are commonly used as indicators of atmospheric evaporative demand through measuring the water loss with time either by observation of depth or mass change. Evaporation pans are widely used in comparison with atmometers as indicators of reference evaporation. Evaporation pans have even been recommended as an alternative to the Penman and Penman-Monteith approach for estimating reference evaporation (Doorenbos and Pruitt 1977; Jensen *et al.* 1990; Allen *et al.* 1998). A common advantage of pans and atmometers is that they can supply values of evaporation on daily, hourly or even shorter time periods (Messing 1998). The data provided with each time step is an integrated influence from the starting point of measurement. However, evaporation pans used today are relatively large in size and open. For example, errors on the measurements from these devices may occur due to accumulation of dirt, wind waves, animals and heat storage of the pan (Doorenbos and Pruitt 1977; Jensen *et al.*1990; Allen *et al.* 1998). Atmometers on the other hand are small and thus ensure a fast response (Messing 1998). They are cheap, have a low water requirement and are easy to install and record (Chang 1968; Doorenbos 1976; Messing 1998). The main disadvantages of atmometers can be the difficulty of keeping the evaporating surface clean and in an unchanged condition.

Although an atmometer shows the integrated influence of all effective micro-meteorological measures, the forms and configuration of the atmometer employed limits the manner of its exposure to the surrounding and its response. In addition, there is a difficulty of interpreting the data obtained from the measurement. As a result, the earlier studies on atmometers especially focused on the sensitivity of the atmometer surface and its response to the main microclimatic variables (Livingstone 1935; Holmes and Robertson 1958; Mukammal 1961; Wilcox 1963; Wilcox and Sly 1974). These studies also related the measured values with potential evaporation and crop consumption for irrigation purposes (Jessep 1964; Korven and Wilcox 1964; Shannon 1966). Furthermore, the type of assembly, evaporation surface, ease of mounting and a system of having all season evaporative surfaces were studied (Livingstone 1935; Carder 1960; Wilcox 1967).

Unlike the earlier works, recent studies focused on simulating the actively evaporating leaf surface using porous ceramic plates. Green and variable density fabric cover was used to simulate the canopy resistance of a reference crop for irrigation scheduling and hydrological monitoring (Altenhofen 1985; Broner and Law 1991; Fontaine and Todd 1993; Parchomchuk *et al.* 2000; Alam and Trooien 2001). In any type of atmometer the amount of water, which evaporated in any given time can be measured by making two consecutive readings of the level of water in the tube electronically or visually or through weighing the water reservoir.

The aim of this chapter is to assess the type and nature of atmometers, principle and relation with actual and reference evaporation measured using other methods.

3.2 PRINCIPLES AND THEORY OF ATMOMETERS

Atmometers are either porous porcelain bodies or porous paper wick devices (Chang 1968; Rosenberg *et al.* 1983). They generally consist of an evaporating surface, a water reservoir and a mechanism, which controls the back flow of water from the evaporating surface. According to Anonymous (1961), the actual evaporation from natural solid porous surfaces takes places in two stages: diffusion of water either as liquid or vapour through the solid to the surface and removal of water vapour from surface. Under these circumstances the evaporation rate from the surface depends on (1) water vapour pressure deficit near the evaporation surface, (2) the circulation of air near the evaporation surface, and (3) energy flux density available for evaporation at the surface (Fontaine and Todd 1993).

The mounting and installation of the parts of atmometers varies with the evaporative surface used (Livingstone 1935). Basically there are two types of assembly used with most atmometers. In the first type of assembly, the reservoir is connected to the evaporation surface with a tube and suction feeds the evaporating surface. The second type of assembly is similar in principle to the Piche atmometer when the evaporation surface is in direct contact with the reservoir and gravity feeds the surface. In both systems, the assembly is made to maintain continuity of water flow from the reservoir to the evaporation surface while evaporation proceeds from the top of the evaporating surface. Atmospheric pressure on the surface of liquid maintains the flow of water through the supply tube to the evaporating surface.

The back flow of water or entrance of rain within the earlier models of atmometers was controlled with a check valve or shield. The Livingstone-Thone wool mercury check valve is the most common type of check valve used with Bellani plate and Livingstone atmometers and it is made of mercury and wool. Furthermore Carder (1960) assessed and used other types of

check valves such as the modified Shive mercury U-tube check valve (mercury in U shaped tube valve) and fritted glass check valve (fritted glass and mercury). The atmometer assembly was based on a suction feed that used a check valve to prevent the water from back flow into the reservoir during rain. The recently modified atmometer model ET-gage uses a suction feed mount with an impervious cover at the top of the evaporation surface (Alam and Trooien 2001).

The atmometer reservoir is used as a water storage as well as a measuring device. The reservoir can be of glass, a bottle cylinder, a beaker, a burette or a flask depending on the measurement, mounting and assembly technique (Livingstone 1935; Carder 1960; Feldhake and Boyer 1988, 1990; Qian *et al.* 1996; Jiang *et al.* 1998).

Distilled water is usually used with atmometers to avoid blockage of the evaporation surface. However, since the porous porcelain atmometer is sensitive to frost, an alternative liquid, which does not freeze has also been used. Wilcox (1967) used a mixture of 22 % methanol and 78 % distilled water avoid freezing at -32 °C.

The evaporation from the atmometers correlated with actual evaporation based on the assumption that evaporation from these surfaces is a meteorologically controlled entity. The response of atmometers to microclimatic measures has been widely studied (Livingstone 1935; Holmes and Robertson 1958; Carder 1960; Mukammal 1961; Feldhake and Boyer 1988, 1990; Alam and Trooien 2001). However there is disagreement on the interpretation of the data. Livingstone (1935) and Shannon (1966) and similarly Halkias *et al.* (1955) as cited by Dilley and Helmond (1973) reported higher correlation of the difference of water loss of black and white Bellani atmometers with solar irradiance. A schematic illustration of Bellani atmometer is shown in Fig. 3.1. A number of studies also reported the existence of the relation between the aerodynamic term of Penman and Penman-Monteith evaporation equations and Piche atmometer evaporation.

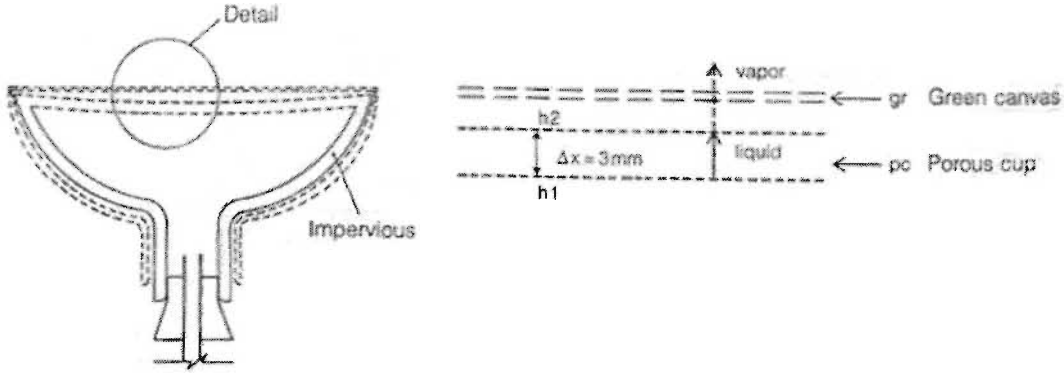

Fig. 3.1 Schematic description of the ceramic cup (Bellani plate) (Broner and Law 1991)

Similarly Mukammal (1961) reported a greater response of atmometer evaporation to wind speed than to solar irradiance. Wilcox and Sly (1974) used a second-degree polynomial equation to relate Bellani plate and Carborundum atmometers to actual evaporation. Jessep (1964) linearly related atmometer evaporation to the pan evaporation. Feldhake and Boyer (1988) recommended the black Bellani atmometer alone be used to estimate potential evaporation. Dilley and Helmond (1973) used a shaded and unshaded synthetic sponge as an evaporation surface to estimate net irradiance and potential evaporation.

3.2.1 Theoretical Evaluation of Modified Atmometer

Recently, the evaporating surface of a modified Bellani plate atmometer, with various density green canvas covers has been used to simulate the actively evaporating saturated leaf condition. Altenhofen (1985) reported the correlation of evaporation measured using a Bellani plate atmometer with a green canvas cover to mimic alfalfa-based reference evaporation calculated using the Penman approach. Based on Altenhofen (1985), Broner and Law (1991) theoretically evaluated and compared the evaporation of the atmometer surface with that of an actively transpiring leaf.

The physical evaluation was performed from the measurements of hydraulic conductivity of the evaporation surface based on the assumption of the maximum possible daily evaporation rate of a leaf. Darcy's law of water flow was used to calculate the water potential difference between reservoir and evaporation surface needed to keep water flow through:

$$q = K_h \frac{\Delta h}{\Delta x} \qquad 3.1$$

where q is flow rate (m s^{-1}), K_h is hydraulic conductivity (m s^{-1}), Δh (= h_2 - h_1) is the pressure head difference across the Bellani cup (m) (Fig. 3.1) and Δx is cup thickness (m). The relative humidity between canvas cover and ceramic cup was evaluated from the assumed air temperature and water holding capacity of reservoir using the Kelvin equation:

$$h_2 = \frac{RT \ln(e/e_s)}{V} \qquad 3.2$$

where h_2 is water potential at the upper surface of cup (m), T is absolute temperature below canvas cover (K), R is the gas constant (8.3143 J mol^{-1} K^{-1}), V is the molar volume of water (18 $\times$ 10^{-6} m^3 mol^{-1}), e is water vapour pressure between canvas cover and ceramic cup (kPa) and e_s is the saturation water vapour pressure (kPa) at temperature T (Broner and Law 1991).

The use of rough green canvas cover is aimed at simulating the reflection coefficient of solar irradiance by plant leaves as well as the water vapour diffusion resistance of leaves. Broner and Law (1991) evaluated the radiation property of evaporation surface. The green

colour and water content between plate and canvas enable the atmometer to simulate the reaction of plant to the reflection of solar irradiance and absorption of long wave irradiance. Broner and Law (1991) also assumed similarity of long wave emission from the evaluation leaf and atmometer surface temperature measurement. Furthermore the use of PVC as a reservoir reduces the warming effect of water in the reservoir, compared to the metal used in pans (Chapter 2).

Based on the Broner and Law (1991) evaluation, the atmometer with brand name ET-gage is mounted with three different fabric covers named canvas 30, canvas 54 and Gore-Tex is made to simulate different evaporation conditions (Alam and Trooien 2001). The fabric options are designed to have different densities to simulate different diffusion resistances:

1. the canvas cover 30 is made to have similar diffusion resistance of grass from one meter;
2. the canvas cover 54 is calibrated against the leaf resistance of alfalfa from one meter;
3. the less dense (Gore-Tex) fabric was made to estimate crop water use at canopy height of tall crops (Altenhofen 1992) cited by Alam and Trooien (2001).

Modification in shape of evaporation surface and the addition of an electronic recording system improves the importance of the atmometer as a field tool. According to Gimabelluca *et al.* (1992), the inclusion of electronics with atmometers often improves resolution, accuracy, response time, short-interval measurement capability, unattended operation and portability. Parchomchuk *et al.* (2000) used the modified atmometer together with a data logger to automatically schedule irrigation. Alam and Trooien (2001) compared the evaporation of the flat and convex shaped evaporative surface of modified atmometer and reported better sensitivity of a convex shaped evaporating surface in comparison with the Penman-Monteith approach of estimating reference evaporation.

3.3 EVAPORATIVE SURFACE AND ATMOMETER TYPES

3.3.1 Introduction

There are numerous designs of atmometers (Fig. 3.2). Livingstone (1935) found that the evaporative surface is the main distinguishing feature among the different atmometer types. The evaporative surface used with most common atmometer types is porous porcelain with different shape and size, porous disc, carborundum, cloth, sponge and blotting paper. The colour of the evaporating surface is made in order to improve the sensitivity of atmometers. Black and white coloured atmometers are used as measures of solar irradiance as well as potential evaporation (Livingstone 1935; Wilcox 1963; Shannon 1966). The green canvas cover is made in order to simulate the reflection of solar irradiance from a plant surface (Altenhofen 1985; Broner and

Law 1991). Livingstone (1935) and Doorenbos (1976) gave a detailed description of the most common ones used.

3.3.2 Piche and Carborundum Atmometers

The Piche atmometer was first introduced in 1872 (Livingstone 1935; Thom *et al.* 1981; Brutsaert 1982) (see Fig. 3.2*a*). The assembly of the Piche atmometer consists of an inverted long graduated glass tube of 200 to 300 mm (Guyot 1997) and 10-mm inside diameter (Brutsaert 1982). The tube is closed at one end. In the original model the base (open flat end) of the glass tube is closed with a disc of blotting paper (Livingstone 1935). Circular filter paper, cloth, carborundum and porous disc (Carder 1960; Chang 1968; van Zyl *et al.* 1987) held in position with a small disc and metal clip are also used as an evaporating surface. Water soaks into the evaporating surface and then evaporates. The assembly is easy to prime compared to other types (Carder 1960). The original version of the instrument has a small hole in the middle of the paper for air, but for recent versions the hole is in the tube. It requires frequent changing of the evaporating surface.

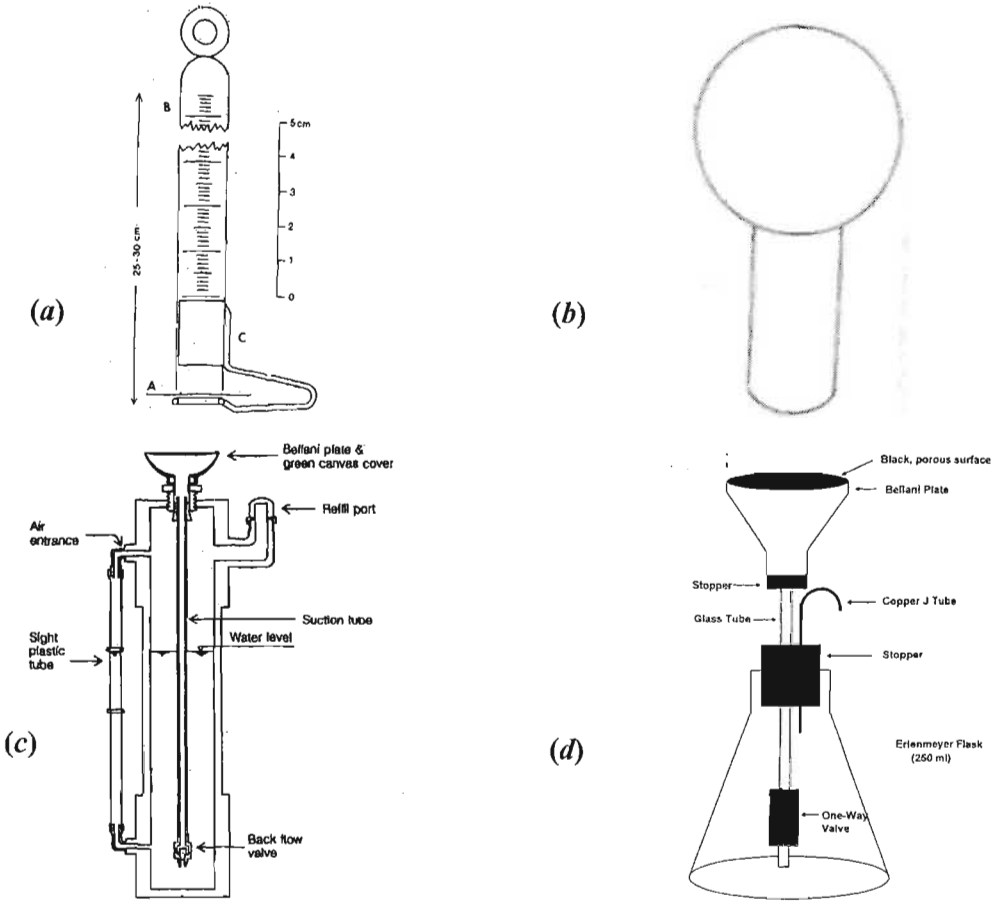

Fig. 3.2 Atmometer types: (*a*) Piche atmometer (Jacobs and Linclaen 1983) (*b*) Livingstone atmometer (Livingstone 1935) (*c*) modified Bellani plate by Law and Israel (1988) (cited by Broner and Law 1991) (*d*) black Bellani plate (Qian *et al.* 1996)

The difference in the readings at different times will give the volume rate of water evaporated. The atmometer is usually placed in a Stevenson screen (Stanhill 1962; Doorenbos 1976; Brutsaert 1982) or covered with a transparent shield (Carder 1960).

The evaporation rate measured using a Piche atmometer has been correlated with potential evaporation in various studies. However, the sensitivity of Piche or carborundum atmometer evaporation to wind and water vapour pressure deficit has been demonstrated in many studies (Mukammal 1961; Stanhill 1962; Fitzpatrick and Stern 1966; Thom *et al.* 1981; van Zyl *et al.* 1987; Papainnoun *et al.* 1996; Messing 1998). The evaporation rate of a Piche atmometer in a shelter not exposed to solar irradiance is very difficult to relate to actual evaporation (Brutsaert 1982). As a result, Piche atmometer evaporation rate is used for estimating the aerodynamic component of Penman and Penman-Monteith equations. Stanhill (1962) and then independently Bouchet (1963) as cited in Papaioannou *et al.* (1996) were the first to realize the sensitivity of the device to water vapour pressure deficit and wind speed and suggested a linear regression relationship for the second term of the Penman equation as:

$$\frac{\gamma}{\gamma + \Delta} E_a = aE_{pi} + b \qquad 3.3$$

where a and b are empirical constants, $E_a = f(u)(e_s - e_a)$ is in mm day^{-1} and E_{pi} is evaporation from the Piche atmometer (mm day^{-1}). Table 3.1 shows values for a and b derived by correlation from different studies. Recently, Papaioannou *et al.* (1996) reviewed and used monthly variable values of a and b and suggested a site calibration to obtain the necessary monthly relationship. Further to this, as Brutsaert (1982) cited, Brochet and Gerbier (1972) proposed an empirical formula as a substitute for the Penman equation as a function of Piche evaporation and solar irradiance measurements.

Table 3.1 The a and b linear regression coefficients derived from Piche atmometer evaporation and the aerodynamic term of the Penman and Penman-Monteith equation

Author	Value of coefficient		Type of evaporating surface
	a	b	
Stanhill (1962)	0.1469	0.118	Disc of blotting paper
Bouchet (1963)[1]	0.1469		Disc of blotting paper
Fitzpatrick and Stern (1966)	0.6210	0.172	Disc of blotting paper
Thom *et al.* (1982)	0.4000		Disc of blotting paper
van Zyl *et al.* (1987)[2]	0.0180	0.090	Disc of blotting paper
van Zyl *et al.* (1987)[2]	0.0080	0.060	Carborundum

[1]Reported in Brutsaert (1982), [2]expressed as mm hour^{-1}

3.3.3 Livingstone Atmometer

The Livingstone atmometer consists of a hollow porous porcelain of 50-mm diameter and 3-mm thick wall sphere evaporating surface (Fig. 3.2*b*). Based on the Livingstone (1935) description, the evaporating surface was made to be spherical in order to integrate the effect of wind, water vapour pressure deficit and solar irradiance uniformly from all directions except downward at the narrow cylindrical neck, which is glazed and connected to a supply tube. The evaporation surface of a Livingstone atmometer is attached to a glass or metal tube dipping into a reservoir. A check valve is used to control back flow of water during rain. The capillary rise within the pores maintains the supply of water to the surface. As various studies indicated, the surface is easily broken by frost.

The Livingstone atmometer evaporation relationship to potential evaporation and other microclimatic measures has been confirmed in many studies. Livingstone (1935) and Janes (1960), Shannon (1966) and Halkias *et al.* (1955) as cited by Dilley and Helmond (1973) found higher correlation between solar irradiance or net irradiance and different evaporation from black and white surface Livingstone atmometers.

3.3.4 Bellani Plate Atmometer

According to Doorenbos (1976) and Livingstone (1935), the evaporative surface of Bellani plate atmometers is a porous ceramic disc, with flat circular shape connected to the large end of a glazed ceramic funnel and proposed by Bellani (Fig. 3.2*d*). Most of the time, the reservoir of water is attached with a check valve using a supply tube to the evaporative surface. The evaporating surface is about 3-mm thick and has a high enough porosity to supply the maximum potential evaporation rate (Livingstone 1935). Carder (1960) mentioned that the need of a check valve is a disadvantage of the Bellani plate atmometer mounts.

The response of the Bellani plate surface to microclimate measures has been widely studied in comparison with other types (Livingstone 1935; Holmes and Robertson 1958; Carder 1960; Mukammal 1961; Wilcox 1963; Wilcox and Sly 1974; Feldhake and Boyer 1988, 1990; Qian *et al.* 1996; Jiang *et al.* 1998). The white and black evaporating surface has been used to estimate water potential, solar irradiance, net irradiance and crop water consumption. Some studies found the black Bellani plate to be more reliable and other studies less reliable for estimating potential evaporation in comparison to the other types of evaporimeters (Holmes and Robertson 1958; Mukammal 1961; Feldhake and Boyer 1988; Qian *et al.* 1996).

3.3.5 Modified Atmometer

The modified atmometer is a recent modification of a white Bellani plate evaporating surface with a fabric cover (Fig. 3.3a). The evaporation surface is made to have a 79-mm diameter similar to the cross sectional area of the reservoir and a sight glass is attached for visual reading. The proportionality of cross section area between Bellani plates and reservoirs allowed the decrease in depth of evaporation to be read on the graduated glass plastic tube mounted on the side of the reservoir. In the earlier models, a plastic check valve at the end supply tube and with present models Teflon and PTFE (poly-tetra-fluoro-ethylene) membranes at the top evaporation surface are used to prevent the entrance of precipitation to the reservoir. The atmometer is usually placed at a 1-m height in order to estimate reference evaporation from grass and alfalfa (Altenhofen 1985; Broner and Law 1991; Alam and Trooien 2001) and at a canopy height to estimate crop consumption (Altenhofen 1992) (cited by Alam and Trooien 2001).

The canvas cover used resulted in three different resistances to evaporation. According to Broner and Law (1991), the green canvas is 100 % acrylic and non-fading. The canvas model design 30 was made to have maximum resistance whereas Gore-Tex has the least resistance to evaporation. The resistance of canvas model 54 has been designed to be in-between the two models for the evaporation (Alam and Trooien 2001). The Gore-Tex cover was recommended to be adjusted with canopy height except at early stage of growth. Parchomchuk *et al.* (2000) used canvas cover 54 with a data logger for automatic irrigation scheduling. Canvas 30 and 54 are adjusted for one-meter height measurement.

The Bellani plate employed with the modified Altenhofen (1985) atmometer was flat. Alam and Trooien (2001) used a convex surface with a white PTFE (poly-tetra-fluoro-ethylene) membrane (top part of deposable wafer) in between the canvas cover and the evaporating surface. Alam and Trooien (2001) reported a higher degree of correlation between atmometer-measured evaporation using a flat-shaped Bellani plate covered with Gore-Tex cover and evaporation calculated using a modified alfalfa-based Penman approach. Alam and Trooien (2001) also reported similar results using a canvas 30 covering a convex plate and Penman-Monteith approach for a grass surface. According to Alam and Trooien (2001), the modification of the atmometer (ET-gage) to include a PTFE membrane and a convex shaped evaporating surface replaces the need for a check valve and improves the rainwater shading by reducing the evaporation measurement depression. In addition to this, the shape of surface helps in mounting and creating better contact of the canvas cover (fabric).

CHAPTER 4

ESTIMATION AND ASSUMPTION OF THE PENMAN-MONTEITH APPROACH

4.1 INTRODUCTION

The derivation of the Penman-Monteith approach (Eq. 2.12) includes the available energy term (I_{net} - G) and the biologically-based canopy and physically-based aerodynamic resistance term based on the implicit assumption of uniform surface and neutral atmospheric condition. It includes all the important parameters that govern the energy exchange and the corresponding latent heat flux density from a uniform surface of vegetation. The approximations applied and estimations of parameters limit its estimation accuracy of evaporation.

The application of the Penman-Monteith approach of estimating reference evaporation of a specific crop depends on the accuracy of quantifying the radiative term as well as the aerodynamic term (Allen *et al.* 1989, 1994*a*, 1994*b*). None of the parameters of the expression are directly measured at a weather station. In many practical applications I_{net}, G, r_c and r_a are estimated using a theoretical approach or an empirical correlation with commonly measured microclimatic measures (Allen *et al.* 1994*a*, 1994*b*; De Bruin and Stricker 2000; Ortega-Farias *et al.* 2000).

As shown by many studies, net irradiance is the dominant term in the expression (Eq. 2.12). Penman (1956) expressed the net irradiance as two to three times the value of the aerodynamic component of the Penman (1948) approach (Eq. 2.7). With the Penman and Penman-Monteith estimate of reference evaporation, the microclimatic measures solar irradiance, which is the most important component of the net irradiance estimation (Ross 1975; Nott and Savage 1985; De Bruin and Stricker 2000), air temperature and water vapour pressure are used. In some instances even the estimated solar irradiance is recommended in the absence of direct measurement (Doorenbos and Pruitt 1977; Allen *et al.* 1994*b*, 1998). The estimation approach followed with soil heat flux density is different. It is either ignored or estimated as a function of estimated net irradiance. As a result, the evaluation of the estimation technique used for soil heat flux density and its use with the Penman-Monteith and energy balance approaches for estimating reference evaporation needs attention.

The aerodynamic term of the Penman-Monteith equation includes the aerodynamic and canopy resistance terms. Unlike the energy terms measuring aerodynamic and canopy resistance on hourly and daily bases is impractical (Savage *et al.* 1997). Empirical assumptions and approximations are always used for the reference evaporation estimate.

The aim of this chapter is to review the assumptions as well as estimation methods and techniques of the radiative term (net irradiance and soil heat flux density) and the aerodynamic term (aerodynamic resistance and canopy resistance) of grass and alfalfa-based Penman-Monteith reference evaporation estimation approach.

4.2 AVAILABLE ENERGY TERM

4.2.1 Introduction

The available energy flux density (I_{net} - G) is the primary and a dominant climatic factor controlling evaporation under non-advective conditions when water is not limiting (Mukammal 1961; Linacre 1968; Jensen *et al.* 1990; Savage *et al.* 1997). The available energy flux density differs only in small amount from net irradiance (Savage *et al.* 1997) and it is the most important parameter affecting reference evaporation (Liasat and Snyder 1998). Soil heat flux density (G) is usually approximated as function of I_{net} (Allen *et al.* 1994*b*, Allen 1996, Allen *et al.* 1998).

4.2.2 Net Irradiance

Net irradiance is the net result of the surface radiation balance in solar irradiance domain (0.15 μm to 4 μm) and the long wave irradiance domain (3 μm to 100 μm) (Amarakoon and Chen 1999, Ortega-Faries *et al.* 2000). It is usually measured with a net radiometer. According to Savage *et al.* (1997), a net radiometer requires regular, weekly, checks for dirt and punctures as well as "milky appearance" on the dome and replacement or calibration under similar conditions. Also for use in reference evaporation equations, the net radiometer must be measured over irrigated grass. It is an expensive measurement and the sensor voltage to net irradiance sensitivity changes rapidly in comparison with other sensors (Liasat and Snyder 1998).

In the absence of direct measurement, I_{net} can be computed from the measurement of its components as:

$$I_{net} = I_s - rI_s + L_d - L_u \qquad 4.1$$

where I_s is the incoming solar irradiance (W m^{-2}), rI_s is the reflected solar irradiance (W m^{-2}), L_d is the incoming long wave irradiance (W m^{-2}) and L_u is upward long wave irradiance (W m^{-2}).

Most of the components of Eq. 4.1 are not measured directly at a weather station. Especially, direct measurement of reflected solar irradiance, long wave irradiance between the atmosphere and surface are seldom available. Therefore L_d - L_u is generally estimated using a theoretical or empirical approach from the regularly measured meteorological data. Penman (1948) estimated L_d - L_u from a single equation incorporating the Stefan-Boltzmann law of radiation based on the empirical expression due to Brunt (1932) and Angstrom (1924), which relates the net long wave irradiance L_d - L_u from the atmosphere to water vapour pressure and cloudiness:

$$L_u - L_u = (c + d\sqrt{e}\,)\sigma T^4 (a + b\frac{n}{N}) \qquad 4.2$$

where e is actual water vapour pressure (mb), T the air temperature (K) and σ the Stefan-Boltzmann constant (= 5.673×10^{-8} W m^{-2} K^{-4}), n the sunshine duration (h) and N the potential sunshine duration of the day (h) (Penman 1956). The values of *a, b, c* and *d* varies from place to place. The equation was recommended by Doorenbos and Pruitt (1977) for use with the modified FAO Penman equation. In a similar manner, Wright (1982) gave estimates of net long wave irradiance L_d - L_u computed as a function of minimum and maximum air temperature and solar irradiance:

$$L_u - L_d = \sigma \frac{\left(T_{\max}^4 + T_{\min}^4\right)}{2}(c + d\sqrt{e}\,)\,(b\frac{I_s}{I_a} + a) \qquad 4.3$$

where T_{max} and T_{min} are absolute maximum and minimum air temperatures (K), I_a is clear sky irradiance (W m^{-2}) and a and b are constants. Allen *et al.* (1994*b*, 1998) also recommended the formulation for daily net irradiance computation with Penman-Monteith approach.

Dong *et al.* (1992) estimated net irradiance for the daytime where net long wave irradiance is estimated as:

$$L_d - L_u = 0.89\varepsilon_s[\varepsilon_a(1-c)\sigma T^4 + cT^4 - \sigma T_s^4] \qquad 4.4$$

where T_s is the surface temperature (K), c an empirically-evaluated cloudiness factor, ε_a the clear sky emissivity using the Satterlund (1979) formulation and ε_s the emissivity of the surface. Dong *et al.* (1992) also used the same factor 0.89 for the net short wave irradiance ((1 - r) I_s). Liasat and Snyder (1998) evaluated the error of estimation on the reference evaporation with the use of Eq. 4.4 and Venture *et al.* (1999) used Eq. 4.4 to estimate net irradiance with the Penman-Monteith approach.

As an alternative to the theoretical approach, Monteith and Unsworth (1990), gave a formulation for I_{net} with L_d - L_u empirically evaluated as a function of air temperature T_a in °C:

$$L_d - L_u = (a + bT_a) f(I_s / I_o). \quad 4.5$$

The unpublished and undated Campbell Scientific Inc. application notes recommended its use with Penman-Monteith approach for estimating hourly reference evaporation.

Different from the radiation balance approach, net irradiance is often empirically estimated using the equation developed through correlation with common weather data from a weather station. The most common regression is with solar irradiance:

$$I_{net} = aI_s - b \quad 4.6$$

where a and b are constants that vary with location, crop, season, time of year and sky condition (Linacre 1968; Jensen 1974; Denmead 1976; Hatfield and Fuchs 1990; Jensen *et al.* 1990). Rosenberg *et al.* (1983) and Jensen *et al.* (1990) gave a summary of these equations.

4.2.2.1 Solar irradiance

The incoming short wave solar irradiance has most of its energy contained in the wavelength range from 0.1 to 4 μm (Brutsaert 1982). Solar irradiance is measured using a radiometer. The number of meteorological stations measuring solar irradiance are however limited. According to Thornton and Running (1999) global evaluation of weather stations with solar irradiance to air temperature recording is 1:500. In most places the solar irradiance is estimated from theoretical models or simpler empirical formulae.

As numerous studies indicated, Angstrom (1924) was the first to suggest a linear relationship between solar irradiance and sunshine duration:

$$I_s = I_a \left(a + (1 - a) \frac{n}{N} \right) \quad 4.7$$

where I_a is solar irradiance arriving at a horizontal surface if clear perfect cloudless days were present (W m^{-2}) and a is a constant. As Brutsaert (1982) indicated the total cloudless days are scarce and calibration of Eq. 4.7 may be impossible. As a result, they proposed the use of the Prescott (1940) formulation in terms of extraterrestrial irradiance (I_o) that is calculated from position of a place, solar constant, position of sun and time of year is mentioned as a useful tool for weekly and monthly average estimation of solar irradiance (cited from Brutsaert 1982):

$$I_s = I_o\left(a + b\frac{n}{N}\right) \qquad 4.8$$

where a and b are constants, which are related to location, season and state of atmosphere in many studies (Glover and McCulloch 1958; Reid 1985; Revfeim 1997). Tanner and Pelton (1960) and Brutsaert (1982) also indicated the use of mean fractional cloud cover (c) in the absence of sunshine duration as $n/N = 1 - c$. Various similar relationships are also presented in Chang (1968), Rosenberg *et al.* (1983) and Jensen *et al.* (1990) reports. Doorenbos and Pruitt (1977) and Allen *et al.* (1994*b*, 1998) recommended the use of Eq. 4.8 in the absence of solar irradiance data for reference evaporation estimation with Penman and Penman-Monteith approach.

Other empirical methods of estimating solar irradiance (like Bristow and Campbell 1984; Hunt *et al.* 1998; Goodin *et al.* 1999; Thornton and Running 1999; Mahmood and Hubbard 2002) are also developed from air temperature, rainfall, relative humidity and other geographical information for crop modelling and other purposes.

4.2.2.2 Reflected solar irradiance

Reflected solar irradiance is part of incoming solar irradiance reflected by the surface encountered. The nature of the surface determines the reflection of solar irradiance. The ratio of reflected short wave solar irradiance to the incident solar irradiance for solar wave band is referred as the reflection coefficient (r):

$$r = \frac{rI_s}{I_s} \times 100. \qquad 4.9$$

As in various studies indicated, the reflection coefficient of most natural surfaces also depends on the direction of incoming solar irradiance. In the literature the term albedo is used extensively for the reflection coefficient. Monteith (1973) suggests that albedo be used exclusively of the visible light energy and the term reflection coefficient be used for the total short wave solar irradiance.

The incident and reflected component of solar irradiance can be measured at the same time using a sensor called an albedometer and then reflection coefficient is calculated (Amarakoon and Chen 1999: Savage 2001*a*). However most often the reflection coefficient (r) is assumed constant for a crop or estimated as a function of altitude of sun or day of the year. Wright (1982) estimated the variable coefficient as a function of the day of year for an alfalfa

reference crop. Dong *et al.* (1992) gave empirical formulations of variable reflection coefficient as a function of solar altitude. Table 4.1 shows some of the assumed reflection coefficient values reported for some crops.

4.2.3 Net Long Wave Irradiance

Net long wave irradiance is also called effective outgoing irradiance or effective terrestrial irradiance. It is described as the algebraic sum of the upward and the downward long wave irradiance:

$$L_{net} = L_d - L_u \tag{4.10}$$

where L_{net} is net long wave irradiance (W m^{-2}). Long wave irradiance can be measured directly or indirectly using pyrgeometers or pyranometers (Guyot 1997), but these instruments are expensive and too delicate for routine weather measurement (Aubinet 1994).

4.2.3.1 Upward long wave irradiance

Most natural surfaces can be treated as a "full radiator" which emits "terrestrial" or long wave irradiance (Monteith 1973). The intensity of any surface for long wave irradiance is based on the Stefan-Boltzmann law of radiation:

$$L = \varepsilon_s \sigma T_s^4 \tag{4.11}$$

where L the long wave irradiance from the surface (W m^{-2}), ε_s the surface emissivity (unit less). and T_s is the surface temperature (K). However, the widely measured air temperature is used in estimating crop surface emittance instead of surface temperature using Eq. 4.11 (Brutsaert 1982). Jensen and Aslyng (1967) gave a formulation, which relates the outgoing long wave irradiance as a function of air temperature at screen height and surface temperature:

$$L_u = \sigma T^4 + \sigma\left(T_s^4 - T^4\right). \tag{4.12}$$

Table 4.1 Assumed reflection coefficient (r) and reference crop

Author	Crop	Coefficient (r)	Combination method
Fitzpatrick and Stern (1965)	Cotton and grass	0.18	Penman 1948
Doorenbos and Pruitt (1977)	Grass	0.25	FAO Modified Penman
Weiss (1982*b*)	Alfalfa	0.24	FAO Modified Penman
Allen *et al.* (1994*b*, 1998)	Grass	0.23	Penman-Monteith
De Bruin and Stricker (2000)	Grass	0.23	Penman-Monteith

Similarly as Amarakoon and Chen (1999) cited, Holtslag and Van Ulden (1983) measured the surface temperature with an infrared thermometer and used the measurement to parameterize the outgoing long wave irradiance. The emissivity of natural surface on earth surface varies and in many practical applications it is simply assumed as one (Brutsaert 1982).

Dong *et al.* (1992) proposed the estimation of upward long wave irradiance in terms of clear sky emissivity, surface emissivity, air and surface temperature as:

$$L_u = (1-\varepsilon_s)[\varepsilon_a(1-c)\,\sigma T^4 + c\sigma T^4 + ck] + \varepsilon_s \sigma T_s^4 . \qquad 4.13$$

Monteith (1973) and Monteith and Unsworth (1990) also gave a linear approximation to Eq. 4.11 for a defined air temperature range as:

$$L_u = a + bT \qquad 4.14$$

where a and b are constants. Monteith and Unsworth (1990) gave a value of 320 for a and 5.2 for b for air temperature T in °C.

4.2.4 Downward Long Wave Irradiance

The atmosphere of the earth emits long wave irradiance. However according to Prata (1996), there are few direct measurements of this quantity. An alternative technique of measuring incoming long wave irradiance is from Eq. 4.1 as a residual. Weiss (1982*a*) found that the residual method works well during daytime and under clear sky conditions.

Because of the dynamic nature of atmosphere, the best estimation of incoming long wave irradiance is more difficult to obtain since it must be an integrated value variation in water vapour pressure and temperature of the cloud. In the majority of practical applications incoming long wave irradiance is estimated indirectly, using an empirical equation computed from the equations that describes emissivity of clear sky and cloudiness together with Eq. 4.11 from routinely collected microclimatic measures.

4.2.4.1 Clear sky emissivity

Under clear skies, the long wave irradiance of the earth's atmosphere originates mainly from three major components of atmosphere: water vapour, carbon dioxide and ozone (Idso and Jackson 1969). Therefore more accurate methods of calculating the atmospheric irradiance under clear skies require vertical profile data of humidity and air temperature (Brutsaert 1982).

The long wave irradiance from the sky may be described in terms of an emissivity as:

$$\varepsilon_a = \frac{L_d}{\sigma T_s^4} \qquad 4.15$$

where ε_a is apparent emissivity of clear sky (Unsworth and Monteith 1975; Prata 1996). As cited in most literature, Angstrom (1924) and Brunt (1932) derived two of the earliest and most widely used estimates of clear sky atmosphere emittance, from screen height water vapour pressure (e). The Angstrom and Brunt equations took the form:

$$\varepsilon_a = a + b10^{ce} \qquad 4.16$$

and

$$\varepsilon_a = \alpha + \beta\sqrt{e} \qquad 4.17$$

respectively, where a, b, α, β and c are empirical coefficients. Brunt (1932), as cited by Jensen *et al.* (1990), also used the same form of expression for net emissivity later used by Penman (1948), Doorenbos and Pruitt (1977) and Allen *et al.* (1998) for the computation of reference evaporation.

Swinbank (1963) and Idso and Jackson (1969) developed an empirical equation for clear sky emissivity and net emissivity using air temperature (T) at screen height:

$$\varepsilon_a = [f(T)]^a . \qquad 4.18$$

Unsworth and Monteith (1975) and Monteith and Unsworth (1990) gave linear approximations of Eq. 4.18 for a defined air temperature range:

$$L_d = a + bT \qquad 4.19$$

where a is 213 and b is 5.5 for air temperature in °C. The mathematical combination of Eqs 4.14 and 4.19 result in an expression for the net long wave irradiance of clear sky (Monteith and Unsworth 1990):

$$L_{net} = 0.003T_a - 0.107 \qquad 4.20$$

where T_a is the air temperature (°C). In the unpublished and undated Campbell Scientific Inc. notes, Eq. 4.20 is described as atmospheric emittance minus crop emittance under clear sky irradiance (Appendix 2.1) and its use recommended for estimating hourly net irradiance with Penman-Monteith approach.

Referring to an earlier idea of Angstrom (1924) and Brunt (1932), Brutsaert (1975) developed an equation for estimating clear sky emittance that depends only on water vapour pressure (e) at screen height based on the radiative transfer theory and some approximation:

$$\varepsilon_a = c\, e^{1/7}. \qquad 4.21$$

After detailed revision of Eq. 4.18 and 4.21, Satterlund (1979) and Idso (1981) recommended an equation that involved both water vapour pressure (e) and air temperature (T):

$$\varepsilon_a = a\,(1 - \exp\,(-e^{(T/b)})) \qquad 4.22a$$

and

$$\varepsilon_a = a + b\, e \exp\,(c/T) \qquad 4.22b$$

respectively. Other similar empirical expressions for clear sky emittance are also given from dew point temperature (Berdahl and Fromberg 1982, Berdahl and Martin 1984) and from air temperature (Prata 1996). Aase and Idso (1978) compared the equation of Idso and Jackson (1969) and Brutsaert (1975) and found comparable results for air temperature above 0 °C. Dong *et al.* (1992) evaluated Eqs 4.21, 4.22*a* and 4.22*b* and found that the Eq. 4.22*a* formulation had better estimation accuracy for clear sky conditions. Hatfield *et al.* (1983*b*) also compared Eqs 4.18, 4.21, 4.22*a* and 4.22*b* and found that Eq. 4.22*b* had a higher correlation coefficient than the others. So it is clear that most of the equations are limited in accuracy for global use due to their empirical nature of formulation. However, the Brutsaert (1975) formulation and its modification are used in various places and seems to give reasonable estimate because of its theoretical bases of derivation. Amarakoon and Chen (1999) and Ortega-Farias *et al.* (2000) used Eq. 4.21 and its modification in the estimation of net irradiance in different places and similarly Weiss (1982*b*) used the estimation with Modified FAO Penman approach of estimating reference evaporation.

4.2.4.2 Cloudiness

Beneath a cloudy sky, the flux density of long wave irradiance received at the ground has two components: radiation emitted by water vapour and carbon dioxide below the cloud base; and radiation emitted by water droplets forming the base (Unsworth and Monteith 1975).

Clouds have a strong influence on the long wave irradiance exchange. On cloudy nights the sky irradiance is almost as large as terrestrial irradiance in the radiation balance (Nott and Savage 1985). In meteorological stations cloudiness is measured visually in eighths (oktas) and tenths. However a non-linear approximation of cloudiness is usually derived to evaluate the

cloud cover of atmosphere for downward long wave irradiance as:

$$f = 1 + a\,c^m \qquad 4.23a$$

and net long wave irradiance:

$$f = 1 - b\,c^m \qquad 4.23b$$

where a, m (= 2) and b are constants and c is fractional cloud cover in tenths (Oke 1978; Brutsaert 1982). As an alternative to cloud cover, a percentage of sunshine hours (n/N) or fractional solar irradiance related to clear sky solar irradiance (I_s/I_a) or extraterrestrial irradiance (I_s/I_o) is used to calibrate either clear sky net long wave irradiance or downward long wave irradiance. Penman (1948) estimated the net long wave irradiance for clear sky and evaluated cloudiness as:

$$f = a + b\frac{n}{N}. \qquad 4.24$$

Doorenbos and Pruitt (1977) presented a table to convert cloudiness expressed in eighths (oktas) or tenths to n/N and vice versa and used the equation to evaluate cloudiness. Jensen *et al.* (1990), Dong *et al.* (1992), Allen *et al.* (1994*b*, 1998) and Liasat and Snyder (1998) also recommended Eq. 4.24 to adjust the cloud cover either with n/N or I_s/I_a ratio in estimating I_{net}. Similarly the unpublished Campbell (undated) notes used a non-linear equation based on I_s/I_o ratio and some constants (a = 7.9 and b = 0.034) for estimating cloudiness with Eq. 4.20:

$$f = b\exp(aI_s / I_o)/[1 + b\exp(aI_s / I_o)]. \qquad 4.25$$

Dong *et al.* (1992) gave a formulation for the incoming long wave irradiance of cloudy sky from air temperature, clear sky emisivity and additional coefficients:

$$L_d = \varepsilon_a (1 - c)\sigma T_a^4 + c\sigma T_a^4 + ck \qquad 4.26$$

where c is fractional cloud cover evaluated empirically from clear sky irradiance and solar irradiances (Eq. 4.24), ε_a is clear sky emissivity estimated using Eq. 4.22*b* and k is correction factor for the difference between air temperature cloud base temperature.

The other difficulty of adjusting the cloudiness effect on estimating net long wave irradiance lies in distinguishing between clear and cloudy condition of atmosphere. An arbitrarily defined value of fraction of sunshine (n/N) or irradiance (I_s/I_a *or* I_s/I_o) or cloudiness (c) is used in several studies. Dong *et al.* (1992) and Allen *et al.* (1998) used values of 0.7 and Weiss (1982*a*) a value 0.85 and above as clear sky condition.

4.2.5 Soil Heat Flux Density

Soil heat flux density is defined as the amount of energy flux density entering or leaving a layer of soil at a given time with units of J m^{-2} s^{-1} or W m^{-2} (Nott and Savage 1985). Over a land cover with vegetation, the daily mean value of soil heat flux density is often one or more orders of magnitude smaller than the major term in the energy balance (Brutsaert 1982). As Hatfield and Fuchs (1990) indicated the amount of net irradiance partitioned into soil heat flux density is a function of soil water content and ground cover. In the study of Berkowicz and Prahm (1982) and Clothier *et al.* (1986), it is evaluated as 10 to 30 % of net irradiance. It is usually ignored for a daily time step since the daytime value tended to be canceled by nighttime values. However it is an important component of the energy balance in the evaluation of hourly or shorter time periods (Savage 2002*b*). Hatfield and Allen (1996) indicated the probable existence of bias with the approach followed in the estimation of reference evaporation when soil heat flux density is ignored.

Soil heat flux density is directly measured using a device called soil heat flux plates normally placed perpendicular to the direction of heat flow and correcting the measured flux for the heat storage between the flux plates and the soil surface (Choundry *et al.* 1987; Savage *et al.* 1997). As Brutsaert (1982) reviewed, although soil heat flux plates are simple to use, their construction, calibration and installation requires great care. An alternative to the direct measurement of soil heat flux density estimation is either to calculate from soil temperature gradient and water content measurement or from the use of theoretical or empirical equations. Provided that the thermal conductivity (K_T) of soil is known and soil temperature gradient ($\delta T/\delta Z$) is measured, soil heat flux density may be computed as:

$$G = -K_T \frac{\delta T}{\delta Z} \qquad 4.27$$

(Brutsaert 1982; Rosenberg *et al.* 1983; Jensen *et al.* 1990). But according to Brutsaert (1982), since K_T depends on soil water content and temperature gradient, the method is suitable only at larger depths.

The empirical method of estimating soil heat flux density involves relating soil heat flux density with other major components of the energy balance. Based on the assumption of proportionality, sensible heat flux is taken as obvious choice by Brutsaert (1982) and Berkowicz and Parham (1982):

$$G = C_h F_h \qquad 4.28$$

where C_h is the proportionality parameter. In the computation of evaporation using the Penman and Penman-Monteith approach, the soil heat flux density is commonly related in a similar manner to the net irradiance or neglected. Allen *et al.* (1994*a*) reported soil heat flux density

varying between 0.4 to 0.5 I_{net} under forage grass during nighttime hours. Choudhury *et al.* (1987) included the leaf area index (*LAI*) for the prediction of soil heat flux density in addition to net irradiance under day light condition as:

$$G = 0.4e^{-0.5LAI} I_{net} \qquad 4.29$$

where e is natural number. Allen *et al.* (1998) and Jensen *et al.* (1990) gave a relation between soil heat flux density and air temperature for periods longer than a day, assuming soil temperature follows the change with air temperature:

$$G = C_v \frac{T_i - T_{i+1}}{\Delta t} \Delta z \qquad 4.30$$

where C_v is volumetric soil heat capacity (J m^{-3} $°C^{-1}$), T_i is the air temperature at time i (°C), T_{i+1} is air temperature at time i+1 (°C), Δz is depth of measurement (m) and Δt is time interval in days.

4.3 RESISTANCE TERM

4.3.1 Introduction

Measurement of latent heat flux density from vegetation surface using the Penman-Monteith approach (Eq. 2.12) needs consideration of the physiological and aerodynamic resistance to the process. According to Savage *et al.* (1997) continuous or daily measurement of aerodynamic and canopy resistance is not practical. Often these resistances are derived from extrapolation of the wind, air temperature and water vapour pressure profile down to the canopy surface when they linked in series with stomatal resistance.

4.3.2 Aerodynamic Resistance

The aerodynamic resistance (r_a) is governed by atmospheric turbulence. It may be evaluated using the momentum theory as:

$$r_a = \frac{\left[\ln\left(\frac{Z_m - d + Z_M}{Z_M}\right) + \psi_M\right]\left[\ln\left(\frac{Z_h - d + Z_H}{Z_H}\right) + \psi_H\right]}{k^2 u} \qquad 4.31$$

where Z_m is the height of wind speed measurement (m), d is zero plane displacement height (m), Z_h is the height of measurement air temperature and water vapour pressure (m), Z_M and Z_H are roughness parameters for momentum and sensible and latent heat respectively (m), Ψ_H and Ψ_M are the stability factors for sensible and latent heat and momentum respectively and k is von Karman's constant (= 0.41) (Campbell and Norman 1998). Under neutral atmospheric condition, with the assumption of source and sink of momentum, sensible and latent heat similarity, the stability factor can be assumed zero ($\Psi_M = \Psi_H = 0$) for more practical use. Furthermore the aerodynamic resistance can be dependent on the accuracy of estimating the

value of roughness length (Z_M and Z_H) and Zero plane displacement height (d) that depends mainly on the soil cover, leaf area and structure of canopy (Shaw and Perior 1982; Hatfield and Fuchs 1990). The estimation of the roughness parameter and zero plane displacement may be evaluated as a function of crop height given in Thom (1975), Brutsaert (1982), Allen *et al.* (1989) and Campbell and Norman (1998). Thom and Oliver (1977) gave a further simplified empirical expression of Eq. 4.31 as:

$$r_a = 4.72[\ln(2/Z_H)/(1+0.54u_2). \qquad 4.32$$

De Bruin and Stricker (2000) used Eq. 4.32 for the estimation of r_a in the grass Penman-Monteith approach.

4.3.3 Physiological Canopy Resistance

For a vegetation surface, the physiological canopy resistance depends on both physiological property of the vegetation and water content of soil in addition to the microclimate. The stomatal resistance of leaf for water vapour diffusion can be calculated from the dimension and populations of stomata (Milthorpe and Penman 1967 cited by Berkowicz and Prahm 1982) or measured by diffusion porometers (Sharma 1985). However it is very difficult for practical use. For the purpose of estimating fluxes of momentum, latent and sensible heat from routine meteorological data, simple relations are developed for practical use. Allen *et al.* (1989) estimated canopy resistance of grass and alfalfa reference crop as function of effective *LAI*:

$$r_c = r_i / 0.5LAI \qquad 4.33$$

where r_i is an average minimum day value stomatal resistance of a single leaf. For a height of grass less than 0.15 m, the *LAI* is estimated as:

$$LAI = 0.24h_c \qquad 4.34a$$

and 0.5 m height of alfalfa and tall grass:

$$LAI = 5.5 + 1.5\ln h_c \qquad 4.34b$$

where h_c is crop height in meter. Based on these relationships and Jensen *et al.* (1990) evaluation, an average value of 70 s m^{-1} is recommended for average daily value in Allen *et al.* (1998). Allen *et al.* (1989) gave a value of r_i =100 s m^{-1} for grass and alfalfa reference crop. Based on this result, the unpublished Campbell (undated), Jensen *et al.* (1990) and Allen *et al.* (1994*b*, 1998) recommended the approximation of canopy resistance of between 70 and 700 s m^{-1} with the Penman-Monteith approach for grass reference crops. However recently Venture *et al.* (1999) also reported an improvement in estimation accuracy of the method with use of canopy resistance value less than 70 s m^{-1}.

4.4 ROADMAP RESTATED

Measured data are used to test the assumptions of the Penman-Monteith approach (Chapter 6) and the performance of ET-gage evaporimeter and the micrometeorological techniques for measuring evaporation is investigated in Chapter 7. The cost and accuracy consideration of the various methods for estimating evaporation are dealt within Chapter 8.

CHAPTER 5

GENERAL MATERIALS AND METHODS

5.1 SITE DESCRIPTION

A turf grass grown in the Agrometeorology site of the Faculty of Science and Agriculture, University of Natal, in KwaZulu-Natal, in South Africa was used as the main study area. The site is located at latitude ≈ 29.97 ^{0}S, longitude ≈ 30.95 ^{0}E and altitude ≈ 620 m. Data from the site were collected from December 27, 2001 to July 12, 2002 and from November 1, 2002 to December 29, 2002. During the experiment, the turf grass was maintained at an average height of 0.12 m and frequently watered in addition to rain.

5.2 INSTRUMENTATION OVERVIEW

Two independent weather station systems and one evaporimeter were used to estimate reference evaporation from the short turf grass. The basic difference between the two weather station systems lies in the data logging system used. The first system employed more advanced and sophisticated multi-channel measurement and control data loggers (CR7X, 21X, Campbell Scientific Inc., Logan, Utah, USA)[1]. The second system consisted of one single channel Hobo Event logger (H07-002-04; http://www.onsetcomp.com/product/3648_event.html) [1] and one Hobo H8 relative humidity, air temperature and two external channel logger (H08-007-02, Hobo H8, http://www.onsetcomp.com/product/3653_rh.html). The Hobo loggers have no control capability. An ET-gage atmometer (Model E, A, ET-gage^R, ET-gage Company, Loveland, USA)[1] was directly connected to a data logging system (Hobo Event logger or a pulse port of a CR7X and 21X data logger), which was also used to measure the reference evaporation. In addition to this, net radiometer, soil heat flux plates, infrared thermometer (IRT) and thermocouples connected to one of the Campbell data loggers were used for additional measurements of the radiation balance and energy balance components.

Sensible heat flux density, soil heat flux density, net irradiance and radiation balance components from the short grass were calculated and measured using the STEB technique, soil heat flux plates and net radiometers respectively.

[1] Mention of a commercial company in this thesis does not imply an endorsement

The atmometers (ET-gage), reduced set Penman-Monteith approach and STEB estimate of reference evaporation were compared with the grass and alfalfa based Penman-Monteith approach. The Penman-Monteith approach of estimating reference evaporation using microclimatic measures from the Hobo H8 weather station system was compared with reference evaporation calculated using AWS measurement.

Air temperature and relative humidity were measured from naturally ventilated Stevenson screen and radiation shields. The performance of the home-made seven-plate plastic radiation shield was compared with the standard six- and twelve-plate Gill radiation shields (Models 413011, 41002, R M Young, Traverse city, Michigan, USA) [1]. The variability of naturally ventilated radiation shield was evaluated using air temperature and relative humidity measurement comparison. The variability between different air temperature and relative humidity sensors was also compared.

The soil water content, soil temperature and surface temperature were measured using a ThetaProbe (ML2X-UM-1.21 56/012, Delta-T Devices, Cambridge, UK) [1], soil thermocouple and infrared thermometer (ftp://ftp.campbellsci.com/pub/outgoing/lit/b_irts-p.pdf).

5.3 AUTOMATIC WEATHER STATION

5.3.1 Solar Irradiance

The pyranometers used for the measurement of solar irradiance were two types. Three CM3 pyranometers (serial numbers 025870, 993283, 993297), Kipp and Zonen[1], Delft, Holland were used with CR7X and 21X data loggers. The sensor consists of a thermopile sensor, a housing, glass dome and a cable with nominal resistance of 125 Ω, which generates a microvolt signal proportional to solar irradiance. The sensor spectral response lies between 0.3 to 3 μm. Its angle field of view (FOV) is 180^0 and it is designed for continuous outdoor use.

The second type of pyranometer used is an Apogee silicon pyranometer sensor (serial number 1228), model PYR from Apogee Instrument Inc., Logan, Utah, USA[1]. The sensor is a highly stable silicon photovoltaic detector (blue enhanced) mounted in a cosine-corrected head. This sensor was connected to a Hobo H8 logger. The Apogee pyranometer sensor is flush mounted

[1] Mention of a commercial company in this thesis does not imply an endorsement

in a PVC gray body that blocks the solar radiation at very low angles. The sensor spectral response is between 0.3 to 1.1 μm. It generates a millivolt signal proportional to solar irradiance. The sensor has a much larger voltage output per unit of irradiance than the Kipp and Zonen CM3 and LI-200SZ LI-COR pyranometers. This large voltage output allowed the Apogee PYR sensor to be used with either Hobo H08-007-02 or the Campbell data loggers.

A differential output voltage instruction P2 (Appendix 5) was used for the CR7X data logger and single-ended output voltage P1 for the 21X data logger. The Hobo H8 was used to measure the voltage from the Apogee pyranometers. To convert the thermopile output voltage to solar irradiance (W m^{-2}) an appropriate multiplier (W m^{-2} mV^{-1}) was used for each solar irradiance sensor.

5.3.2 Rain Gauge

Three small rectangular shaped electronic Rain-O-Matic rain gauges (Rain-O-Matic, http://www.pronamic.com3_in_1_dansk.htm) were used to measure rainfall. The sensor consists of a box, a self-emptying spoon, magnet and the electrical board with flat base. The self-emptying spoon below the rain collector was set to a 1 mm resolution with the magnet kept in position to maintain the spoon by an anchor. An Event Hobo logger was used to record rainfall at every one second. The pulse ports of CR7X and 21X were also used to record the number of pulses of recorded rainfall every 10 or 30 second intervals.

5.3.3 Relative Humidity and Air Temperature

Air temperature and relative humidity measurements were accomplished using two models of air temperature and humidity probes. The Campbell Scientific Inc. model CS500 (serial numbers CR0710077, S5030025, R2020010, S4650042) temperature and relative humidity probe (Vaisala CS500, Campbell Scientific Inc., Logan, Utah, USA) sensors have a platinum resistance temperature detector (1000 Ω PRT) and a Vaisala intercap capacity relative humidity sensor. Each probe was measured using two single-ended analog input channels: one for temperature and the other for relative humidity. One Campbell Scientific Inc. model HMP35C temperature and humidity probe (HMP35C, Campbell Scientific Inc.) that uses a 100-kΩ thermistor and Vaisala capacity polymer H chip was also used for measuring air temperature and relative humidity. The program instruction P11 provided a DC excitation voltage that switched and digitally controlled the analog output channel for the air temperature and relative humidity measurements using two single ended analog input channels of the CR7X data logger.

The Hobo H8 logger (H08-007-02) contains an internal temperature and humidity sensor. A thermistor temperature and user replaceable humidity sensor were used to measure temperature and relative humidity of the air. To avoid condensation, the loggers were placed within the radiation shields and Stevenson screens.

5.3.4 Wind Speed and Direction

Two three-cup wind speed and direction (Model 03001, R M Young, Traverse city, Michigan, USA) sensors were used to measure wind speed and direction at one and two meters height. The cup wheel rotation produces an AC sine wave voltage signal with frequency proportional to the wind speed. The turning factor of the anemometer is 0.75 m with a distance constant 2.3 m (63 % recovery). The wind vain position is sensed with a 10-kΩ potentiometer and an output signal is developed that is proportional to the mechanical azimuth angle range of 360^0 and electrical of 352^0. An additional ceramic heated needle anemometer, which consists of a ceramic needle (platinum resistance thermometer), was used to measure wind speed at one meter.

Wind speed was measured using pulse instruction P3 of the CR7X and 21X data loggers (Appendix 5). Instruction P4 and P11 were used to measure temperature of heated and unheated platinum ceramic needle anemometer using the 21X data loggers. A full bridge resistance measurement was used to measure the electronic resistance corresponding to the heated and unheated states ceramic needle anemometer. From the measurement of temperature difference, the logger calculated the wind speed from the polynomial given by the supplier. Wind direction was measured using a single-ended analog input channel and measured as degrees from magnetic north in a clockwise direction. Instruction P4 with excitation voltage was used to measure the wind direction. The wind vane was positioned north-south with respect to the wind speed sensor pointing north and regularly cleaned with distilled water and tissue paper. Similarly the cups of wind speed sensors were cleaned with distilled water and tissue paper and a regular check done to the flexibility of the wheels.

5.4 ADDITIONAL INSTRUMENTS AND SOIL ANALYSIS

5.4.1 Net Radiometer

Two types of net radiometers were used. The first model, the CNR1 (Kipp and Zonen, Delft, Holland, Fig. 5.1) component net radiometer (serial number 990192), has two CM3 pyranometers (Section 5.3.1) and two CG3 pyrgeometers to measure the four components of the radiation balance separately and net radiation as a whole.

Fig. 5.1 Component net radiometer CNR1 for measuring the incident, reflected solar irradiance and incoming and outgoing long wave irradiance above a short grass surface (photograph, Savage 2001). The upper and lower CM3's are shown on the right

The total spectral response of the sensors is between 0.3 to 50 μm with a time response of 18 s. This spectral range covers both short wave irradiance (0.3 to 3 μm) and long wave irradiance (5 to 50 μm). The CG3 pyrgeometers consist of thermopile sensors, a housing and a silicon window with a nominal resistance of 150 Ω. The silicon window serves both as an environmental protection and a wave band filter. The pyrgeometers are flat with field of view of 150^0. The black paint of the sensor absorbs the irradiance and converts it into heat. The component net radiometer also has a built-in level, a thermistor temperature sensor (YSI 44032) and a heater.

The sensor was mounted horizontally using a spirit level with one pyranometer and one pyrgeometer facing down and the other pair facing up (Fig. 5.1). The sky long wave and solar irradiance were measured using the upper sensors. Grass surface long wave and reflected solar irradiance were measured using the lower sensors. The pyrgeometer windows were cleaned every week using alcohol and camera lens tissue paper. Distilled water and similar tissue paper were used

to clean the domes of pyranometers in addition to soft facial tissue and camel hair used for the body.

The long wave emittance of grass and sky was calculated as the sum of measured pyrgeometers ($CG3_{up}$ and $CG3_{down}$) and the sensor emittance calculated from the Stefan-Boltzmann law as a function of its body temperature (T) measured using the YSI thermistor:

$$L = CG3 + \sigma T^4 . \qquad 5.1$$

The emissivity of the darkened sensor surface was assumed to be one. Whenever measurement of net irradiance only is needed, the measurement of body temperature can be ignored. The difference of sky and surface measured long wave irradiance can be used as a measure of net long wave irradiance. To avoid dew deposition on the sensor surface, a heater was used during the nighttime with switch control from the data logger.

A net radiometer (REBS Q*6.7.1, Radiation and Energy Balance System Inc., Seattle, USA)[1] was used to measure the net irradiance in addition to the CNR1. The sensor has a spectral response between 0.25 and 60 μm and a time constant of 30 seconds. The sensor has 60 junction thermocouples with a nominal resistance of 4 Ω and generates a millivolt signal proportional to the net irradiance. The thermopile is mounted in a glass reinforced plastic frame with a built-in level. The black paint absorbs the internally reflected radiation. The polyethylene plastic is used for a windshield for the sensors.

In addition to the above net radiometer sensors, a miniature net radiometer (Model 310, Middleton and Co Pty Ltd., Melbourne, Australia)[1] was also used to measure net irradiance from the evaporation surface of an ET-gage evaporimeter. Initially the sensor was calibrated against the CNR1 component net radiometer. The domes of the sensor were replaced every morning whenever condensation of water vapour was observed.

To minimize shading from metal supports, the net radiometers were positioned with their head facing north-south or south to north directions. The sensors were mounted horizontally using a spirit level with the domes facing the sky and grass at a 1 m height above ground. The domes were cleaned using distilled water and dried using facial tissue. The silica gel was replaced after the colour changed from blue-white to pink.

[1] Mention of a commercial company in this thesis does not imply an endorsement

A differential output voltage instruction P2 and single ended output voltage instructions P1 were used with CR7X and 21X data loggers. In each case, the appropriate multiplier was used to convert the measurement voltage to net irradiance.

5.4.2 Infrared Thermometer (IRT) and Thermocouples

Infrared temperature sensors and thermocouples Type E (chromel-constantan) were used to measure surface temperature. The IRTS-P sensor contains a twisted and shielded pair of type K thermocouples (chromel–alumel), one seeing the target temperature and the other for measuring the sensor body temperature. The sensor is designed to have a field of view such that the target diameter to distance away from the object is 1:3. The sensor was laboratory calibrated by measuring the surface temperature of stirred water using a magnetic stirrer. This surface water temperature was independently measured using type E thermocouples. In the field, the IRTS-P sensor was placed at an angle of 45^0 to view the grass surface and at 90^0 to the ET-gage evaporimeter surface. In addition to the IRTS-P, thermocouples (one type E 0.5 mm and three type E 0.254 mm diameter) were used to measure the surface temperature of the grass surface and ET-gage evaporation surfaces as well as the body temperature of ET-gage. Seven type E thermocouples (0.5 mm diameter) were also used to measure air temperature within the naturally ventilated radiation shields and Stevenson screens. Two exposed fine wire thermocouples type E (75 μm diameter) were also used to measure air temperature at 1.5 and 2.0 m above the grass surface.

The grass and ET-gage evaporation surface temperature was measured to calculate the sensible heat flux density with air temperature and wind speed measured above the grass and ET-gage evaporative surfaces. The surface temperature of grass and the ET-gage evaporimeter was also measured using type E thermocouples. These measurements together with air temperature and wind speed measurements allowed the sensible heat flux density to be calculated.

5.3.3 ET-gage

Atmometers (manual model A and electronic model E, ET-gage) were used to measure evaporation from the grass and crop surfaces. The device consists of cylindrical plastic container, porous ceramic evaporative surface (porcelain), fabric cover and in case of model E CMOS electronics (see Fig. 5.2).

Fig. 5.2 Main parts of ET-gage atmometer (photograph, Savage 2001) from left to right: the complete unit, the ET-gage evaporation surface, the electronic board for model E and the glass sight tube. The diameter of the ET-gage evaporating sensor is 79 mm

The device has a graduated glass sight tube attached to indicate the water level in the reservoir. The conduit, the suction tubes, was used to connect the main reservoir with porous ceramic surface. The electrical and visual resolution of the ET-gage is 0.254 and 0.5 mm respectively. The sensitivity of the evaporation surface was evaluated with evaporation measured from the surface using the STEB technique.

The priming of ET-gage was accomplished with distilled water and a syringe. The reservoir was filled with distilled water and connected to the ceramic cup after air bubbles were removed. The ceramic cup was covered with the bottom wafer and the canvas cover kept upside down to allow water to soak. For model E a syringe was used to avoid air bubbles, using a suction tube from the glass measuring vial on the circuit board. The priming was completed after the ceramic cup is connected using a suction tube. Four AA-size alkaline dry cell batteries were used to power the circuit and activate the valve of the system.

The device uses three different types of fabric cover at the top of ceramic evaporation surfaces: canvas cover 30, canvas cover 54 and Gore-Tex. The evaporation measurement was conducted using two covers (canvas 30 and 54) at three sites. The ET-gage model A with canvas 54 was used at Cedara weather station (latitude ≈ 29.58 ^{0}S, longitude ≈ 30.28 ^{0}E, altitude ≈ 1076 m). The two electronic models with canvas cover 30 and 54 were used at the Agrometeorology site and one with canvas 54 was used at Ukulinga farm (latitude ≈ 29.67 ^{0}S, longitude ≈ 30.40 ^{0}E, altitude ≈ 775 m). The devices were mounted to wooden posts with the evaporating surface at 1 m above the ground surface. Two thin twine wires of length 153 mm were placed at the top of the cylinder to avoid the interference of birds with the system. Telephone wire was connected to the circuit board

to connect to the analog pulse input channel of loggers (CR7X, 21X) and Event Hobo loggers (H07-002-04). The device height, diameter and gross mass are 566 mm, 79 mm and 2.5 kg respectively (Fig. 5.2).

5.4.4 Soil Heat Flux Plates, ThetaProbe and Soil Thermocouples

Soil heat flux plates HFT3 (Radiation Energy Balance Systems Inc., Seattle, USA) (serial number 91300, 913031), uses a thermopile to generate a voltage difference across a plate corresponding to the soil heat flux density. The physical dimension of circular plates is 38.2 mm diameter and 3.91 mm thickness. The measurement range of the sensor lies between –100 and 100 W m^{-2}.

Two soil heat flux plates were buried at a depth of 80 mm. Averaging soil thermocouples probe (TCAV Type-E, Campbell Scientific Inc., Logan, Utah, USA) and ThetaProbe soil water content sensors were used to calculate stored soil heat flux density. Four type E thermocouples connected in parallel were used to measure the average soil temperature above the plates. Two thermocouples were placed at 20 mm and the other two at 60 mm depths. One ThetaProbe was buried in the turf grass to measure soil water content above the soil heat flux plates. The upper pins were placed horizontally in undisturbed soil facing north at a depth of 25 mm. The measured voltage was transformed into volumetric soil water content using the equation given for mineral soil (Appendix 4). The soil water content and soil temperature were measured to calculate the stored heat flux density and this was added to the soil heat flux density measured using the soil heat flux plates.

A diagrammatic representation of the installation of soil heat flux plates and soil thermocouples for the determination of soil heat flux density is shown (Fig. 5.3). A hoe and spade were used to cut the soil in vertical and horizontal positions.

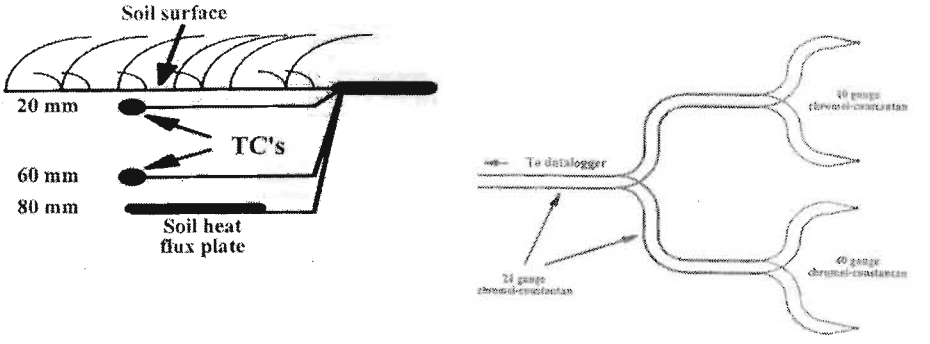

Fig. 5.3 Diagrammatic representation of soil heat flux plates and soil thermocouples (Savage *et al.* 1997)

The soil was replaced carefully in a hole minimizing the disturbance but ensuring good contact between sensors and soil.

5.4.5 Radiation Shields

Three types of naturally ventilated radiation shields were used: standard and small Stevenson screen, manufactured Gill multi-plate radiation shields and home-made plastic and metal multi-plate radiation shields (Fig. 5.4). The standard Stevenson screens were used as the standard. All shelters were in an east-west line to maintain the dominant north-south wind direction.

The standard and small Stevenson screens (910 mm × 720 mm × 460 mm and 300 mm × 270 mm × 200 mm) are wooden louvered shelters. The existing double louvered white rectangular of the larger standard Stevenson screen was cleaned and painted with whitewash paint. The Stevenson screen was mounted so that the steel angle iron legs base was at one meter above ground. The standard Stevenson screen was used for the calibration and comparison of different models of electronic temperature and humidity probes.

Fig. 5.4 Radiation shields from left to right: top standard Stevenson screen (910 mm × 720 mm × 460 mm), small Stevenson screen (300 mm × 200 mm × 270 mm) and bottom twelve-plate Gill radiation shield, six-plate Gill radiation shield, seven-metal plate home made radiation shield, seven-plate large size plastic home-made radiation shield, seven-plate small size plastic home made radiation shield

The Stevenson screen air temperature and relative humidity was measured using the Vaisala CS500, Hobo H8 and thermocouple type E sensors. The small single louvered Stevenson screen, which differs in size and door position, was used with the Hobo H8 logger and thermocouple type E sensors.

The twelve-plate Gill thermoplastic radiation shield was used with the HMP35C temperature and humidity probe and type E thermocouples. The six-plate thermoplastic Gill radiation shield is commonly used in South Africa and was used to shelter type E thermocouples and CS500 air temperature and relative humidity sensors.

Home-made radiation shields with a design similar to original Gill multi-plate radiation shield were used for measuring air temperature and relative humidity. One type uses plastic plates (Savage 2002*b*) and another metal plates (Science Workshops, University of Natal, Pietermaritzburg, South Africa). The seven-plate plastic radiation shields were made to have two different designs of plates of diameter 180 mm and 140 mm respectively. Furthermore it was modified to accommodate the Hobo H8 logger in addition to the CS500 temperature and humidity probe. White paint was applied to the internal and external parts of the shields. The metal plate of the radiation shield has a diameter of 100 mm. Each metal plate was painted black internally and white for the external parts. The seven-plate metal radiation shield was used with type E thermocouples.

5.4.6 Organic Matter Content Determination

Organic matter content of soil was determined by adding 10 ml of potassium dichromate solution (1N K_2CrO_2) and 20 ml H_2SO_4 to a 0.5 g sample of soil (that has previously air dried, grinded and passed through a 0.5 mm sieve) contained in a 500 ml Erlenmeyer flask. The solution was left to stand for 20 minutes after which 170 ml deionized water, 10 ml of 85 % H_3PO_4, 0.2 g NaF and 10 drops of ferroin indicator were added. After adding each chemical solution, the mixture was mixed by swirling. This procedure was also performed for a blank sample. The blank sample flask was titrated using ferrous ammonium sulphate (Fe $(NH_4)_2(SO_4)$). The titrated volume for which the blank sample turned from dark green–blue to dark brownish black was noted and used to estimate the concentration of the ferrous ammonium sulphate used (Walkley 1947). The titrated volume for which the soil sample solution was turned to dark brownish black was also noted and used to estimate the percentage of organic carbon and subsequent organic matter using a factor. The calculations performed are shown in Appendix 4.

5.6 OPERATION DESCRIPTIONS AND USE OF DATA LOGGING EQUIPMENT

5.6.1 Description of Data Loggers

5.6.1.1 Multi-channel loggers and power

For collecting microclimatic measures, data loggers used were one CR7X (Fig. 5.5 *A*) and two 21X (Fig. 5.5 *B*) Campbell Scientific Inc. data loggers (http://www.campbelsci.com/loggers.html). Each data logger was powered using two lead acid rechargeable batteries (12 V) connected to an electrical charger. The data logger with battery ground was connected to ground using a lightning rod to reduce lightning damage. The rod was banged into the soil to a depth of 300 mm. The loggers were covered with a white plastic box to avoid solar heating and entry of rain. Silica gel placed inside the data logger was used to create a non-condensing environment.

5.6.1.2 Hobo loggers and power

Two types of Hobo data logger were used to collect data from devices and sensors. Two event recording single channel (H07-002-04, Fig. 5.5 *D*) and four point measuring four-channel Hobo H8 (H08-007-02 Fig. 5.5 *C*) loggers were used to measure microclimatic variables. All loggers were placed in radiation shields. Small dry cell batteries were used to power the loggers.

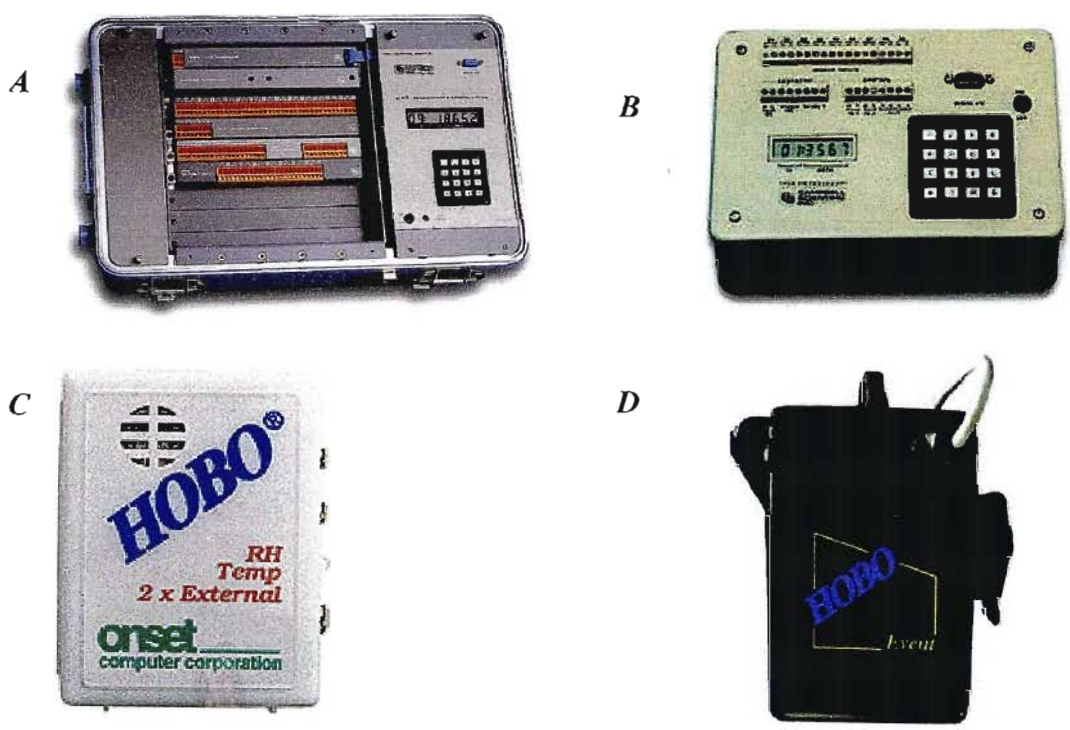

Fig. 5.5 Data loggers: (***A***) CR7X, (***B***) 21X (***C***) Hobo H8 logger (H08-007-002) and (***D***) Event Hobo logger (H07-002-04)

5.6.2 Program and Data Transfer and Statistical Procedures

For the CR7X and 21X data loggers manual data logger programming and monitoring is possible using an eight-digit LCD screen display. An alternative option is *via* the RS-232 port using an interface. The PC208W data logger supporting software was used to download programs and data using a storage module. Hobo logger programming and monitoring was achieved with the help of Boxcar software with the Hobo logger connected to PC *via* serial port.

The data was analyzed with excel worksheet and PlotIT for windows version 3.2. The statistical analysis includes regression analysis of calculated and measured variables, with confidence limit and error of estimates.

5.6.2 Programming

The program used for measurements is shown in Appendix 3. The CR7X and 21X program were created using PC208W (Campbell Scientific Inc.) software. The instructions are characterized by input processing (P30 - P66), output processing (P69 - P82) and control instruction (P85 - P98) in measurement table 1 and table 2 (Appendix 5). Table 1 and table 2 have similar execution intervals. The output interval for CR7X and 21X loggers was 15 minutes.

CHAPTER 6

ASSESSMENT OF ESTIMATION AND ASSUMPTIONS OF PENMAN-MONTEITH APPROACH

6.1 INTRODUCTION

In this chapter the accuracy and usefulness of the estimation and assumption of the available energy used in the Penman-Monteith approach for estimating reference evaporation for a short unstressed grass surface are investigated. From 15-minute data a comparison is made between measured and estimated parameters for hourly and daily procedures. The accuracy of the formulation for net long wave irradiance, the assumption of a fixed reflection coefficient value and soil heat flux density are compared with measured values. The performance of the net irradiance and emissivity estimation based on water vapour pressure and air temperature are also compared. The Monteith and Unsworth (1990) formulation of clear sky atmospheric minus crop surface emittance was evaluated and compared with actual measurements. A comparative analysis using linear regression is performed between the estimated hourly reference evaporation calculated from measured and estimated available energy parameters (I_{net} - G) from:

a) Measured net irradiance and estimated soil heat flux density (G)
b) Estimated net irradiance with assumed constant reflection coefficient (r = 23 %, r = 25 %) and estimated soil heat flux density (G)
c) Estimated net irradiance with empirically estimated reflection coefficient (r empirically estimated) and estimated soil heat flux density (G)
d) Measured net irradiance with soil heat flux density ignored (G)
e) Estimated net irradiance with soil heat flux density ignored (G)

The sensitivity of estimation under these assumptions is statistically compared.

6.2 MATERIALS AND METHODS

The Campbell Scientific Inc. (undated) application note discusses the estimation of hourly grass-based Penman-Monteith equation:

$$ET_o = \left[\frac{\Delta(I_{net} - G)}{\lambda(\Delta + \gamma)} + \frac{\gamma^* M_w (e_s - e_a)}{R\Theta r_v (\Delta + \gamma)} \right] / \rho_w \qquad 6.1$$

where ET_o is grass reference evaporation (mm s^{-1}), I_{net} is net irradiance (kW m^{-2}), G is the soil heat flux density (kW m^{-2}), M_w is the molecular mass of water (= 0.018 kg mol^{-1}), R is gas constant (= 8.3143 × 10^{-3} kJ mol^{-1} K^{-1}), Θ is Kelvin temperature (= 293 K), (e_s - e_a) is water vapour pressure deficit of the air (kPa), λ latent heat vaporization of water (= 2450 kJ kg^{-1}), r_v is canopy (r_c) plus aerodynamic boundary layer resistance (r_a) of water vapour (s m^{-1}), Δ is the slope of saturation water vapour pressure function (Pa K^{-1}), γ^* is apparent psychrometric constant (Pa K^{-1}) and ρ_w is density of water (kg m^{-3}). A spreadsheet (Savage 2002*a*) based on Eq. 6.1 was used to calculate grass reference evaporation. Appendix 2.1 presents the procedures for estimating the parameters using an AWS with data logger and a computer.

6.2.1 Experimental Data Collection and Weather Data Analysis

6.2.1.1 Net irradiance

The net irradiance from the short grass was measured using a component net radiometer (Fig. 5.1). The CNR1 component net radiometer consists of two CM3 pyranometers and two CG3 pyrgeometers and measures the four components of radiation balance separately:

$$I_{net} = I_s \downarrow - rI_s \uparrow + L_d \downarrow - L_u \uparrow \qquad 6.2$$

where I_s is solar irradiance (W m^{-2}), rI_s is the reflected solar irradiance (W m^{-2}), L_d is the downward long wave irradiance (W m^{-2}) and L_u is the upward long wave irradiance (W m^{-2}). The CNR1 was regarded as the standard for all radiation measurements and estimates of net irradiance in this work. The pyranometers were used to measure the incident and reflected solar irradiance. The pyrgeometers and thermistor temperature sensor (YSI 44032) were used to measure the upward and downward emittance and the CNR1 body temperature respectively. The upward and downward long wave irradiance were computed as a sum of pyrgeometers ($CG3_{up}$ and $CG3_{down}$) measurement and the sensor emittance calculated from Stefan-Boltzmann law of radiation (Eq. 4.11) as a function of its surface temperature using Eq. 5.1. The emissivity of the CNR1 surface (ε_s) was assumed to be one. An additional two separate but similar model CM3 pyranometers and REBS Q*6.7.1 net radiometer were also used to measure irradiance above the short grass surface.

Comparison of REBS Q*6.7.1 net irradiance with the CNR1 results in a high correlation coefficient (r^2 = 0.99), and slope and intercept were 1.07 and -14.18 W m^{-2} respectively, using the CNR1 net irradiance as the independent measurement (data not shown).

6.2.1.2 Soil heat flux density

Soil heat flux density for the short turf grass was measured using two HFT3 soil heat flux plates. The measured soil heat flux plates were corrected for the stored heat above plates. Measurements of soil temperature using TCAV Type E parallel thermocouples and soil water content measured using a ThetaProbe were used to calculate stored soil heat flux density. The 15-minute soil heat flux density was calculated as:

$$G = F_s + F_{stored} \quad 6.3$$

where the stored soil heat flux density (F_{stored}) was calculated as:

$$F_{stored} = \rho_{soil} \Delta z_{soil} dT_{soil} c_{soil} / dt \quad 6.4$$

where ρ_{soil} is the bulk density of the soil (= 1200 kg m^{-3}), Δz_{soil} is the soil depth (80 mm), dT_{soil} is change in soil temperature (K) during a measurement interval dt (= 900 s), c_{soil} ($c_{soil} = c_{dsoil} + \Theta c_w$) is the specific heat capacity of soil (J kg^{-1} K^{-1}), c_{dsoil} is specific heat capacity of dry soil (= 837 J kg^{-1} K^{-1}), Θ is the gravimetric soil water content (kg of water in kg of soil) and c_w specific heat capacity of water (= 4190 J kg^{-1} K^{-1}). The soil heat flux density (F_s) is measured with soil heat flux plates (W m^{-2}) (Savage *et al.* 1997).

6.2.1.3 Automatic weather station (AWS)

An AWS was used to collect the following data: solar irradiance, rainfall, wind speed, relative humidity, air and surface temperature. The three-cup wind speed and direction sensor at 2 meter and heated ceramic needle anemometer at 1 meter were used to collect the wind speed and wind direction data. Relative humidity and air temperature were measured with Vaisala CS500 air temperature and relative humidity sensors. Actual water vapour pressure (kPa) was calculated as the product of the fractional (sample) 15-minute relative humidity (RH) and saturation water vapour pressure computed from the average air temperature (T_a) in °C as:

$$e_a = 0.6108[\exp(17.2694 T_a /(237.3 + T_a))](RH/100). \quad 6.5$$

Rain data was collected using a Rain-O-Matic rain gauge.

A logger scan rate of 30 seconds was used for all the measurements. The output-averaging period was 15 minute.

6.2.2 Methods

The primary input data of Eq. 6.1 is the available energy component (I_{net} - G), which supplies or diminishes the energy at the grass surface. The procedures for estimating net irradiance (I_{net}), as a function of estimated net long wave irradiance (L_{net}) and reflection coefficient (r) evaluated by comparison with measurements, are presented in Table 6.1. The assumed and empirically estimated (Dong *et al.* 1992) reflection coefficients are compared with measured. The clear sky emissivity parameterization based on water vapour pressure, air temperature or both which were compared with the Monteith and Unsworth (1990) formulation of atmospheric emittance minus crop surface emittance (Eq. 4.20) are presented in Table 6.2. In the estimation of net long wave irradiance (Eq. 4.10), the cloudiness was evaluated using a formulation given in the unpublished Campbell (undated) application note. The emittance of the grass surface was calculated using Eq. 4.11, assuming surface emissivity (ε_s) equal to 0.98 (Savage *et al.* 1997). Brunt (1932) clear sky emittance used a calibrated coefficient while for the other formulations the original coefficients were used for the comparison. Dong *et al.* (1992) daytime hourly net irradiance estimation procedure used the clear sky emissivity (ε_a) formulation of Satterlund (1979).

Table 6.1 Procedures for the estimation of net irradiance (I_{net}) (T_a and T are hourly average air temperature in °C and in K respectively)

Method	Formulations for net irradiance
Campbell (undated) (Appendix 2)	$I_{net} = (1-r)I_s + (0.0003T_a - 0.107)\times 10^{-3} \times c$ $c = 1 - 1/(1 + 0.034\exp(7.9I_s / I_o))$ $r = 0.23$
Dong *et al.* (1992)[1]	$I_{net} = 0.89[(1-r)I_s + \varepsilon_a(1-c)\sigma T^4 + c\sigma T^4 - 0.98\sigma T^4]$ $r = 0.0015\phi + 0.386\exp(-0.0188\phi)$ $c = 1.33 - 1.33I_s / I_a$ $I_a = (0.79 - \frac{3.75}{\phi})I_s$
FAO (1998)[2] (Appendix 2)	$I_{net} = (1-r)I_s - (0.34 + 0.14\sqrt{e})(1.35I_s / I_a - 0.35)\sigma T^4$ $r = 0.23$
Ortega-Farias *et al.* (2000)[3]	$I_{net} = (1-r)I_s + 0.98(1.31(e/T)^{1/7} - 1)\sigma T^4 \times c$ $r = 0.25$

[1] e is in mbar, [2] e is in kPa, [2] T is given as maximum (T_{max}) and minimum (T_{min}) air temperature average for daily estimate, [3] the cloudiness (c) is evaluated with unpublished and undated Campbell Scientific Inc. procedure and the water vapour pressure e is in hPa, ϕ is solar altitude in degrees, r is reflection coefficient, I_a is solar irradiance in clear sky day (W m^{-2}), I_o is extraterrestrial irradiance (W m^{-2}), I_{net} is net irradiance (W m^{-2}), I_s is solar irradiance (W m^{-2})

Table 6.2 Formulation of clear sky emissivity compared with Monteith and Unsworth (1990) formulations (hourly average water vapour pressure e in millibars, air temperature T in Kelvin and dew point temperature T_{dp} in °C)

Method	Formulations for clear sky emissivity (ε_a)
Brunt (1932)[1]	$\varepsilon_a = 0.44 + 0.08\sqrt{e}$
Idso and Jackson (1969)	$\varepsilon_a = 1 - 0.26\exp(-7.77\times10^{4}(273-T)^{2})$
Brutsaert (1975) - 1	$\varepsilon_a = 1.24\,(e/T)^{1/7}$
Brutsaert (1975) - 2	$\varepsilon_a = 0.533\,e^{1/7}$
Satterlund (1979)	$\varepsilon_a = 1.08(1-\exp(-e^{T/2016}))$
Idso (1981)	$\varepsilon_a = 0.70 + 5.95\times10^{-5}\,e\exp(1500/T)$
Berdahl and Martin (1984)	$\varepsilon_a = 0.711 + 0.56\,(T_{dp}/100) + 0.73\,(T_{dp}/100)^{2}$
Prata (1996)[2]	$\varepsilon_a = 1-(1+46.5\,(e/T))\exp(-(1.2+3.0\times46.5(e/T))^{0.5})$

[1]Corrected coefficient, [2]water vapour pressure e in hPa

The FAO daily procedure was used to estimate the daily net irradiance using the fourth power of maximum (T_{max}) and minimum (T_{min}) air temperature in Kelvin (Table 6.1). The procedure was evaluated for the daytime data based on the day length calculation using a spreadsheet.

The measured soil heat flux density was compared with estimated hourly soil heat flux density, which is usually approximated as 10 % and 50 % of the estimated net irradiance for day and night time respectively.

The sensitivity of Eq. 6.1 was assessed using a regression analysis (Savage 1998, spreadsheet) for the available energy (I_{net} - G) from the measured and estimated net irradiance, estimated reflection coefficient, estimated soil heat flux density and ignored soil heat flux density using the Campbell (undated) available energy (I_{net} - G) calculation procedures. The water vapour pressure deficit was computed as a difference between saturation water vapour pressure and actual water vapour pressure (Eq. 6.5). The aerodynamic resistance was evaluated from logarithmic wind profile function (Eq. 4.31) for a neutral atmosphere. The canopy resistance was assumed constant as a function time of day (daytime value of 70 s m^{-1} and nighttime value of 700 s m^{-1}). The procedures for estimating extraterrestrial solar irradiance, solar altitude, clear sky solar irradiance cloudiness used are presented in Appendix 2. A rejection criterion was used to discard all unreliable data.

6.3 EVALUATION OF THE ESTIMATION OF AVAILABLE ENERGY TERM

6.3.1 Reflection Coefficient

The accuracy in the estimation of net irradiance for the reference crop depends on the measured incident solar irradiance, estimated reflected solar irradiance and net long wave irradiance. The assumption of a constant reflection coefficient (Allan *et al.* 1998; Campbell undated) and empirical estimation (Dong *et al.* 1992) as a function of solar irradiance and solar altitude (ϕ) (Table 6.1) respectively avoids the need for measuring the reflected component of solar irradiance for the estimation of net irradiance. The approximation of a constant reflected solar irradiance used with reference crop varies from 23 % to 25 % of solar irradiance (Table 4.1).

The clear daytime hourly calculated reflection coefficient of short grass surface was observed to vary between 15 to 22.6 % of measured solar irradiance. A comparison of measured average reflection coefficient and the Campbell (undated) assumed reflection coefficient (23 %) of short grass showed an overestimation of reflection coefficient by 5 %. Fig. 6.1 shows the measured and empirically estimated (Dong *et al.* 1992) hourly reflection coefficient of selected three clear days of the year 2002 (55, 124, and 157). The measured reflection coefficient shows a variation below the approximated percentage (23 %) for the whole day. Fig. 6.1 also shows Dong *et al.* (1992) empirical estimation of reflection coefficient. The Dong *et al.* (1992) empirical approximation overestimated the measured but follows a similar trend to the variation of the hourly measured clear day reflection coefficient. Local calibration of the coefficient may improve the estimate of empirical formulation since it is a solar altitude dependent formulation.

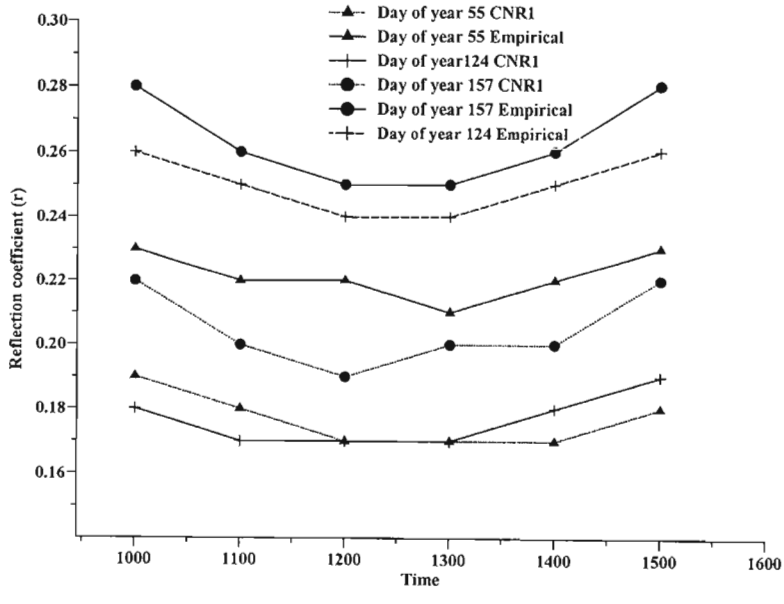

Fig. 6.1 Measured and empirically estimated (Dong *et al.* 1992) reflection coefficient of short grass surface for selected clear days of the year 2002, at the Agrometeorology site

6.3.2 Soil Heat Flux Density

The measurement or estimation of soil heat flux density (G) is important for calculating latent heat flux using the energy balance equation. A procedure for the approximation of soil heat flux density (G) from the estimated net irradiance for the Penman-Monteith approach of estimating reference evaporation was recommended by Allan *et al.* (1998) and Campbell (undated).

As Snyder *et al.* (2000) pointed out, the approximation was based on soil heat flux plate measurement at a depth of 100 mm. Figs 6.2*a* and 6.2*b* shows net irradiance, soil heat flux plate at 80 mm, surface soil heat flux density, stored soil heat flux density, soil water content and wind speed (from one meter) of clear day of year 55 and cloudy day of year 96, 2002. Plate heat flux density measurement with the stored heat flux density was calculated by averaging three consecutive 15-minute measurements (Fig. 6.2*a*). Most of the time the corrected surface soil heat flux density and stored soil heat flux density were higher than the estimated values in the morning hours and lower in the afternoon where the estimated soil heat flux density is assumed to be as 10 and 50 % of net irradiance during day and night time respectively.

The soil heat flux density of the grass surface is sensitive to soil temperature and soil water content changes - a similar result has also been reported in various studies. There was more variation in the soil heat flux density than with calculated stored heat flux density. As Malek (1993) and Savage (2002*b*) observed and Figs 6.2*a* and 6.2*b* show, cloudiness, wind speed and wind direction variation could also be possible factors in the surface soil heat flux density variations. The wind speed was measured using a more sensitive PRTD wind speed sensor at one-meter height. As Figs 6.2*a* and 6.2*b* show, the major contribution of soil heat flux density is from the stored soil heat flux density than that measured with plates. More research on the method of estimation of soil heat flux density for short time periods is needed.

The scatter plot of daytime hourly computed net irradiance and soil heat flux density of surface, soil heat flux density of plate and stored soil heat flux density from 15 minute data is shown in Figs 6.3*a*, 6.3*b*, 6.4. The daytime ratio of hourly stored and plate-measured soil heat flux density to net irradiance varies between -27.7 to 10.4 and -68.8 to 24.4 respectively. Similarly the ratio of soil heat flux density to net irradiance varies between -92.8 to 13.8, excluding the extreme outliers observed due to sudden change of soil temperature.

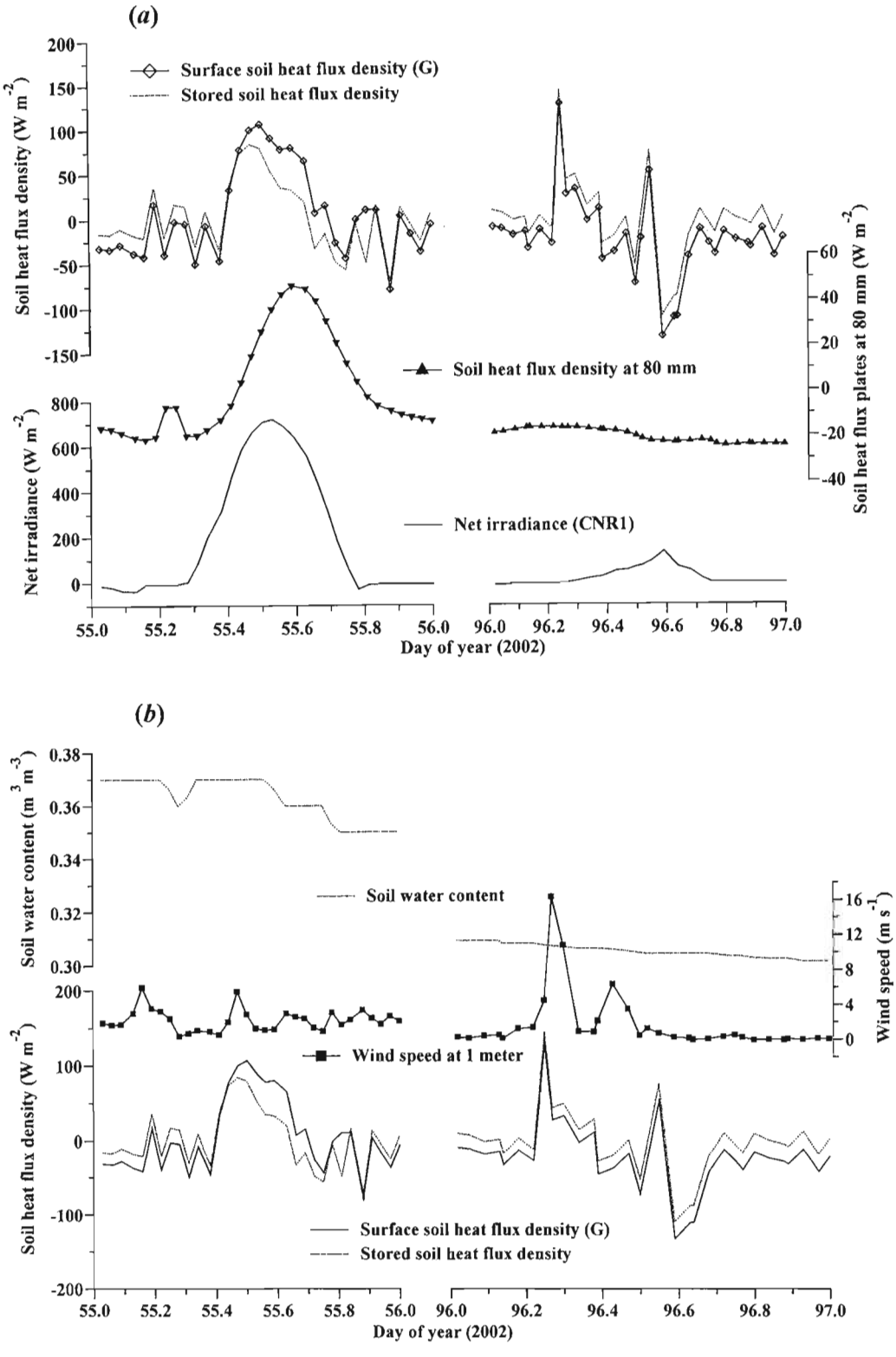

Fig. 6.2 (*a*) Soil heat flux density measured using soil heat flux plates at 80 mm (F_s), stored (F_{stored}) and corrected soil heat flux density (G) and net irradiance (*b*) Stored (F_{stored}) and corrected soil heat flux density (G), wind speed at 1 meter and soil water content for clear and cloudy days of year 55 and 96, 2002, at the Agrometeorology site

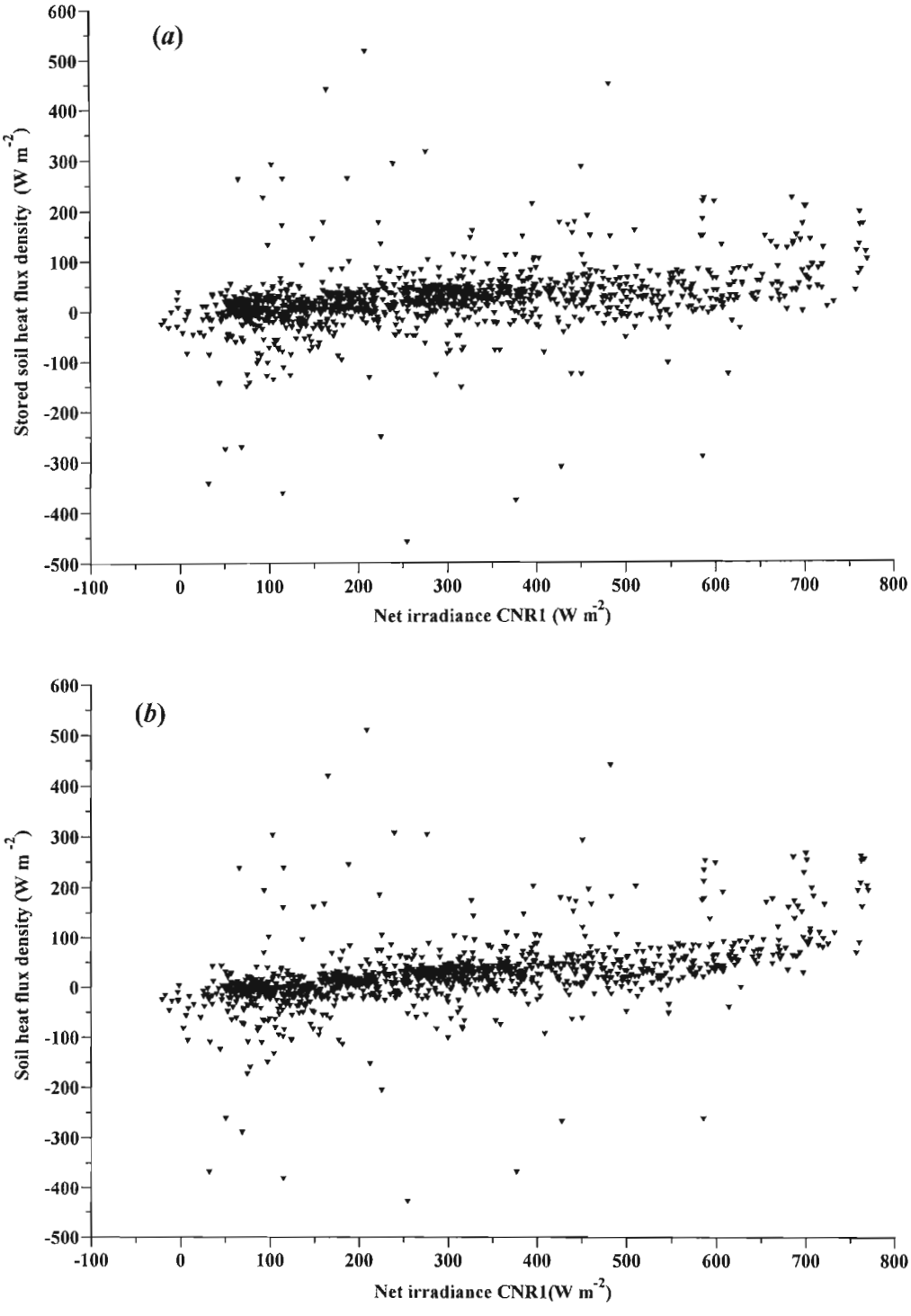

Fig. 6.3 Hourly measured net irradiance using the CNR1 *vs* (*a*) daytime calculated stored soil heat flux density of short grass (*b*) daytime surface soil heat flux density of short grass (15 minute averages) for the period of measurement between December 27, 2001 to July 12, 2002, at the Agrometeorology site

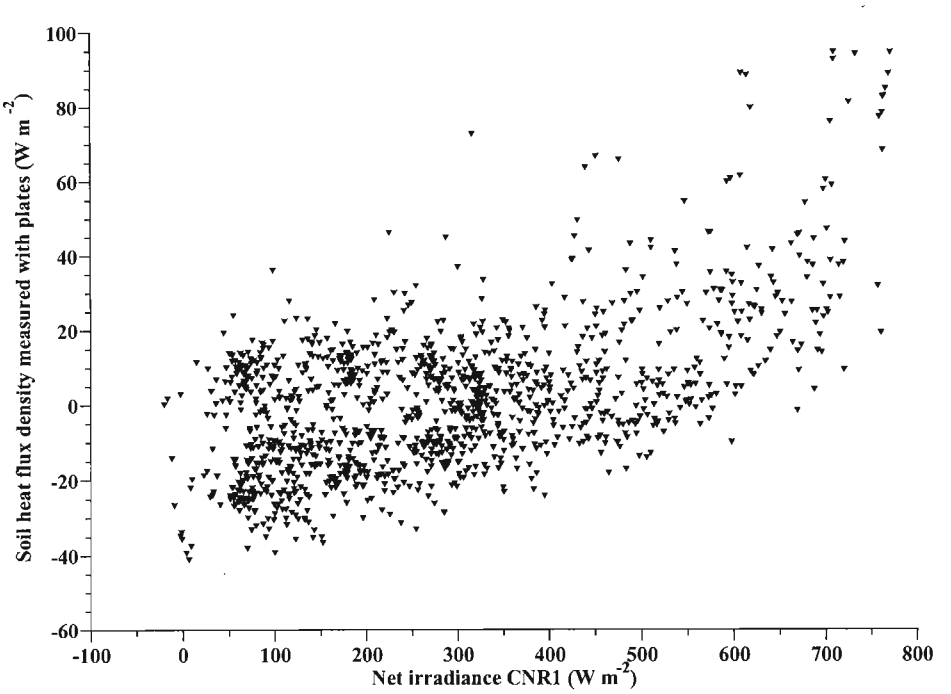

Fig. 6.4 Hourly measured net irradiance using CNR1 *vs* daytime soil heat flux density measured at 80 mm using soil heat flux plates (15 minute average) for the period of measurement between December 27, 2001 to July 12, 2002, at the Agrometeorology site

6.3.3 Atmospheric Minus Crop Emittance

The third approximation with available energy in the implementation of Penman-Monteith approach depends on the net long wave approximation either as a function of air temperature and/or water vapour pressure measured at two meters. The difficulty in the estimation of net long wave irradiance lies with the estimation of the incoming long wave irradiance. Most of the approximations used the empirical correlation of air temperature and/or water vapour pressure or dew point temperature.

The Monteith and Unsworth (1990) linear approximation of atmospheric minus crop emittance under clear sky (Eq. 4.20) is based on a limited range of air temperatures. The measurement of clear day net long wave irradiance (L_{net}) in this study revealed a logarithmic relation rather than a linear one with daytime air temperature variation (Fig. 6.5*a*). A plot of measured net long wave irradiance versus Monteith and Unsworth (1990) estimate of atmospheric minus crop emittance is shown in Fig. 6.5*b*. The estimated hourly atmospheric minus crop emittance of grass surface was between -10 to -100 W m^{-2} when the measured net long wave irradiance varied between -150 and 10 W m^{-2}. Furthermore, the comparison with other similar empirical parameterisations showed a lower correlation for hourly estimate of net long wave irradiance (Table 6.3).

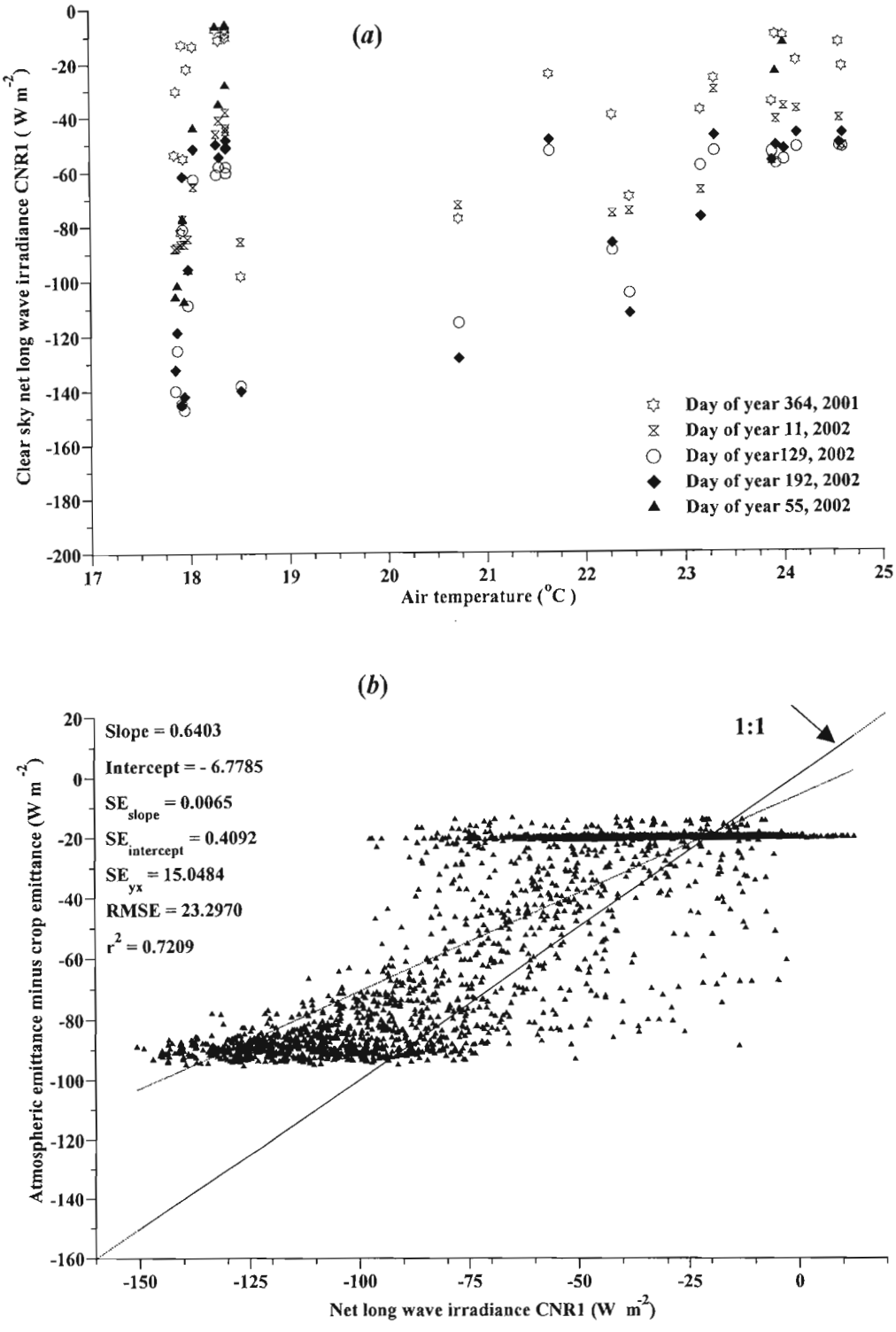

Fig. 6.5 (*a*) Hourly average air temperature *vs* clear sky net long wave irradiance (L_{net}) measured using the CNR1 for selected clear days of year 2002 (*b*) hourly CNR1 net long wave irradiance *vs* Monteith and Unsworth (1990) atmospheric emittance minus crop emittance for the period of measurement between December 27, 2001 to July 12, 2002, at the Agrometeorology site

Table 6.3 Statistical results of the comparisons between formulations of net long wave irradiance (W m^{-2}) for hourly data, for the period of measurement between December 27, 2001 to July 12, 2002, at the Agrometeorology site

Method (n = 3795)	r^2	Slope	Intercept (W m^{-2})	MSE_{uns} (W m^{-2})	MSE_{sys} (W m^{-2})	RMSE (W m^{-2})	S_{yx} (W m^{-2})
Brunt (1932)	0.79	0.81	1.59	15.92	13.10	20.61	15.93
Idso and Jackson (1969)	0.70	0.40	-6.60	9.83	32.93	34.36	9.83
Brutsaert (1975) - 1	0.79	0.63	1.84	12.28	19.12	20.04	12.28
Brutsaert (1975) - 2	0.79	0.69	1.00	13.45	20.37	20.41	13.46
Satterlund (1979)	0.76	0.86	-2.37	18.51	6.98	19.79	18.52
Idso (1981	0.78	0.53	4.09	1076	32.94	34.65	10.76
Berdahl and Martin (1984)	0.79	0.65	0.98	12.58	23.20	26.39	12.59
Monteith and Unsworth (1990)[1]	0.72	0.64	-6.78	15.04	17.71	23.28	15.05
Prata (1996)	0.79	0.59	0.83	11.42	26.81	29.14	11.43

1 and 2 refers to the formulation in Table 6.2, [1]Eq. 4.20, r^2 is correlation coefficient, MSE_{uns} is unsystematic mean square error, MSE_{sys} is systematic mean square error, RMSE is the root mean square error, S_{yx} is standard error of estimate y on x

The comparison shows higher relative accuracy of the calculated net long wave irradiance using the corrected coefficient of Brunt (1932), which is based on water vapour pressure, and the Satterlund (1979) parameterization, which incorporate water vapour pressure and air temperature (Table 6.3). These formulations of net long wave irradiance show higher correlation coefficient, lower mean systematic error (MSE_{sys}) and lower underestimation compared to the Monteith and Unsworth (1990) formulation. Brutsaert (1975) and Berdahl and Martin (1984) formulation was also show good correlation coefficients.

6.3.4 Net Irradiance Comparison

The statistical result of comparison following the procedures of estimation net irradiance based on the Monteith and Unsworth (1990) emissivity formulation (Eq. 4.20) given in the unpublished Campbell (undated) notes, FAO (1998), Dong *et al.* (1992) and Ortega-Farias *et al.* (2000) is presented in Table 6.4. The estimation of cloudiness followed the procedure presented in each study. For the Monteith and Unsworth (1990) and Ortega-Farias *et al.* (2000) formulations, cloudiness was evaluated with the same equation given in the Campbell (undated) note.

Table 6.4 Statistical comparisons of procedures for estimating net irradiance (W m^{-2}), at Agrometeorology site

Methods	r^2	Slope	Intercept (W m^{-2})	MSE_{uns} (W m^{-2})	MSE_{sys} (W m^{-2})	RMSE (W m^{-2})	S_{yx} (W m^{-2})
Procedures compared for hourly estimate of net irradiance (n = 3795)							
Campbell (undated)	0.99	0.92	16.8	19.73	17.44	26.34	19.74
FAO (1998)	0.98	0.98	19.73	22.82	18.52	29.39	22.82
Ortega-Farias *et al.* (2000)	0.96	0.96	18.95	17.66	17.19	24.64	17.66
Procedures compared for solar irradiance greater than 100 W m^{-2} (n = 1349)							
Campbell (undated)	0.99	0.92	21.81	19.25	14.99	24.40	19.26
FAO (1998)	0.98	0.94	37.59	24.64	23.56	34.09	24.66
Ortega-Farias *et al.* (2000)	0.99	0.94	27.48	16.16	14.91	21.99	16.17
Dong *et al.* (1992)	0.98	1.02	4.48	24.85	10.54	26.99	24.87
Daily net irradiance estimation procedure (MJ m^{-2})							
FAO (1998) (n = 148)[1]	0.93	0.87	-0.55	0.97	1.70	1.99	0.980
FAO (1998) (n = 163)	0.97	0.77	1.01	0.73	1.56	1.56	0.740

[1]Maximum and minimum air temperature estimated from daytime using day length calculation (spreadsheet), r^2 is correlation coefficient, MSE_{uns}, MSE_{sys}, RMSE are unsystematic, systematic and root mean square errors, S_{yx} is standard error of estimate of y on x

Fig. 6.6 shows daytime net irradiance estimated using the procedures and measured values using the CNR1. The maximum difference was noted in the midday hours. For the hourly estimation procedures, Dong *et al.* (1992) considers solar irradiance above a solar altitude of 10^0 and then these data were compared to three other methods for which the solar irradiance was greater than 100 W m^{-2}. The result showed comparatively lower mean systematic error (MSE_{sys}) and 2 % error compared to the others (Table 6.4). Although there is an underestimation and relatively poor estimation of net long wave irradiance using the Monteith and Unsworth (1990) formulation and an overestimation of the reflected solar irradiance (Fig. 6.5*b*), the net irradiance estimation procedure of Campbell (undated) gives a relatively similar result to other methods. This may be because solar irradiance is the major contributor of net irradiance and underestimation of the net long wave estimate tends to cancel out the reflected solar irradiance overestimation. The correlation coefficient (r^2) is higher and slope is close to one with almost similar mean systematic (MSE_{sys}) and unsystematic error (MSE_{uns}) for the other procedures. All the procedures except that of Dong *et al.* (1992) underestimated the measured net irradiance. Campbell (undated) procedure underestimated the measured net irradiance by 8 %. The slope and intercept of estimated net irradiance was significantly different from one and zero for all procedures.

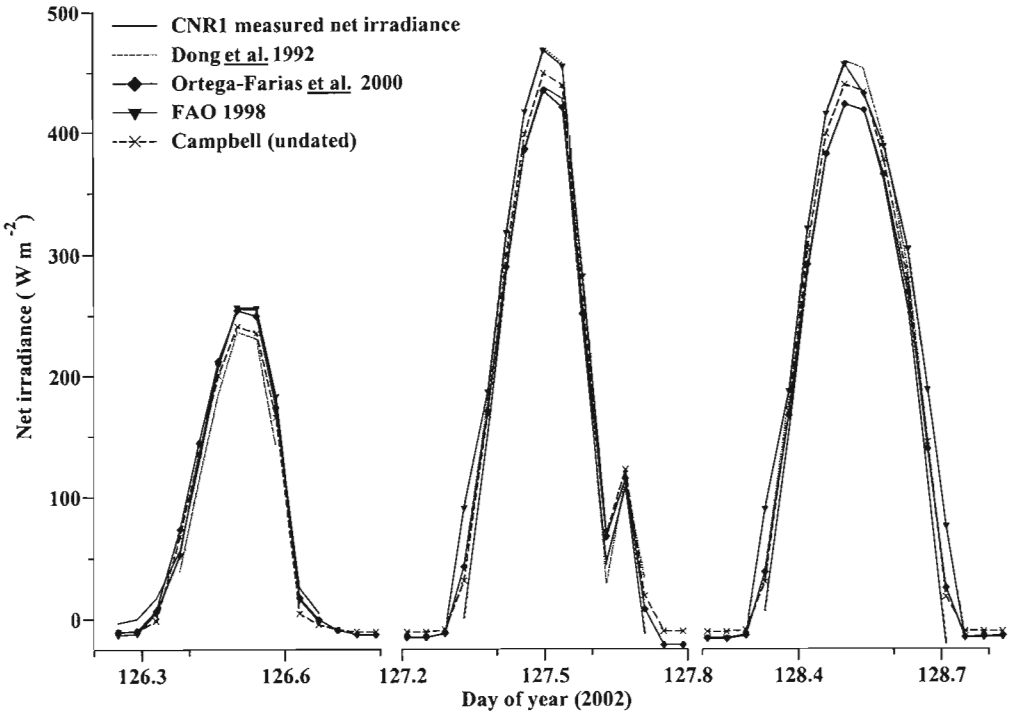

Fig. 6.6 Net irradiance estimated using four different procedures (Campbell undated, Dong *et al.* 1992, FAO 1998, Ortega-Farias *et al.* 2000) and measured using the CNR1 for days of the year 126, 127 and 128, 2002, at the Agrometeorology site

FAO daily procedure of estimating net irradiance from daily maximum and minimum air temperature was compared with estimated net irradiance calculated from measured air temperature based on the day length calculation. The first procedure showed higher correlation with measured net irradiance (CNR1) but with greater underestimation. Table 6.4 shows the statistical result of comparison between measured and estimated net irradiance.

In the absence of direct measurements, with local calibration of empirical coefficients using hourly data, a reasonable estimate of net irradiance can be obtained with all the procedures used for reference evaporation estimation purposes.

6.4 ESTIMATION SENSITIVITY OF THE PENMAN-MONTEITH APPROACH

The available energy in the Penman-Monteith formulation is an important term, which could result in greater error than the aerodynamic term. The sensitivity of the approach for three cases of reflection coefficient assumptions with estimated net irradiance and two cases of soil heat flux density assumptions with measured and estimated available energy (I_{net} - G) is considered.

In Table 6.5 a statistical summary is provided for the comparison between the estimated grass Penman-Monteith (Eq. 6.1) latent heat using measured available energy and that estimated for the following cases:

(*a*) measured net irradiance and estimated soil heat flux density,

(*b*) estimated net irradiance using (r = 23 %, 25 %) and estimated soil heat flux density,

(*c*) estimated net irradiance using Dong *et al.* (1992) empirically estimated reflection coefficient and estimated soil heat flux density,

(*d*) measure net irradiance but ignored soil heat flux density ($G = 0$) and

(*e*) estimated net irradiance (r = 23 %) and ignored soil heat flux density ($G = 0$).

The differences in mean hourly value of latent heat (L_vF_w) estimated from measured (I_{net} - G) and estimated from (I_{net} - G), correlation coefficient (r^2), standard mean square error (RMSE), unsystematic (MSE_{uns}) and systematic (MSE_{sys}) mean square error are shown in Table 6.5.

In Fig. 6.7 the scatter plot shows a comparison between measured hourly available energy (I_{net} - G) and estimated values calculated using Campbell (undated) procedures. It shows the underestimation of measured available energy (I_{net} - G) by 7 %.

Table 6.5 Statistical result of grass Penman-Monteith sensitivity error of assumptions and approximation with available energy term (I_{net} - G) (n = 2453 for hourly data, for the period of measurement between December 27, 2001 to July 12, 2002, at the Agrometeorology site)

Statistical test parameters	Grass Penman-Monteith latent heat flux estimate (L_vF_w)					
	Case *a*	Case *b* (r = 23 %)	Case *b* (r = 25 %)	Case *c* ($r = E$)	Case *d*	Case *E*
Slope	1.00	0.98	0.96	0.98	1.08	1.05
Intercept (W m^{-2})	-3.09	-1.08	-0.92	-1.97	-5.05	-2.82
Correlation coefficient (r^2)	0.97	0.97	0.97	0.97	0.97	0.97
Index of agreement	0.99	0.99	0.99	0.99	0.99	0.99
MAE (W m^{-2})	6.37	7.56	7.86	7.57	7.99	8.24
MSE_{uns} (W m^{-2})	10.86	11.54	12.90	11.42	11.87	12.14
MSE_{sys} (W m^{-2})	2.89	1.11	4.57	3.80	5.25	3.59
RMSE (W m^{-2})	11.24	11.91	12.28	12.04	12.98	12.65
Mean x (W m^{-2})	68.66	68.66	68.66	68.66	68.66	68.66
Mean Y (W m^{-2})	65.77	66.08	64.94	65.15	69.12	69.52
Mean difference error (W m^{-2})	2.89	2.58	3.72	3.51	-0.46	-0.86

MAE is the mean absolute error, MSE_{sys}, MSE_{uns} and RMSE are the systematic, unsystematic and root mean square error respectively, r is the E empirically estimated reflection coefficient (Dong *et al.* 1992)

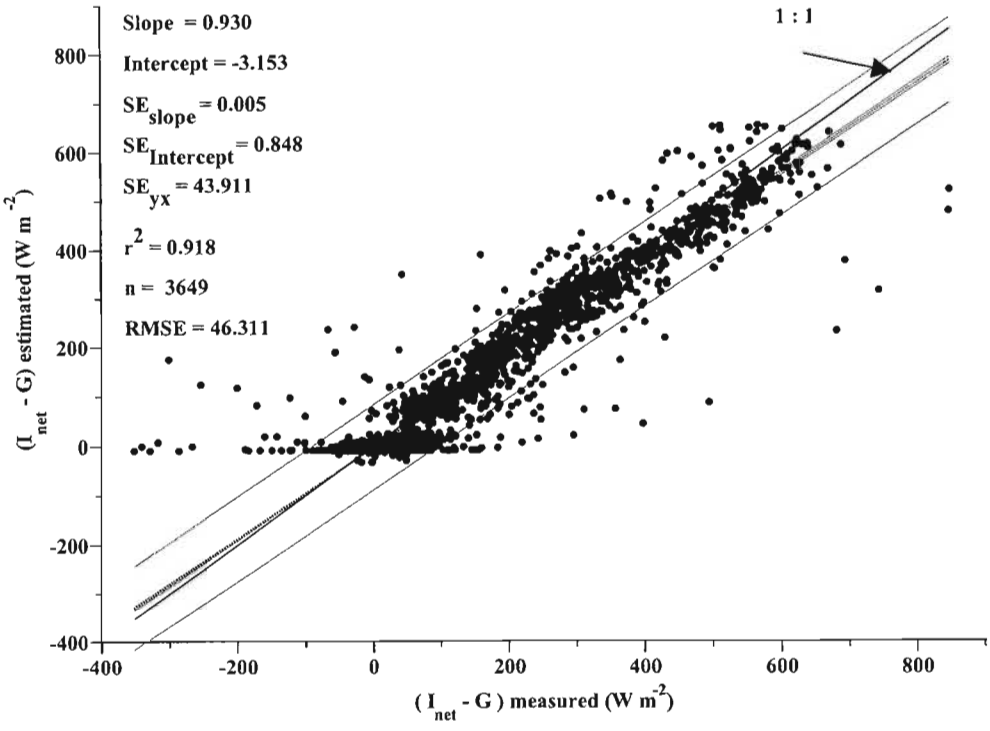

Fig. 6.7 Measured hourly available energy *vs* estimated with Campbell (undated) procedure. The wide 95 % confidence belts are for single predicted value and narrow belts are for predicted population mean value for the period of measurement between December 27, 2001 to July 12, 2002, at the Agrometeorology site

The underestimated net irradiance and the variable soil heat flux density tend to cancel each other. For all cases, the correlation coefficient (r^2) is high and the slope is close to one. Higher deviation of slope is observed for the case where soil heat flux density is neglected and I_{net} is measured and resulted in an 8 % overestimate and relatively higher mean systematic error (MSE_{sys}) compared to the estimated value of case (*a*). De Bruin and Striker (2000) also reported similar overestimation of the evaporation estimate. The estimated reflection coefficient tends to underestimate the latent heat. The higher unsystematic mean square error (MSE_{uns}), root mean square error (RMSE) and 4 % underestimation are observed due to assumption of the 25 % reflection coefficient and estimated soil heat flux density on the latent heat estimate.

Table 6.5 shows the dependence of the Penman-Monteith reference evaporation estimate on various methods of estimating/measuring net irradiance and soil heat flux density. When net irradiance is measured and soil heat flux density estimated a better estimate of reference evaporation is obtained. However, in the absence of direct measurement of net irradiance, estimated reflection coefficient as 23 % of solar irradiance and soil heat flux density

(as 10 and 50 % of I_{net} for day and night-time respectively) can give acceptable results. Moreover a local calibration can yield a better estimate of the parameters.

6.5 CONCLUSIONS

The measured soil heat flux density was variable depending on the net irradiance, wind speed, cloudiness and soil water content. There was no clear relation between measured surface soil heat flux density and net irradiance. The commonly-used estimate of reflection coefficient overestimated the measured reflection coefficient of the grass surface. Moreover, measured clear sky net long wave irradiance was observed to show a logarithmic relation to the daytime measured clear sky air temperature. The estimation accuracy of the linear atmospheric minus crop surface emittance formulation of Monteith and Unsworth (1990) was also observed to be limited to a certain range of net long wave irradiance estimated and showed less agreement for the Agrometeorology site. This estimation approach underestimated the measured net long wave irradiance. As a net result the Campbell (undated) procedure to estimate net irradiance was observed to underestimate the measured net irradiance. Furthermore, the estimated available energy underestimated the measured. The assumption that soil heat flux can be neglected, introduces a relatively greater mean systematic error apart from the random error on the reference latent heat estimate. The grass Penman-Monteith estimated latent heat was overestimated due to ignored soil heat flux density and underestimated due to the estimated soil heat flux density. The estimated reflection coefficient also underestimated the latent heat.

Estimating or measuring soil heat flux density and net long wave irradiance is difficult. Therefore the best option of estimating the available energy in the absence of direct measurement can be obtained by calibrating the net irradiance and soil heat flux density estimation approach. The use of this estimation approach, which accounts more of the microclimate measures, can be more accurate.

CHAPTER 7

PERFORMANCE OF ET-GAGE EVAPORIMETER AND MICROMETEOROLOGICAL TECHNIQUES FOR MEASURING EVAPORATION

7.1 INTRODUCTION

Simpler and less expensive methods of reference evaporation estimation, using the ET-gage evaporimeter and two micrometeorological techniques are evaluated. The measured ET-gage and the reduced set Penman-Monteith reference evaporation estimates are compared with grass and alfalfa based Penman-Monteith reference evaporation estimates from full set of AWS data. The usefulness of the reduced set assumption are investigated using an hourly and daily time step. Furthermore, the ET-gage evaporimeter measurement of reference evaporation is compared with STEB measures of reference evaporation. The sensitivity of the ET-gage evaporimeter to microclimate measures is investigated by comparison with reference evaporation estimates of Penman-Monteith and STEB using wind speed, air temperature and water vapour pressure, which were all measured at 1 and 2 meter heights for the Agrometeorology site. For Ukulinga (under shade) and Cedara, these measurements were at 2 meter height. The response of the ET-gage evaporative surface to microclimate measures is investigated using measurements of the STEB.

The STEB measure of reference evaporation is compared with the grass based Penman-Monteith approach. The error of using estimated available energy (I_{net} - G) is investigated with the technique. The STEB is evaluated for stability using corrected and uncorrected sensible heat measurements.

7.2 MATERIALS AND METHODS

7.2.1 Instrumentation

7.2.1.1 *ET-gage*

The ET-gage evaporimeter (with canvas 30 and 54) located at the Agrometeorology site was used to measure evaporation from short and long grass surfaces for 155 and 86 days (in 2001 and 2002) respectively. The ET-gage with canvas 30 was placed in the middle of the short grass (0.12 m) area close to an AWS. The ET-gage with canvas 54 was placed in an area of long grass (0.50 m). It was placed 50 m away from an AWS. In another experiment at the same site, two ET-gages were covered with canvas 54 and placed within a short grass area for 19 days. The ET-gages were placed close to each other, 300 mm apart, with evaporation surface 1 m above the canopy surface. Campbell Scientific CR7X and 21X data loggers were used to collect the data every 30 seconds and to store the 15-minute cumulative measures.

ET-gage evaporation measurements from Cedara and Ukulinga were used to investigate the sensitivity of the evaporimeter to different microclimates. The Cedara ET-gage measurement (ET-gage, Model A) was collected from an ET-gage evaporimeter placed within short grass 500 m away from an AWS. The data from the Cedara ET-gage was collected visually (every morning at 8:00 am). The Ukulinga measure (ET-gage, Model E) was for a tomato crop grown under white colour shade adjacent to an AWS. The solar irradiance transmission of the white colour shade was 76 %. The 21X data logger was used to collect the data.

7.2.1.2 Automatic weather station (AWS)

An AWS was used to measure the microclimatic variables required to compute hourly and daily reference evaporation using the Penman-Monteith approach at the Agrometeorology site. Solar irradiance was measured using the CNR1 component net radiometer and rainfall measured using a Rain-O-Matic rain gauge. The data was collected at every 30 seconds and totalled every 15-minutes. The wind speed was measured using two three-cup anemometers in conjunction with a wind direction sensor at one and two meters. Similarly, two Vaisala CS500 air temperature and relative humidity sensors in their Gill shield were used at a height of one and two meters. The average 15-minute solar irradiance, wind speed and air temperature data were collected from the 30-second scan rates. Using Eq. 6.5, water vapour pressure was calculated from the sampled 15-minute relative humidity and average air temperature. In addition to this measurement, data collected from the Cedara and Ukulinga AWS systems were used to compute reference evaporation. Data measured from the sensors were collected using the CR7X and 21X data loggers.

7.2.1.3 Infrared thermometer (IRT) and additional instruments

The energy balance of the grass surface at the Agrometeorology site and ET-gage evaporation surface were evaluated from the measured surface temperature. The Apogee IRTS-P infrared thermometer (IRT) was used to monitor the surface temperature of the short grass surface. The IRT was placed at a height of 1.5 m and positioned to face south at an angle of 45^0 below the horizontal. Measurements were taken every 30 seconds and averaged every 15-minutes. Thermocouples (type E, 0.5 and 0.254 mm in diameter) were also used to measure the surface temperature of the grass. The data was collected using data loggers (CR7X, 21X).

Measurements of the ET-gage surface were collected using an Apogee IRT, Model 310 Middleton miniature net radiometer and two thermocouples (type E, 0.254 mm diameter). The IRT was positioned 90^0 angle to the centre of the ET-gage surface and 200 mm above the surface. The 200 mm distance was calculated using the ratio of evaporimeter diameter to distance away ratio of 1:3 given by the manufacturer. Type E thermocouples were placed under the canvas cover of the ET-gage and a second at the base of the PVC reservoir. Using a 21X data logger, 15-minute average data was collected for a 10-second scan rate.

Net irradiance and soil heat flux density of the grass surface was measured using the CNR1 component net radiometer and two soil heat flux plates. The plate heat flux density was added to the stored heat flux density to calculate the soil heat flux density using the procedure described in the previous chapter (Section 6.2.1).

7.2.2 Methods

7.2.3 Reference Evaporation Equations

2.2.2.1 Hourly equations

Two hourly grass based Penman-Monteith approaches were used to estimate reference evaporation from the microclimatic measures. The approach recommended in Campbell (undated) notes is given in Eq. 6.1 and FAO (1998) Penman-Monteith approach in mm h^{-1} is given as:

$$ET_o = \frac{\Delta(I_{net} - G) + \gamma\lambda(37/(T_a + 273))U(e_s - e_a)}{\Delta + \gamma} \qquad 7.1$$

where the net irradiance (I_{net}) is evaluated differently as discussed in previous chapter (see Appendix 2.2 for procedures of calculating the parameters). The reduced set Penman-Monteith

reference evaporation was calculated using the approximated wind speed and estimated water vapour pressure (kPa) from the previous day minimum air temperature ($T_{p\,min}$) as:

$$e_a(T_{p\,\min}) = 0.6108\exp(17.2694T_{p\,\min}/(237.3+T_{p\,\min})). \quad 7.2$$

Alfalfa based Penman-Monteith reference evaporation was estimated using Eq. 6.1 where the canopy resistance (r_c) and aerodynamic resistance (r_a) were evaluated using Eqs 4.31 and 4.33 (Allen *et al.* 1989; Jensen *et al.* 1990).

7.2.2.2 Daily equations

The 24-hour Penman-Monteith approach of FAO (Eq. 2.13) and cumulative hourly Penman-Monteith version of Campbell (undated) (Eq. 6.1) and FAO (Eq. 7.1) were used to estimate daily reference evaporation (mm), where the daily value of Eqs 6.1 and 7.1 were calculated as:

$$\text{daily reference evaporation} = \sum_{i=1}^{24} ET_o . \quad 7.3$$

The daily water vapour pressure deficit (*VPD,* kPa) using the reduced set assumptions was estimated using the daily maximum (T_{max}) and minimum (T_{min}) air temperature and previous day minimum air temperature ($T_{p\,min}$) as:

$$VPD = \frac{e_s(T_{\max})+e_s(T_{\min})}{2} - e_a(T_{p\,\min}) . \quad 7.4$$

7.2.3 Energy Balance Equations

7.2.3.1 Surface temperature energy balance (STEB)

The simplified energy balance equation (I_{net} - L_vF_w - F_h - G = *0*) can be used to express the energy balance of grass and the ET-gage evaporation surfaces. For calculating latent heat flux (L_vF_w) as a residue from the equation, the net irradiance (I_{net}) and soil heat flux density (G) of grass surface were measured as described in Chapter 6 (Section 6.2.1). In the case of the ET-gage, G would represent the heat flux density stored in the canvas cover and ceramic.

The net irradiance and the net change in internal energy flux density of the evaporation surface (ceramic porcelain plus canvas cover) of the ET-gage were obtained using the miniature net radiometer and thermocouple (type E, 0.254 mm diameter). The density of ceramic (ρ_c = porcelain) was taken as 2450 kg m^{-3} (http://www.technoceramic.com/technical.htm.). The specific heat capacity of the evaporation surface (c_s) was calculated from specific heat capacity of water on the pore spaces of surface (c_w = 4190 J kg^{-1} K^{-1}) and specific heat capacity of ceramic surface (c_c = 1085 J kg^{-1} K^{-1}) (Glenn 2003). The water content of the evaporation surface was assumed to be 25 % of

the total volume of evaporation surface, although the value did not significantly alter the calculation. The ceramic thickness (Δz) is 3 mm (Altenhofen 1985; Broner and Law 1991). The difference of surface temperature (dT) of the ceramic over time interval dt (= 900 s) was used to estimate the stored heat of the evaporating surface:

stored heat flux density in ceramic $= \rho_c \, c_s \, \Delta z \, dT / dt$. 7.5

The miniature net radiometer was positioned so as to view 80 % of the evaporation surface of the ET-gage. The view factor (F) was calculated as:

$$F = \frac{A}{A + \pi d} \qquad 7.6$$

where A is the area of ceramic evaporation surface (m^2) and d is the diameter of surface (= 79 mm) (Savage *et al.* 1997).

The sensible heat energy flux density of grass and ET-gage surfaces may be expressed using a resistance law (Eq. 2.9), assuming the surface temperature (T_s) measured with infrared thermometer (IRT) and thermocouple (T_c) equals T_o. Eq. 2.9 was then solved iteratively after r_a was corrected for stability using the Campbell and Norman (1998) and Monteith (1973) procedures.

Simplified aerodynamic resistance equation (Eq. 4.31) can be rewritten and the parameter estimated as:

$$r_a = \left[\frac{\ln((z - d + z_H)/z_H)}{k u_*} \right] + \Psi_M \qquad 7.7a$$

where u_* is the friction velocity (m s^{-1}) defined by:

$$u_* = \frac{k u}{\ln[(z - d - z_M)/z_M] + \Psi_M} \qquad 7.7b$$

where z is the measurement height of wind speed and air temperature (m), h_c is crop surface height (m), d is the zero plane displacement (= 0.67 h_c), z_M is momentum roughness parameter (= 0.12 h_c), z_H is sensible heat roughness parameter (= 0.1 z_M) after Smith (1991), k is von Karman's constant (= 0.41) and Ψ_M is dimensionless momentum stability correction factor (cited from Savage *et al.* 1997).

Monin-Obukhov (1946) defined an atmospheric stability parameter (ξ) as:

$$\xi = \frac{-kzgF_h}{c_p \rho T_a u_*^3} \qquad 7.7c$$

where g is the gravitational acceleration (= 9.8 m s^{-1}), F_h is the sensible heat flux density (W m^{-2}) and T is the air temperature (K), ρ is density of air (kg m^{-3}) and c_p specific heat capacity of air (J kg^{-1} K^{-1}).

The Campbell and Norman (1998) stability correction for unstable atmospheric condition ($\xi < 0$), the stability correction factor for sensible heat (Ψ_H = dimensionless) is calculated as:

$$\Psi_H = -2\ln\left[\frac{1+\sqrt{1+16\xi}}{2}\right] \qquad 7.8a$$

and for momentum (Ψ_M):

$$\Psi_M = 0.6\Psi_H . \qquad 7.8b$$

For stable conditions ($\xi > 0$) the stability parameters are calculated from

$$\Psi_M = \Psi_H = 6\ln(1+\xi). \qquad 7.8c$$

The initial value of F_h was calculated using the uncorrected r_a from Eq. 4.31 (assuming $\Psi_M = \Psi_H = 0$). Based on the sign of stability (ξ), Ψ_M and Ψ_H were calculated from Eqs 7.8*a*, 7.8*b* and 7.8*c*. Then r_a and u_* were calculated from Eqs 7.7*a* and 7.7*b*. The sensible heat flux was then calculated from Eq. 2.9 using the corrected r_a value.

The Monteith (1973) stability correction is computationally more simpler. The empirical approach consists of two steps. The uncorrected aerodynamic resistance was calculated as:

$$r_a = \frac{[\ln(\frac{z-d}{z_M})]}{ku^2} \qquad 7.9a$$

and then the corrected value as:

$$r_{am} = r_a\left[1-\left[\frac{n(z-d)g(T_s-T_a)}{Tu^2}\right]\right] \qquad 7.9b$$

where T is average temperature of the surface (T_s) and air (T_a) in Kelvin and n is a number that describes atmospheric stability conditions (n = 5 is taken as the best estimate for transpiring plants). For r_{am} less than 15 s m^{-1}, 15 s m^{-1} was used to calculate sensible heat flux density (Kjelgaard *et al.* 1996).

In a similar manner, the sensible heat flux density from the ET-gage evaporation surface (STEB, with and without correction) was calculated using Eq. 2.9. In each case the calculated aerodynamic resistance from Eqs 4.31, 7.7*a* and 7.9*b* were added to the mean canvas 54 diffusion resistances. The canvas 54 diffusion resistances were assumed to be equal to 200 s m^{-1}, which is the maximum value of alfalfa leaf diffusion resistance (Altenhofen 1985). The Altenhofen (1985) diffusion resistance measurement for the ceramic surface canvas 54 was between 100 and 300 s m^{-1}.

The 15-minute evaporation measure computed using the STEB technique and the stability correction procedure Monteith (1973) ($STEB_{MC}$) and Campbell and Norman (1998) ($STEB_{CC}$) and without stability correction ($STEB_{UN}$) and with estimated (I_{net} - G) were totalled and compared with the daily measure of reference evaporation of ET-gage and Penman-Monteith using measured I_{net} - G values.

7.3 PENMAN-MONTEITH APPROACH

7.3.1 Introduction

The estimate of reference evaporation using the grass- and alfalfa-based Penman-Monteith method normally requires measurement of the four microclimatic measures: solar irradiance, air temperature, relative humidity and wind speed. However, the reduced set Penman-Monteith requires the measurement of solar irradiance and air temperature, an approximation of wind speed and an assumption to the water vapour pressure to compute reference evaporation. The reduced set Penman-Monteith approach has been compared with grass Penman-Monteith and was reported to have a 10 % error (unpublished Campbell Scientific Inc. 1998).

The significance of the reduced set Penman-Monteith approach, reported by the unpublished Campbell Scientific Inc. (1998) application notes, is based on the assumption that the previous day minimum air temperature is approximately equal to the dew point temperature and the use of approximated wind speed as 2 m s^{-1} or 3 m s^{-1}or average wind speed of the area. The limited data requirement of the reduced set Penman-Monteith approach is attractive. However the validity of the assumption depends on the climate of the location since the minimum air temperature can be greater than the dew point temperature in an arid environment where the wind speed can play a great role. So the performance of the reduced set Penman-Monteith method has focused on the assumptions and potential for wider climate application. Savage *et al.* (1998) showed a 38 % underestimation of daily reference evaporation due to water vapour pressure estimated from the previous day minimum air temperature and use of surrogate wind speed (1.3 m s^{-1}) in comparison to

the hourly sum (for a day) of grass Penman-Monteith reference evaporation estimate. In this chapter, the assumptions and reliability of the approach for this particular measurement site are investigated. The hourly sum of the reduced set Penman-Monteith estimate of reference evaporation is compared with the grass-based Penman-Monteith using two procedures using hourly data and one procedure using daily data. The reduced set Penman-Monteith reference evaporation calculated from the daily water vapour pressure deficit estimate of T_{min} and T_{max} using Eq. 7.4 and approximated wind speed (2 m s^{-1}) is compared with hourly sum of grass Penman-Monteith (Eqs 6.1, 7.1) and daily Penman-Monteith estimate (Eq. 2.13).

7.3.2 Comparison of the Reduced Set Penman-Monteith Approach

The measured and estimated water vapour pressure deficit (*VPD*), net irradiance, wind speed and estimated latent heat for days of year 54 (summer, 23 February) and 188 (winter, 7 July), 2002 are shown in Fig. 7.1. The average wind speed measured at the site was 1.03 m s^{-1}. It was only for 17 % of the period that a wind speed was greater than or equal to 2 m s^{-1}.

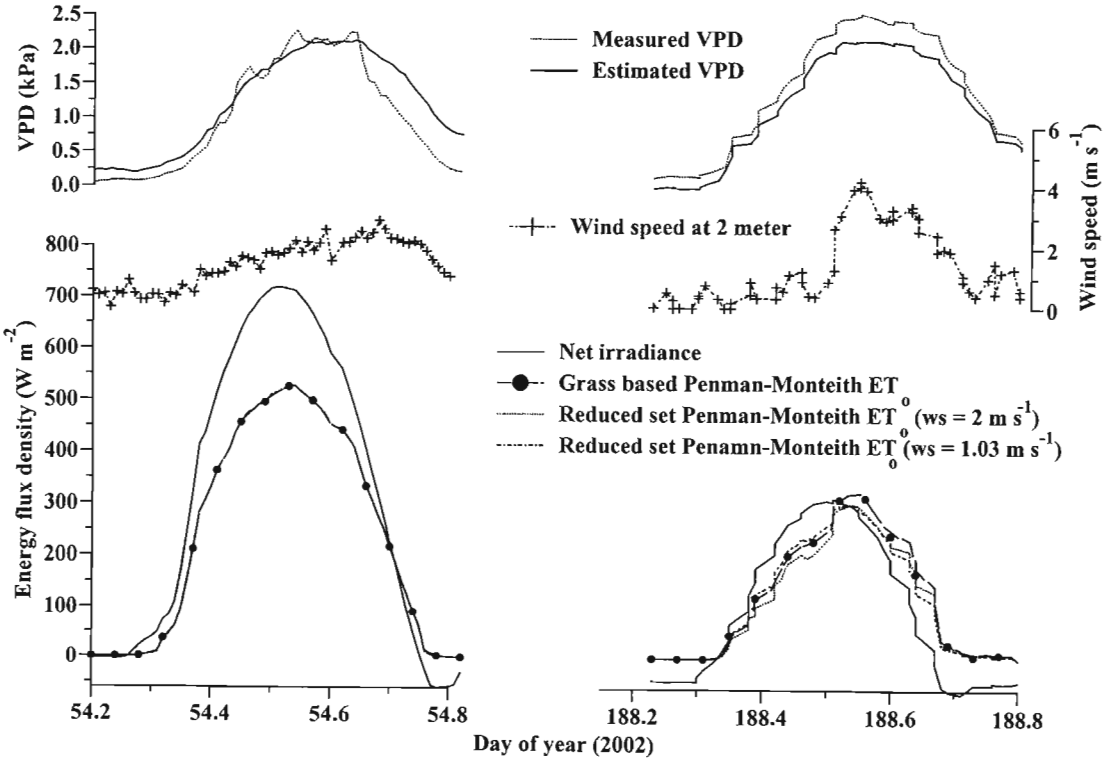

Fig. 7.1 Diurnal variation of net irradiance, measured and estimated water vapour pressure deficit (*VPD*), wind speed from 2 meter and hourly sum of estimated reduced set grass Penman-Monteith reference evaporation (using 2 and 1.03 m s^{-1} wind speed (ws)) and grass Penman-Monteith reference evaporation for the days of year 54 and 188, 2002, at the Agrometeorology site. Note: 250 W m^{-2} latent heat is equivalent to a reference evaporation (mm h^{-1}) of 0.37

The reference evaporation comparison of hourly sum and daily reduced set Penman-Monteith reference evaporation, using 2 and 1.03 m s^{-1} wind speed is shown (Table 7.1, Figs 7.2*a,* 7.2*b*). The regression analysis indicates that the slope of grass reduced set Penman-Monteith estimate (with 2 m s^{-1}) compared to the grass Penman-Monteith reference evaporation (Eq. 6.1) relationship is not significantly different from one ($\alpha = 0.05$) and the overestimate of the reference evaporation was only 2 %. However the reduced set Penman-Monteith reference evaporation estimate using a wind speed 1.03 m s^{-1} was 10 % greater compared to hourly sum of grass Penman-Monteith estimate (Eq. 6.1). The reference evaporation was very well estimated when a 2 m s^{-1} wind speed was used. Table 7.1 and Fig. 7.2*b* shows the correlation of daily procedure of reference evaporation estimate of reduced set Penman-Monteith using Eq. 2.13 and hourly sum of Eq. 7.1 when water vapour pressure deficit was estimated from Eq. 7.4 and a wind speed of 2 m s^{-1} was used.

Table 7.1 Statistical data associated with grass-based Penman-Monteith reference evaporation (GPM) and reduced set Penman-Monteith (RPM) using two hourly and one daily procedure (mm day^{-1}) (n = 155, for the period December 27, 2001 to July 12, 2002, at the Agrometeorology site)

Statistical Information	Campbell hourly grass Penman-Monteith (Eq. 6.1) *vs*				FAO hourly grass Penman-Monteith (Eq. 7.1) *vs*		
	RPM-2	RPM-1.03	24-GPM	24-RPM	RPM-2	24-RPM	24-GPM
r^2	0.987	0.981	0.918	0.720	0.955	0.650	0.893
Intercept (mm)	-0.077[1]	-0.072[2]	0.191	-0.187	0.092[1]	-0.384	-0.177[2]
Slope	1.029[1]	1.101	0.900	0.683	1.038[1]	0.639	0.874
$SE_{intercept}$ (mm)	0.030	0.039	0.070	0.112	0.068	0.140	0.091
SE_{slope}	0.009	0.012	0.022	0.034	0.018	0.038	0.025
S_{yx} (mm)	0.167	0.219	0.389	0.617	0.332	0.690	0.447
MSE_{uns}(mm)	0.027	0.047	0.149	0.375	0.109	0.470	0.197
MSE_{sys} (mm)	0.001	0.070	0.031	1.440	0.052	2.891	0.403
RMSE (mm)	0.169	0.342	0.424	1.347	0.400	1.833	0.774

[1]Null hypothesis is that slope is 1 and intercept 0; statistically significant at the 99 % level of significance, [2]null hypothesis is that slope is 1 and intercept 0; statistically significant at the 95 % level of significance, GPM is the grass based hourly (Eqs 6.1, 7.1) and 24-GPM is the daily (Eq. 2.13) Penman-Monteith, 24-RPM is the daily reduced set Penman-Monteith (Eq. 2.13) using a wind speed of 2 m s^{-1}, RPM-2, RPM-1.03 is the hourly sum of reduced set Penman-Monteith using wind speed of 2 and 1.03 m s^{-1} respectively, SE_{slope} is the standard error of slope, $SE_{intercept}$ is the standard error of intercept, S_{xy} is the standard error of estimate of y on x, MSE_{sys}, MSE_{uns}, RMSE are systematic, unsystematic and root mean square errors respectively, r^2 is the correlation coefficient

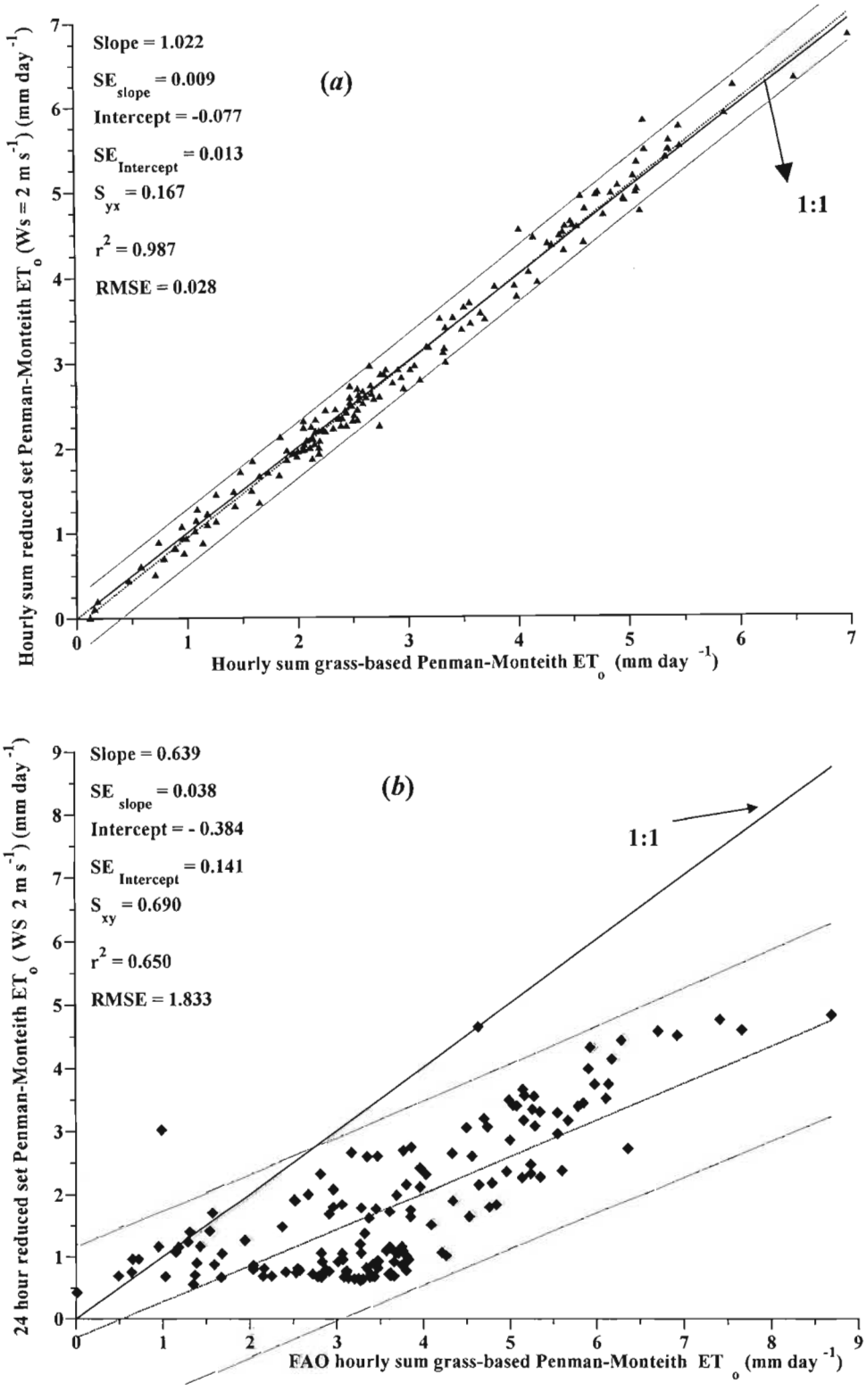

Fig. 7.2 Comparison of hourly sum of grass-based Penman-Monteith ET_o (Eqs 6.1, 7.1) *vs* (***a***) sum of hourly reduced set Penman-Monteith ET_o (Eq. 6.1) and (***b***) daily reduced set Penman-Monteith ET_o estimate (Eq. 2.13)) using wind speed of 2 m s^{-1} for measurement period between December 27, 2001 to July 12, 2002, at the Agrometeorology site

The r^2 value of daily procedure of reduced set estimate was much lower compared to the hourly estimate. This may be the result of the poor estimate of the daily water vapour pressure deficit (*VPD*) from T_{max} and T_{min}. A similar result was also reported by Savage *et al.* (1998). Table 7.1 shows the statistical summary of hourly sum and daily procedure estimate of grass Penman-Monteith reference evaporation estimate. The daily procedure of reference evaporation estimate (Eq. 2.13) underestimated the reference evaporation by 13 % compared to both procedures of hourly grass reference evaporation estimate (Eqs 6.1, 7.1).

The use of hourly procedures better described the microclimate than the daily estimate. Even the hourly reduced set Penman-Monteith showed comparatively better accuracy than the daily reduced set and full set grass reference evaporation estimate using an estimated wind speed of 2 m s^{-1} for the site.

7.4 SURFACE TEMPERATURE ENERGY BALANCE (STEB)

7.4.1 Introduction

Surface temperature, when measured remotely, offers a method for measuring evaporation using a simplified energy balance of the crop surface (Eq. 2.9). The STEB technique of measuring latent heat has three principal variables: the available energy flux density I_{net} - G, surface-air temperature difference T_o - T_z and aerodynamic resistance r_a. Hatfield *et al.* (1984) found a 10 % or less error when using the STEB method in measuring evaporation under full ground cover. Several studies have used the STEB method to calculate evaporation (Hatfield *et al.* 1983*a*; Hatfield *et al.* 1984; Choudhury *et al.* 1986; Huband and Monteith 1986; Choudhury *et al.* 1987; van Zyl and de Jager 1992; Kjelgaard *et al.* 1994, 1996; Lukangu 1997; Savage *et al.* 1997).

The technique has been applied using estimated and measured available energy. Kjelgaard *et al.* (1996) found the method gives good results using estimated available energy. Choudhury *et al.* (1987) used an estimated soil heat flux density (Eq. 4.29) to estimate evaporation from a wheat crop and obtained a correlation coefficient of 0.97 and standard error 3.9 W m^{-2}. Furthermore the Monteith (1973) adjustment coefficient and Campbell and Norman (1998) iteration procedures for atmospheric stability correction were applied to the aerodynamic resistance for different crops. The evaporation term calculated as a residual of STEB with and without corrected aerodynamic resistance was compared with Bowen ratio, lysimeter and Penman-Monteith methods from different crop surfaces (Hatfield *et al.* 1984; van Zyl and de Jager 1992; Kjelgaard *et al.* 1994, 1996; Lukangu 1997). van Zyl and de Jager (1992) found that the Monteith (1973) stability corrected

reference evaporation to be reliable in the presence of advective energy in comparison with lysimeter evaporation for a short grass surface.

Full and uniform canopy cover is the requirement for successful application of the technique, which is the ideal character of a reference crop. The STEB measure of reference evaporation is evaluated for the short grass surface. The stability-corrected and uncorrected STEB estimate of reference evaporation is compared with hourly grass based Penman-Monteith estimates. The STEB-measured evaporation using measured and estimated available energy (I_{net} - G) is compared with the hourly grass based Penman Monteith reference evaporation estimate.

7.4.2 Measurement of Sensible Heat and Aerodynamic Resistance

The sensible heat from a short grass surface was evaluated from the surface-air temperature difference and aerodynamic resistance using Eq. 2.9. The surface-air temperature difference is a driving force of heat flow. It determines the sign and magnitude of sensible heat flux density. The aerodynamic resistance of sensible heat flux density is governed by atmosphere turbulence of atmosphere and also determines the magnitude of the flux.

The grass surface to air temperature difference (T_s - T_a), wind speed and sensible heat flux density F_h for cloudless days of year 365 (2001), 1, and 9 (2002) are shown in (Figs 7.3*a*, 7.3*b*). The daytime average temperature of grass surface was 4.3, 4.4 and 5.6 °C warmer than air temperature at 2 meter above the grass surface for the days of year 1 and 9 (2002) and 365 (2001) respectively. While the grass surface was 6.5 and 6.7 °C cooler than air temperature on the day of year 159 (2002) from 2 and 1 meter respectively. The stability correction Monteith (1973) procedure for aerodynamic resistance (Eqs 7.9*a*, 7.9*b*) was observed to be very sensitive to a higher and lower than zero grass surface-air temperature difference (see Figs 7.3*a*, 7.3*b*) and resulted in a higher sensible heat relative to the uncorrected and Campbell and Norman (1998) stability corrected sensible heat. Similar results were also reported for maize and potato crop surfaces (Kjelgaard *et al.* 1996). The sensible heat calculated from Campbell and Norman (1998) procedure stability correction of aerodynamic resistance closely followed the uncorrected sensible heat. Most of the time the sensible heat calculated with corrected aerodynamic resistance of Monteith (1973) and Campbell and Norman (1998) procedure were in close agreement, with the uncorrected for the (T_s - T_a) difference close to zero.

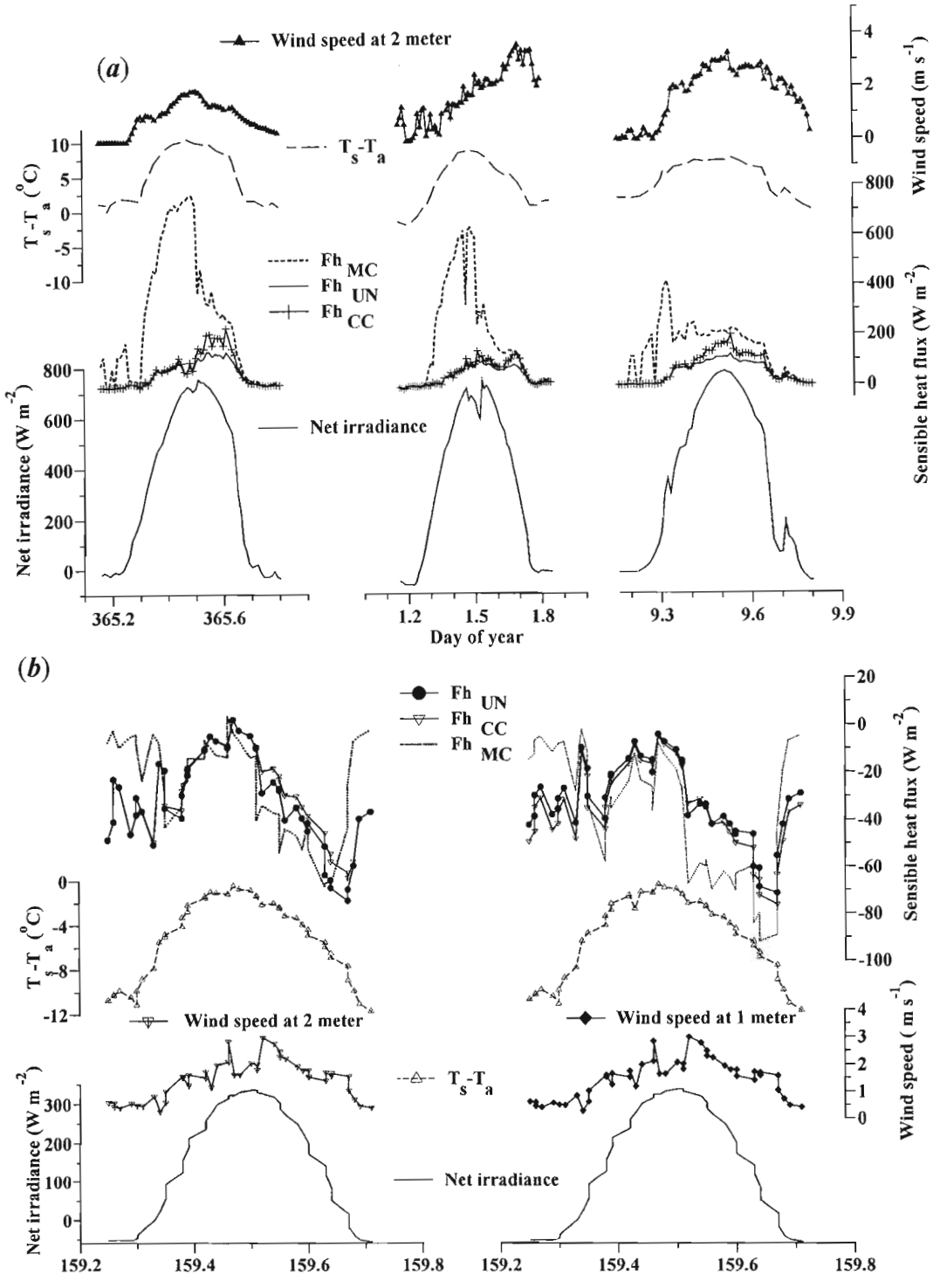

Fig. 7.3 Diurnal variation of sensible heat flux density (F_h), net irradiance, grass surface-air temperature difference (T_s - T_a) and (***a***) wind speed at 2 meter for the days of year 365 (2001) and 1, 9 (2002) (***b***) wind speed measured from 1 and 2 meter for the day of year 159 (2002) ($_{UN}$ is the uncorrected, $_{CC}$ is the Campbell and Norman (1998) corrected, $_{MC}$ is the Monteith (1973) corrected), at the Agrometeorology site

7.4.3 Measurement of Evaporation Using the STEB

A statistical comparison of the 15-minute cumulative daily evaporation from STEB measure (with and without atmospheric stability correction) and hourly sum of grass based Penman-Monteith reference evaporation (Eq. 6.1) using the measured available energy flux density I_{net} - G is shown in (Table 7.2; Figs 7.4*a*, 7.4*b*, 7.5*a*, 7.5*b*,). Compared to the corrected, the uncorrected STEB evaporation estimates a better correlate with grass Penman-Monteith estimate of reference evaporation.

A regression analysis (Table 7.2, Figs 7.4*a*, 7.4*b*) shows that the uncorrected $STEB_{UN}$ and Campbell and Norman (1998) procedure corrected $STEB_{CC}$ evaporation measure overestimate the evaporation by 9 % and 6 % compared to the grass-based Penman-Monteith estimate respectively. The Monteith (1973) procedure using corrected $STEB_{MC}$ underestimate the daily evaporation by 4 % but with greater RMSE (Fig. 7.5*a*). The slope of the $STEB_{MC}$ estimate is not significantly different from one (α = 0.05). However, the slope and intercept of the regression $STEB_{UN}$ and $STEB_{CC}$ were found to differ from one and zero significantly.

Table 7.2 Daily sum of 15-minute sum of STEB reference evaporation compared with hourly sum of Penman-Monteith reference evaporation estimates (mm) (n =155 days for the period December 27, 2001 to July 12, 2002, at the Agrometeorology site)

Statistical	$STEB_{UN}$	$STEB_{CC}$	$STEB_{MC}$	STEB (I_{net} - G)
Correlation coefficient (r^2)	0.955	0.938	0.715	0.936
Intercept (mm)	0.478	0.467	0.652	0.253
Slope	1.105	1.086	0.963[1]	1.176
Standard error of intercept ($SE_{intercept}$) (mm)	0.064	0.074	0.162	0.082
Standard error of slope (SE_{slope})	0.019	0.023	0.049	0.025
Average (mm)	3.772	3.705	3.522	3.759
Standard error of estimate of y on x, S_{yx} (mm)	0.335	0.391	0.852	0.433
MSE_{uns} (mm)	0.111	0.151	0.717	0.185
MSE_{sys} (mm)	0.648	0.539	0.296	0.668
Root mean square error (RMSE) (mm)	0.871	0.831	1.001	0.923

[1]The slope is 1 at 95 % significance level, MSE_{uns} and MSE_{sys} are the unsystematic and systematic root mean square errors respectively, S_{yx} is the, $_{CC}$ indicated the Campbell and Norman (1998) procedure corrected, $_{MC}$ the Monteith (1973) procedure corrected, $_{UN}$ the uncorrected and I_{net} - G the STEB with estimated available energy flux density

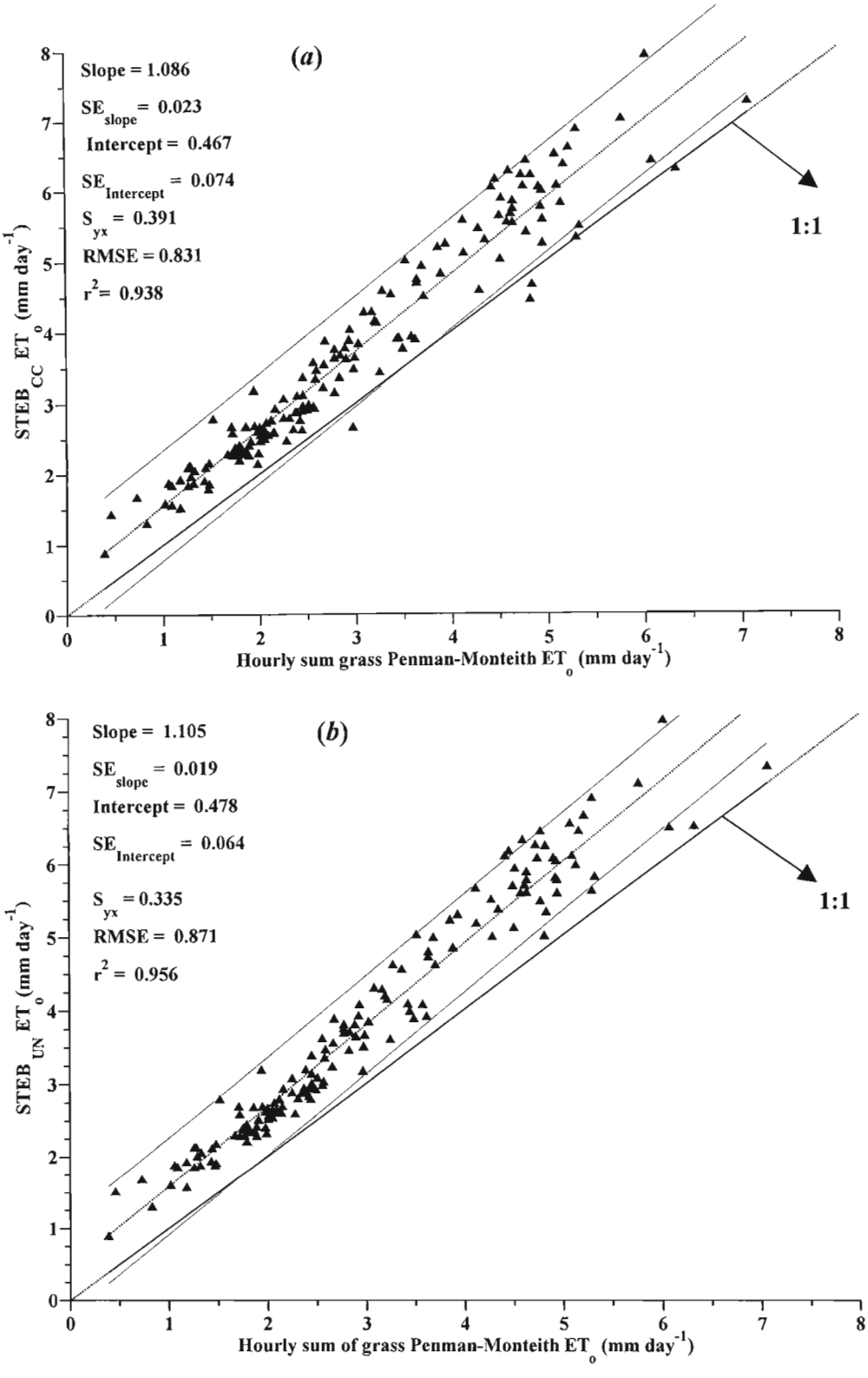

Fig. 7.4 Comparison of daily values of grass Penman-Monteith ET_o *vs* (***a***) Campbell and Norman (1998) procedure corrected STEB ET_o ($STEB_{CC}$) and (***b***) uncorrected STEB ET_o ($STEB_{UN}$) for the measurement period between December 27, 2001 to July 12, 2002, at the Agrometeorology site

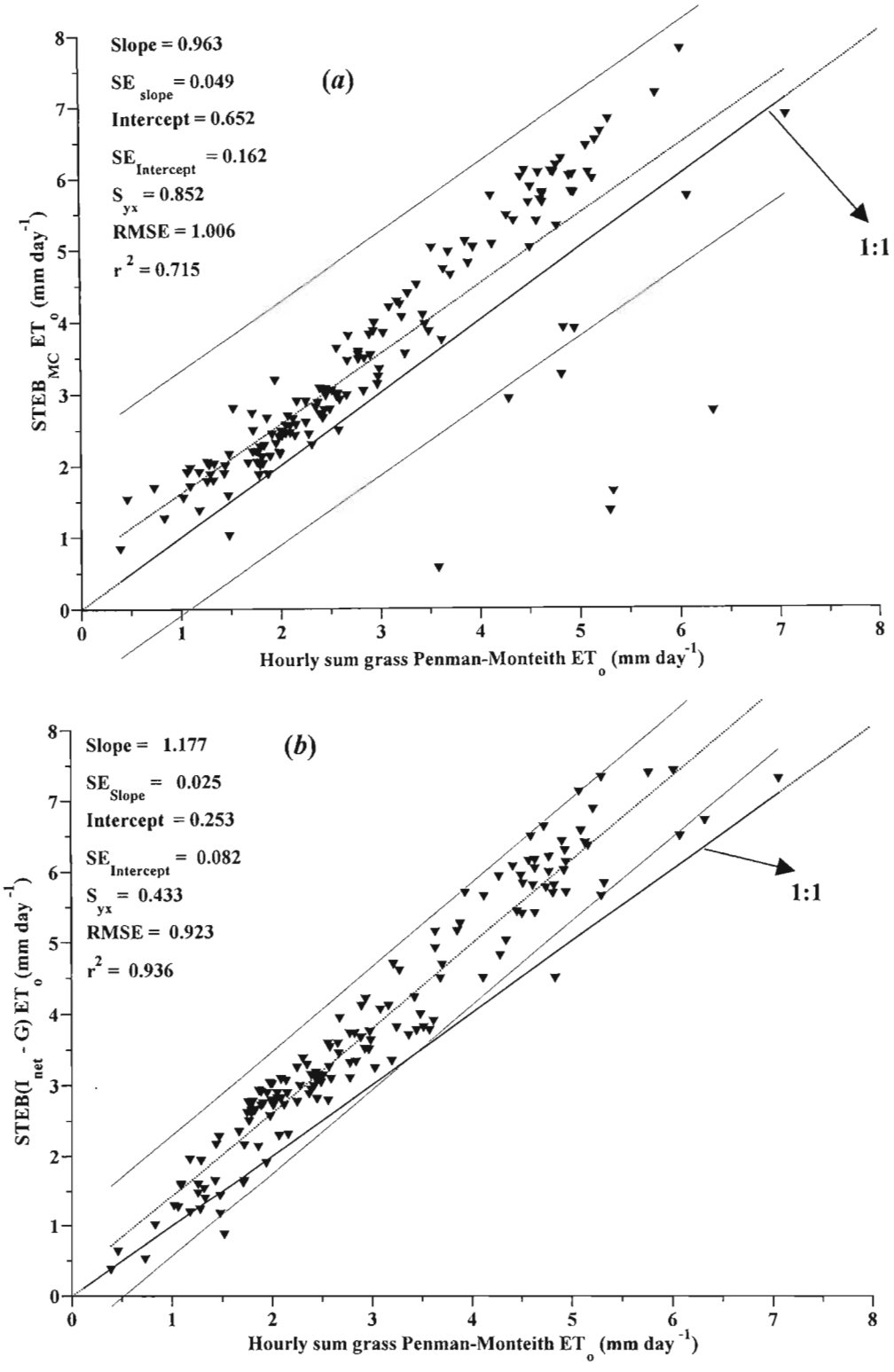

Fig. 7.5 A comparison of daily values of reference evaporation determined using grass Penman-Monteith *vs* (***a***) Monteith (1973) procedure corrected STEB values ($STEB_{MC}$) and (***b***) uncorrected STEB using estimated available energy (STEB (I_{net} - G) ET_o) values for the measurement period between December 27, 2001 to July 12, 2002, at the Agrometeorology site

Using the Campbell (undated) notes estimate of (I_{net} - G), the daily sum of 15-minute $STEB_{UN}$ evaporation estimates *vs* hourly sum of grass Penman-Monteith reference evaporation (Table 7.2, Fig. 7.5*b*) resulted in an r^2 value 0.936 but with larger RMSE. However, the use of locally calibrated estimation approach of $I_{net} - G$, can improve the accuracy.

7.5. ET-GAGE REFERENCE EVAPORATION

7.5.1 Introduction

Evaporation rate (measured with ET-gage) is based on the change of water level of evaporation surface connected to a reservoir. The performance of the device with canvas 30 and 54 were compared with alfalfa- and grass-based Penman-Monteith and STEB uncorrected reference evaporation estimates. Broner and Law (1991) and Alam and Trooien (2001) reported similarity of the cumulative of three and seven days visual measure of ET-gage and alfalfa-based modified Penman and grass-based Penman-Monteith reference evaporation estimate respectively. Three day cumulative evaporation measure showed 81 % agreement with grass based Penman-Monteith estimate (Alam and Trooien 2001). The performance of the electronic and visual reading of evaporimeter is investigated as daily reference evaporation estimate in comparison with grass and alfalfa based Penman-Monteith and STEB uncorrected estimate of reference evaporation.

The sensitivity of the device is investigated from the evaporation measure for three different microclimates. The STEB measure of evaporation at the Agrometeorology site from the ceramic evaporation surface is compared to the cumulative ET-gage measure.

7.5.2 ET-gage Comparison with Micrometeorological Techniques

The daily electronic evaporation measure of ET-gage using canvas 30 was from 0 to 8.3 mm while using canvas 54 the range was from 0 to 10.1 mm. Daily measures of evaporation with canvas 30 *vs* grass-based reference evaporation estimate of Penman-Monteith (Campbell undated) results in an r^2 value 0.79 and slope 0.88 (Fig. 7.6*a*). The result indicated the underestimation of the reference evaporation by 12 % (Figs 7.6*a*, 7.6*b*). The STEB uncorrected estimates resulted in a lower correlation and higher RMSE (Fig. 7.7*a*). The long grass canvas 54 ET-gage measure of evaporation correlated well with the alfalfa-based reference evaporation estimate of Penman-Monteith (Fig. 7.7*b*, Table 7.3). The r^2 value was 0.66 and RMSE was 1.30 for the long grass. The r^2 value was lower but the underestimation was minimal compared to canvas 30. The slope and intercept were not significantly different from one and zero ($\alpha = 0.05$).

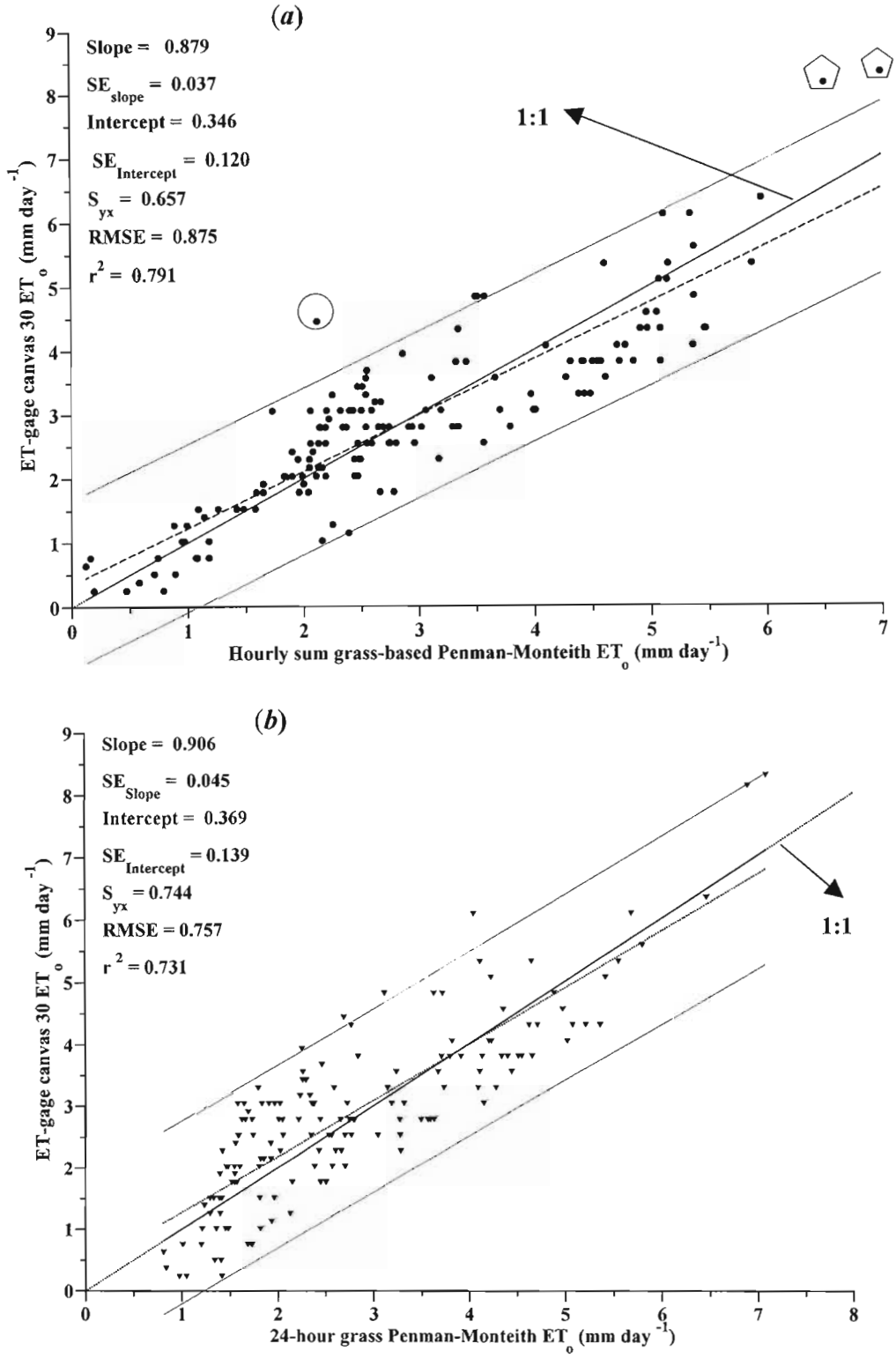

Fig. 7.6 Comparison of daily values of ET-gage canvas 30 evaporation reference evaporation (ET_o) measure *vs* (***a***) hourly sum of grass Penman-Monteith (Eq. 6.1) and (***b***) daily grass Penman-Monteith (Eq. 2.13) for the period of measurement between December 27, 2001 to July 12, 2002, at the Agrometeorology site

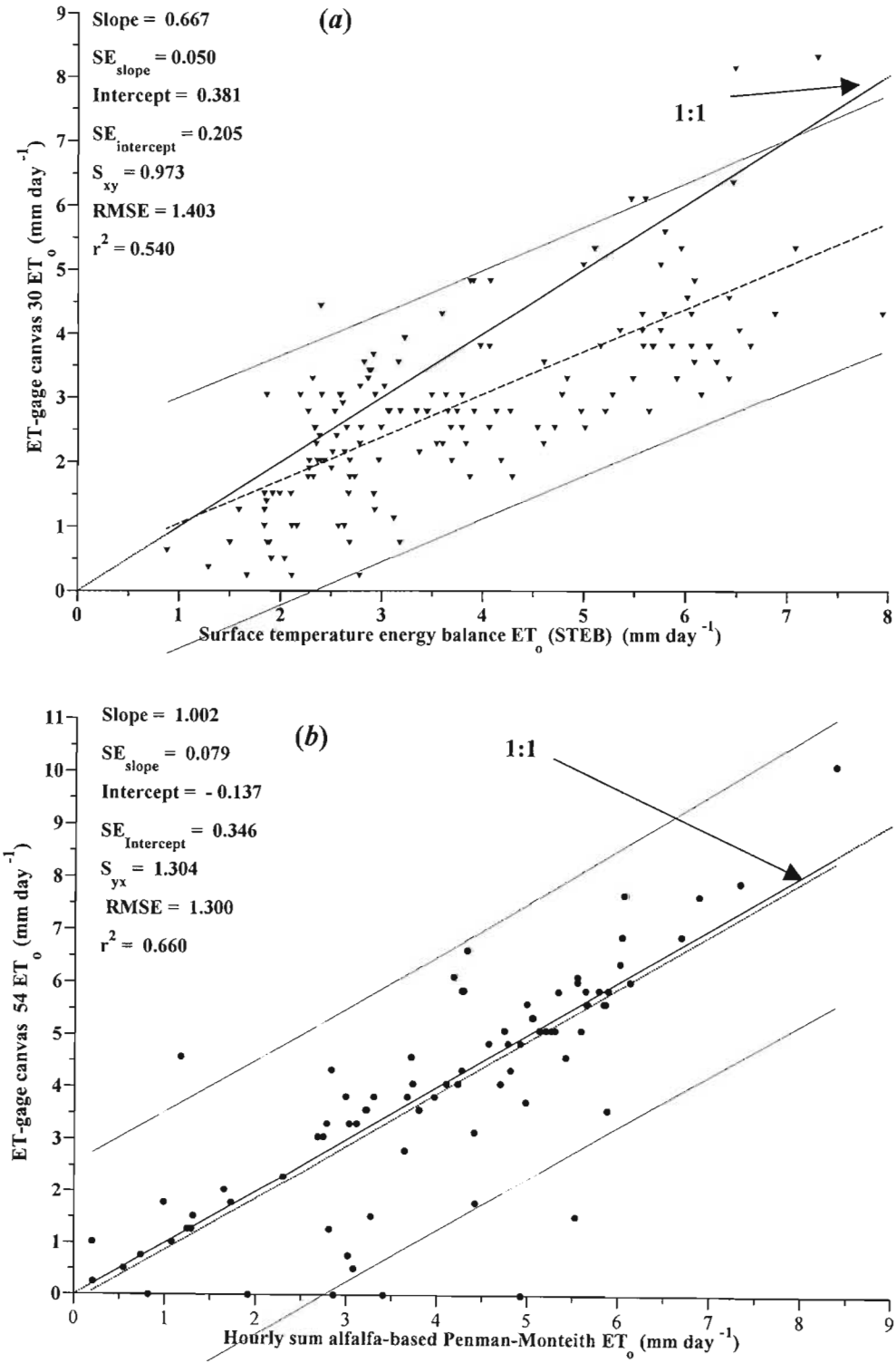

Fig. 7.7 Comparison of daily values of reference evaporation (ET_o) (*a*) uncorrected STEB evaporation *vs* ET-gage canvas 30 and (*b*) hourly sum alfalfa-based Penman-Monteith (Eq. 6.1) *vs* ET-gage canvas 54 evaporation for the period of measurement between December 27, 2001 to July 12, 2002, at the Agrometeorology site

Table 7.3 Comparison of daily ET-gage evaporation *vs* grass (GPM) and alfalfa (ALPM) based Penman-Monteith reference evaporation (Eq. 6.1) and STEB estimate of reference evaporation for short and long grass at the Agrometeorology site

(A) Canvas 30 (n = 152, for period of measurement between December 27, 2001 to July 12, 2002)

Models	r^2	Intercept (mm)	Slope	$SE_{intercept}$ (mm)	SE_{slope}	S_{yx} (mm)	MSE_{uns} (mm)	MSE_{sys} (mm)	RMSE (mm)
GPM	0.791	0.346	0.879	0.120	0.037	0.657	0.426	0.031	0.675
STEB	0.540	0.381[1]	0.667	0.205	0.050	0.973	0.935	1.034	1.403
GPM*	0.732	0.369	0.905	0.139	0.045	0.744	0.546	0.027	0.757

(B) Canvas 54 (n = 84, for period of measurement between December 27, 2001 to July 12, 2002)

Models	r^2	Intercept (mm)	Slope	$SE_{intercept}$ (mm)	SE_{slope}	S_{yx} (mm)	MSE_{uns} (mm)	MSE_{sys} (mm)	RMSE (mm)
ALPM	0.661	-0.137[1]	1.002[1]	0.346	0.079	1.304	1.660	0.017	1.295
STEB	0.468	-0.877[1]	1.017[1]	0.585	0.119	1.633	2.602	0.714	1.821

*Daily grass Penman-Monteith reference evaporation estimated using Eq. 2.13, [1]statistically significant at the 95 % level of confidence, r^2 is the correlation coefficient, MSE_{uns}, MSE_{sys} and RMSE are the unsystematic, systematic and root mean square error respectively, SE_{slope} and $SE_{intercept}$ are the standard error of slope and intercept respectively, S_{yx} is the standard error of estimate of y on x

Three daily data points were excluded from the comparison for the reason of incomplete data measurement of AWS and power failure and priming date of ET-gage. In Fig. 7.6*a* the data point outside the confidence limit indicated by a circle was characterized with rapid change of water vapour pressure deficit and wind speed relative to solar irradiance while the two points indicated by surrounding polygon (upper right) were during clear summer skies for which there was a rapid change of water vapour pressure and variable wind speed.

The 40 days of cumulative evaporation measure of ET-gage canvas 30 and 54 are shown (Fig. 7.8). The measurements were in close agreement with the micrometeorological estimates for the first few days with the difference increasing with time. The canvas 54 response was variable as can be seen in Fig. 7.8. There was a lag in the response of ET-gage canvas 54 reference evaporation on day of year 47 (2002). A higher late response of canvas 54 was noticed starting on day of year 51, 2002 after priming. The canvas 30 measurements remained lower than the hourly sum of Penman-Monteith grass reference evaporation estimates. The STEB measures were much higher than the rest. The average and total evaporation values for the 152 days period is given (Table 7.4).

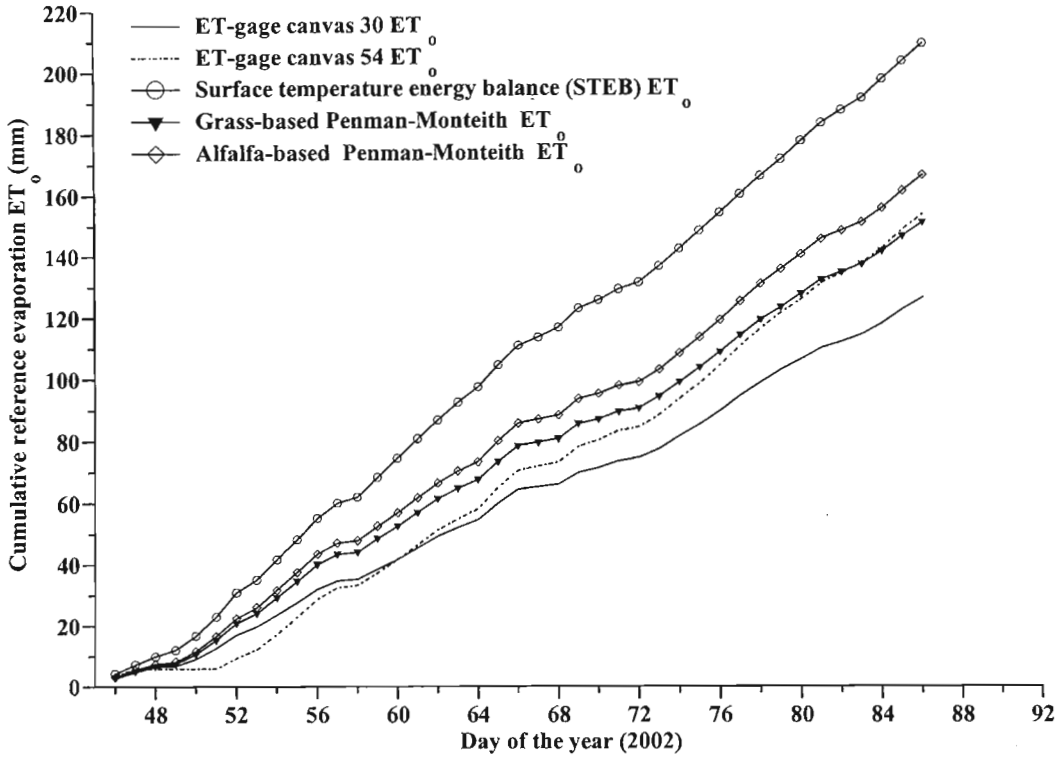

Fig. 7.8 Cumulative evaporation of ET-gage (canvas 30 and 54), hourly sum of grass and alfalfa-based Penman-Monteith reference evaporation and uncorrected STEB measured values (February 14 to March 31, 2002), at the Agrometeorology site

Table 7.4 Average (Avera) and total ET-gage reference evaporation values for three sites (mm day^{-1}) for the ET-gage canvas 30 and for ET-gage canvas 54 compared with hourly sum of Penman-Monteith estimates for grass (GPM), alfalfa (ALPM), the reduced set (RPM) (Eq. 6.1) and the uncorrected STEB reference evaporation estimates

Site	ET-gage (mm)		GPM (mm)		ALPM (mm)		RPM (mm)[1]		STEB (mm)	
	Avera	Total	Avera	Total	Avera	Total	Avera	Total	Avera	Total
Agrometeorology site										
Canvas 30 (n = 152)	2.896	440.2	2.901	441.0			2.89	438.6	3.768	572.7
Canvas 54 (n = 84)	3.852	323.6			3.983	334.3				
Ukulinga (n = 21)										
Canvas 54	2.17	45.47	1.09	22.9	1.19	24.97				
Cedara[2] (n = 225)										
Canvas 54	3.39	762.2	2.55	574.1	3.21	721.3				

[1]Using wind speed of 2 m s^{-1}, [2]ET-gage Model A (manual)

Another indication of ET-gage performance is to analyse how the ET-gage reference evaporation tracks the daily reference evaporation rate (canvas 30, 54). The daily ET-gage measure is shown in Fig. 7.9. From days of year 56 up to 68, 2002 the canvas 30-measured evaporation followed the same trained to the hourly sum of Penman-Monteith grass reference evaporation but always lower. The significant variation of canvas 30 measures was noticed when the average of two ET-gage with canvas 30 was used from days of year 156 up to 168, 2002. The canvas 54 measure followed an irregular pattern compared to the micrometeorological estimate.

7.5.3 ET-gage Sensitivity

The comparison of ET-gage evaporation measures for different microclimates and comparison with the Penman-Monteith approach could be used as an indication of the sensitivity of ET-gage to the microclimate measure. Tables 7.4 and 7.5 show comparisons of measured ET-gage evaporation rate for three different microclimates with computed reference evaporation from the sum of hourly grass and alfalfa based Penman-Monteith approach.

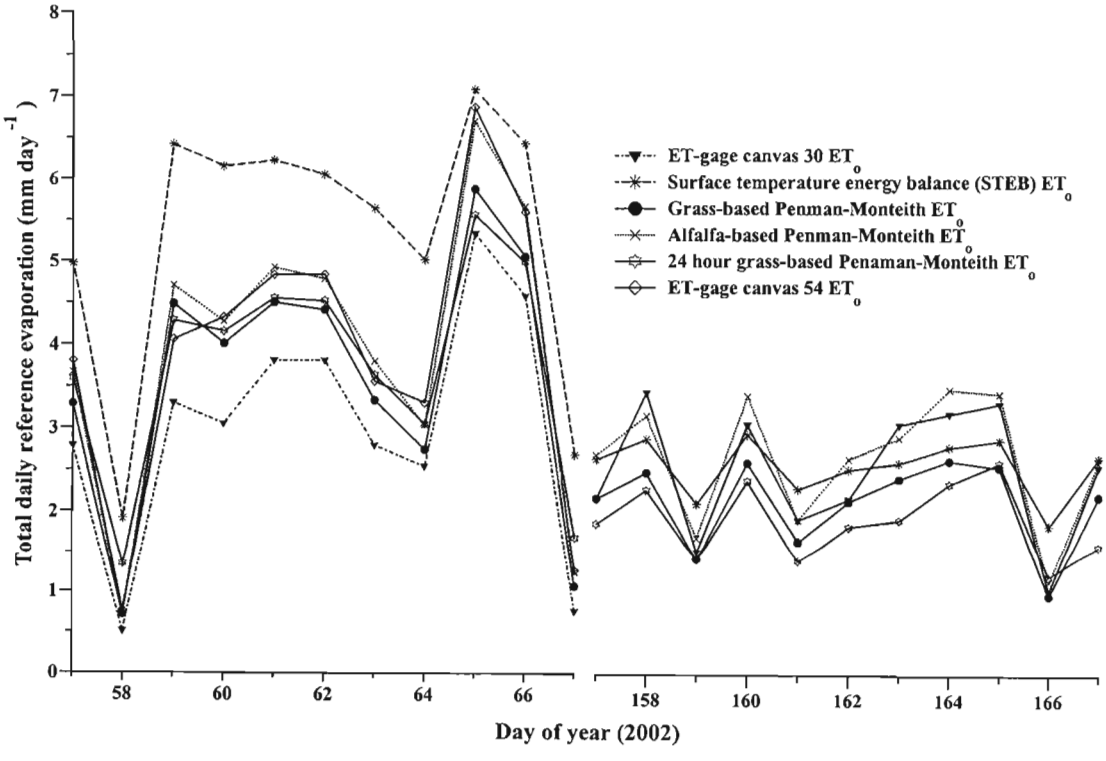

Fig. 7.9 Daily variation of ET-gage (canvas 30 and 54) evaporation, hourly grass and alfalfa based Penman-Monteith ET_o, uncorrected STEB and daily grass Penman-Monteith reference evaporation estimate, at the Agrometeorology site

Table 7.5 Statistical summaries of ET-gage 54 evaporation measures and hourly sum alfalfa evaporation based on the Penman-Monteith method for two different microclimates (Ukulinga under shade, Cedara short grass) in mm days^{-1}

Site	r^2	Intercept (mm)	Slope	SE_{Int} (mm)	SE_{Slope}	S_{yx} (mm)	MSE_{uns} (mm)	MSE_{sys} (mm)	RMSE (mm)
Ukulinga (n = 21)	0.316	-0.136	1.933	0.823	0.653	1.243	1.399	1.103	1.582
Cedara (n = 225)	0.770	-0.688	1.270	0.160	0.048	0.827	0.678	0.120	0.893

r^2 is the correlation coefficient, MSE_{uns}, MSE_{sys} and RMSE are the unsystematic, systematic and root mean square error respectively, SE_{slope} and SE_{int} are the standard error of slope and intercept respectively, S_{yx} is the standard error of estimate of y on x, Ukulinga measurement period between July 1 to 16, 2002, Cedara measurement period between April 10 to December 31, 2002

The 21 days of evaporation measurement using the ET-gage (canvas 54) for a tomato crop (under white colour shade, solar irradiance transmittance 76 %) was higher than hourly sum of alfalfa based Penman-Monteith estimate. The total evaporation was almost twice that of the alfalfa-based Penman-Monteith estimate.

The sensitivity of ET-gage measure to variation of wind speed, relative humidity and air temperature measure from one and two meters compared to hourly sum of grass Penman-Monteith and STEB is shown in Table 7.6. The measurement of evaporation using the ET-gage was equally sensitive to the two and one meter measurement of the microclimate measures.

Table 7.6 Regression of ET-gage canvas 30 *vs* grass-based hourly sum of Penman-Monteith (GPM) evaporation and STEB estimated from a wind speed, air temperature and relative humidity measured from 1 and 2 meters respectively (n = 108 days)

Models	r^2	Intercept (mm)	Slope	$SE_{Intercept}$ (mm)	SE_{Slope}	S_{yx} (mm)	MSE_{uns} (mm)	MSE_{sys} (mm)	RMSE (mm)
GPM (2 m)	0.668	0.496	0.877[1]	0.161	0.060	0.679	0.452	0.056	0.713
GPM (1 m)	0.668	0.483	0.857[1]	0.162	0.059	0.679	0.453	0.040	0.702
STEB (2 m)	0.398	0.637[1]	0.634	0.256	0.076	0.915	0.821	0.456	1.130
STEB (1 m)	0.378	0.694	0.610	0.260	0.076	0.930	0.848	0.519	1.169

[1]The slope and intercept significantly different from 1 and 0 at 99 % confidence level, r^2 is the correlation coefficient, MSE_{uns}, MSE_{sys} and RMSE are the unsystematic, systematic and root mean square error respectively, SE_{slope} and $SE_{intercept}$ are the standard errors of slope and intercept respectively, S_{yx} is the standard errors of estimate of y on x, at the Agrometeorology site. The measurement period is between February 13 to July 12, 2002

The short and long grass ET-gage measurements at the Agrometeorology site were similar to the hourly sum of grass and alfalfa based Penman-Monteith estimate (Table 7.4). The average and total measure for canvas 30 was 0.2 % lower than hourly sum of grass Penman-Monteith estimate while for canvas 54 the measurements were 3 % greater than the hourly sum of alfalfa Penman-Monteith respectively. Similarly a 6 % overestimation of the visual average and total measure of canvas 54 evaporation from Cedara were noticed when it was compared with hourly sum of alfalfa Penman-Monteith estimate. The Cedara canvas 54 measure overestimated the hourly sum of alfalfa Penman-Monteith estimate by 27 % (Table 7.5). This large difference may be due to the resolution limit and bias of the visual reading. The Agrometeorology site visual reading of canvas 30 (n = 144 days) and 54 (n = 75 days) were more than 2 % and 6 % of the average and 4 % and 13 % of total electronically recorded evaporation measure respectively. The 21 days of shade measurements at Ukulinga of ET-gage showed more response to the water vapour pressure deficit than to solar irradiance. During the measurement period, the daily 15-minute water vapour pressure deficit variability was greater than that for solar irradiance. The maximum measured water vapour pressure deficit was 2.94 kPa and solar irradiance 564.9 W m^{-2} under shade.

The similarity of daytime total evaporation measure with STEB from the surface of ET-gage (canvas 54) and evaporation measure of ET-gage revealed the sensitivity of the device to microclimatic changes. Fig. 7.10 and Table 7.7 show 19 days of cumulative evaporation for two ET-gage (canvas 54) evaporimeters and that for the STEB estimate of the evaporation surface of the ET-gage. The ET-gage measure was 7.3 % higher than the uncorrected STEB estimate of the surface. The significant difference between the ET-gage measured and STEB estimate was shown on days of year 208, 210, 214, 218 and 220, 2002.

Fig. 7.10 shows the change in the cumulative evaporation measure of ET-gage canvas 54 and the uncorrected STEB measure. The ET-gage measure was higher than that for the STEB method on days of year 208, 210 and 214. However the response of the ET-gage remained lower than the STEB measure on days of year 218 and 220, 2002. The water vapour pressure deficit, wind speed, net irradiance from the ET-gage surface, surface-body (T_s - T_b) and surface-air (T_s - T_a) temperature difference are shown in Fig. 7.11.

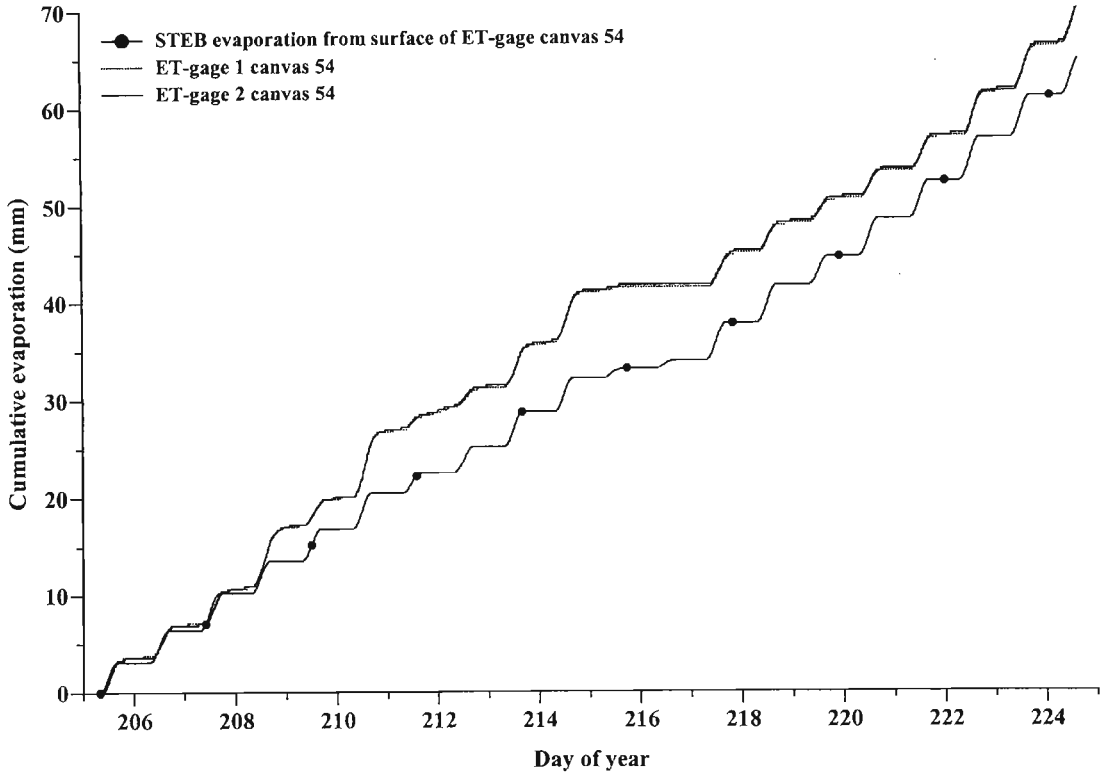

Fig. 7.10 Cumulative evaporation record of two ET-gage canvas 54 (ET-gage 1 and ET-gage 2) measures for which there is no cumulative difference, and STEB evaporation estimate from the ET-gage canvas 54 evaporation surface (July 24 to August 12, 2002, at the Agrometeorology site)

Table 7.7 Cumulative evaporation of two ET-gages and STEB evaporation from the evaporation surface using IRT and thermocouple type E, (T_c) diameter 0.254 mm, using air temperature, wind speed and relative humidity measured from 1 and 2 meters respectively, at the Agrometeorology site for period of measurement between July 24 and August 12, 2002

		ET-gage (mm)	$STEB_{UN}$[1] (mm)	$STEB_{CC}$[2] (mm)	$STEB_{MC}$[3] (mm)
IRT	1 meter	69.85	64.87	65.06	57.67
	2 meter		64.73	65.04	57.13
T_c	1 meter	69.85	64.92	65.10	57.77
	2 meter		64.79	65.08	63.71

[1] uncorrected STEB evaporation estimate

[2] Campbell and Norman (1998) procedure corrected STEB evaporation estimate

[3] Monteith (1973) procedure corrected STEB evaporation estimate

In addition to this Fig. 7.11 shows the 24-hour sum of 15-minute evaporation measure from the two ET-gage evaporimeters and the STEB measures for the cloudless days of year 208, 210, 218 and 220, 2002. The net irradiance from the ET-gage surface was fairly similar for the four days (Fig. 7.11). The higher water vapour pressure deficit with variable wind speed for days of year 208 and 210 resulted in lower difference of surface-body (T_s - T_b) and surface-air (T_s - T_a) temperature and resulted in greater ET-gage response with increase in body temperature even in the late evening compared to the other two days. A similar situation was observed on day of year 214 (2002). The relatively lower water vapour pressure deficit and constant wind speed was observed to result in a higher difference of T_s - T_b and T_s - T_a and lower response of ET-gage for the days of year 218 and 220 (decreased body temperature). This indicates the sensitivity of the ET-gage to microclimate measures and variation of body temperature of ET-gage with wind speed and water vapour pressure deficit in addition to the net irradiance as a possible cause of lag in response of the ET-gage evaporimeter. The minimum temperature of the ceramic surface and body of ET-gage were 2.64 °C and -0.42 °C respectively.

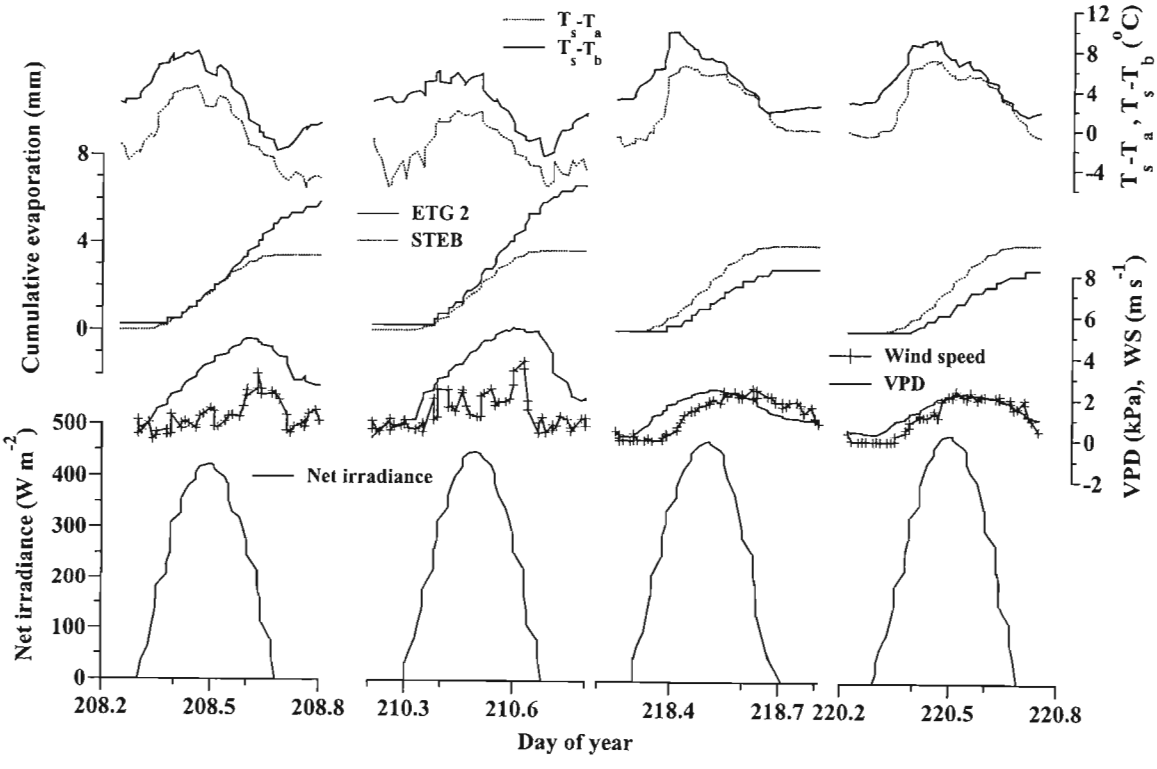

Fig. 7.11 Microclimatic measure and response of ET-gage canvas 54 for four days in 2002 (T_s - T_a is the surface-air temperature difference, T_s - T_b is the surface-body of ET-gage temperature difference, *VPD* is the water vapour pressure deficit, ET-gage measured evaporation (ETG 2), ET-gage surface energy balance (STEB) estimate of evaporation), at the Agrometeorology site

7.6 CONCLUSIONS

The hourly-reduced set Penman-Monteith estimate of reference evaporation was within the specified accuracy range limit of the Penman-Monteith estimates when wind speed was approximated as 2 or 1.03 m s^{-1} for the period of measurement. The reference evaporation was underestimated to a greater extent when water vapour pressure deficit was estimated from the daily maximum and minimum air temperature and previous day minimum air temperature. The reference evaporation estimated using STEB method was affected by the stability correction procedure applied using aerodynamic resistance. The STEB reference evaporation estimate was overestimated when uncorrected and Campbell and Norman (1998) procedure corrected aerodynamic resistance was used. The STEB reference evaporation estimate was underestimated when aerodynamic resistance was corrected using the Monteith (1973) procedure and resulted in lower agreement by comparison with the Penman-Monteith estimate using data from a complete AWS. The agreement of ET-gage daily evaporation measures, using canvas 30 and 54 and grass and alfalfa based Penman-Monteith estimate were above 60 % except for the Ukulinga site for which measurements were under shade. The electronic measurement correlated better with the reference Penman-Monteith evaporation estimate compared with the visual measure. The average and total visual ET-gage measurement of reference evaporation using canvas 30 and 54 were 6 % and 13 % higher than their electronic counterparts respectively.

The sensitivity of the ET-gage evaporimeter was observed to be dependent on the microclimate. The shade measurement showed a lower correlation with the alfalfa-based Penman-Monteith estimate. The Cedara visual measurement showed good correlation if daily measures were used but showed much greater overestimation than at the Agrometeorology site, which used the electronic measurement method. The STEB measurement of reference evaporation from the ET-gage surface revealed the equal importance of the microclimatic measure to the ET-gage response in a specific microclimate and found the late evening response of the ET-gage to correlate with the water vapour pressure deficit and wind speed measures.

CHAPTER 8

COST, MATERIALS AND ACCURACY CONSIDERATIONS FOR MICROCLIMATIC AND REFERENCE EVAPORATION MEASURES

8.1 INTRODUCTION

One of the limitations in using micrometeorological techniques to estimate evaporation at many different locations is the investment cost of the systems. The use of AWS for estimating reference evaporation requires an enclosure, a data logger, sensors, and evaporation program and communication equipment. The use of an AWS for the online estimation of reference evaporation is important in sharing resources and information, accessing real time information and irrigation control. However its wider application and use may be limited due to the high investment cost.

One full AWS system may be used on a farm but the environmental conditions may be different at different places within the farm, particularly if the topography is not uniform. This undulating topography may necessitate the use of two or more AWS systems. This chapter considers systems complimentary to the traditional full AWS system of collecting microclimatic data for calculating reference evaporation. The material and cost of each system with due consideration to accuracy is given. The sensitivity of grass-based hourly Penman-Monteith reference evaporation estimates to the various micrometeorological measures of the complimentary weather station is also investigated. The effect of resolution and point measurement on the estimate of reference evaporation is investigated and comparisons of reference evaporation with the ET-gage evaporimeter performed. The accuracy of various air temperature and relative humidity sensors placed in naturally ventilated radiation shields and those placed in a standard Stevenson screen is investigated. Measurement comparisons using home-made radiation shields are made.

The aim of this chapter is to investigate the accuracy of data from a less expensive weather station system that may be used as a complimentary system to traditional AWS systems. Comparisons are made in terms of reference evaporation estimate calculated from the measurement data from both systems as well as the accuracy, resolution and cost of the individual sensor/sensors measurements.

8.2 MATERIALS AND METHODS

Microclimatic measurements and reference evaporation calculations were performed for a period of 58 days (from November 1 to December 29, 2002) above a short grass surface at the Agrometeorology site. Different methods and sensors were used to determine reference evaporation.

8.2.1 Reference Evaporation and Microclimatic Measures

We used as our standard the AWS system and subsequent reference evaporation calculation based on the Campbell Scientific Inc. data acquisition system. The data acquisition system includes a data logger, sensors, peripheral equipment (e.g. communication devices), battery, regulator, charging source and appropriate software (Savage 2001*b*).

Three complimentary weather station systems/reference evaporation systems were used (Table 8.1):

1) Hobo logging weather station;
2) the reduced set evaporation weather station (ET101, Campbell Scientific Inc., Logan Utah, USA) and;
3) the ET-gage evaporimeter for determing reference evaporation.

The reduced set evaporation weather station includes all the sensors of AWS (Table 8.2) except relative humidity, wind speed and direction sensors.

Table 8.1 Standard and complimentary weather station systems/reference evaporation systems

Weather station systems		Data logging, sensors and communication systems
Standard AWS Systems		CR10X data logger, pyranometer, Vaisala CS500, rain gauge, wind speed and direction senor, radiation shield model 41301
Complimentary weather station systems/evaporation systems		
	Reduced set ET_o station (ET101)	CR10X, pyranometer, CS200 temperature probe[1], rain gauge
	Hobo weather station	Hobo logger (Hobo H8, Hobo Temp, Hobo Thermocouple), Event Hobo logger, pyranometer, rain gauge, radiation shield
	Evaporimeter	Event Hobo logger, ET-gage Model E (electronic and manual), ET-gage Model A (manual)

[1]ftp://ftp.campbellsci.com/pub/outgoing/lit/eto.pdf

Table 8.2 AWS and reduced set evaporation weather station data acquisition system (options of sensors, data loggers and communication systems) available for routine collection of microclimatic measure, potential accuracy and present cost

Parameters	Instruments / sensors	Accuracy	Cost (R)[2]	Calibration[1] /comment
Solar irradiance	LI-200SZ (Pyranometer) sensor	±3 to 5 %	1914.03	Annual
Air temperature and relative humidity	CS500 sensor	±0.5 to 0.8 °C (0 to 60 °C)	2870.00	Annual
		±3 % (10 to 90 % RH)		
		±6 % (90 to 100 % RH)		
Air temperature	Thermistor CS200 sensor	±1.25 to 2 °C	246.00	Annual, can be used without radiation shield
Wind speed	Model 03001 sensor	±0.5 m s^{-1}	4159.95	Annual
Rainfall	Rain-O-Matic sensor	1 mm / tip	253.71	Annual
	Professional sensor	0.1 mm / tip	1345.62	
Data handling	CR10X (6 differential channels) data logger		13674.30	
	CR510 (2 differential channels) data logger		8618.40	
	CR200 (5 single ended channels) data logger[3]		4481.57	
Communication	CSM1 CSL Card Storage module		4678.91	
	CSMC1M 1M byte memory card		1131.11	
	MCR1 CSL memory card reader		6055.77	
Radiations shield	Model 41301		1394.00	
Data processing	Loggernet support software		4061.71	
Power supply	Battery (VA10SB)		110.36	
	Solar panel (VA12SP)		844.14	
	Solar panel (VA20SP)		1355.33	
	Regulator (VAREG)		140.65	

[1]Savage (1996), [2]Campbell Scientific Africa, the cost includes VAT of 14 % and assumes an exchange rate of 1$ = R 8.20

The Vaisala CS500 air temperature and relative humidity sensor, CM3 pyranometer, wind speed and direction (Model 3001), precipitation (Rain-O-Matic rain gauge) and data logger (CR7X) were used as a part of reduced set evaporation weather station and AWS data acquisition system. Normally however, a CR10X data logger could be used for this application but with less accuracy compared to CR7X.

The Hobo weather station can be set up using Hobo loggers, radiation shields, rain gauge, appropriate software, batteries, solar irradiance sensors and an amplifier depending on the solar irradiance sensor and Hobo logger (Table 8.3).

Table 8.3 Details of the Hobo logging weather station sensors available for collection of various microclimatic measures and the ET-gage evaporimeter

Parameter	Instruments/sensors	Accuracy	Cost (R)[1]
Solar irradiance	Apogee (PYR) sensor	±2 %	1703.00
Solar irradiance	LI-200SZ sensor	±3 to 5%	1914.00
Air temperature	Hobo H8 logger	±0.7 °C	1157.37
Relative humidity	Hobo H8 logger	±5 % RH	
	Two external channels (0 to 2.5V)	10 mV resolution	
Air temperature	Hobo Temp logger	±0.7 °C	675.12
Air temperature	Hobo Thermocouple logger	±0.7 °C	779.00
Rainfall	Rain-O-Matic sensor	1 mm / tip	253.71
Data collection	Event Hobo logger		1068.34
	Hobo Shuttle		1973.00
Data processing	Boxcar software		259.67
Radiation shield	Hobo radiation shield (RS1)		1231.22
Power	Battery		15.00
Amplification	Amplifier (×100)		400.00
	ET-gage		
Evaporation	Model A (manual)	±0.254 mm	1886.00
Evaporation	Model E (electronic and manual)	±0.5 mm	5116.00
Power	Battery		28.00

[1]http://www.enviromon.co.za, http://www.onsetcomp.com/product.html, Campbell Scientific Africa, the cost includes VAT at 14 %, and assumes exchange rate of 1$ = R 8.20

One Onset Computer Hobo H8 logger (H08-007-02) and one event recording Event Hobo logger (H07-002-04) together with Apogee PYR pyranometer and home-made radiation shield (Savage 2002*b*) were used to form the Hobo H8 weather station.

The ET-gage evaporimeter (Model E) can be used to measure evaporation electronically and manually (Table 8.3). Two ET-gage sensors connected to the CR7X data logger and Event Hobo logger respectively were used to measure reference evaporation. The output circuit of the Model E ET-gage is made to pull the signal line down to 0 volts for about 2 seconds while the ET-gage measuring-vial fills. Similarly the Event Hobo logger was adjusted to the 2-second event-recording interval. The second ET-gage was connected to the pulse port of CR7X data logger and recorded every 10 s. Assuming daily mean evaporation rate is 11 mm, the memory Event Hobo logger can last 185 days.

8.2.2 Radiation Shields

Air temperature and relative humidity data were collected from naturally ventilated home-made two plastic seven-plate and one metal seven-plate and six- and twelve-plate Gill (Model 41002, 41301, R M Young) radiation shields (Fig. 5.4). In addition to the multi-plate radiation shields, a single louvered small (300 mm × 200 mm × 270 mm) and a double louvered standard size Stevenson screen (910 mm × 720 mm × 640 mm) were used to measure air temperature and relative humidity and compare the performance of home-made radiation shields in terms of cost and efficiency. Seven thermocouples (type E, 0.5 mm diameter), four Vaisala CS500, one HMP35C temperature and humidity probe and four Hobo H8 loggers were placed in the different shields (Table 8.4). Additionally unshielded two fine-wire thermocouples (type E, 75 μm diameter) were used for air temperature measurement at 1.5 and 2 meters.

All the sensors were connected to a CR7X data logger. Air temperature and relative humidity were measured every 10 s. The 5-minute sample and 15 and 60-minute average air temperature and water vapour pressure and sample relative humidity were collected from the sensors housed in the reference Stevenson screen and each of the shields (Table 8.4). The 5-minute sample relative humidity and air temperature were collected and water vapour pressure calculated from the Hobo H8 loggers.

Table 8.4 Description of the radiation shields used, the air temperature and relative humidity sensors, height of measurement and estimated cost

Radiation shield	Height	Sensors[2]	Descriptions	Cost (R)[1]
Standard Stevenson screen	1.5 m Standard	Hobo H8, Type E (0.5 diameter), CS500)(RTD)	Humitter 50YC S4650042	3135.74
Small Stevenson screen	1.5 m Small	Hobo H8 (Thermistor), Type E (0.5 diameter)		436.21
Six-plate Gill Radiation shield	2 m (Standard in AWS)	Type E (0.5 diameter), CS500 (RTD)	Humitter 50YC R0710077	1394.00
Twelve-plate Gill radiation shield	2 m	Type E (0.5 mm diameter), HMP35C (Thermistor)		1394.00
Seven-plate metal home-made radiation shield	2 m (100 mm diameter)	Type E (0.5 mm diameter)		428.00
Seven-small plate plastic home-made radiation shield	2 m (140 mm diameter)	Hobo H8, Type E (0.5 mm diameter), CS500 (RTD)	Vaisala 50YC R2020010	428.00
Seven-large plate plastic home-made radiation shield	2 m (190 mm diameter)	Hobo H8, Type E (0.5 mm diameter), CS500 (RTD)	Humitter 50YC S5030025	428.00

[1]Price includes VAT of 14 % and assumes an exchange rate of 1$ of R 8.20,
[2]RTD is resistance thermometer detector, Type E thermocouples used

8.2.3 Accuracy and Cost Estimation Methodology

Reference evaporation was calculated from the microclimatic measures using the standard AWS system and the complimentary reduced set evaporation weather station, Hobo H8 weather station systems and reference evaporation measured using ET-gage evaporimeter. The spreadsheet-based Penman-Monteith algorithm implemented in the data logger program of the standard weather station systems was utilized to calculate hourly grass and alfalfa based reference evaporation. The accuracy involved with each system was compared and evaluated using regression analysis.

The possible least investment cost of each data acquisition system was considered based on the present market price of sensors, loggers and additional cost requirement for the implementation of the systems (see Tables 8.2 and 8.3). The performance of the different electronic air temperature and relative humidity (RH) sensors housed in naturally ventilated radiation shields were compared. Air temperature measured using a thermocouple (type E, 0.5 mm diameter) and water vapour pressure measured using Vaisala CS500 placed in a standard Stevenson screen were used as the reference standard. The regressions of air temperature measured in the Stevenson screen and between the different shields were used to compare the accuracy and advantage of home-made radiation shields.

8.3 MICROCLIMATIC MEASURE AND RADIATION SHIELDS

8.3.1 Introduction

Air temperature and relative humidity are the primary microclimatic measures that are routinely measured along with solar irradiance, wind speed, wind direction and precipitation. The measurement of air temperature and relative humidity are affected by ventilation and solar and long wave irradiance. The use of a radiation shield and application of ventilation reduces the measurement error. The error of free air measurement of air temperature using an unshielded thermocouple for example depends on the diameter of the wire and ventilation. For air speeds greater than or equal to 0.4 m s^{-1}, the radiation error is less than 0.5 °C for a wire diameter (thermocouple) less than or equal to 75 μm (Tanner 1979).

Different types of naturally-ventilated and forced-aspirated radiation shields are commonly used in weather stations. In the case of a non-automatic weather station, the standard for housing sensors is a naturally ventilated Stevenson screen. The six-plate Gill radiation shield is considered as a standard for AWS use. Naturally-ventilated, one small and one standard Stevenson screen, two low cost home-made small and large size seven-plate plastic radiation shields and one low cost home-made seven-plate metal radiation shield and six- and twelve-plate Gill radiation shield are compared with air temperature and relative humidity measurements obtained using a thermocouple (type E), CS500, HMP35C and Hobo H8 sensors mounted in each shield (Table 8.4). Air temperature and relative humidity measurements using Hobo H8 and thermocouples (type E) are compared with CS500 and HMP35C probes mounted in the home-made plastic radiation shields and the metal plate radiation shield.

8.3.2 Comparison of Air Temperature and Relative Humidity Sensors

Air temperature and relative humidity were measured using four different electronic sensors placed in the Stevenson screens. The air temperature measurements using thermocouples (type E) were compared to the one HMP35C (thermistor), four CS500 (RTD) and four Hobo H8 (thermistor) measurements. Averages of the air temperature differences ranging from 0.01 to 0.7 °C were noted between the thermocouples (type E), CS500, HMP35C and Hobo H8 sensors. The averages of the air temperature differences among the thermocouple (type E) were between 0.01 to 0.05 °C, 0.1 to 0.7 °C with Hobo H8, 0.3 °C with HMP35C and 0.02 to 0.4 °C with Hobo H8 sensors (data not shown). The maximum difference of 0.7 °C was noted for one CS500, which was within the accuracy limit range of sensors.

The relative humidity differences observed among the different electronic capacitance sensors were between 0.42 and 7.82 % (data not shown). The differences in relative humidity measurements were greater for Hobo H8 than CS500 and HMP35C sensor. Differences of 6.97 to 7.82 % were noticed with four Hobo H8 sensors. The 15 and 60-minute sample relative humidity difference were between 0.99 to 6.97 % for the four CS500 and one HMP35C sensors (data not shown). A greater measurement difference was observed with one CS500 sensor, which was above the range of maximum accuracy limit of sensor specified by the manufacturer.

8.3.3 Performance of Home-Made Radiation Shields

A good temperature radiation shield should remove solar irradiance, equilibrate infrared long wave irradiance and minimize the blocking of airflow to the temperature sensor (Lin and Hubbard 1999). Hubbard *et al.* (2001) and Lin *et al.* (2001) studied and reported the efficiency of the solar and infrared long wave irradiance shield effectiveness and wind flow character of four different radiation shields. Due to variation in geometric design, nature and colour of the naturally ventilated radiation shields, the airflow character inside the shield and radiation shield effectiveness is likely to differ. The performance of the home-made plastic radiation shield was determined through the comparison of air temperature and RH measurement as well as cost. Tables 8.4, 8.5, 8.6, 8.7 and 8.8 shows the costs and averages, mean daily maximum and minimum of the air temperature and water vapour pressure differences measured from shields and small Stevenson screen against the standard Stevenson screen measure.

Table 8.5 Air temperature differences relative to 0.5 mm diameter thermocouple placed in the standard Stevenson screen: average, mean of the daily maximum and minimum and standard deviation of the air temperature differences measured from 5-minute sample and 15 and 60-minute averages of the home-made radiation shield and small Stevenson screen measurements (measurement period from November 1 to December 29, 2002)

Sensors in radiation shield thermocouple (type E) as a reference		Seven-large plastic plate home-made radiation shield			Seven-small plastic plate home-made radiation shield			Small size Stevenson screen		
		Measurement period (minute)								
		5	15	60	5	15	60	5	15	60
CS500	Average difference									
		0.05	0.03	0.03	0.02	0.05	0.04			
	Mean of maximum daily difference									
		1.30	0.98	0.78	1.43	1.14	0.91			
	Mean of minimum daily difference									
		-0.65	-0.54	-0.38	-0.72	-0.52	-0.42			
	SD	0.43	0.41	0.39	0.50	0.48	0.46			
Type E	Average difference									
		0.02	0.02	0.02	0.003	0.03	0.03	0.20	0.22	0.21
	Mean of maximum difference									
		1.33	0.79	0.60	1.29	0.87	0.67	1.72	1.45	1.28
	Mean of minimum difference									
		-0.68	-0.52	-0.35	-0.76	-0.46	-0.34	-0.61	-0.54	-0.44
	SD	0.33	0.32	0.31	0.36	0.34	0.33	0.52	0.57	0.37
Hobo H8	Average difference									
		0.10			0.06			0.36		
	Mean of maximum difference									
		1.30			1.17			2.29		
	Mean of minimum difference									
		-0.65			-0.71			-0.72		
	SD	0.39			0.46			0.78		
n		2941	4241	1061	2941	4241	1061	2941	4241	1061

SD is standard deviation of the average differences

Table 8.6 Air temperature differences relative to 0.5 mm diameter type E thermocouple placed in the standard Stevenson screen: average, mean of the daily maximum and minimum and standard deviation of the air temperature differences from sample 5-minute, averages of 15 and 60-minute measurements of twelve- and six-plate Gill radiation shields (measurement period from November 1 to December 29, 2002)

Sensors in radiation shield thermocouple (type E) as a reference		Twelve-plate Gill radiation shield (HMP35C sensor)			Six-plate Gill radiation shield (CS500 sensor) [1]			Standard Stevenson screen (CS500 sensor)		
		Measurement period (minute)								
		5	15	60	5	15	60	5	15	60
HMP35C CS500	Average difference									
		0.65	0.02	0.02	0.71	0.12	0.14	-0.02	0.02	0.01
	Mean of maximum daily difference									
		1.18	0.70	0.52	2.42	1.44	1.12	0.75	0.32	0.19
	Mean of minimum daily difference									
		-0.49	-0.40	-0.29	-0.66	-0.55	-0.42	-0.57	-0.26	-0.15
	SD	0.31	0.29	0.27	0.61	0.57	0.53	0.18	0.11	0.09
Type E Hobo H8	Average difference									
		0.08	0.01	0.02	0.02	0.06	0.06	0.05 [2]		
	Mean of maximum daily difference									
		1.18	0.79	0.58	1.42	0.94	0.72	0.83		
	Mean of minimum daily difference									
		-0.49	-0.40	-0.28	-0.82	-0.50	-0.37	-0.58		
	SD	0.30	0.30	0.28	0.39	0.37	0.35	0.20		
n		2941	4241	1037	2941	4241	1037	2941	4241	1037

[1]technical problem with CS500 sensor, [2]Hobo H8, SD is standard deviation of the average differences

8.3.3.1 Radiation shield design

In order to keep the cost of an AWS minimum, an alternatives to the expensive six-and twelve-plate Gill radiation shields for air temperature and relative humidity sensors were considered. Inexpensive plastic dish plates and simple geometry, based on the original design of the six-plate Gill radiation shields were used to assemble the plates (Savage 2002*b*). The spacing between plates is made to be flexible with a minimum limit of 14 mm and connected using three plastic pillars with bolts and nuts. The leading edge of the plate encourages the flow of air into the plate. Seven plates were arranged to accommodate the CS500 and Hobo H8 logger in the space provided at the middle of the lower five plates. As Fig. 8.1 illustrates the suitable angle edge and spacing between plates

was found that satisfied the radiation shield requirement in comparison with the other radiation shields.

8.3.3.2 Minute values

Using the 15 and 60-minute data an average of 0.03 °C and 0.05 °C increase in the air temperature measurement relative to the standard size Stevenson screen was noticed for the home-made plastic radiation shields (Table 8.5). The differences were generally similar to the Gill multi-plate radiation shields (Table 8.6). The small Stevenson screen air temperature measures were much higher than the radiation shields. An average air temperature difference of 0.22 °C was observed in comparison with standard Stevenson screen measurement. The highest average difference was noticed during daytime hours. The average air temperature difference for the metal radiation shield was greater during the day and lower during night compared to the standard Stevenson screen air temperature and similar results were also noticed from free air fine wire thermocouple measurements. This may be due to the higher conductivity of the metal compared to the wood and plastic.

Table 8.7 Air temperature differences relative to a 0.5 mm diameter type E thermocouple placed in the standard Stevenson screen: average, mean of the daily maximum and minimum and standard deviation of the air temperature differences measured from 5-minute sample and 15 and 60-minute averages of free air at 1.5 and 2 meters and from home-made metal plate radiation shield measurements (measurement period from November 1 to December 29, 2002)

Sensors in radiation shield thermocouple (type E) as a reference		Type E thermocouple at 1.5 meter free air			Type E thermocouple at 2 meter free air			Seven-metal plate home-made radiation shield		
		Measurement period (minute)								
		5	15	60	5	15	60	5	15	60
Type E (75 μm diameter)	Average difference									
		0.05	0.03	0.03	0.05	0.02	0.02	0.06	0.06	0.06
	Mean of maximum daily difference									
		2.14	0.88	0.70	1.76	0.81	0.63	1.53	1.01	0.76
	Mean of minimum daily difference									
		-1.49	-0.62	-0.43	-0.85	-0.55	-0.39	-0.81	-0.62	-0.44
	SD	0.53	0.39	0.38	0.54	0.39	0.37	0.39	0.39	0.37
n		2941	4150	1061	2063	3855	1061	2941	4241	1061

SD is the standard deviation of the average difference

Table 8.8 Water vapour pressure differences relative to that measured using a Vaisala CS500 sensor placed in the standard Stevenson screen: average, mean of the daily maximum and minimum and standard deviation of the water vapour pressure differences measured from 5-minute sample and 15 and 60-minute averages of the home-made radiation shield, Gill multi-plate radiation shields and Stevenson screens (measurement period from November 1 to December 29, 2002)

Sensors in radiation shield Vaisala CS500 as a reference		Seven-large plastic plate home-made Radiation shield			Seven-small plastic plate home-made Radiation shield			Standard Stevenson screen	Small Stevenson screen
		Measurement period (minute)							
		5	15	60	5	15	60	5	5
CS500	Average difference (kPa)								
		0.010	0.006	0.006	0.061	0.003	0.003		
	Mean of maximum daily difference								
		0.09	0.04	0.03	0.20	0.05	0.04		
	Mean of minimum daily difference								
		-0.08	-0.02	-0.02	-0.06	-0.06	-0.05		
	SD	0.029	0.017	0.02	0.016	0.063	0.036		
Hobo H8	Average difference								
		0.10			0.065			0.069	0.386
	Mean of maximum daily difference								
		0.23			0.20			0.22	0.64
	Mean of minimum daily difference								
		-0.03			-0.06			-0.05	0.18
	SD	0.076			0.065			0.060	0.125
Sensors in shield		Twelve-plate Gill (HMP35C sensor)			Six-plate Gill (CS500 sensor) [1]				
HMP35C CS500	Average difference								
		0.036	0.014	0.014	-0.003	0.004	0.003		
	Mean of maximum daily difference								
		0.11	0.05	0.04	0.07	0.05	0.03		
	Mean of minimum daily difference								
		-0.01	-0.01	-0.01	-0.10	-0.02	-0.02		
	SD	0.028	0.019	0.018	0.026	0.021	0.019		
n		2941	4241	1061	2941	4241	1061	2941	2941

[1]Technical problem with CS500 sensor, SD is standard deviation of the average differences

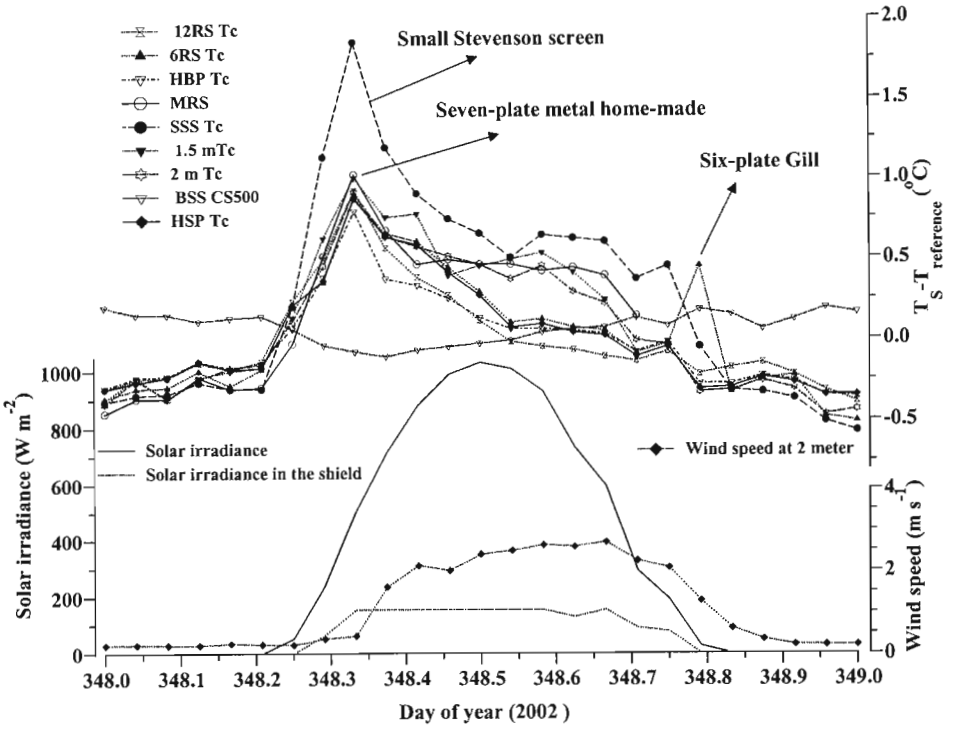

Fig. 8.1 Air temperature difference (T_s - $T_{reference}$) from the radiation shields and the standard Stevenson screens (day of year 348, 2002), wind speed at 2 meter, solar irradiance measured inside and outside a home-made radiation shield, T_c is the thermocouple type E, 12RS and 6RS are the twelve- and six-plate Gill radiation shields respectively, HBP, HSP and MRS are seven-plate large and small size plastic and seven-plate metal home made radiation shields respectively, SSS is the small size Stevenson screen, 1.5 m Tc and 2 m Tc are the free air 1 and 2 meter above surface thermocouple type E (75 μm diameter) measurements, BSS is the standard Stevenson screen CS500 sensor)

The home-made naturally ventilated radiation shield with air temperature and relative humidity sensor increased the 60 minute measurement of air temperature by 0.04 °C and water vapour pressure by 0.01 kPa compared to the standard Stevenson screen measurement (Tables 8.5, 8.8).

Figs 8.1 and 8.2 shows wind speed, solar irradiance (inside and outside shield) and differences of air temperature and water vapour pressure inside radiation shields and Stevenson screens for the day of year 348, 2002. The significant feature of Fig. 8.1 is the large differences in air temperature between standard Stevenson screen and radiation shields between 07h00 and 08h00. Fig. 8.3 shows air temperature and water vapour pressure differences, wind speed and solar irradiance for the morning hours of day of year 348, 2002. The radiation shield is warmer at low solar irradiance levels creating a higher difference in air temperature.

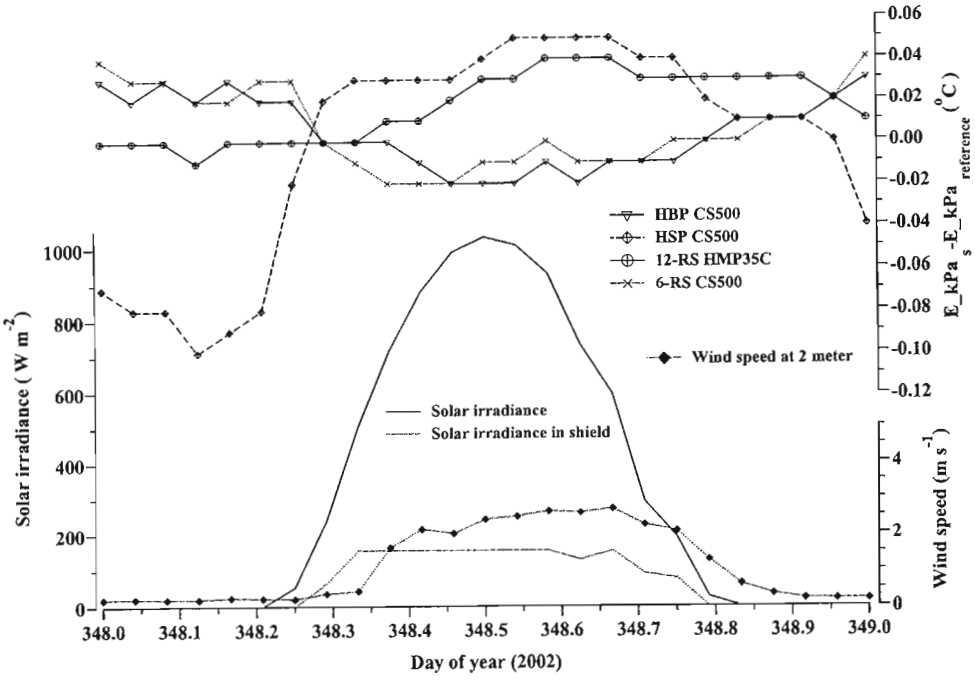

Fig. 8.2 Diurnal variation of water vapour pressure differences (E_kPa_s - $E\_kPa_{reference}$), wind speed and solar irradiance from shields and Stevenson screens for day of year 348, 2002. The subscript $_s$ stands for the water vapour pressure measured in the seven-plate large (HBP), seven-plate small (HSP) size home made plastic radiation shields and six- and twelve-plate Gill radiation shields (6-RS, 12-RS), the reference of water vapour pressure measured using Vaisala CS500 placed in standard Stevenson screen

Such a difference was common for all clear days. The reason seems to be that the radiation shields and small Stevenson screen allow an excessive amount of solar irradiance at low solar elevation into the shield or screen. However the phenomena was minimum on clear afternoon from west although similar amount of solar irradiance was measured from inside the shields. The difference in air temperature remains smaller than morning hours. This could have arisen because of the relatively lower wind speed that resulted in insufficient ventilation. Lin *et al.* (2001) also reported insufficient ventilation of naturally ventilated radiation shields for ambient wind speeds less than 5 m s^{-1}. The value was closer to the maximum wind speed measured for the site. Fig. 8.1 also shows that the air temperature in the shields and in the small Stevenson screen increases very rapidly between 08h00 to 09h00 hours. Fig. 8.2 shows the pattern of water vapour pressure difference for the same day of the year. The average water vapour pressure difference measured in the home-made radiation shield was similar to the six- and twelve-Gill plate radiation shields (Table 8.8). The maximum difference in water vapour pressure was 0.003 kPa for CS500 and 0.009 kPa for Hobo H8.

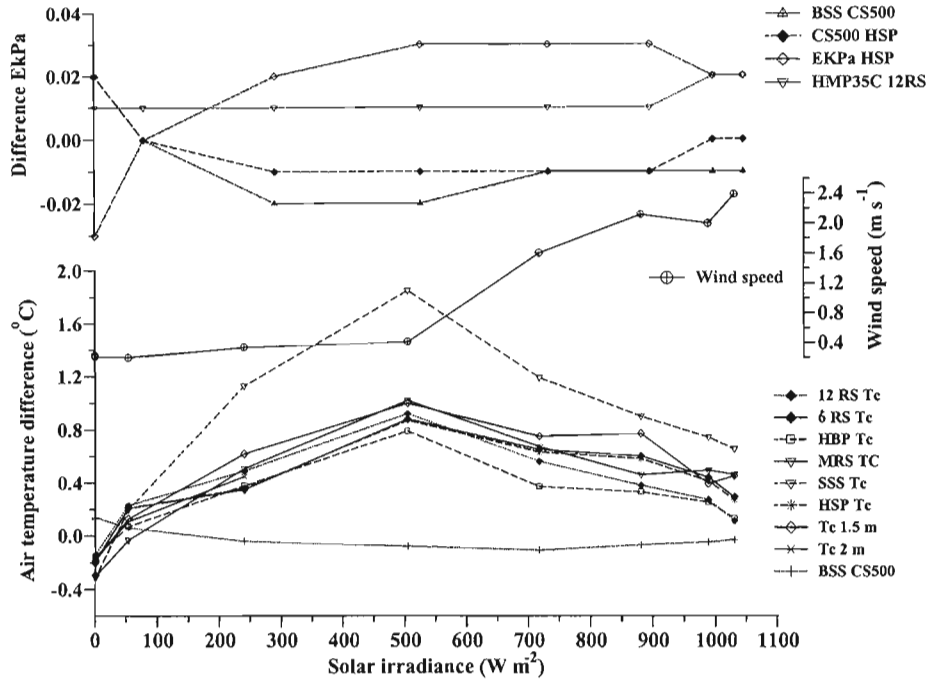

Fig. 8.3 Variation of air temperature, water vapour pressure differences *(E_kPa)* and wind speed as a function of solar irradiance in the morning hours of day of year 348, 2002. (BSS and SSS are the large and small size Stevenson screen, 12RS, 6RS are the twelve- and six-plate Gill radiation shields, HBP, HSP, and MRS are the seven-plate home made small and large size plastic and metal radiation shields, Tc1.5 m and Tc 2 m are the free air thermocouples placed at 1.5 and 2 meter (type E thermocouples, 75 μm diameter))

The maximum difference of water vapour pressure was noted for the small Stevenson screens. As Fig. 8.2 shows, the water vapour pressure difference for the small home-made radiation shield (HSP) was greater during the night time hours compared to the daytime. This may due to a build-up of humidity in the shield at low wind speed.

The averages of the air temperature differences measured using fine wire thermocouples (75 μm) in free air were similar to the metal home-made radiation shield measurement of air temperature. Although the measurements were taken from two different heights, this did not affect the averages of the differences (Table 8.7). The comparison between the home-made radiation shield and the Stevenson screen shows a satisfactory linear relationship (Table 8.9, Figs 8.4, 8.5). The correlation between the radiation shields and the Stevenson screen was excellent for the measurement period (see Figs 8.4, 8.5). Similar agreement was also observed with six- and twelve-plates Gill radiation shields (Table. 8.9).

Table 8.9 Comparisons of 60-minute average air temperature measured in the radiation shields and Stevenson screens. Reference type E thermocouple (0.5 mm diameter) (n =1061 hours corresponds to the period November 1 to December 29, 2002)

Radiation shield and screens	r^2	Intercept (°C)	Slope	RMSE (°C)	S_{yx} (°C)	Average (°C)		
						Daily mean	Daily max	Daily min
Standard Stevenson screen	1.000	0.00	1.000	0.000	0.000	19.62	25.79	14.59
Twelve-plate Gill	0.997	-0.17	1.009	0.285	0.281	19.64	25.60	14.54
Six-plate Gill	0.996	-0.36	1.021	0.359	0.337	19.68	25.98	14.50
Seven-large plastic plate	0.997	-0.24	1.013	0.308	0.300	19.64	25.87	14.54
Seven-small plastic plate	0.996	-0.22	1.013	0.329	0.320	19.66	25.90	14.55
Seven- metal plate	0.996	-0.44	1.025	0.374	0.346	19.68	26.18	14.45
Small Stevenson screen	0.992	-0.70	1.047	0.595	0.502	19.83	26.57	14.41

r^2 is correlation coefficient, RMSE is root mean square error, S_{yx} is error estimate of y on x

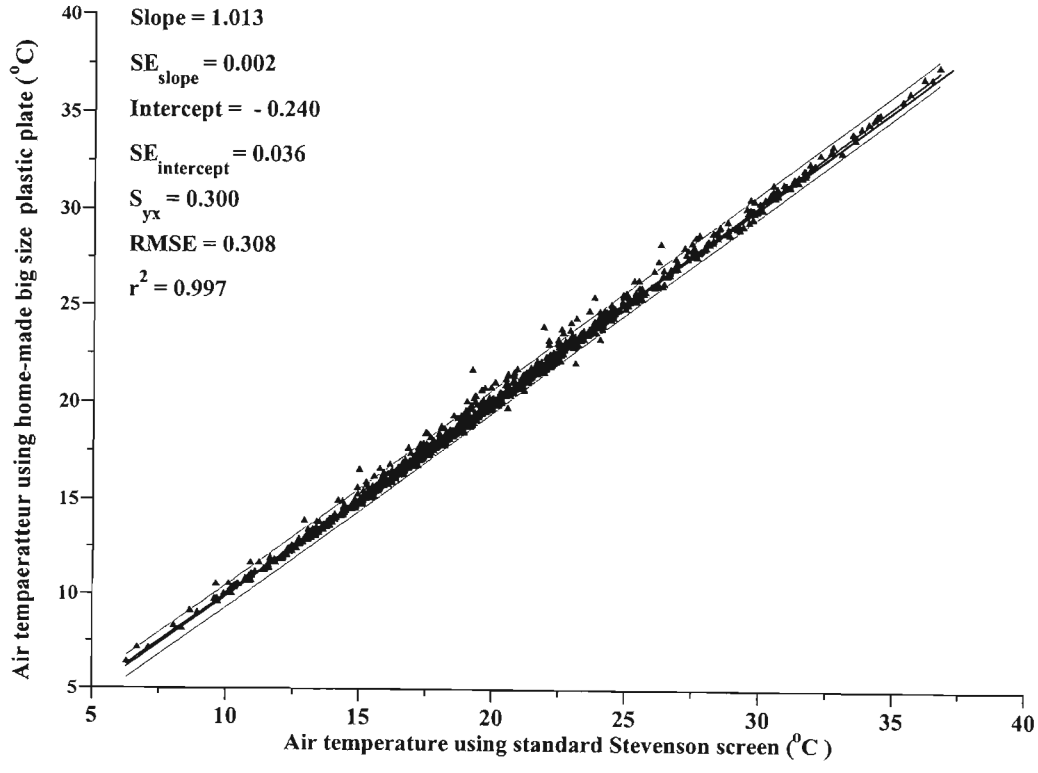

Fig. 8.4 Air temperature measurement comparison between that measured in the home-made large size seven-plate radiation shield and that in the standard Stevenson screen for hourly averages for the period 6 November to 20 December, 2002

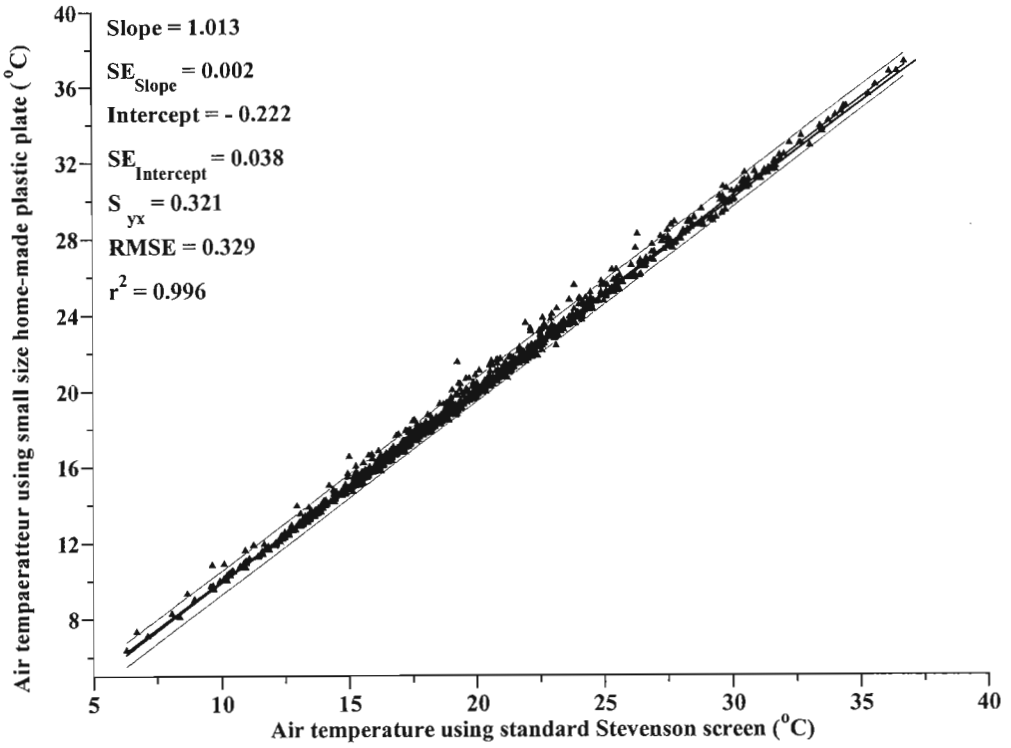

Fig. 8.5 Air temperature measurement comparison between that measured in the home-made small size seven-plate radiation shield and that in the standard Stevenson screen for hourly averages for the period 6 November to 20 December, 2002

8.3.4 Conclusions

Relative to the standard Stevenson screen measurements, higher daily maximum and minimum average of the air temperature difference was measured in the single louvered small Stevenson screen and metal radiation shield. All of the radiation shields and the small Stevenson screen air temperature and relative humidity measures experienced a radiation error at low solar elevation when wind speed was low particularly between 08h00 and 09h00. A 60-minute maximum air temperature difference of up to 2.5 °C was noted in the morning hours of cloudless days for the small Stevenson screen. The average of the air temperature differences was highest for the metal radiation shield and next to the highest small Stevenson screen. The metal radiation shield air temperature differences were the lowest of all the shields during the night time. Both sizes of the home-made plastic radiation shield provided almost similar air temperature and relative humidity differences that were not significantly different from those observed for the manufactured six- and twelve- plate Gill radiation shields. The large sized home-made plastic radiation shield provided smaller average measurement differences compared to the small plastic radiation shields. Generally

the home-made plastic radiation shields were a bit warmer during the day and cooler during the night than the six- and twelve-plate Gill radiation shield when compared to the standard Stevenson screen. The use of home-made radiation shields saves 70 % of the cost of six- and twelve-plate Gill radiation shields.

The different air temperature and relative humidity sensors provided different accuracy levels. The maximum air temperature difference measured was 0.7 °C for one CS500 sensor and 7.82 % relative humidity for one Hobo H8 sensor. Except for one CS500 and one Hobo H8 sensor, which exceeded the maximum limit of accuracy specified by the manufacturer, the other air temperature and relative humidity sensors were within their specified range of accuracy

8.4 COMPARISON OF DIFFERENT REFERENCE EVAPORATION ESTIMATING SYSTEMS

8.4.1 Introduction

The use of AWS data acquisition systems is increasing and online computation of reference evaporation is possible using the Penman-Monteith approach for an hourly time step. The system can also be used to collect data at high frequency and through communication with radio and cell phone from remote sites (Mottram *et al.* 1991). These stations collect solar irradiance, air temperature, relative humidity, precipitation, wind speed and wind direction data. This information can be stored in the station data logger for further processing using the Penman-Monteith approach. Hess (1996) reported greater significance of the sum of hourly reference evaporation estimates from an AWS compared to the daily reference evaporation estimates based on conventional synoptic weather observations twice per day. In developing countries or at a farm level accessing or affording more than one AWS system is however very expensive. Complimentary or alternative options evaluated in terms of cost and accuracy include the reduced set evaporation weather station, the ET-gage evaporimeter and Hobo H8 weather station system. Comparisons in this section focus on microclimatic measurement and calculating reference evaporation. All comparisons are relative to measurements made using a standard AWS system (Table 8.1).

8.4.2 Solar Irradiance Comparison

The frequency and the resolution limit of the Hobo H8 data-logging system could result in a difference in the solar irradiance relative to the AWS system. The Hobo H8 logger can measure a voltage of between 0 and 2.5 V DC but it has a resolution limit of 10 mV. The use of low cost solar irradiance sensor (Apogee PYR sensor) with a sensitivity of 3.86 W m^{-2} mV^{-1} results in a solar

irradiance resolution limit of 38 W m^{-2} (Fig. 8.6). The Hobo H8 resolution limit is noticeable in the case of 15-minute measurements but less so for 60-minute data correlation periods (data not shown). The average 60-minute solar irradiance obtained, using 5-minute point measurements using the Hobo H8 logger shows 98 % agreement with 10 second CM3 solar irradiance measurement using the CR7X logger (60-minute average) but with more scatter. Most data points outside the belts (Fig. 8.6) correspond to cloudy days (data point within the circle measured on cloudy days of year 338 (12h30) and 341 (09h30), 2002). Fig. 8.7 illustrates the measured solar irradiance for the clear days of year 311 and 329, 2002 respectively. The maximum deviation of measurement was observed during the mid-day and this can be expected to be more in cloudy days since it is a point measurement. However, Figs 8.6 and 8.7 illustrates that using 5-minute averaging period for the Hobo logging system improves the solar irradiance measurement of the Hobo H8 weather system. The time lag of CM3 (thermopile) sensor also contributes to some degree, which is greater than that for the Apogee PYR (silicon) sensor.

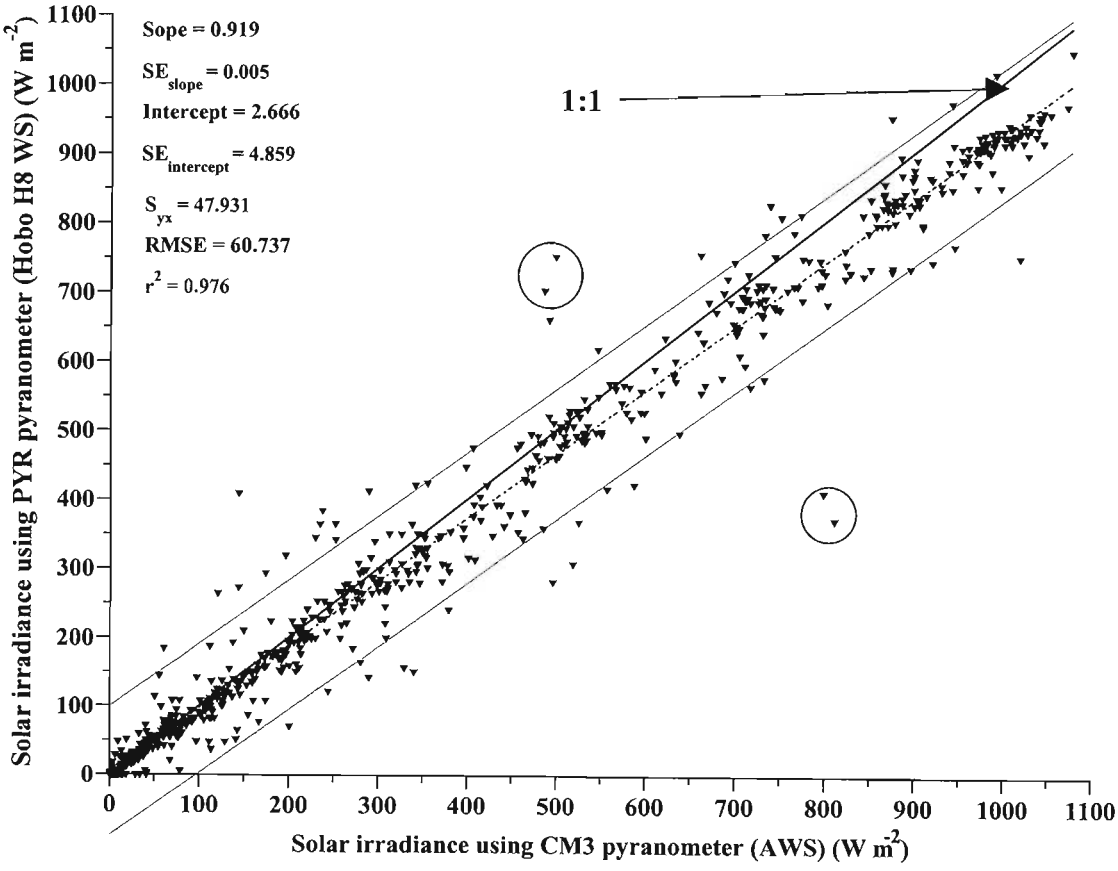

Fig. 8.6 Regression of the hourly average solar irradiance using Hobo H8 weather station (PYR is the Apogee pyranometer) and AWS (CM3 pyranometer) for day of year November 1 to December 29, 2002. The average of twelve consecutive 5-minutes Hobo H8 and 360 consecutive 10-second CR7X solar irradiance measurement were used as the 60-minute value

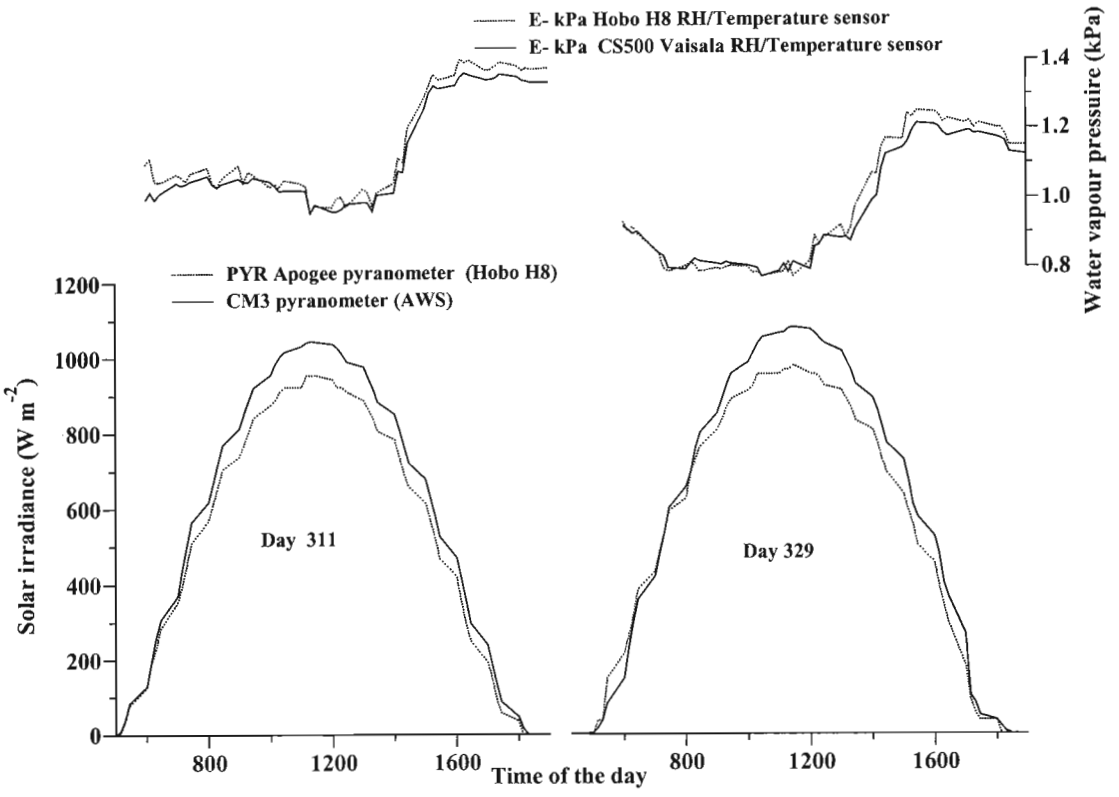

Fig. 8.7 The 15-minute interval solar irradiance and water vapour pressure measurements for two clear days of year (311 and 329, 2002) for an AWS (CM3 pyranometer and CS500 Vaisala RH/Temperature sensors connected to a CR7X data logger) and Hobo weather station (Apogee PYR pyranometer and Hobo H8 logger) systems

8.4.3 Air Temperature and Relative Humidity Comparisons

Air temperature is considered the second most important microclimate measure, which can affect the reference evaporation calculation besides solar irradiance. High frequency CS500 air temperature and relative humidity measurement using CR7X and 5-minute averaging of Hobo H8 logger were used to calculate the water vapour pressure. A comparison of 15-minute average air temperature measurement from 5-minute Hobo H8 and CR500 is shown in Fig. 8.8. The 5-minute average of Hobo H8 air temperature measurement is within 0.005 % of the high frequency CS500 measurement. Similarly the calculated Hobo H8 water vapour pressure was in close agreement with the AWS CS500 measurement but most of time greater than the CS500 measurement (Figs 8.7, 8.9). Using a 15-minute average water vapour pressure, calculated from the 5-minute point air temperature and relative humidity (RH) (Eq. 6.5) measurements were 98 % in agreement with 10-second interval measurement of the CR7X logger (15-minute average, Fig. 8.9).

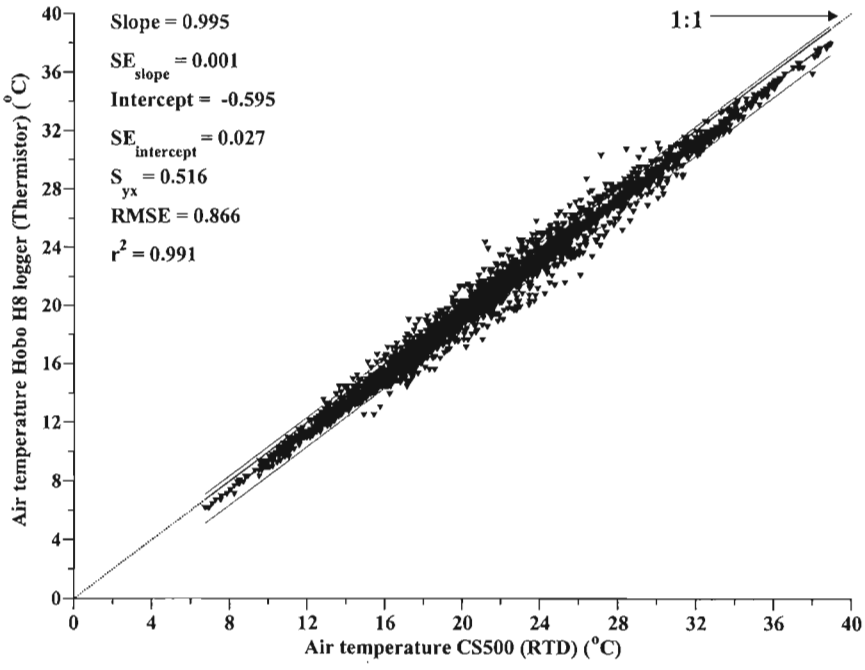

Fig. 8.8 Regression of the 15-minute interval average air temperature using AWS (CS500) and Hobo weather station (Hobo H8) for days November 1 to December 29, 2002. The average of three consecutive five minute Hobo H8 air temperature measurement were used as the 15-minute value

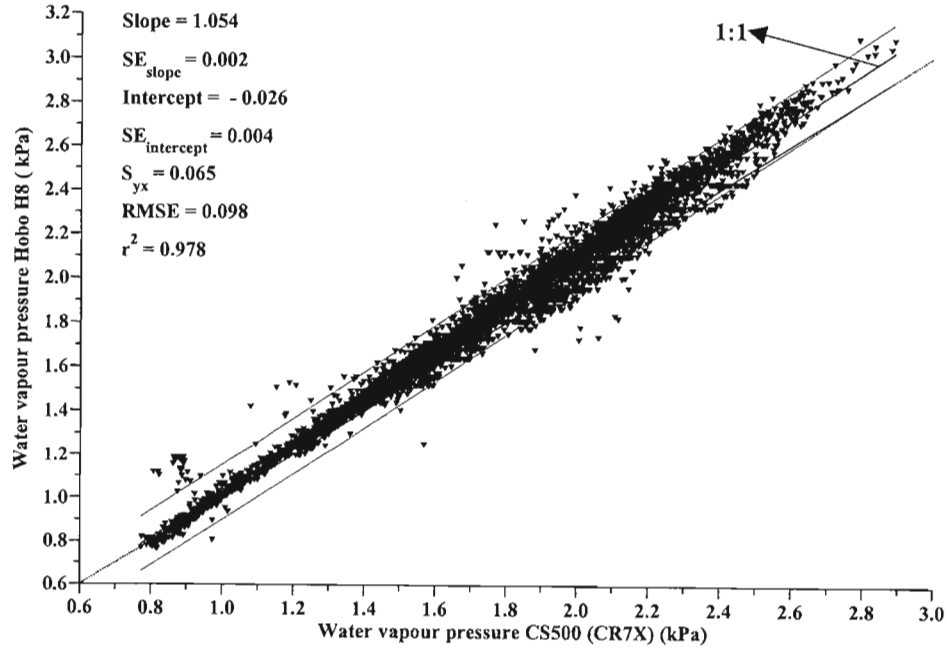

Fig. 8.9 Regression of the 15-minute water vapour pressure measurements using an AWS (CS500) *vs* that Hobo weather station (Hobo H8 logger) for days November 1 to December 29, 2002. The average of three consecutive five minute Hobo H8 air temperature and relative humidity measurement were used to calculate the 15-minute value

As Fig. 8.7 shows, the water vapour pressure varies from 0.8 to 1.4 kPa for the daytime hours but the water vapour pressure estimated from previous day minimum air temperature was 1.19 and 1.12 kPa for the days of year 311 and 329 respectively. Hobo H8 measurement of water vapour pressure better describes the actual water vapour pressure than that estimated from the minimum air temperature of previous day.

8.4.4 Wind speed and Rainfall

In various studies, wind speed is considered as the least important microclimatic measure for calculating evaporation. For the measurement period, the hourly wind speed varied between 0.2 to 4.7 m s^{-1}. The average hourly wind speed was 1.24 m s^{-1}. However, the possible use of the wind speed sensor with the Hobo H8 weather station system is still of concern and needs more research. The estimated wind speed (2 m s^{-1}) at 2 meter for the reduced set reference evaporation or Hobo H8 weather station system is greater than the average wind speed measured.

Rainfall was measured using a Rain-O-Matic rain gauge connected to an Event Hobo logger and another to a CR7X data logger. The cumulative record was equal using the two loggers (Fig. 8.10). However the Event Hobo logger timing of record could also be more accurate for the high frequency measurements (1 second).

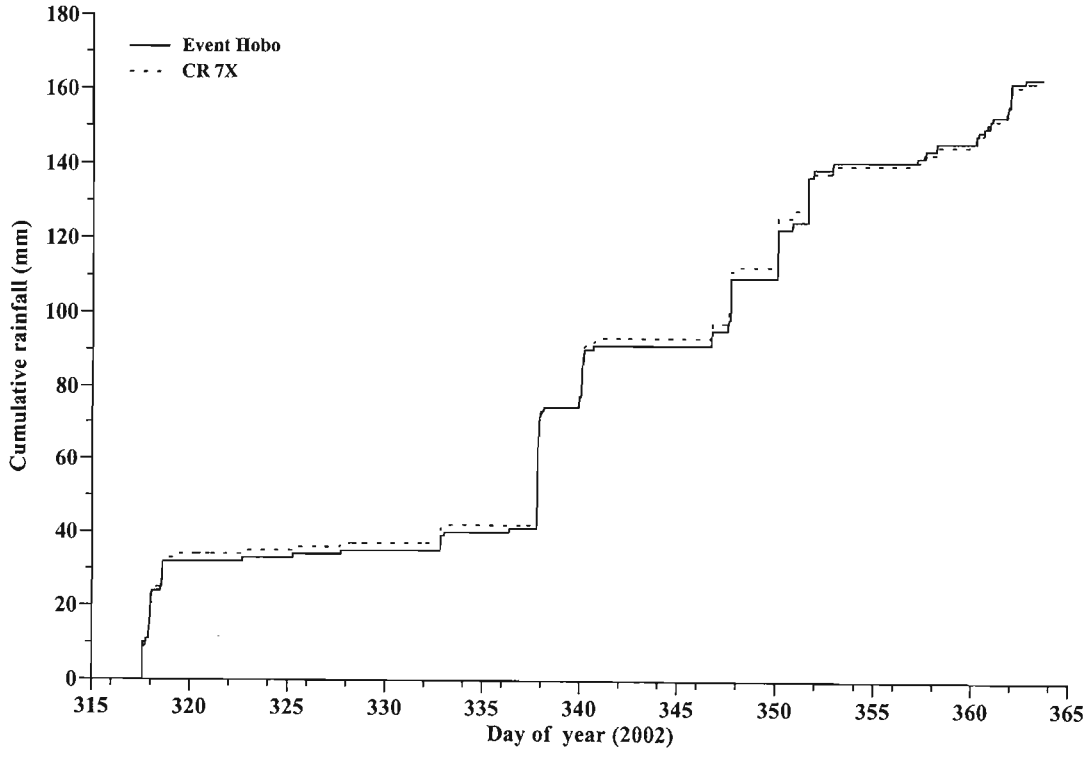

Fig. 8.10 Cumulative rainfall collected using a Hobo Event and CR7X loggers

8.4.5 Microclimatic Measures and Reference Evaporation Calculation

The importance of solar irradiance, air temperature and relative humidity and wind speed on reference evaporation estimates can be determined using a sensitivity analysis. A 10 % maximum error of the Penman-Monteith grass reference evaporation using an estimate for wind speed and water vapour pressure was reported in the unpublished Campbell Scientific Inc. (1998) application notes. However the relative importance of these microclimatic measures can be site- or time-dependent.

Unlike the standard AWS, the reduced set reference evaporation weather station (Campbell Scientific Inc. application notes 1998) avoids the need for measuring relative humidity and wind speed and direction. In the constantly changing microclimate, low frequency measurement of these microclimate variables can be worthwhile compared to using an estimated value (see Fig. 8.7). The low frequency Hobo H8 weather station air temperature, water vapour pressure and solar irradiance measurement compared well with their AWS counterparts. As Fig. 8.11 illustrates, using a 5-minute averaging period for the Hobo logger improves the solar irradiance measurement and reference latent heat estimate of Hobo H8 weather station system.

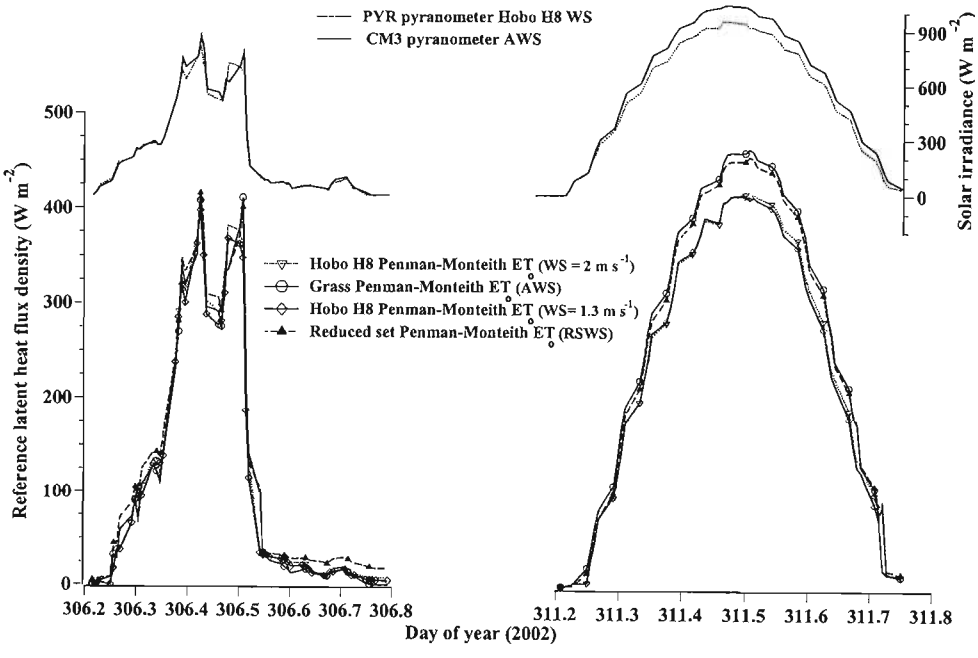

Fig. 8.11 Hourly reference latent heat flux density estimated using grass Penman-Monteith using AWS, using Hobo H8 weather stations (wind speed 2 and 1.3 m s^{-1}) and using the reduced set evaporation weather station (RSWS) (solar irradiance measured using the Apogee PYR pyranometer connected to a Hobo H8 data logger and a CM3 pyranometer connected to a CR7X data logger)

8.4.6 Automatic Weather Station (AWS) System

Table 8.2 shows the minimum possible options of sensors, loggers and peripheral equipment that can be used as part of an AWS system and reduced set evaporation weather station (without wind speed and direction and RH sensors). The maximum expected measurement error of sensors, based on the manufacturer specification of accuracy and present cost from supplier were presented previously (Table 8.2).

An AWS system can be easily equipped with electronic sensors, which allow the measurement of microclimatic measures and the calculation of reference evaporation with greater accuracy and at a different time step. For the calculation of reference evaporation, the CR10X can be replaced with CR200 and CR510 data loggers. Based on the estimation of minimum investment cost, the AWS component cost is given in Table 8.2. Depending on how the data is telecommunicated, data logger type and power source, the minimum investment cost of an AWS system (using materials in Table 8.2) can vary from R29,805 ($3635) to R47,170 ($5752). However the proper function and continuous use of the AWS needs also consideration of the hidden costs associated with ease of sensors use, site visitation, data analysis, waiting time of delivery, repair, and calibration and shipping cost.

The CR510 and CR200 data loggers are less expensive than CR10X. Their difference is that CR510 and CR200 have four and five single ended channels respectively while the CR10X has twelve single ended channels. The CR510 and CR200 also have two pulse and two excitation channels respectively. Furthermore the CR200 is incapable of keypad and multiplexer use. The CR200 data logger supports the direct RS-232 communications only. The inclusion of additional sensors to the CR200 logger is limited. Also the CR200 cannot be interrogated in the field and cannot display real-time data unless a laptop computer is connected. However the channel number are enough for measurement of five microclimatic measures. As a unit, the use of CR510 and CR200 logger can save 13 % and 24 % of the investment cost of the CR10X AWS system. However the per channel comparison showed the CR10X logger is cheaper than the CR510. Other major cost-increasing factors of reduced set evaporation weather station and AWS is the repair and calibration cost. It is much higher than for a Hobo weather station and ET-gage because of its complexity. Cost saving of the complimentary systems is assessed from the use for the estimate of reference evaporation and microclimate measures based on a number of factors: (*a*) accuracy; (*b*) the rapid availability of real-time information; (*c*) additional uses and users; (*d*) ease and complexity. Although the cost of each system may vary from country to country, as can be seen

from Tables 8.2 and 8.3, the complimentary options provide significant cost saving and reasonable accuracy compared to the conventional real time AWS measure. The investment cost of each system can be further minimized when large quantities are purchased thereby reducing shipping costs. The final decision as to which systems is most suitable may revolve around data telecommunication issues relative to the option of making frequent site visits. In the case of the Hobo weather system, frequent site visits would be needed if data is required for irrigation scheduling applications. The cost in time of these visits would need to be factored into the calculation. This cannot however be done here since the cost would vary for each application depending on the distance involved.

The 58 days (November 1 to December 29, 2002) reference evaporation calculation was used for the inter-comparison between the AWS and reduced set evaporation weather station, Hobo H8 weather station microclimatic measures and ET-gage evaporation measures. Since grass and alfalfa-based Penman-Monteith reference evaporation estimate using an AWS is considered as accurate for the alfalfa and short grass, the good agreement of alfalfa and grass based Penman-Monteith estimate using reduced set evaporation weather station, Hobo H8 weather station and ET-gage relative to AWS illustrates the relative accuracy of the grass and alfalfa-based Penman-Monteith reference evaporation estimate using systems and ET-gage measures.

8.4.7 Reduced Set Evaporation Weather Station (RSWS) Systems

The reduced set evaporation weather station system estimate of reference evaporation using the grass Penman-Monteith (assuming the wind speed is 2 m s^{-1}) describes 91 % of the relationship with the AWS estimate (grass Penman-Monteith) (Fig. 8.12). For the 58 days of measurement, the assumptions and approximations resulted in 13 % overestimation with reduced agreement compared to the result discussed in Chapter 7 (Section 7.5). This shows the variation of the accuracy of the estimate and variability of the system efficiency with season. Table 8.10 presents the average, total and standard deviation of daily reference evaporation measure of reduced set Penman-Monteith (RPM) and grass Penman-Monteith (GPM). The daily sum of hourly reduced set Penman-Monteith (RPM) estimate of reference evaporation was 18.5 % higher than grass Penman-Monteith (GPM) estimate from AWS. It is believed that the main bias may be the result of the water vapour pressure estimate, which could be a seasonally dependent.

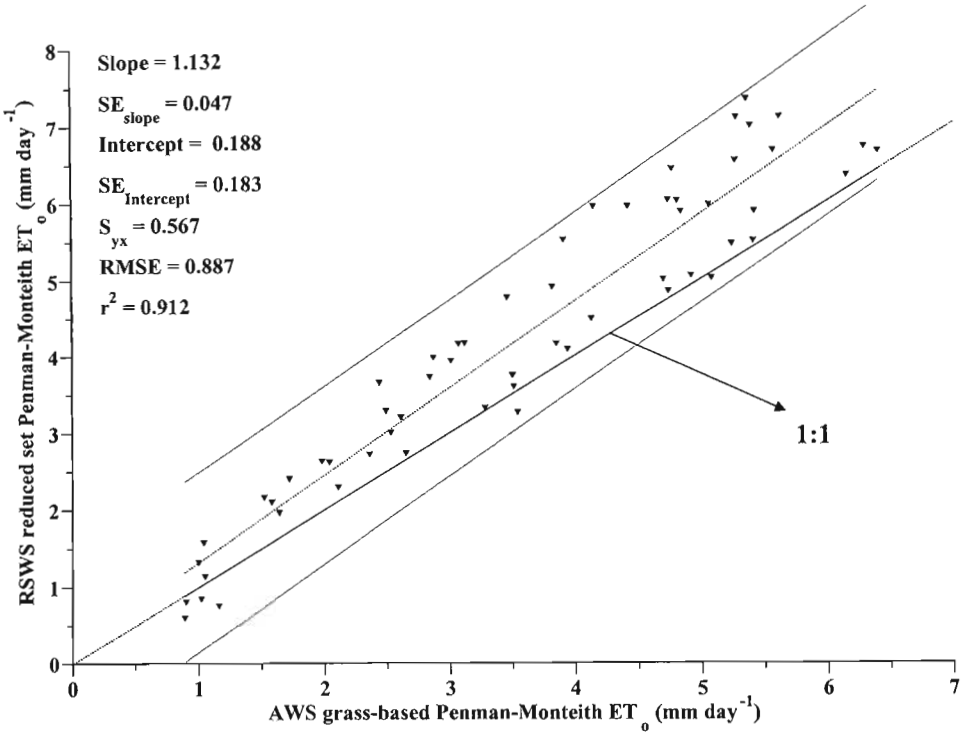

Fig. 8.12 Regression of daily grass reference evaporation estimate of Penman-Monteith using hourly sum of reduced set evaporation weather station and AWS systems for period of measurement November 1 to December 29, 2002

The investment cost saving in using the reduced set evaporation weather station is limited. The major cost of the AWS system is related to the data logger, communication system and hidden costs (Table 8.2). The minimum sensor cost in relation to the whole system is only 26 %. It is only 18 to 27 % of the investment cost that can be saved by using reduced set reference evaporation weather station system.

Table 8.10 Comparison between reference evaporation estimated for the period November 1 to December 29, 2002, using grass-based and alfalfa-based Penman-Monteith (GPM, ALPM) using AWS, Hobo H8 WS (HPM, using 2 and 1.3 m s^{-1}), reduced set evaporation weather station (RPM), ET-gage (Canvas 30, Canvas 54)

Method	AWS		RSWS	Hobo H8		ET-gage	
	GPM	ALPM	RPM	HPM2	HPM1.3	Canvas 30	Canvas 54
Average (mm)	3.56	3.99	4.21	3.34	3.21	3.27	4.06
SD (mm)	0.89	1.60	1.90	1.51	1.45	1.77	2.10
Total (mm)	206.21	231.24	244.31	193.75	186.26	189.48	235.46

SD is the standard deviation of daily reference evaporation estimate

The real-time access of information is the main advantage of reduced set evaporation weather station compared to Hobo weather station and ET-gage. The expected life time and robustness of the AWS system and reduced set evaporation weather station is also a major advantage of the more expensive systems.

8.4.8 ET-gage Evaporimeter

The evaporation measurements using an ET-gage evaporimeter could be useful in remote areas and for automatic irrigation scheduling. The device connected to a CR10X data logger was used for automatic irrigation by Parchomchuk *et al.* (2000) who reported a 70 % reduction of water loss for a growth season. The ease of use of the ET-gage as an evaporation-measuring device and cost makes the ET-gage a good alternative in remote areas where regular visits are not possible. The use of manual ET-gage (Model A) can minimize the cost even further but limit the accuracy of measurement compared to the electronic model E. At the present exchange rate, model A and E costs R1886 ($230) and R5116 ($624) respectively. Both models can be used without a data logger and computer but the use of Model E without a data logger results in higher investment cost compared to model A. The investment cost of the ET-gage (Model E) is 45 % and 24 % lower than the CR10X AWS investment cost when the Event Hobo logger and CR200 data logger are used as the data logging system respectively (Tables 8.2 and 8.3).

The 58 days (November 1 to December 29, 2002), 15-minute microclimatic measure from an AWS allowed the comparison between the AWS estimate of grass or alfalfa Penman-Monteith and ET-gage reference evaporation measure to be made over a time scale that ranged from two seconds to many days. The cumulative two-second-evaporation recorded using an Event Hobo logger and canvas 54 is shown in Fig. 8.13. According to Fig. 8.14 the Event Hobo recorded evaporation from canvas 54 is in good agreement with the reference evaporation estimated from hourly alfalfa based Penman-Monteith estimate. Similar agreement also observed using the canvas 30 measurements and grass Penman-Monteith estimate from the same CR7X logger (Figs 8.13, 8.15). However, the range can be wide up to ± 3.5.

ET-gage evaporation measure can be recorded either visually using a site tube or electronically. The electronic record gives a higher resolution (0.254 mm compared to 0.5 mm for the visual measurement) and increases the accuracy of measurement.

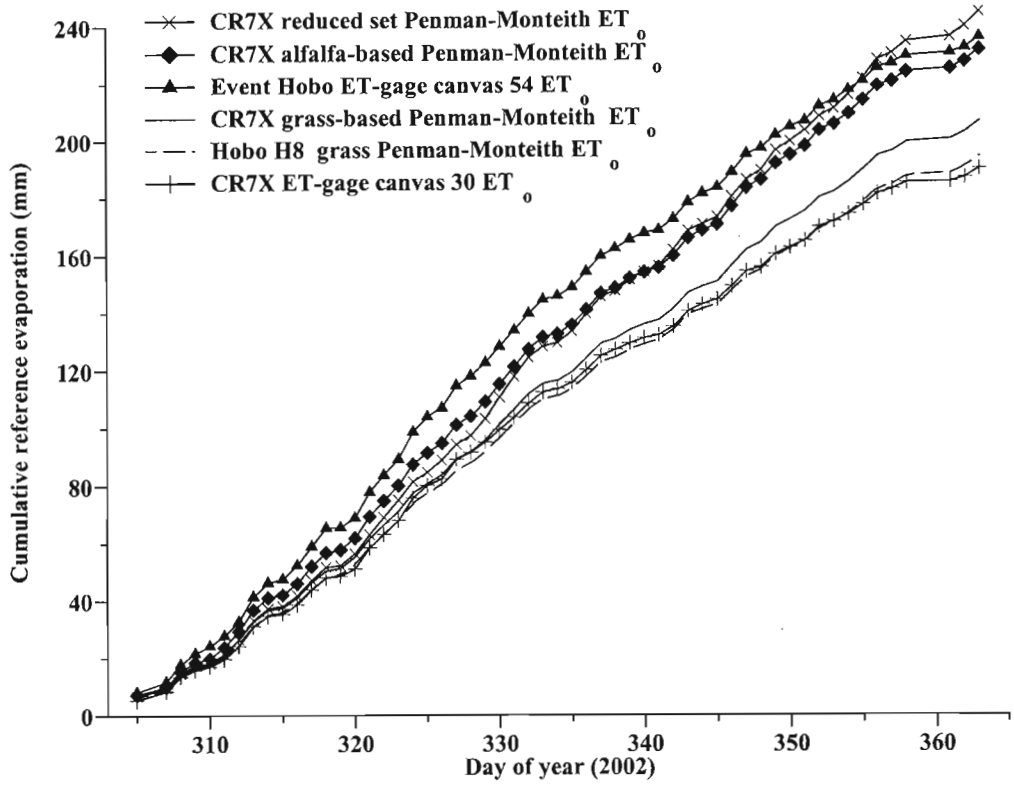

Fig. 8.13 Cumulative reference evaporation measured using an ET-gage evaporimeter (canvas 30 and 54), grass Penman-Monteith reference evaporation using Hobo H8 weather station (using a wind speed of 2 m s^{-1}), reduced set evaporation weather station (using a wind speed of 2 m s^{-1}) and AWS (grass and alfalfa based Penman-Monteith) reference evaporation (ET_o)

Using the Event Hobo logger instead of the multi-channel loggers, the ET-gage (canvas 54) (Figs 8.13, 8.14) measurement of reference evaporation shows a good agreement to the hourly alfalfa based Penman-Monteith of AWS estimate. However the ET-gage exhibits some lag after sunset that does not occur in the AWS estimates (Fig. 8.13). The 58 days canvas 30 and 54 ET-gage cumulative evaporation measures were only 8.12 % less than and 3.12 % more than sum of hourly grass and alfalfa based Penman-Monteith (GPM, ALPM) estimate respectively (Table 8.10). Although the agreement was lower than Hobo H8 weather station and reduced set evaporation weather station estimates, the slope and intercept regression values were not significantly different from one and zero respectively (α = 0.01). The agreement between the sum of hourly grass and alfalfa-based Penman-Monteith evaporation is 88 % for both canvas covers (Figs 8.14, 8.15).

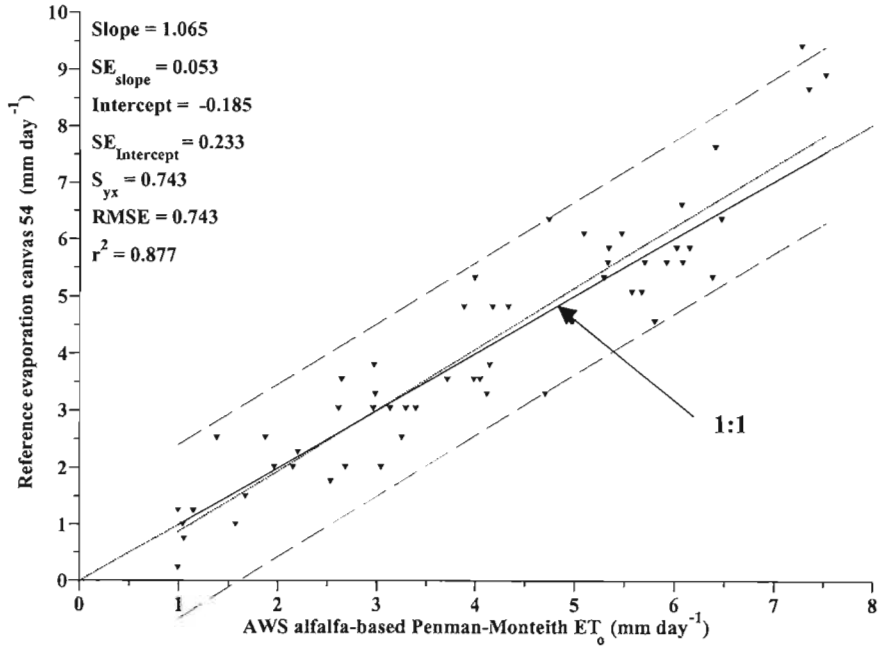

Fig. 8.14 Regression of hourly sum of daily Penman-Monteith grass reference evaporation estimate using an AWS system and ET-gage (canvas 54) reference evaporation (ET_o) measures for days November 1 to December 29, 2002

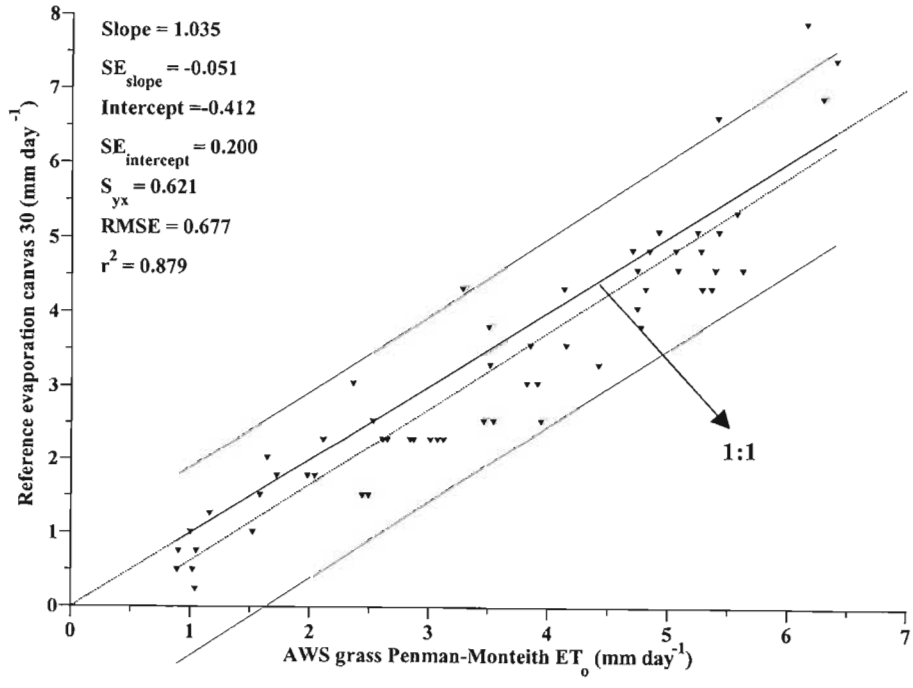

Fig. 8.15 Regression of hourly sum of daily Penman-Monteith grass reference evaporation (ET_o) estimate using an AWS system and ET-gage (canvas 30) reference evaporation measures for days November 1 to December 29, 2002

Figs 8.13,14, 15 show that the ET-gage evaporimeter measure is as accurate as the other systems but with more daily variation. As an evaporation device, the ET-gage can be an effective tool in terms of accuracy and cost for irrigation purposes compared to complimentary systems. However, its use in different microclimates needs consideration as discussed in Chapter 7 (Section 7.5). Furthermore, its advantage is limited to gathering information on evaporation data only. Nevertheless the frequency of measurement is also limited since it only measures cumulative evaporation.

8.4.9 Hobo Logging Weather Station (Hobo WS)

The Hobo weather station is fairly portable compared to the AWS system and reduced set evaporation weather station (RSWS) systems. The Hobo logger is a simple logger with memory and internal relative humidity and/or air temperature sensor. The Hobo weather station can have air temperature and/or relative humidity sensors and/or external channels capable of supporting additional external sensors. A disadvantage of the Hobo H8 RH/temp sensor is that the relative humidity sensor may be damaged in condensing environments. Care needs to be taken to ensure that water can freely drain from the sensor area by positioning the unit in the flat position and upside down. The long-term effect of possible condensation, with the sensor housed in a radiation shield, needs further investigation.

The Event Hobo logger is an event-recording logger with a capability of recording event at a frequency of one-second from rain gauges and atmometer model E ET-gage (http://www.onsetcomp.com/3648_event.html). Specifically, the Hobo H8 logger weather station has an air temperature and a relative humidity sensor and two external channels capable of supporting two additional external sensors, usually temperature and voltage sensors. Table 8.3 shows the potential accuracy, cost of weather station using three Hobo loggers and associated sensors.

Using the Hobo logger type as reference for the Hobo weather station system (Hobo H8, Hobo Temp, Hobo Thermocouple http://www.onsetcomp.com/3654_temp.html), an Event Hobo logger, Rain-O-Matic rain gauge, radiation shield, three different Hobo weather stations can be set up using the equipment and sensors presented in Table 8.3. The minimum estimated cost of a Hobo Temp weather station is 31 % of a CR10X AWS system. As a result, the number of Hobo weather stations for monitoring the microclimate of an area can be increased significantly. However the advantage of using Hobo Temp is limited compared to the Hobo H8 system. Hobo Temp and Hobo

Thermocouple can only be used for daily reference evaporation estimate using the measured maximum and minimum air temperature, estimated wind speed and estimated water vapour pressure. As a unit, the Hobo H8 data logger is more expensive than the Hobo Temp and Hobo thermocouple. However the per channel comparison showed the Hobo H8 data logger is less expensive than Hobo Temp and Hobo Thermocouple data loggers by 48 % and 63 % respectively. The Hobo H8 weather station system allows measurement of solar irradiance and one other external sensor in addition to the relative humidity and air temperature measurements. The Hobo Shuttle may be used with Hobo weather station systems provided that continuous data collection is the priority of the user. The inclusion of solar irradiance and Hobo shuttle can improve the Hobo H8 system with an increase in investment cost by 12 % and 14 % respectively. Furthermore, use of a home-made radiation shield can reduce the system cost by 3 %.

The new micro station data logger (H21-002, http://onsetcomp.com/7910_weather.html) is 32 % more expensive than the Hobo H8 weather system used in this study. Generally the Hobo weather station system is less complex than the AWS or reduced set evaporation weather station systems.

Although the accuracy of Hobo H8 weather station reference evaporation estimate depends on the approximated wind speed, the 58 days measurement showed good agreement with AWS measurements. The same 58 days were used for the comparison of hourly sum of grass Penman-Monteith reference evaporation estimate from Hobo H8 weather station (HPM) (Table 8.10, Figs 8.16, 8.17). The linear regression shows 99 % agreement compared to AWS (GPM) estimate. The intercept is not significantly different from zero at $\alpha = 0.01$ when wind speed was approximated as 2 m s^{-1}. The reference latent heat flux density for two days computed from AWS (GPM) and the Hobo H8 weather station is shown in Fig. 8.11. The point measurement of solar irradiance for cloudy days (day of year 306, 2002) could affect the Hobo H8 weather station reference latent heat flux density estimate more than the AWS estimate relative to a clear day (day of year 311, 2002). The maximum difference on clear days (day of year 311, 2002) occurs at the midday hours, while on cloudy days (day of year 306, 2002) the estimate is almost the same. This may be the result of high frequency measurement and time lag of CM3 measurement. The measurement of relative humidity further increases the accuracy of evaporation estimate compared to the reduced set evaporation weather station estimate.

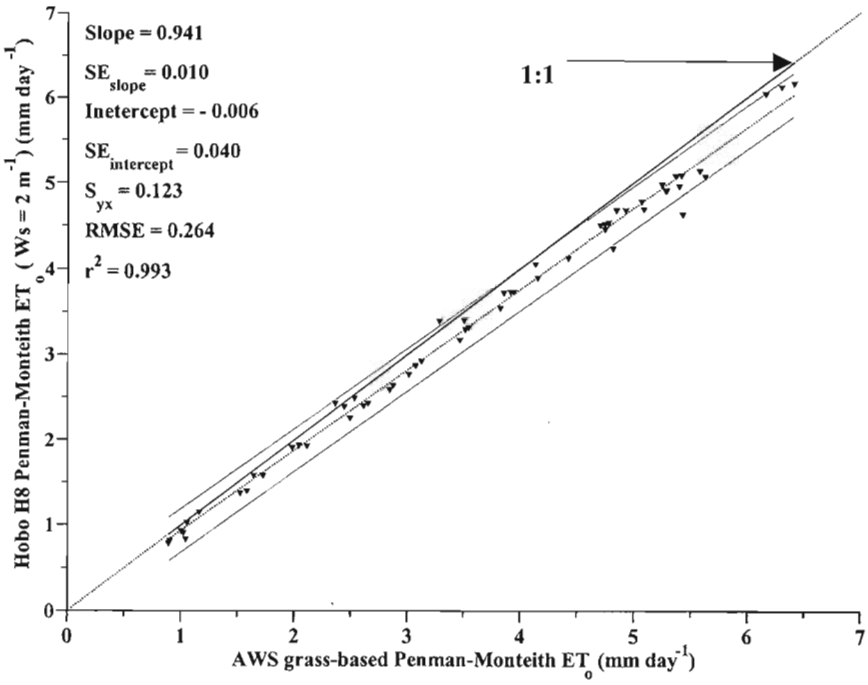

Fig. 8.16 Regression of hourly sum of daily grass-based Penman-Monteith reference evaporation estimated using AWS and Hobo H8 weather station assuming wind speed is 2 m s^{-1} for days November 1 to December 29, 2002

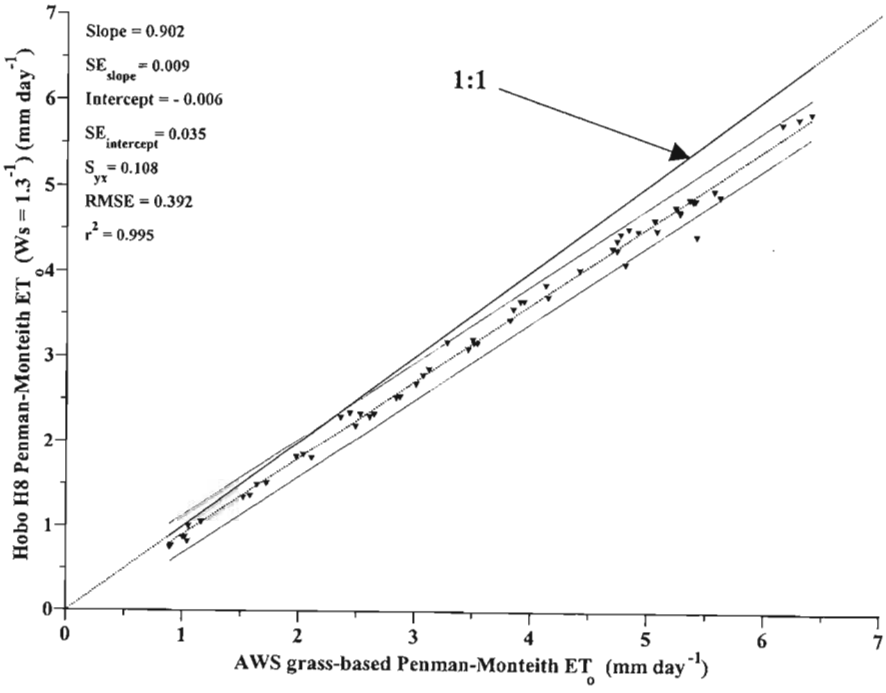

Fig. 8.17 Regression of hourly sum of daily grass-based Penman-Monteith reference evaporation estimated using AWS and Hobo H8 weather station assuming wind speed is 1.3 m s^{-1} for days November 1 to December 29, 2002

8.4.9.1 Event Hobo logger

As a simple test of Event Hobo logger robustness, two electronically recording ET-gages (Model E) and a rain gauge were placed side by side connected to Event Hobo and 21X (for seven days) and CR7X (for 47 days) loggers respectively. The 24-hour sum of recorded evaporation of the 21X and Event Hobo is shown in Fig. 8.18 (3 days in August, 2002). Seven day two ET-gage cumulative records were 53.3 mm for both loggers. The agreement of the recorded measures between the two loggers remains the same except for the lag created due to the ET-gage response. The total rain recorded over 47 days was equal between the CR7X logger and the Event Hobo logger (Fig. 8.10). The performance of Event Hobo logger as an event-recording logger for the two ET-gage and rain gauge sensors were in good agreement with 21X and CR7X loggers. Furthermore the Event Hobo-recorded evaporation of ET-gage (canvas 54) was in close agreement to the alfalfa-based reference evaporation estimate of Penman-Monteith using the CR7X logger (Fig. 8.14). However the difference in frequency of measurement resulted in small differences of event timing using rain gauge (Fig. 8.10).

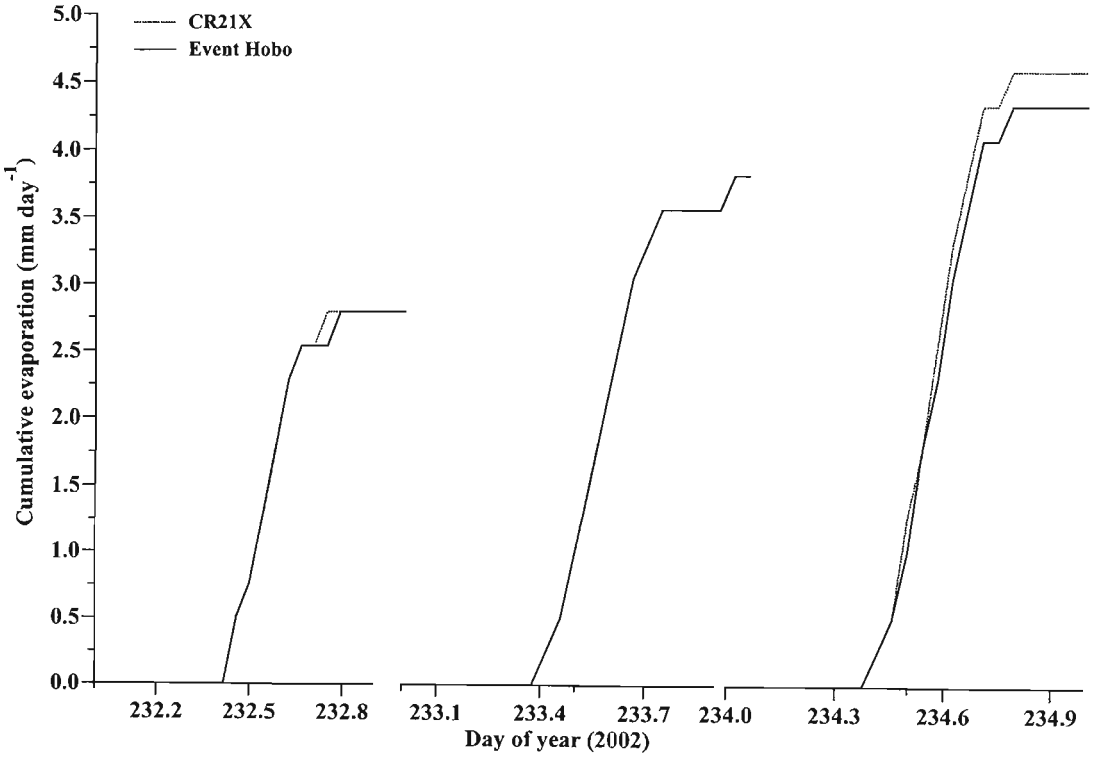

Fig. 8.18 Daily cumulative record of ET-gage (canvas 54) reference evaporation measured using 21X and Event Hobo loggers (3 days in August, 2002)

8.4.9.2 Limitation of Hobo logging weather station

The Hobo logger weather station is inexpensive and user friendly compared to the AWS system and the reduced set evaporation weather station system. The main limitation of the Hobo system lies in the need for high frequency measurements, which is limited by the memory capacity of logger, and the absence of data telecommunication capability. For example, the memory of the Hobo H8 logger lasts 13 days when a 5-minute interval is used for air temperature and relative humidity. However the biggest disadvantage of the Hobo system lies in their lack of data telecommunication. The additional use of external sensors and an increase in frequency of the measurements limit the memory and increase frequency of visits to the Hobo weather station. Furthermore, the logger can be affected by radiation, humidity and rain. The Hobo logger therefore requires a radiation shield. The humidity sensor can be damaged during condensing events. However, the use of a weatherproof cover can reduce its damage in the open environment. The resolution limit and absence of wind speed and direction measuring systems are other drawbacks of the system. Also, the Hobo logger cannot be interrogated in the field and cannot display real-time data unless Hobo Shuttle or a laptop computer is connected.

A recorded voltage was noticed without external voltage sensors connected when using the Hobo H8 logger. The recorded voltage was constant for a given logger but variable in value between Hobo loggers. Measurement of voltage without external sensor using launched Hobo H8 logger can give the offset value. The deduction of this offset from the measured voltage can decrease the voltage measurement error of Hobo H8 weather station. Hobo H8 logger use can also be limited to the resolution of the connected sensor. The resolution can be improved using a temperature independent amplifier. Alternatively a pyranometer with a larger irradiance to voltage multiplier, such as the Apogee PYR sensor can be used.

Care is needed when connecting the Event Hobo logger since touching of the two connecting wires can be recorded as an event. This problem can be solved using the Shuttle Hobo logger, which is capable of collecting data and programming the Hobo loggers. Alternatively the Event Hobo logger could be disconnected from the ET-gage early in the morning or during clear days for the rain gauge.

8.5 CONCLUSIONS

In general there was reasonable agreement between the alternative or complimentary systems and the AWS estimate of reference evaporation using the hourly Penman-Monteith approach. However, when estimating reference evaporation, the minimum investment cost of an AWS system was equivalent to having six Hobo H8 weather stations systems or three ET-gage evaporimeters (Model E plus Event Hobo logger). In terms of cost and accuracy, the Hobo weather station and ET-gage measures of evaporation are better complimentary systems compared to the reduced set evaporation weather station. In general however, the cheaper systems should be used to compliment measurements collected using AWS systems.

The Hobo H8 weather station was found to be a simple and relatively low cost system that allowed continuous data logging of air temperature, relative humidity, rainfall and other measurements. The water vapour pressure was within 5 % of the AWS measures. The solar irradiance was within 8 % of the AWS measures but with more scatter. The addition of an amplifier to the Hobo system may improve the solar irradiance measure and the voltage resolution limit. Above all, the reference evaporation estimate was within 6 % of the AWS estimate. The Event Hobo data logger was capable of recording rainfall data to a similar accuracy of the other multi-channel data loggers. The greater accuracy of reference evaporation estimate compared to reduce set and ET-gage evaporimeter, low investment cost requirement and ease of use of the Hobo H8 weather station system makes it ideal for complimenting more expensive methods of estimating reference evaporation.

ET-gage measurements of reference evaporation (canvas 30 and 54) were about 4 % and 7 % greater than the grass and alfalfa-based Penman-Monteith reference evaporation estimate using an AWS respectively. The daily agreement was relatively lower compared to the reduced set evaporation weather station and Hobo H8 weather station system reference evaporation estimates, but the cumulative and average measures were in better agreement compared to the others. The relatively low investment cost and accuracy are the main advantages of the ET-gage evaporimeter. However, it is limited to reference evaporation measurements only. Although the accuracy and resolution is limited, the investment cost was a minimum through the use of Model A. The use of an Event Hobo logger with the ET-gage (Model E) evaporimeter was found to give better results with little increase in investment cost.

CHAPTER 9

DISCUSSION, CONCLUSIONS AND RECOMMENDATIONS FOR FUTURE WORK

9.1 DISCUSSION AND CONCLUSIONS

9.1.1 Introduction

A proper and wide application of irrigation scheduling and management of water resources requires an accurate and inexpensive technique or approach for estimating the actual evaporation. The approach of using a crop factor and reference evaporation depends on the accuracy of reference evaporation estimate. Micrometeorological methods (Penman-Monteith and STEB) for estimating reference evaporation could be relatively the best option rather than an absolute method (lysimetry). However, the application of the techniques is limited due to: 1) the cost; 2) the assumptions and approximations made when estimating reference evaporation due to limited data, inaccurate data and theoretical assumptions made. All of these factors impact on the accuracy of grass and alfalfa Penman-Monteith and STEB grass reference evaporation estimates. This work has investigated:

- available energy estimate for the Penman-Monteith;
- stability correction procedure for the STEB estimate.

The reliability of inexpensive and flexible reference evaporation and microclimate measuring options was also investigated, where the following were used:

- reduced set evaporation weather station;
- ET-gage evaporimeter and;
- Hobo weather station.

The investment cost and accuracy of each system was noted. In addition, the possible use of home-made plastic radiation shields was explored. Recommendations for the improvement of the Hobo weather station and the ET-gage evaporimeter were presented.

9.1.2 Reliability of Assumptions and Approximation of Penman-Monteith

Different approaches are developed for estimating the available energy term for the grass and alfalfa based Penman-Monteith approach for calculating reference evaporation. The different approaches of estimating hourly net irradiance evaluated in this study showed similar results. Their accuracy was within 10 % of the measured net irradiance. A maximum deviation was

noted for the Campbell (undated) procedure, which underestimated by 8 %. The atmospheric minus crop emittance estimate was limited to a certain range of values compared to the measured values. The linear approach of atmospheric minus crop emittance estimate underestimated the measured net long wave irradiance and showed lower agreement compared to the other similar clear sky empirical formulations. The clear sky daytime net long wave irradiance estimation from air temperature was closer to a logarithmic than to a linear relationship. The estimated reflected solar irradiance was overestimated for the reference crop. The estimation was 5 % more than the measured average. The measured hourly surface soil heat flux density was more variable depending on the cloud cover, net irradiance, wind speed and soil water content. The approximation of soil heat flux density was closer to the soil heat flux density measured using soil heat flux plates than surface soil heat flux density. The overall result observed on the available energy estimation (Campbell undated) was a cancellation of energy balance components, with that overestimated cancelling with those that were underestimated. As a result, the estimated available energy flux density of Campbell (undated) was in good agreement with measured or at least estimated to within 7 % of the measured values. However, the use of locally calibrated coefficients, developed from hourly data can improve the estimation accuracy of the approach.

The Campbell (undated) procedure for hourly grass Penman-Monteith reference evaporation underestimated when using an estimated reflection coefficient and estimated soil heat flux density but overestimated when soil heat flux density was simply ignored. The Penman-Monteith grass reference evaporation estimate was more sensitive to the ignored soil heat flux density than to an approximated value.

9.1.3 Surface Temperature Energy Balance Techniques (STEB)

The STEB estimate of reference evaporation was overestimated compared to the grass reference evaporation Penman-Monteith estimate. The STEB reference evaporation estimate using the Campbell and Norman (1998) stability correction procedure and uncorrected STEB estimate overestimated the grass reference evaporation Penman-Monteith estimate by 8 % and 11 % respectively. The Monteith (1973) procedure applied to the corrected STEB estimate underestimated grass reference evaporation by 4 %. The performance of the STEB estimate was found to be affected by the stability correction procedure. The overestimate of reference evaporation using estimated available energy was 7 % more compared to the uncorrected STEB estimate. The surface-air temperature difference was found to have a greater effect on the Monteith (1973) correction procedure compared to that of Campbell and Norman (1998).

9.1.4 Reduced Set Penman-Monteith Approach

Hourly and daily procedures for estimating Penman-Monteith reference evaporation using a reduced set of input data showed time and procedure dependent errors. More error was observed when using a daily procedure. The daily procedure underestimated the reference evaporation by 36 % for the Agrometeorology site. This may be because of the poor estimate of water vapour pressure deficit from daily maximum and minimum air temperature. The maximum overestimation of hourly reference evaporation estimate using the reduced set grass Penman-Monteith method was observed to be 13 % (November 1 to December 29, 2002), which was more than the first period estimate of error (December 27, 2001 to July 12, 2002). For the same site, the second period of measurement the reduced set estimate was 10 % greater. This indicates the possible existence of an accuracy that varies with seasons. The approximation of wind speed as 2 m s^{-1} with hourly estimated reference evaporation showed good results for the main site used. The reduced set Penman-Monteith assumptions and approximations were relatively effective for hourly and shorter time periods compared to the use with a daily procedure.

The use and access of a reduced set evaporation weather station system is greatly dependent on the cost of the system. As the investment cost analysis showed, the system cost was more or less similar to that of the full AWS system. Only 18 to 27 % of investment cost of AWS could be saved through the use of a reduced set evaporation weather station system. Since the cost of the relative humidity and wind speed sensors are only 26 % of the investment cost required for the AWS, it may be more worth having these sensors than replacing them with approximations.

9.1.5 Performance of the ET-gage Evaporimeter

Electronic model ET-gage (Model E) evaporimeter together with an Event Hobo data logger was an effective system for daily reference evaporation measurement in terms of accuracy and investment cost. The agreement with grass and alfalfa Penman-Monteith reference evaporation estimate was found to be above 60 % except when measurements were under shade. The maximum daily underestimate of grass reference evaporation estimate using canvas 30 was 12 % with much more similar average and cumulative reference evaporation measures. The maximum daily overestimate of canvas 54 evaporation measurements was observed under shade netting (solar irradiance transmittance 76 %). The cumulative measurement was almost twice as much as the alfalfa Penman-Monteith reference evaporation estimate. Although there were limited measurements, the shade netting ET-gage response was more sensitive to measured water vapour pressure deficit than to the solar irradiance. As a daily measure, the Cedara visual reading (canvas 54, ET-gage mode A) showed 77 % agreement to the alfalfa Penman-Monteith

reference evaporation estimate. However, the visual reading overestimated the alfalfa Penman-Monteith estimate by 26 %. The electronic measure increased the accuracy of daily ET-gage evaporimeter reference evaporation measure, compared to the visual reading. The use of an Event Hobo logger with the electronic ET-gage evaporimeter was found to minimize the investment cost by 50 % compared to the use of a CR10X data logger.

There was little difference between the ET-gage reference evaporation measured at a height of 1 meter, compared to that measured at 2 meter. Reference evaporation estimated using AWS measurements at both heights confirmed this result.

Cumulative evaporation estimates from a saturated ET-gage evaporation surface using the STEB method was within 7 % of the cumulative ET-gage canvas 54 evaporation. The late evening response of the ET-gage was observed to relate to the daytime water vapour pressure deficit and wind speed.

9.1.6 Hobo H8 Weather Station

The Hobo H8 weather station microclimate measure of reference evaporation was found to be reasonable compared to the AWS measures at a much-reduced cost. The water vapour pressure was in close agreement to the AWS system measure. It was within 5 % of the high frequency measure of AWS. The Hobo H8 solar irradiance measure was found to be within 8 % of the AWS measure. The cumulative error was a 6 % underestimate of the hourly grass Penman-Monteith reference evaporation estimate when wind speed was assumed to be 2 m s^{-1}. The high frequency point microclimatic measurement using the system was found to give relatively better results and improved accuracy compared to the reduced set evaporation weather station system. In terms of ease, portability, cost and accuracy, the Hobo system was adequate for the microclimatic measure and reference evaporation calculation compared to the reduced set evaporation weather station system. The major limitation of the Hobo system is the absence of data telecommunication capability and memory limit.

9.1.7 Radiation Shield

Accurate measurements of air temperature and relative humidity were obtained using the plastic home-made radiation shields. The maximum average air temperature and water vapour pressure difference were 0.05 °C (using small sized home-made seven-plate plastic radiation shields) and 0.006 kPa (using the large sized home-made seven-plate plastic radiation shields) relative to measurements made in a standard Stevenson screen. The difference was almost similar to the six- and twelve-plate Gill radiation shields. With all radiation shields, the highest air temperature difference was observed in the morning hours of clear days when the solar

elevation and wind speed was low. The highest average of the air temperature difference was obtained from the single louvered small Stevenson screen and home made seven-plate metal radiation shield. The efficiency of the small Stevenson screen and seven-plate metal radiation shield seems to be limited in the open environment when wind speed is low.

9.2 RECOMMENDATIONS FOR FUTURE STUDY

There is a need for more research on the performance of the ET-gage evaporimeter in a closed environment to find the causes of the overestimation in shade environments. The use of ET-gage model E with a data logger is recommended compared to model A. In addition to this, the use of Hobo H8 weather station system needs further investigation on the techniques to measure wind speed using voltage-measuring sensors. The motivation for more research is the simplicity and minimum investment cost requirement of systems and the need of wide technology transfer of the applications. The clear sky air temperature and net long wave irradiance relation may be better expressed using a logarithmic relation. More study and correlation is needed to improve and develop a better hourly relation for future use.

REFERENCES

Aase JK, Idso SB (1978) A comparison of two formula types for calculating long wave radiation from the atmosphere. Water Resource Res 14: 623-625

Alam M, Trooien JL (2001) Estimating reference evapotranspiration with an atmometers. App Eng Agric 17: 153-158

Al-Ghobari HM (2000) Estimation of reference evapotranspiration for southern region of Saudi-Arabia. Irrig Sci 19: 81-86

Allen RG (1996) Assessing integrity of weather data for reference evaporation estimation. J Irrig Drain Eng ASCE 122: 97-106

Allen RG, Jensen ME, Wright JL, Burman RD (1989) Operation estimation of reference evaporation. Agron J 81: 650-662

Allen RG, Pereira LS, Raes D, Smith M (1998) Crop evapotranspiration: guideline for computing crop water requirement. FAO Irrigation and Drainage Paper 56. FAO, Rome, pp 1-209

Allen RG, Pruitt WO (1986) Rational use of the FAO Blaney-Criddle formula. J Irrig Drain Div ASCE 112: 139-155

Allen RG, Smith M, Pereira LS, Perrier A (1994*a*) An update for the definition of reference evapotranspiration. ICID Bull 43: 1-34

Allen RG, Smith M, Pereira LS, Perrier A (1994*b*) An update for the calculation of reference evapotranspiration. ICID Bull 43: 35-92

Altenhofen J (1985) A modified atmometer for on-farm evapotranspiration determination. In: Proc National Conference on Advances in Evapotranspiration. ASAE, Chicago IL, USA, pp 177-184

Altenhofen J (1992) ETgage: a field device for simulating ET. In: Proc Irrigation Association Conference. The Irrigation Association, Fairfax, USA, pp 12-20

Alves I, Pereira LS (2000) Modeling surface resistance from climatic variables? Agric Water Manage 42: 371-385

Amarakoon D, Chen A (1999) Estimating daytime net radiation using routine meteorological data in Jamaica. Caribbean J Sci 35: 132-141

Angstrom A (1924) Solar and terrestrial radiation. Quart J Roy Meteorol Soc 50: 121-125

Anonymous (1961) Handbook of Meteorological Instruments Part I. Instruments for Surface Observation, London: Her Majesty's Stationery Office, London, UK

Apogee Instrument Inc (2002) Infrared-red thermocouple sensor: Model IRTS-P. [Online.] [2 p.] Available at ftp://ftp.campbellsci.com/pub/outgoing/lit/b_irts-p.pdf (accessed 3 December 2002; verified 25 May 2003). Apogee Instruments Inc, Logan, Utah, USA

Aubinet M (1994) Long wave sky radiation parameterizations. Solar Ener 53: 147-154

Bekhøi International (2002) Rain-O-Matic. [Online.] [3 p.] Available at http://www.pronamic.com/3_in_1_dansk.htm (accessed 3 December 2002; verified May 2003). Bekhøi International, Hagemannsvej, 78600 Silkeborg, Denmark

Berdahl P, Fromberg R (1982) The thermal radiance of clear sky. Solar Ener 29: 299-314

Berdahl P, Martin M (1984) Emissivity of clear skies. Solar Ener 32: 663-664

Berkowicz R, Prahm LP (1982) Sensible heat flux estimation from routine meteorological data by the resistance method. J Appl Meteorol 21: 1845-1865

Blaney HF, Criddle WD (1950) Determining water requirement in irrigated areas from climatological and irrigation data. USDA, SCS, TP 96, pp 1-48

Bouchet RJ (1963) 'Evapotranspiration r'eelle e'vapotranspiration potentielle, et production agricole', ann. Agron 14: 743-824

Bristow KL, Campbell GS (1984) On the relationship between incoming solar radiation and daily maximum and minimum temperature. Agric For Meteorol 31: 159-166

Brochet P, Gerbier N (1972) 'Un m'thode de calcul de l' evapotranspiration potentielle'. Ann Agron 21: 31-49

Broner I, Law RAP (1991) Evaluation of modified atmometer for estimating reference evaporation. Irrig Sci 12: 21-26

Brunt D (1932) Notes on radiation in the atmosphere. Quart J Roy Meteorol Soc 58: 389-418

Brutsaert W (1975) On the derivable formula for the long-wave radiation from clear skies. Water Resource Res 11: 743-744

Brutsaert W (1982) Evaporation in the Atmosphere. Reidel, Dordrecht, Holland

Burman RD, Nixon PR, Wright JL, Pruitt WO (1980) Water requirement. In: Jensen ME (ed) Design and Operation of Farm Irrigation Systems. ASAE, New York, USA, pp 819-825

Campbell GS (undated) On-line measurement of potential evapotranspiration with Campbell Scientific automated weather station. Application note produced by Campbell Scientific Inc. in corporation with G S Campbell

Campbell GS, Norman JM (1998) An Introduction to Environmental Biophysics. 2nd ed Springer-Verlag, New York, USA

Campbell Scientific Inc. (1998) Reduced set evapotranspiration station. Application notes 4-T, Logan, Utah, USA

Campbell Scientific Inc (2002) Evapotranspiration Monitoring Stations: Models ET101 and ET106. [Online.] [4 p.] Available at ftp://ftp.campbellsci.com/pub/outgoing/lit/eto.pdf (accessed 3 December 2002; verified 25 May 2003). Campbell Scientific Inc, Logan, Utah, USA

Campbell Scientific Inc (2002) Data logger product line. [Online.] [4 p.] Available at http://www.campbellsci.com/logger.html (accessed 3 December 2002; verified 25 May 2003). Campbell Scientific Inc, Logan, Utah, USA

Carder AC (1960) Atmometer assemblies, a comparison. Can J Plant Sci 40: 700-706

Chang J (1968) Climate and Agriculture. Aldine, Chicago, USA

Chouduhury BJ, Idso SB, Reginato RJ (1987) Analysis of an empirical model for soil heat flux under a growing wheat crop for estimating evaporation by an infrared-temperature based energy balance equation. Agric For Meteorol 39: 283-297

Choudhury BJ, Reginato RJ, Idso SB (1986) Analysis of infrared temperature observations over wheat and calculation latent heat flux. Agric For Meteorol 37: 75-88

Christen JE (1968) Pan evaporation and evapotranspiration from climatic data. J Irrig Drain Div ASCE 94: 243-265

Christen JE, Hargreaves GH (1969) Irrigation requirement from evaporation. Trans Int Comm Irrig Drain III: 23.569-23.596

Clothier BE, Clauson KL, Pinter IR, Moran MS, Reginato RJ, Jackson RD (1986) Estimation of soil heat flux from net radiation during the growth of alfalfa. Agric For Meteorol 37: 319-329

De Bruin HAR, Stricker JN (2000) Evaporation of grass under non-restricted soil moisture conditions. Hydro Sci J 45: 39-406

Denmead OT (1976) Temperate cereals. In: Monteith JL (ed) Vegetation and the Atmosphere. Vol.2, Academic Press, New York, USA, pp 1-30

Dilley AC, Helmond I (1973) The estimation of net radiation and potential evapotranspiration using atmometer measurement. Agric Meteorol 12: 1-11

Dong A, Grattan SR, Carrol JJ, Prashar CRK (1992) Estimation of daytime net radiation over well-watered grass. J Irrig Drain Div ASCE 118: 467-479

Doorenbos J (1976) Agro-meteorology field station. FAO Irrigation and Drainage Paper 27. FAO, Rome, pp 1-94

Doorenbos J, Pruitt WO (1977) Guideline for predicting crop water requirements. FAO Irrigation and Drainage Paper 24. FAO, Rome, pp 1-107

Dusek DA, Howell TA (1996) Effectes of instrument shelters on air temperature and humidity measurements. In: Proc Evapotranspiration and Irrigation Scheduling. ASAE, St. Joseph, Michigan, USA, pp 491-496

Environmon (2002) Environmental Monitoring and Control Systems: MC systems instruments price list. October 2002. [Online.] [8 p.] Available at http://www.enviromon.co.za (accessed 15 December 2002; verified 25 May 2003). Cape Town, South Africa

Feldhake CM, Boyer DG (1988) Use of Bellani plate evaporimeter for estimation of PET. Agric For Meteorol 42: 219-227

Feldhake CM, Boyer DG (1990) Bellani evaporation variation in hill-land pasture. Agric For Meteorol 51: 211-222

Fitzpatrick EA, Stern WR (1965) Components of radiation balance of irrigated plots in a dry monsoonal environment. J Appl Meteorol 4: 649-660

Fitzpatrick EA, Stern WR (1966) Estimation of potential evaporation using alternative data in Penman's formula. Agric Meteorol 3: 224-239

Fontaine TA, Todd DE (1993) Measurements of evaporation with ceramic Bellani plate atmometers. Water Res Bull 29: 785-795

Giambelluca TW, Mckenna DL, Ekern PC (1992) An automated recording atmometer: calibration and testing. Agric For Meteorol 62: 109-125

Glenn E (2003) Hypertext book thermal physics. [Online.] [5 p.] Available at http://hypertextbook.com/physics/thermal/heat-sensible/ (accessed February 18, 2003; verified may 25 2003).

Glover J, McCulloch JSG (1958) The empirical relationship between solar radiation and hours of sunshine. Quart J Roy Meterol Soc 84: 172-175

Goodin DG, Hutchinson JMS, Vanderlip RL, Knapp MC (1999) Estimating solar irradiance for crop modeling using daily air temperature data. Agron J 91: 845-851

Guyot G (1997) Physics of the Environment and Climate. John Wiley and Sons, Paris, France

Halkias NA, Veihmeyer FS, Hendrickson AH (1955) Determing water needs of crops from climatic data. Hilgardia 24: 207-233

Hargreaves GH, Samani ZA (1982) Estimating potential evapotranspiration. J Irrig Drain Div ASCE 108: 225-230

Hargreaves GH, Samani ZA (1985) Reference evapotranspiration from temperature. Appl Eng Agric 1: 97-99

Hashim F, Habibian MT (1979) Limitation of temperature method in estimating crop evapotranspiration in arid-zone agriculture development project. Agric Meteorol 20: 237-247

Hatfield JL, Allen RG (1996) Evapotranspiration estimates under deficient water supplies. J Irrig Drain Eng ASCE 122: 301-307

Hatfield JL, Fuchs M (1990) Evapotranspiration models. In: Hoffman GH, Howell TA, Solomon KH, Management of Farm Irrigation Systems. ASAE, St. Joseph, Michigan, USA, pp 33-54

Hatfield JL, Perrier A, Jackson RD (1983*a*) Estimation of evapotranspiration one time-of-day using remote sensed surface temperature. Agric Water Manage 32: 41-53

Hatfield JL, Reginato RJ, Idso SB (1983*b*) Comparison of long wave radiation calculation methods over the United States. Water Resource Res 19: 285-288

Hatfield JL, Reginato RJ, Idso SB (1984) Evaluation of canopy temperature-evapotranspiration models over various crops. Agric For Meteorol 32: 41-53

Hess T (1996) A comparison between evapotranspiration calculated from an automatic weather station and conventional weather data implication for Irrigation scheduling in the UK. In: Proc Evapotranspiration and Irrigation Scheduling. ASAE, St. Joseph, Michigan, USA, pp 516-521

Holmos RM, Robertson GW (1958) Conversion of latent evaporation to potential evapotranspiration. Can J Plant Sci 38: 164-172

Holtslag AM, Van Ulden AP (1983) A simple scheme for daytime estimate of surface fluxes from routine weather data. J Appl Meteorol 22: 517-529

Hope AS, Evans SM (1992) Estimating reference evaporation in the central valley of California using Linacre model. Water Resource Bull 28: 695-702

Huband NDS, Monteith JL (1986) Radiative surface temperature and energy balance of wheat canopy. Boundary Layer Meteorol 36: 107-116

Hubbard KG, Lin X, Walter-Shea EA (2001) The effectiveness of the ASOS, MMTS, Gill and CRS air temperature radiation shields. J Atmos Oceanic Technol 18: 851-864

Hunt LA, Kuchar L, Swanton CJ (1998) Estimation of solar radiation for use in crop modeling. Agric For Meteorol 91: 293-217

Idso SB (1981) A set of equations for full spectrum and 8-14 μm and 10.5-12.5 μm thermal radiation from cloudless skies. Water Resource Res 17: 295-304

Idso SB, Jackson RD (1969) Thermal radiation from the atmosphere. J Geophys Res 74: 5397-5402

Jacobs AFG, Linclaen A EE (1983) Evaporation data from a Piche evaporimeter. J Hydro 60: 367-382

Janes B (1960) Estimation of potential evapotranspiration from vegetable crops from net solar radiation. Proc Am Soc Hortic Sci 76: 582-589

Jensen ME (1966) Empirical methods of predicting or estimating evapotranspiration-using radiation. In: Proc Conference on Evapotranspiration. ASAE, St. Joseph, Michigan, USA, pp 49-53

Jensen ME (1974) Consumptive use of water and irrigation water requirements. (ed) Rep Tech Com Irrig Water Requirements. Am Soc Civ Eng, Irrig Drain Div, USA, pp 1-227

Jensen SE, Aslyng HC (1967) Net radiation and long-wave radiation at Copenhagen 1962-1964. Archivfδr Meteoroloie, Geophysik und Bioklimatologie 15: 127-139

Jensen ME, Burman RD, Allen RG (1990) Evapotranspiration and irrigation water requirements. ASCE Manuals and Reports on Engineering Practices No 70. ASCE, New York

Jensen ME, Haise HR (1963) Estimating evapotranspiration from solar radiation. J Irrig Drain Div ASCE IR 4: 15-41

Jessep CT (1964) The development testing and calibration of portable atmometers suitable for field use. Neth J Agric 7: 205-216

Jiang H, Fry JD, Wiest SC (1998) Variability in turf grass water requirement on golf course. HortSci 33: 689-691

Kjelgaard JF, Stockle CO, Evans RG (1996) Accuracy of canopy energy balance for determing daily evapotranspiration. Irrig Sci 16: 149-157

Kjelgaard JF, Stockle CO, Evans RG, Villar Mir JM, Campbell GS (1994) Evaluation methods to estimate corn evapotranspiration from short-time interval weather data. ASAE 37: 1825-1833

Korven P, Wilcox JC (1964) Correlation between evaporation from Bellani plate and evapotranspiration from orchard. Can J Plant Sci 45: 132-138

Law RP, Israel I (1988) Evaluation of atmometer performance as a tool for irrigation scheduling. ASAE, paper No 88-2504 presented at winter meeting, Chicago IL, USA

Liasat MC, Snyder RL (1998) Data error on net radiation and evaporation estimation. Agric Meteorol 91: 209-221

Lin X, Hubbard KG (1999) Microclimate inside air temperature radiation shield. Unpublished Ph D thesis, Report to High Plane Climate Center, University of Nebraska, Lincoln, USA

Lin X, Kenneth, Hubbard KG (2001) Air flow characteristics of commonly used temperature radiation shields. J Atmos Oceanic Technol 18: 239-339

Linacre ET (1968) Estimating net radiation flux. Agric Meteorol 5: 49-63

Linacre ET (1977) A simple formula for estimating evaporation rates in various climates, using temperature data alone. Agric Meteorol 18: 409-424

Linacre ET (1988) Simplification of Penman's formula. Paper presented at the 26th Congress of International Geographical Union, Sydney, Australia

Livingstone B (1935) Atmometers of porous porcelain and paper, their use in physiological ecology. Ecol 16: 438-471

Lukangu G (1997) Bowen ratio and surface temperature techniques for measuring evaporation from cabbage. Unpublished MScAgric thesis. Department of Agronomy, University of Natal, Pietermaritzburg, South Africa

Mahmood R, Hubbard KG (2002) Effect of time of temperature observation and estimation of daily solar radiation for the northern great plains USA. Agron J 94: 723-733

Makkink GF (1957) Testing the Penman formula by means of Lysimeters. J Instn Wat Engrs 11: 277-288

Malek E (1993) Rapid change of surface soil heat flux and its effect on the estimation of evaporation. J Hydro 142: 89-97

Merva G, Fernandez A (1985) A simplification Penman's Equation for humid regions. ASAE 28: 819-825

Messing I (1998) A simple practical evaporimeter: comparison of Anderson evaporimeter with Class-A Pan, Piche atmometer and Penman evaporation. Arid soil Res Rehabilitation 12: 275-290

Milthorpe FL, Penman HL (1967) The diffusion conductivity of the stomata of wheat leaves. J Exp Bot 18: 422- 431

Mottram R, de Jager JM, Savage MJ (1991) Telecommunications networking data for use in agricultural systems. Water SA 17: 243-248

Monteith JL (1965) Evaporation and environment. In: Fogg GE The State and Movement of Water in Living Organisms. Vol. 19, Sympos Soc Exp Biol, Swansea Cambridge, Academic Press, New York, pp 205-234

Monteith JL (1973) Principles of Environmental Physics. Edward Arnold, London, UK

Monteith JL, Unsworth MH (1990) Principles of Environmental Physics. 2nded, Butterworth Heinemann, Johannesburg, South Africa

Mukammal EI (1961) Evaporation pans and atmometers. In: Proc Hydrology Symposium No 2: Evaporation. Toronto, Ontario, Queens Printer, Ottawa Canada, pp 84-105

Nott K, Savage MJ (1985) Radiation in Namib Desert. Madoqua 14: 165-172

Obukhov AM (1946) Turbulence in atmosphere with non-uniform temperature. Trudy Insti: Teoret. Goefiz. AN-SSSR No.1 (English translation (1971) Boundary-Layer Meteorol 2: 7-29

Oke TR (1978) Boundary Layer Climate. Menthuen, London, UK

Ortega-Farias S, Antonioletti R, Olioso A (2000) Net radiation model evaluation at an hourly time step for Mediterranean condition. Agronomie 20: 157-164

Onset Computer Corporation (2002) Temperature data loggers. [Online.] [4 p.] Available at http://www.onsetcomputer.com/product/3654_temp.html (accessed 3 December 2002; verified 25 May 2002). Onset Computer Corporation, 470 MacArthur Blvd., Bourne, MA 02532

Onset Computer Corporation (2002) Relative humidity data loggers. [Online.] [6 p.] Available at http://www.onsetcomputer.com/product/3653_rh.html (accessed 3 December 2002; verified 25 May 2002). Onset Computer Corporation, 470 MacArthur Blvd., Bourne, MA 02532

Onset Computer Corporation (2002) Event /rainfall data loggers. [Online.] [2 p.] Available at http://www.onsetcomputer.com (accessed 3 December 2002; verified 25 May 2002). Onset Computer Corporation, 470 MacArthur Blvd., Bourne, MA 02532

Onset Computer Corporation (2002) Weather station. [Online.] [2 p.] Available at http://www.onsetcomputer.com (accessed April 2003; verified 25 May 2002). Onset Computer Corporation, 470 MacArthur, Blvd., Bourne, MA 02532

Papaioannou G, Vouraki, Kerkides (1996) Piche evaporimeter data as a substitute for Penman equation's aerodynamic term. Agric For Meteorol 82: 83-92

Parchomchuk P, Berard R, Van Der Gulik TW (2000) Automated irrigation scheduling using an electronic atmometer. International Water Irrig 20: 28-32

Penman HL (1948) Natural evaporation from open water, bare soil and grass. Proc Roy Soc A 193: 120-146

Penman HL (1956) Evaporation: An introductory survey. Neth J Agric Sci 4: 9-29

Prata AJ (1996) A new long-wave formula for estimating downward clear-sky radiation at the surface. Quart J Roy Meteorol Soc 122: 1127-1151

Prescott CH (1940) Evaporation from water surface in relation to solar radiation. Trans R Soc A 64: 114-155

Priestley CHB, Taylor RJ (1972) On the assessment of surface heat flux and evaporation using large-scale parameters. Mon Weath Rev 100: 81-92

Qian YL, Fry JD, Wiest S, Pham WS (1996) Estimating turf grass evapotranspiration using atmometers and the Penman-Monteith model. Crop Sci 36: 699-704

Ravikiran Pottery Works (2003) All type of technical ceramics: technical properties. [Online.] [2 p.] Available at http://www.technoceramic.com/technical.htm (accessed February 18, 2003; verified May 25 2003). Caroline exports Pvt Ltd, Parekh nager industrial estate, Maharashtra, India

Reid PCM (1985) Evaluation of the coefficients of the Ångström formula for the estimation of solar radiation in South Africa. South African J Plant Soil 3: 45-48

Revfeim KJ (1997) On the relationship between radiation and mean daily sunshine. Agric For Meteorol 86: 183-191

Rosenberg NJ, Blad BL, Verma SB (1983) Microclimate: The Biological Environment. 2nded, John Wiley and Sons, New York, USA

Ross J (1975) Momentum, mass and heat exchange in plant community. In: Monteith JL (ed). Vegetation and the Atmosphere. Vol. 1, Academic Press, London, UK, pp 13-55

Satterlund D (1979) An improved equation for estimating long wave radiation from the atmosphere. Water Resource Res 15: 1649-1650

Savage MJ (1996) Calibration and use of sensors to quantify the microclimate. Paper presented to South Africa Soc Crop Prod, Bloemfonteine, South Africa

Savage MJ (1998) A spreadsheet calculating statistical parameter for model evaluation. Soil–plant-atmosphere continuum research unit, school of applied environmental science, University of natal, Pietermaritzberg, South Africa

Savage MJ (2001*a*) Introduction to microclimate and automatic weather station systems for measurement and control. Unpublished Agrometeorology course notes, University of Natal, Pietermaritzburg, South Africa

Savage MJ (2001*b*) Unpublished Agrometeorology course notes (PAM2112). University of Natal, Pietermaritzburg, South Africa

Savage MJ (2002*a*) A spreadsheet calculating hourly reference evaporation. Soil–plant-atmosphere, continuum research unit, school of applied environmental science, university of natal, Pietermaritzberg, South Africa

Savage MJ (2002*b*) Personal communication

Savage MJ, Everson CS, Burger C, Annandale JG (1998) Online estimation of reference evaporation using automatic weather stations. Meeting of South African Soc Crop Prod, Stellenbosch, South Africa, pp 23

Savage MJ, Everson CS, Metelerkamp BR (1997) Evaporation measurement above vegetated surface using micrometeorological techniques. Report to the Water Research Commission. WRC report no 349/1/97, ISBN NO 186845 3634, Pietermaritzburg, South Africa, pp 1-228

Shannon JW (1966) Use of atmometer in estimating evapotranspiration. J Irri Drain Div ASCE IR 3: 309-321

Sharma ML (1985) Estimating evapotranspiration. In: Hillel D (ed) Advances in Irrigation Vol. 3, Academic Press, London, UK, pp 213-273

Shaw RH, Perior A (1982) Aerodynamic roughness of plant canopy: A numerical experiment. Agric For Meteorol 26: 51-65

Smith M (1991) Report on the expert consultation on proceeding for revision of FAO guideline for crop water requirement. Food and Agriculture Organization of the United Nation (FAO), Rome, Italy

Snyder RL, Paw U KT, Wahbeh H (2000) Estimating soil heat flux density. In: Proc 24th Conference on Agricultural and Forest Meteorology. AMS, Davis, California, USA, pp 124

Stanhill G (1962) The use of Piche evaporimeter in the calculation of evaporation. Quart J Roy Meteorol Soc 88: 81-82

Steiner JL, Howell TA, Schneider AD (1991) Lysimetric evaluation of daily potential evapotranspiration models for grain sorghum. Agron J 83: 240-247

Stewart JB (1983) A discussion of the relationship between the principal forms of the combination equation for estimating crop evaporation. Agric Meteorol 30: 111-127

Swinbank WC (1963) Long wave radiation from clear skies. Quart J Roy Meteorol Soc 89: 339-348.

Tanner CB (1979) Temperature: Critique I. In: Tibbitts TW, Kozlowski TT (ed) Controlled Environment Guidelines for Plant Research. Proceedings of the Controlled Environments Working Conference, March 12-14, 1979. Madison, Wisconsin, Academic Press, New York, USA, pp 117-130

Tanner CB, Pelton WL (1960) Potential evapotranspiration estimate by the approximate energy balance methods of Penman. J Geophys Res 65: 3409-3413

Thom AS (1975) Momentum, mass and heat exchange in plant community. In: Monteith JL (ed) Vegetation and the Atmosphere. Vol.1, Academic Press, London, UK, pp 57-109

Thom AS, Oliver HR (1977) On Penman's equation for estimating regional evaporation. Quart J Roy Meteorol Soc 103: 345-357

Thom AS, Thony JL, Vauclin M (1981) On the proper employment of evaporation pans and atmometers in estimation potential transpiration. Quart J Roy Meteorol Soc 107: 711-736

Thornthwaite CW (1948) An approach towards a rational classification of climate. Geog Res 38: 55-80

Thornton PE, Running SW (1999) An improved algorithm for estimating incident daily solar radiation from measurement of temperature, humidity and precipitation. Agric For Meteorol 93: 211-228

Unsworth MH, Monteith JL (1975) Long wave radiation at the ground: I angular distribution of incoming radiation. Quart J Roy Meteorol Soc 101: 13-24

van Zyl WH, de Jager JM, Maree CJ (1987) Estimating evapotranspiration from wheat using weather measurement and Carborundum or Piche evaporimeter. Agric For Meteorol 41: 65-75

van Zyl WH, de Jager JM (1992) Errors in micro-meteorological estimate of reference evapotranspiration to advection. Water SA 18: 255-262

Ventura F, Spanod DP, Snyder RL (1999) An evaluation of common evapotranspiration equations. Irrig Sci 18: 163-170

Weiss A (1982*a*) An experimental study of net radiation, its components and prediction. Agron J 74: 871-875

Weiss A (1982*b*) A quantitative approach to the Pruitt and Doorenbos version of Penman equation. Irrig Sci 4: 267-275

Wilcox JC (1963) Effects of weather on evaporation from Bellani plates and evapotranspiration from Lysimeters. Can J Plant Sci 43: 1-11

Wilcox JC (1967) A simple evaporimeter for use in cold areas. Water Resource Res 3: 433-436

Wilcox JC, Sly WK (1974) Ratio between evapotranspiration from lysimeter and evapotranspiration from small evaporimeters using 2-and 3-hour periods of measurement. Can J Plant Sci 54: 559-564

Wright JL (1982) New evapotranspiration crop coefficient. J Irrig Drain Div ASCE 108: 57-71

APPENDIX

Appendix 1.1 Temperature Methods for Estimating Evaporation

Name of Methods	Author	The formula	Minimum data requirements	Recommended application time	Recommended application	Reference crop	Source
Thornthwaite	Thornthwaite (1948)	$ET = 1.6\left(\frac{l_i}{12}\right)\left(\frac{N_a}{30}\right)\left(\frac{10T}{I}\right)^{ai}$	Air temperature, latitude	Monthly	Climatological and seasonal pattern		Rosenberg *et al.* (1983) and Jensen *et al.* (1990)
SCS Blaney-Criddle	Blaney Criddle (1950)	$ET = KF = \sum kf$ $f = Tp$	Air temperature	Seasonal monthly	Seasonal estimate		Hatfield and Fuchs (1990) and Jensen *et al.* (1990)
FAO Blaney-Criddle	Doorenbos and Pruitt (1977)	$ET_o = a + b(p(0.46T + 8.13))(1 + \frac{0.1h}{1000})$	Air temperature	5 Days	Reference evaporation	Grass alfalfa	Doorenbos and Pruitt (1977); Allen and Pruitt (1986) and Jensen *et al.* (1990)
Linacre	Linacre (1988)*	$ET_o = \frac{\Delta}{\Delta+\gamma}(I_{net} + \frac{\rho C_p}{r_a}(e_s - e_a)/\Delta)$	Air temperature, latitude, altitude	Monthly	Reference evaporation	Grass	Linacre (1977) and Hope and Evans (1992)
Hargreaves	Hargreaves and Samani (1985)	$ET_o = aI_oTD^{0.5}(T + b)$ $TD = T_{max} - T_{min}$	Air temperature, extraterrestrial solar irradiance	10 days	Reference evaporation	Grass	Hargreaves and Samani (1982, 1985); Allen *et al.* (1998) and Jensen *et al.* (1990)

* $I_{net} = 0.63(\frac{570(T_n + 0.006h)}{85 - A}) - 40.0$, $\frac{\rho c_p}{r_a} = 6.0 + 4.0u$, $\frac{e_s - e_a}{\Delta} = 0.0023h + 0.37T + 0.53R + 0.35R_{ann} - 10.9$, $\frac{\Delta}{\Delta+\gamma} = 0.42 + 0.11T + 3\times10^{-5}h$

R = monthly mean temperature range in Kelvin, R_{ann} = the difference between the warmest and coldest monthly mean air temperature in Kelvin, T = air temperature (°C), h = elevation (m), A = latitude (degree), k = monthly consumptive crop coefficients from table, p = mean monthly percentage of annual daytime hours, f = consumptive use factor for growing period, l_i = day length in hour, K = empirical consumptive coefficient for growing period from table, U = wind speed (m s^{-1}), N_a = number of days, I = heat index, TD = difference between mean monthly maximum (T_{max}) and minimum (T_{min}) air temperature (°C), I_o = extraterrestrial solar irradiance (W m^{-2}), λ = specific latent heat of evaporation (MJ kg^{-1}), γ = psychrometric constant (kPa $°C^{-1}$), Δ = slope of saturation vapour pressure *vs* air temperature (kPa $°C^{-1}$), ET = potential evaporation (mm), ET_o = reference evaporation (mm), ρ = density of air (kg m^{-3}), c_p = specific heat capacity of air (kJ kg^{-1} K^{-1}), r_a = aerodynamic resistance (s m^{-1}), T_n = mean monthly air temperature of the following month (°C), e_s is saturation water vapour pressure (kPa), e_a = is actual water vapour pressure (kPa), I_{net} = is net irradiance (W m^{-2}), *a, b, ai* = constants

Appendix 1.2 Radiation Methods for Estimating Evaporation

Name of methods	Author	Formula	Minimum data requirements	Recommended application time	Recommended application	Reference crop	Source
Jensen-Haise	Jensen and Haise (1963)	$ET = C_T(T - T_x)I_s / \lambda$ $C_T = \frac{1}{c_1 + c_2(a/(e_2 + e_1))}$	Air temperature, elevation, solar irradiance	5 days	Climatological and seasonal pattern	Alfalfa	Jensen and Haise (1963) and Jensen *et al.* (1990)
FAO radiation	Doorenbos and Pruitt (1977)	$ET_o = c(\frac{\Delta}{\Delta + \gamma} I_s)$	Air temperature, elevation, solar irradiance	5 days	Reference evaporation	Grass	Doorenbos and Pruitt (1977) and Jensen *et al.* (1990)
Hargreaves	Hargreaves and Samani (1985)	$ET_o = a(\frac{I_s}{\lambda})(T + b)$	Air temperature, solar irradiance	10 days	Reference evaporation	Grass	Hargreaves and Samani (1982, 1985); Allen *et al.* (1998) and Jensen *et al.* (1990)
Modified Makkink	De Bruin and Stricker (2000)	$ET_o = c(\frac{\Delta}{\Delta + \gamma}(I_s - aG))$	Air temperature, elevation, solar irradiance	Daily	Reference evaporation	Grass	De Bruin and Striker (2000)

e_2 and e_1 are the saturation water vapour pressure in the warmest month at mean maximum and minimum air temperature respectively, C_2, C_1 = value calculated as function of altitude, T_x is coefficient value calculated as function of e_1, e_2 and altitude, C_T = temperature coefficient, G = soil heat flux density (W m^{-2}), a, c, b = constant, I_s = solar irradiance (W m^{-2}), λ = specific latent heat of evaporation (MJ kg^{-1}), γ = psychrometric constant (kPa $°C^{-1}$), ET = potential evaporation (mm), ET_o = reference evaporation (mm), ρ = density of air (kg m^{-3}), c_p = specific heat capacity of air (kJ kg^{-1} K^{-1}), r_a = aerodynamic resistance (s m^{-1}), T = air temperature (°C), Δ = slope of saturation vapour pressure *vs* air temperature (kPa $°C^{-1}$)

Appendix 1.3 Reduced Combination Methods and Semi Combination Methods for Estimating Evaporation

Name of methods	Author	The formula	Minimum data requirements	Application time step	Recommended Application	Reference crop	Source
Priestley and Taylor	Priestley and Taylor (1972)	$ET = \frac{\Delta}{\Delta + \gamma}(I_{net} - G)$	Solar irradiance air temperature elevations	10 days	Regional evapotranspiration under wet surface	Large rain feed land areas following rains	Priestley and Taylor (1972) and Jensen *et al.* (1990)
Reduced Penman	Merva and Fernandez (1985)	$ET = \frac{\Delta}{\Delta + \gamma}(I_{net} - G) + \frac{\Delta}{\Delta + \gamma}E_a$	Solar irradiance Air temperature elevations	Similar to pan evaporation	Reference evaporation	Humid area Grass	Marva and Fernandez (1985)
Reduced Penman-Monteith	Allan *et al.* (1998) and Campbell (1998)	$ET_o = (\frac{\Delta}{\Delta + \gamma}(I_{net} - G)) + (\rho c_p (e_s - e)/r_a)/(\lambda[\Delta + \gamma(1 + \frac{r_c}{r_a})])$	Solar irradiance air temperature elevations	Daily	Reference evaporation	Grass	Allan *et al.* (1998) and unpublished Campbell Scientific Inc. (1998)

I_{net} = net irradiance (W m^{-2}), E_a = aerodynamic equation of Penman (mm), ρ = density of air (kg m^{-3}), λ = specific latent heat of evaporation (MJ kg^{-1}), γ = psychrometric constant (kPa $°C^{-1}$), ET = potential evaporation (mm), ET_o= reference evaporation (mm), ρ = density of air (kg m^{-3}), c_p = specific heat capacity of air (kJ kg^{-1} K^{-1}), r_a = aerodynamic resistance (s m^{-1}), G = soil heat flux density (W m^{-2}), e_s = saturation water vapour pressure (kPa), e = actual water vapour pressure (kPa), r_c = canopy resistance (s m^{-1}), Δ = slope of saturation water vapour pressure *vs* air temperature (kPa $°C^{-1}$)

Appendix 1.4 Pan Evaporation Method for Estimating Evaporation

Name of method	Author	Formula	Minimum Data requirement	Application time step	Recommended application	Reference crop	Source
Christian pan evaporation	Christian (1968) and Christian and Hargreaves (1969)	$ET = 0.755E_v C_{T2} C_{w2} C_{H2} C_{s2}$	$T, U, RH, E_v N$	Monthly	Reference evaporation	Grass	Jenson *et al.* (1990)
FAO pan	Doorenbos and Pruitt (1977)	$ET_o = K_p E_v$	$E_v K_p$	10 days	Reference evaporation	Grass	Doorenbos and Pruitt (1977) and Allan *et al.* (1998)

T = air temperature (°C), U = wind speed (m s^{-1}), RH = relative humidity (%), E_v = pan evaporation (mm), K_p = pan coefficient, N = possible sunshine hours (h), C_{T2} = coefficient depends on temperature, C_{w2} = coefficient dependent of wind speed, C_{H2} = coefficient dependent on relative humidity, C_{s2} = coefficient dependent on sunshine hours

Appendix 2.1 Procedure for Calculating Parameters of Campbell Scientific Inc. Hourly Version of the Penman-Monteith Approach

2.1.1 Net Irradiance (kW m^{-2})

Net irradiance is calculated as:

$$I_{net} = a_s I_s + L_{ni} \qquad A1.1$$

where I_s is incident solar irradiance (kW m^{-2}), a_s is the absorptive of crop for solar irradiance (= 1- r), r is reflection coefficient calculated as 23 % of I_s,. and L_{ni} is the atmospheric emittance minus crop emittance (kW m^{-2}) at air temperature (T_a):

$$L_{ni} = f(I_s / I_{so}) L_{nic} \qquad A1.2$$

where (L_{nic}) is estimated clear sky atmospheric emittance minus crop emittance (kW m^{-2}). Given as:

$$L_{nic} = 0.0003 T_a - 0.0107 \qquad A1.3$$

where T_a is air temperature in °C. Cloudiness ($f(I_s/I_{so})$ estimated from solar irradiance (I_s) and extraterrestrial solar irradiance on horizontal surface (I_{so}) (kW m^{-2}). Cloudiness is evaluated as:

$$f(I_s / I_{so}) = 1 - 1/[1 + 0.034 \exp(7.9 I_s / I_{so})]. \qquad A1.4$$

Extraterrestrial solar irradiance on horizontal surface (I_{so}) is calculated as:

$$I_{so} = 1.36 \sin\phi \qquad A1.5$$

where 1.36 is the solar constant in kW m^{-2} and ϕ is the elevation angle of the sun (rad). Sin ϕ computed from:

$$\sin\phi = \sin d \sin L + \cos d \cos L \cos(15(t - t_o)) \qquad A1.6$$

where L is latitude (rad) of the site (positive for northern and negative for southern), t is clock time, t_o is the time of solar noon and d is the solar declination angle approximated using a polynomial as a function of day of the year (J = day of year/100). Sin d is given as:

$$\sin d = 0.37726 - 0.10564J + 1.2458J^2 - 0.75478J^3 + 0.13627J^4 - 0.00572J^5 \qquad A1.7$$

and

$$\cos d = (1 - \sin^2 d)^{1/2} \qquad A1.8$$

Time of solar noon is:

$$t_o = 12.5 - L_c - t_e(h) \qquad A1.9$$

where L_c is a longitude correction (rad) and t_e is the equation of time. The longitude correction (L_c) is calculated as:

$$L_c = (L_s - L)/15 \qquad A1.10$$

where L is longitude (rad) of site and L_s is longitude of standard meridian (rad) closer to the site.

Equation of time (t_e) is calculated using two equations, one for the first half of year and other for the second half.

For the first half of the year:

$$t_e = -0.04056 - 0.74503J + 0.08823J^2 + 2.0516J^3 - 1.8111J^4 + 0.42832J^5 \qquad A1.11$$

where J = (day of year)/100

For the second half of the year (For day of the year > 180):

$$t_e = -0.05039 - 0.33954J + 0.04084J^2 + 1.8928J^3 - 1.7619J^4 + 0.4224J^5 \quad A1.12$$

where J = (day of year-180)/100

2.1.2 Soil Heat Flux Density (*G*)

Estimated as a function of net irradiance (I_{net}):

$G = 0.1I_{net}$ where $I_s > 0$

$G = 0.5I_{net} or 0.5L_{ni}$ where $I_s < 0$ $A1.13$

2.2.3 Psychrometric Constants

Slope of saturation water vapour pressure *vs* temperature relationship (Δ):

$$\Delta = 45.3 + 2.97T + 0.0549T^2 + 0.00223T^3 (Pa/^\circ C) \quad A1.14$$

For the range of air temperature -5 to 45 °C.

The apparent psychrometric constant (γ^*) is given by:

$$\gamma^* = \gamma r_v / r_a \quad A1.15$$

where γ is the thermodynamic psychrometric constant (kPa $^\circ C^{-1}$), r_v is combined canopy (r_c) and aerodynamic (r_a) resistance of water vapour pressure in s m^{-1}. r_a is the convective resistance of heat transfer in s m^{-1} calculated as:

$$r_a = 209/u_2 \quad A1.16$$

where u_2 is wind speed at 2 meter in m s^{-1}. The canopy resistance of reference crop is approximated as 70 s m^{-1} for solar irradiance above 10 W m^{-2} and 700 s m^{-1} for the rest of the day.

The thermodynamic psychrometric constant calculated as:

$$\gamma = \gamma^a \exp(-A/8500) \quad A1.17$$

where γ^a is sea level psychrometric constant (= 67.3 kPa $^\circ C^{-1}$) and A is altitude of site in meters.

2.2.4 Water Vapour Pressure Deficit (VPD)

Water vapour pressure deficit (*VPD*) (kPa) is calculated as:

$$VPD = 0.6108\exp(17.2694T/(237.3+T))(1 - RH/100) \quad A1.18$$

where *RH* is relative humidity (%) and *T* is air temperature in (°C).

Appendix 2.2 Procedures for Calculating Parameters of Hourly and 24-Hour Version FAO Penman-Monteith Approach

2.2.1 Net Irradiance

The net irradiance is calculated as sum of net short wave and net long wave irradiance ($I_{net} = I_{ns} - L_{nl}$). Net short wave irradiance (I_{ns}) is calculated as:

$$I_{ns} = (1-r)I_s \qquad A1.19$$

where I_s is solar irradiance (W m^{-2} or MJ m^{-2} day^{-1}) and r is reflection coefficient calculated as 23 % of solar irradiance.

Net long wave irradiance (L_{nl}):

$$L_{nl} = \sigma\left[\frac{T_{\max}^4 + T_{\min}^4}{2}\right](0.34 - 0.14\sqrt{e_a})(1.35(I_s / I_a) - 0.35) \qquad A1.20$$

where L_{nl} is the net long wave irradiance (MJ m^{-2} day^{-1} or W m^{-2}), δ is the Stefan-Boltzmann's constant (= 4.903 x 10 $^{-9}$ MJ $K^{-4}m^{-2}$ day^{-1}), T_{max} is maximum air temperature of day (K), T_{min} is minimum air temperature of the day (K), e_a is actual water vapour pressure (kPa), I_a is calculated clear sky solar irradiance (MJ m^{-2} day^{-1} or W m^{-2}). The T_{max} and T_{min} replaced by average air temperature for hourly and shorter time step.

Clear sky solar irradiance:

$$I_a = (0.75 + 2\times10^{-5}A)I_{so}) \qquad A1.21$$

where A is altitude of site above see level (m) and I_{so} is the extraterrestrial solar irradiance (MJ m^{-2} day^{-1} or MJ m^{-2} $hour^{-1}$).

For daily time step the extraterrestrial solar irradiance is calculated as:

$$I_{so} = \frac{24(60)}{\pi} G_{cr} d_r [\omega_s \sin\varphi \sin\delta + \cos\varphi \cos\delta \sin\omega_s] \qquad A1.22$$

For hourly and shorter period:

$$I_{so} = \frac{12(60)}{\pi} G_{cr} d_r [(\omega_1 - \omega_2)\sin\varphi \sin\delta + \cos\varphi \cos\delta(\sin\omega_2 - \sin\omega_1)] \qquad A1.23$$

where G_{sc} is the solar constant (= 0.0820 MJ m^{-2} min^{-1}), φ is latitude (rad). d_r is inverse relative distance earth-sun calculated as:

$$d_r = 1 + 0.0033\cos(\frac{2\pi}{365}J). \qquad A1.24$$

Solar declination (δ) (rad) calculated as:

$$\delta = 0.409\sin(\frac{2\pi}{365}J - 1.39). \qquad A1.25$$

ω_s is sun set hour angle (rad) and for 24-hour period calculation is given as:

$$\omega_s = \arccos(-\tan\delta \tan\varphi) \qquad A1.26$$

Sun set hour angle (rad) for hourly and shorter time period is calculated for the beginning of period (ω_1) and the end of period (ω_2) as:

$$\omega_1 = \omega - \frac{\pi t_1}{24}$$
$$\omega_2 = \omega + \frac{\pi t_1}{24} \qquad A1.27$$

where t_1 is length of calculation period (for hourly period = 1). ω is the solar time angle at midpoint of the period (rad):

$$\omega = \frac{\pi}{12}(t + 0.06667(L_s - L) + S_c) - 12 \qquad A1.28$$

Where t is time at mid point of period (hours). S_c is seasonal correction for solar time (hours) is:

$$S_c = 0.1645 \sin 2b - 0.1255 \cos b - 0.025 \sin b \qquad A1.29$$

and

$$b = \frac{2\pi(J - 81)}{364} \qquad A1.30$$

where J is the number of the day in the year, L_s is longitude meridian closer to the site (rad) and L is longitude of site (rad).

2.2.2 Soil Heat Flux Density (G)

For hourly and shorter period during daytime and nighttime period approximated as 10 % and 50 % net irradiance (I_{net}) respectively. The daily soil heat flux density is assumed to be zero.

2.2.3 Psychrometric Constant (γ)

The psychrometric constant (γ) is given by:

$$\gamma = \frac{C_p P}{\varepsilon \lambda} = 0.665 \times 10^{-3} P(kPa^o C^{-1}) \qquad A1.31$$

where P is atmospheric pressure (kPa), λ is latent heat of vaporization (= 2.45 MJ kg^{-1}), C_p is specific heat capacity at constant pressure (=1.013 x 10^{-5} MJ kg^{-1} $^oC^{-1}$) and ε is the ratio of molecular weight of water vapour / dry air (= 0.662). The atmospheric pressure is calculated:

$$P = 101.3\left(\frac{293 - 0.0065Z}{293}\right)^{5.26} \qquad A1.32$$

where Z is elevation of site in meter.

2.2.4 Slope of Saturation to Water Vapour Pressure Curve (Δ)

The slope of saturation to water vapour pressure (kPa $^oC^{-1}$) at a given air temperature is given by:

$$\Delta = \frac{4098[0.6108 \exp(\frac{17.27T}{T + 237.3})]}{(T + 237.3)^2} \qquad A1.33$$

where T is air temperature (^oC)

2.2.5 Water Vapour Pressure Deficit (e_s - e_a)

Hourly and shorter time period actual water vapour pressure deficit (kPa) is calculated as given in Eq. A1.18. The 24-hour water vapour pressure deficit is calculated using measured maximum and minimum air temperature and relative humidity. The saturation water vapour pressure (e_s) (kPa) is given as:

$$e_s = \frac{0.6108\exp\left(\frac{17.27T_{max}}{T_{max}+237.3}\right) + 0.6108\exp\left(\frac{17.27T_{min}}{T_{min}+237.3}\right)}{2} \qquad A1.34$$

and actual water vapour pressure (e_a) as:

$$e_a = \frac{0.6108\exp\left(\frac{17.27T_{max}}{T_{max}+237.3}\right)\left(\frac{RH_{min}}{100}\right) + 0.6108\exp\left(\frac{17.27T_{min}}{T_{min}+237.3}\right)\left(\frac{RH_{max}}{100}\right)}{2} \qquad A1.35$$

where T_{max} is maximum air temperature (°C), T_{min} is minimum air temperature (°C), RH_{max} is maximum relative humidity and RH_{min} is the minimum relative humidity of the day.

Appendix 3.1 The CR7X data logger program for measuring microclimatic measures from the component net radiometer (CNR1), infrared thermometer (IRT), thermocouple type E, soil heat flux plates, soil thermocouples, ThetaProbe, ET-gage, and AWS for determing reference evaporation, radiation balance and the available energy components

```
A program of AWS with air
temperature, wind speed and vapour
pressure measured at  two meters
modified to include additional
sensors to measure the radiation
balance component and soil heat flux
of soil and evaporation from Etgage.

CM3 solar irradiance, Component net
radiometer (CNR1) and Net
radiometer(Q*6.7.1),input location
4,5,6,7,8 and 9 , 12 respectively
placed at 1 m above grass surface
used to measure the components of
radiation balance and net irradiance.
2 soil heat flux plate's; buried in
undisturbed soil at a depth of 80 mm,
wires to the south
 Input location 26 and 27
1 averaging soil temperature
thermocouple  location 29
1 theta probes location to measure
soil water content and soil
temperature to calculate stored soil
heat.
2 Etgage locations 20 and 21 to
measure the latent heat of
evaporation from short grass surface
and long grass surface.
1 Apogee Infrared thermometer (IRT)
and 1 Thermocouple type E at location
23 and 24 to measure surface
temperature

Procedure for using heater with CNR1
Program instruction P87 was used to
heat the sensor starting from 1700 Pm
up to 700 Am in 30 second interval to
avoid dew deposition on sensors
window.

CNR1 measurement
;Lmeas_upper = Ld - sTtherm4;
;Lmeas_lower = Lu - sTtherm4;
;Inet = Is - rIs + Ld - Lu
;Heater and temperature measurements
- wire with red, yellow,
;green, blue, black, white and shield
;Yellow Vsingle-ended for thermistor
- SE11 in this program;
;Green ground for thermistor;
;Red Excitation channel - EX1 in this
program;
;The thermistor is a YSI 44032 (30
kohm at 25 oC)
;The fixed resistance is 247 kohm
(measured to be 249 kohm)
;Black Vheater +; white Vheater -

;{CR7}
*Table 1 Program
  01: 30          Execution Interval
(seconds)

1:  Battery Voltage (P10)
 1: 1           Loc [ Vbattery   ]
;Wiring solar and reflected solar
irradiance sensors
;CM3 993283 Is red 1H blue 1L black G
;CM3 993297 rIs: red 2H blue 1L
2:  Volt (Diff) (P2)
 1: 1           Reps
 2: 4           50 mV Slow Range
 3: 1           In Card
 4: 1           DIFF Channel
 5: 3           Loc [ CM283Wm2   ]
 6: 37.383      Mult
 7: 0.0         Offset

3:  Volt (Diff) (P2)
 1: 1           Reps
 2: 4           50 mV Slow Range
 3: 1           In Card
 4: 2           DIFF Channel
 5: 4           Loc [ CM297Wm2r ]
 6: 41.929      Mult
 7: 0.0         Offset
 ;CNR1 measurements
;Red 3H, blue 3L (Is); white 4H,
black 4L; (rIs)
;Grey 5H, yellow 5L (Lmeas_upper)
;Brown 6H, green 6L (Lmeas_lower)
;Control port switching:
;Yellow from switch electronics to
C1, black to ground
;Thin red to +12 V, black to -
terminal of heater battery
;Two thick red wires to CNR1: black
of CNR1 to one red wire;
;Other red wire to white of CNR1

 5:  Volt (Diff) (P2)
 1: 4           Reps
 2: 4           50 mV Slow Range
 3: 1           In Card
 4: 3           DIFF Channel
 5: 5           Loc [ CNR1_1     ]
 6: 82.305      Mult
 7: 0.0         Offset

5:  Beginning of Loop (P87)
 1: 1           Delay
 2: 4           Loop Count

6:  If (X<=>F) (P89)
 1: 3       -- X Loc [ CM283Wm2   ]
 2: 4           <
 3: 0.0         F
 4: 30          Then Do

7:  Z=F (P30)
 1: 0.0         F
 2: 3       -- Z LOC [ CM283Wm2   ]

8:  End (P95)

9:  End (P95)
; Temperature measurement Thermistor
of CNR1 yellow 7H, green G, red EX1
 card1
10:  Excite Delay Volt (SE) (P4)
 1: 1           Reps
 2: 6           500 mV Slow Range
 3: 1           In Card
 4: 13          SE Channel
 5: 1           Ex Card
 6: 1           Ex Channel
 7: 1           Meas/Ex
 8: 0           Delay (units 0.01 sec)
 9: 1000        mV Excitation
10: 9           Loc [ Vtherm     ]
11: 1           Mult
12: 0.0         Offset
; Wind speed red P1, green G, black G

11:  Pulse (P3)
 1: 1           Reps
 2: 2           In Card
 3: 1           Pulse Input Channel
 4: 21          Low Level AC, Output Hz
 5: 10          Loc [ WS_ms      ]
 6: 0.75        Mult
 7: 0.2         Offset

12:  If (X<=>F) (P89)
 1: 10          X Loc [ WS_ms      ]
 2: 4           <
 3: 0.21        F
 4: 30          Then Do

13:  Z=F (P30)
 1: 0           F
 2: 10          Z LOC [ WS_ms      ]

14:  End (P95)
;wind direction Green 7L,Black/Brown
Ground Card 2
15:  Excite Delay Volt (SE) (P4)
 1: 1           Reps
 2: 7           1500 mV Slow Range
 3: 1           In Card
 4: 14          SE Channel
 5: 1           Ex Card
 6: 2           Ex Channel
 7: 1           Meas/Ex
 8: 2           Delay (units 0.01 sec)
 9: 1000        mV Excitation
10: 11          Loc [ WindDir    ]
11: 0.355       Mult
12: 0.0         Offset

16:  If (X<=>F) (P89)
 1: 11          X Loc [ WindDir    ]
 2: 3           >=
 3: 360         F
 4: 30          Then Do

17:  Z=F (P30)
 1: 0           F
 2: 11          Z LOC [ WindDir    ]
18:  End (P95)
;Net radiometer measuring net
irradiance red 8H, black 8L card1

19:  Volt (Diff) (P2)
 1: 1           Reps
 2: 5           150 mV Slow Range
 3: 1           In Card
 4: 8           DIFF Channel
 5: 12          Loc [ NR_Wm2     ]
 6: 9.4         Mult
 7: 0.0         Offset
; Vaisala CS500 Temperature and
humidity probe Tair purple 9H, RH
brown 9L, yellow 12V
;green G
 card 1
20:  Volt (SE) (P1)
 1: 1           Reps
 2: 8           5000 mV Slow Range
 3: 1           In Card
 4: 17          SE Channel
 5: 13          Loc [ AirTC      ]
 6: 0.1         Mult
 7: -40         Offset

21:  Volt (SE) (P1)
 1: 1           Reps
 2: 8           5000 mV Slow Range
 3: 1           In Card
 4: 18          SE Channel
 5: 14          Loc [ RH         ]
 6: 0.1         Mult
 7: 0.0         Offset

22:  If (X<=>F) (P89)
 1: 14          X Loc [ RH         ]
 2: 3           >=
 3: 100         F
 4: 30          Then Do

23:  If (X<=>F) (P89)
 1: 14          X Loc [ RH         ]
 2: 4           <
 3: 108         F
 4: 30          Then Do

24:  Z=F (P30)
 1: 100         F
 2: 14          Z LOC [ RH         ]

25:  End (P95)

26:  End (P95)
; Vapour pressures calculation card1
27:  Z=X (P31)
```

```
 1: 14        X Loc [ RH         ]
 2: 15        Z LOC [ CSI_1      ]

28:  Z=F (P30)
 1: 100       F
 2: 16        Z LOC [ CSI_R      ]

29:  Z=X/Y (P38)
 1: 15        X Loc [ CSI_1      ]
 2: 16        Y Loc [ CSI_R      ]
 3: 15        Z LOC [ CSI_1      ]

30:  Z=F (P30)
 1: .6108     F
 2: 16        Z LOC [ CSI_R      ]

31:  Z=X*Y (P36)
 1: 16        X Loc [ CSI_R      ]
 2: 15        Y Loc [ CSI_1      ]
 3: 15        Z LOC [ CSI_1      ]

32:  Z=F (P30)
 1: 17.       F
 2: 16        Z LOC [ CSI_R      ]

33:  Z=X (P31)
 1: 16        X Loc [ CSI_R      ]
 2: 17        Z LOC [ CSI_2      ]

34:  Z=F (P30)
 1: .2694     F
 2: 16        Z LOC [ CSI_R      ]

35:  Z=X+Y (P33)
 1: 16        X Loc [ CSI_R      ]
 2: 17        Y Loc [ CSI_2      ]
 3: 17        Z LOC [ CSI_2      ]

36:  Z=X*Y (P36)
 1: 13        X Loc [ AirTC      ]
 2: 17        Y Loc [ CSI_2      ]
 3: 17        Z LOC [ CSI_2      ]

37:  Z=F (P30)
 1: 237.3     F
 2: 16        Z LOC [ CSI_R      ]

38:  Z=X+Y (P33)
 1: 13        X Loc [ AirTC      ]
 2: 16        Y Loc [ CSI_R      ]
 3: 16        Z LOC [ CSI_R      ]

39:  Z=X/Y (P38)
 1: 17        X Loc [ CSI_2      ]
 2: 16        Y Loc [ CSI_R      ]
 3: 16        Z LOC [ CSI_R      ]

40:  Z=EXP(X) (P41)
 1: 16        X Loc [ CSI_R      ]
 2: 16        Z LOC [ CSI_R      ]
;actual vapour pressure card1
41:  Z=X*Y (P36)
 1: 16        X Loc [ CSI_R      ]
 2: 15        Y Loc [ CSI_1      ]
 3: 18        Z LOC [ E_KPA      ]
;Rain with Rain-o-Matic ran gauge of
resolution 1 mm.
White pulse port 2, Green Ground
card2
42:  Pulse (P3)
 1: 1         Reps
 2: 2         In Card
 3: 2         Pulse Input Channel
 4: 2         Switch Closure, All
Counts
 5: 19        Loc [ Rain_mm      ]
 6: 1.0       Mult
 7: 0.0       Offset
; Latent heat of evaporation from
Etgage with canvas cover #30 and #54
at 1 m. Green pulse port 4 and 5,
white Ground. Resolution 0.254 mm per
tip card2
43:  Pulse (P3)
 1: 2         Reps
 2: 2         In Card
 3: 3         Pulse Input Channel
 4: 2         Switch Closure, All
Counts
 5: 20        Loc [ ETgauge_1 ]
 6: .254      Mult
 7: 0         Offset
;Type E TC (surface temperature)
purple 10H, red 10L
card1
44:  Panel Temperature (P17)
 1: 1         In Card
 2: 22        Loc [ Tpanel       ]

45:  Thermocouple Temp (DIFF) (P14)
 1: 1         Reps
 2: 3         15 mV Slow Range
 3: 1         In Card
 4: 10        DIFF Channel
 5: 2         Type E (Chromel-
Constantan)
 6: 22        Ref Temp (Deg. C) Loc [
Tpanel     ]
 7: 23        Loc [ Tsurface     ]
 8: 1.0       Mult
 9: 0.0       Offset
; IRT wiring
;body temperature yellow 11H, red
11L, shield G
;target temperature (black band)
yellow 12H, red 12L, shield G
card1
46:  Thermocouple Temp (DIFF) (P14)
 1: 2         Reps
 2: 3         15 mV Slow Range
 3: 1         In Card
 4: 11        DIFF Channel
 5: 3         Type K (Chromel-Alumel)
 6: 22        Ref Temp (Deg. C) Loc [
Tpanel     ]
 7: 24        Loc [ IRTbody      ]
 8: 1         Mult
 9: 0         Offset
;Soil heat flux plate 1: red 12H
black 12L ;serial no. 91300

47:  Volt (Diff) (P2)
 1: 1         Reps
 2: 2         5000 æV Slow Range
 3: 1         In Card
 4: 12        DIFF Channel
 5: 26        Loc [ Fplate_1     ]
 6: .0404     Mult
 7: 0.0       Offset
;Soil heat flux plate 2: red 13H
black 13L ;serial no. 91303
  card1
48:  Volt (Diff) (P2)
 1: 1         Reps
 2: 2         5000 æV Slow Range
 3: 1         In Card
 4: 13        DIFF Channel
 5: 27        Loc [ Fplate_2     ]
 6: .0394     Mult
 7: 0.0       Offset
; Soil thermocouples (type E) blue
card 2 1H, red card 2 1L
; Buried at a depth of 20 and 60 mm,
wires to the south

50:  Thermocouple Temp (DIFF) (P14)
 1: 1         Reps
 2: 3         15 mV Slow Range
 3: 2         In Card
 4: 1         DIFF Channel
 5: 2         Type E (Chromel-
Constantan)
 6: 22        Ref Temp (Deg. C) Loc [
Tpanel     ]
 7: 29        Loc [ Tsoil        ]
 8: 1.0       Mult
 9: 0.0       Offset
;Thetaprobe ML2 56/012 card 2 yellow
2H, green card 2 2L
;Red 12 V, blue G
;Bury probe horizontally with pins in
undisturbed
;soil, top pin at a depth of 25 mm
51:  Volt (Diff) (P2)
 1: 1         Reps
 2: 7         1500 mV Slow Range
 3: 2         In Card
 4: 2         DIFF Channel
 5: 2         Loc [ Vtheta       ]
 6: .001      Mult
 7: 0.0       Offset
,out put program for 15 minute data
52:  If time is (P92)
 1: 0         Minutes into a
 2: 15        Minute Interval
 3: 10        Set Output Flag High

53:  Set Active Storage Area (P80)
 1: 1         Final Storage
 2: 101       Array ID

54:  Real Time (P77)
 1: 1220      Year,Day,Hour/Minute
(midnight = 2400)
55:  Resolution (P78)
 1: 1         High Resolution
56:  Average (P71)
 1: 6         Reps
 2: 3         Loc [ CM283Wm2     ]
57:  Average (P71)
 1: 1         Reps
 2: 9         Loc [ Vtherm       ]
58:  Average (P71)
 1: 1         Reps
 2: 12        Loc [ NR_Wm2       ]
59:  Average (P71)
 1: 1         Reps
 2: 13        Loc [ AirTC        ]
60:  Sample (P70)
 1: 1         Reps
 2: 14        Loc [ RH           ]

61:  Average (P71)
 1: 1         Reps
 2: 18        Loc [ E_KPA        ]

62:  Wind Vector (P69)
 1: 1         Reps
 2: 0         Samples per Sub-Interval
 3: 0         S, é1, & å(é1) Polar
 4: 10        Wind Speed/East Loc [
WS_ms      ]
 5: 11        Wind Direction/North Loc
[ WindDir    ]

63:  Totalize (P72)
 1: 3         Reps
 2: 19        Loc [ Rain_mm      ]

64:  Average (P71)
 1: 3         Reps
 2: 23        Loc [ Tsurface     ]

65:  Average (P71)
 1: 3         Reps
 2: 26        Loc [ Fplate_1     ]

66:  Average (P71)
 1: 1         Reps
 2: 2         Loc [ Vtheta       ]
*Table 2 Program
  01: 10         Execution Interval
(seconds)

1:  Serial Out (P96)
 1: 30        Storage Module
*Table 3 Subroutines
End Program
-Input Locations-
1 Vbattery   1 0 1
2 Vtheta     1 2 1
3 CM283Wm2   1 3 2
4 CM297Wm2r  1 1 1
5 CNR1_1     5 1 1
6 CNR1_2     9 1 1
7 CNR1_3     9 1 1
8 CNR1_4     17 1 1
9 Vtherm     1 1 1
10 WS_ms     1 3 2
11 WindDir   1 3 2
12 NR_Wm2    1 2 1
13 AirTC     1 4 1
14 RH        1 4 2
15 CSI_1     1 3 3
16 CSI_R     1 8 8
17 CSI_2     1 3 3
18 E_KPA     1 2 1
19 Rain_mm   5 2 1
20 ETgauge_1 5 2 1
21 ETgauge_2 17 2 1
22 Tpanel    1 3 1
23 Tsurface  1 1 1
24 IRTbody   5 2 1
25 Tirt      17 2 1
26 Fplate_1  5 2 1
27 Fplate_2  17 2 1
28 Vtheta    1 0 1
29 Tsoil     1 1 1
```

Appendix 3.2. The 21X data logger program for measuring microclimatic measures from the component net radiometer (CNR1), infrared thermometer (IRT), thermocouple type E, soil thermocouple, soil heat flux plates, ThetaProbe, ET-gage and AWS for determing reference evaporation and available energy and radiation balance components.

```
A program AWS with air temperature,
wind speed and vapour pressure
measured at one and two meters
modified to include additional
sensors to measure the radiation
balance component and soil heat flux
of soil and latent heat of
evaporation from Etgage.
CR21X-1
Component net radiometer (CNR1) and
Net radiometer(Q*6.7.1) CM3 solar
irradiance input location 2,3,4,5,6,
9 , 12 and 21 and 22 respectively
placed at 1 m above grass surface
used to measure the components of
radiation balance and net irradiance.

One Vaisala CS500 Temperature and
humidity probe, one Three cup wind
speed and wind direction sensor
location 7,8,11 and 12 placed at 2m
above ground
1 Apogee Infrared thermometer (IRT)
and 1 Thermocouple type E at location
17,18 and 19 to measure surface
temperature
 procedure using heater with CNR1
Program instruction P87 was used to
heat the sensor starting from 1700 Pm
up to 700 Am in 30 second interval to
avoid dew deposition on sensors
window.

CR21X-2

2 soil heat flux plates input
location 13 and 141
1 averaging soil temperature sensor
location 15
1 theta probe location to measure
soil water content  to stored soil
heat.
Location 16
2 Etgage locations 4 and 5 to measure
the latent heat of evaporation from
short grass surface and long grass
surface.
1 three-cup wind speed and direction
sensor and 1 RTD wind speed sensor,
location 6,7

One Vaisala CS500 Temperature and
humidity probe from 1 meter
Location 17,18
 Rain measurement with Rain-o-Matic
resolution 1 mm
Location 3
RTD Heated ceramic anemometer
Location 9,10,11

;{CR21X}-1

*Table 1 Program
  01: 30.0000    Execution Interval
(seconds)

1:  Batt Voltage (P10)
 1: 1          Loc [ Vbattery   ]
; CNR1 Net component radiometer
; Measurements single ended
;red 1H blue G (Is), CH-1
;white 1L black G,(rIs) CH-2
;Grey 2H , yellow G (Lmeas_upper) CH-
3
;Brown 2L, green G(Lmeas_lower)CH-4

2:  Volt (SE) (P1)
 1: 4          Reps
 2: 3          50 mV Slow Range
 3: 1          SE Channel
 4: 2          Loc [ CNR1_1     ]
 5: 82.305     Mult
 6: 0          Offset

3:  Beginning of Loop (P87)
 1: 1          Delay
 2: 2          Loop Count

4:  If (X<=>F) (P89)
 1: 2      -- X Loc [ CNR1_1     ]
 2: 4          <
 3: 0          F
 4: 30         Then Do

5:  Z=F (P30)
 1: 0          F
 2: 2      -- Z Loc [ CNR1_1     ]

6:  End (P95)

7:  End (P95)
;Heating the CNR1 between 1800 Pm and
600 Am
;Control port switching:
;Yellow from switch electronics to
C1, black to ground
;Thin red to +12 V, black to -
terminal of heater battery
;Two thick red wires to CNR1: black
of CNR1 to one red wire;
;Other red wire to white of CNR1
;heater wiring
; yellow C1, black,G
; red +battery, balck -battery
; purple +CNR1(white), blue -
CNR1(black)
;CM3-283 red CH-6L, blue and black G
;CM3-297 red CH-7H, blue and black G


8:  Time (P18)
 1: 1          Minutes into current day
(maximum 1440)
 2: 0          Mod/By
 3: 20         Loc [ Timeloca   ]

9:  If (X<=>F) (P89)
 1: 20         X Loc [ Timeloca   ]
 2: 4          <
 3: 600        F
 4: 30         Then Do

10:  Do (P86)
 1: 11         Set Flag 1 High

11:  Do (P86)
 1: 41         Set Port 1 High

12:  Else (P94)

13:  Do (P86)
 1: 21         Set Flag 1 Low

14:  Do (P86)
 1: 51         Set Port 1 Low

15:  End (P95)

16:  If (X<=>F) (P89)
 1: 20         X Loc [ Timeloca   ]
 2: 3          >=
 3: 1800       F
 4: 30         Then Do

17:  Do (P86)
 1: 11         Set Flag 1 High

18:  Do (P86)
 1: 41         Set Port 1 High

19:  End (P95)
;Body temperature measurement of CNR1
;Thermostat of CNR1
;yellow 3H, green G, Red EX1 CH-5
;the thermostat is a YSI 44032 (30
kohms at 25 oc)
;the fixed resistance is 247 kohms
(measured to be 249 kohms)

20:  Excite Delay Volt (SE) (P4)
 1: 1          Reps
 2: 4          500 mV Slow Range
 3: 5          SE Channel
 4: 1          Excite all reps w/Exchan
1
 5: 0          Delay (units 0.01 sec)
 6: 1000       mV Excitation
 7: 6          Loc [ Vtherm     ]
 8: 1          Mult
 9: 0          Offset
;wind speed and Wind direction from 2
and 1 meter
;wind speed
;red P1, green/black G P-1

21:  Pulse (P3)
 1: 1          Reps
 2: 1          Pulse Input Channel
 3: 21         Low Level AC, Output Hz
 4: 7          Loc [ WS_ms2     ]
 5: .75        Mult
 6: .2         Offset

22:  If (X<=>F) (P89)
 1: 7          X Loc [ WS_ms2     ]
 2: 4          <
 3: .21        F
 4: 30         Then Do

23:  Z=F (P30)
 1: 0          F
 2: 7          Z Loc [ WS_ms2     ]

24:  End (P95)
; wind direction:
;Green 3L, Black/Brown G CH-6, white
1-EX

25:  Excite Delay Volt (SE) (P4)
 1: 1          Reps
 2: 5          5000 mV Slow Range
 3: 6          SE Channel
 4: 2          Excite all reps w/Exchan
2
 5: 2          Delay (units 0.01 sec)
 6: 1000       mV Excitation
 7: 8          Loc [ WindDir    ]
 8: .355       Mult
 9: 0          Offset

26:  If (X<=>F) (P89)
 1: 8          X Loc [ WindDir    ]
 2: 3          >=
 3: 360        F
 4: 30         Then Do

27:  Z=F (P30)
 1: 0          F
 2: 8          Z Loc [ WindDir    ]

28:  End (P95)

Net radiometer
;red 4H , black G  CH-7
29:  Volt (SE) (P1)
 1: 1          Reps
 2: 4          500 mV Slow Range
 3: 7          SE Channel
 4: 9          Loc [ NRWm2      ]
 5: 9.4        Mult
 6: 0          Offset
;Air temperature and RH measurement
from 1 and 2 meter; Vaisala ;Tair
Purple 4L CH-8;RH brown 4L , yellow
12V ,green G CH-9
```

```
30:  Volt (SE) (P1)
 1: 1          Reps
 2: 5          5000 mV Slow Range
 3: 8          SE Channel
 4: 10         Loc [ AirTc       ]
 5: .1         Mult
 6: -40        Offset

31:  Volt (SE) (P1)
 1: 1          Reps
 2: 5          5000 mV Slow Range
 3: 9          SE Channel
 4: 11         Loc [ RH          ]
 5: .1         Mult
 6: 0          Offset

32:  If (X<=>F) (P89)
 1: 11         X Loc [ RH        ]
 2: 3          >=
 3: 100        F
 4: 30         Then Do

33:  If (X<=>F) (P89)
 1: 11         X Loc [ RH        ]
 2: 4          <
 3: 108        F
 4: 30         Then Do

34:  Z=F (P30)
 1: 100        F
 2: 11         Z Loc [ RH        ]

35:  End (P95)

36:  End (P95)

37:  Z=X (P31)
 1: 11         X Loc [ RH        ]
 2: 12         Z Loc [ CSI       ]

38:  Z=F (P30)
 1: 100        F
 2: 13         Z Loc [ CSI_R     ]

39:  Z=X/Y (P38)
 1: 12         X Loc [ CSI       ]
 2: 13         Y Loc [ CSI_R     ]
 3: 12         Z Loc [ CSI       ]

40:  Z=F (P30)
 1: .6108      F
 2: 13         Z Loc [ CSI_R     ]

41:  Z=X*Y (P36)
 1: 13         X Loc [ CSI_R     ]
 2: 12         Y Loc [ CSI       ]
 3: 12         Z Loc [ CSI       ]

42:  Z=F (P30)
 1: 17         F
 2: 13         Z Loc [ CSI_R     ]

43:  Z=X (P31)
 1: 13         X Loc [ CSI_R     ]
 2: 14         Z Loc [ CSI_2     ]

44:  Z=F (P30)
 1: .2694      F
 2: 13         Z Loc [ CSI_R     ]

45:  Z=X+Y (P33)
 1: 13         X Loc [ CSI_R     ]
 2: 12         Y Loc [ CSI       ]
 3: 14         Z Loc [ CSI_2     ]

46:  Z=X*Y (P36)
 1: 10         X Loc [ AirTc     ]
 2: 14         Y Loc [ CSI_2     ]
 3: 14         Z Loc [ CSI_2     ]

47:  Z=F (P30)
 1: 237.3      F
 2: 13         Z Loc [ CSI_R     ]

48:  Z=X+Y (P33)
 1: 10         X Loc [ AirTc     ]
 2: 13         Y Loc [ CSI_R     ]
 3: 13         Z Loc [ CSI_R     ]

49:  Z=X/Y (P38)
 1: 14         X Loc [ CSI_2     ]
 2: 13         Y Loc [ CSI_R     ]
 3: 13         Z Loc [ CSI_R     ]

50:  Z=EXP(X) (P41)
 1: 13         X Loc [ CSI_R     ]
 2: 13         Z Loc [ CSI_R     ]

51:  Z=X*Y (P36)
 1: 13         X Loc [ CSI_R     ]
 2: 12         Y Loc [ CSI       ]
 3: 15         Z Loc [ E_kPa     ]

52:  Internal Temperature (P17)
 1: 16         Loc [ PaTemp      ]
;Type E TC( surface temperature)
;purple 5H , red G CH-10

53:  Thermocouple Temp (SE) (P13)
 1: 1          Reps
 2: 3          50 mV Slow Range
 3: 10         SE Channel
 4: 2          Type E (Chromel-
Constantan)
 5: 16         Ref Temp (Deg. C) Loc [
PaTemp     ]
 6: 17         Loc [ TCsurface ]
 7: 1          Mult
 8: 0          Offset
; IRT wiring;body temperature yellow
5L red/shield G CH-11;Target
temperature (black band) Yellow 6H,
red/shield G CH-12

54:  Thermocouple Temp (SE) (P13)
 1: 2          Reps
 2: 3          50 mV Slow Range
 3: 11         SE Channel
 4: 3          Type K (Chromel-Alumel)
 5: 16         Ref Temp (Deg. C) Loc [
PaTemp     ]
 6: 18         Loc [ IRTbody_1 ]
 7: 1          Mult
 8: 0          Offset
;CM3 serial number 993297
;calibration factor 26.75 microV/w m-
2

;Solar Irradiance and reflected solar
irradiance measurement with CM3
55:  Volt (SE) (P1)
 1: 1          Reps
 2: 3          50 mV Slow Range
 3: 12         SE Channel
 4: 21         Loc [ CM283       ]
 5: 37.383     Mult
 6: 0.0        Offset
;CM3 serial number 993297
;calibration factor 23.85 microV/wm-2
56:  Volt (SE) (P1)
 1: 1          Reps
 2: 3          50 mV Slow Range
 3: 13         SE Channel
 4: 22         Loc [ CM297       ]
 5: 41.929     Mult
 6: 0.0        Offset



57:  Beginning of Loop (P87)
 1: 1          Delay
 2: 2          Loop Count

58:  If (X<=>F) (P89)
 1: 21     -- X Loc [ CM283      ]
 2: 4          <
 3: 0          F
 4: 30         Then Do

59:  Z=F (P30)
 1: 0          F
 2: 21     -- Z Loc [ CM283      ]

60:  End (P95)

61:  End (P95)

;Prpgogram for 15 M out put data
62:  If time is (P92)
 1: 0          Minutes into a
 2: 15         Minute Interval
 3: 10         Set Output Flag High

63:  Set Active Storage Area (P80)
 1: 1          Final Storage
 2: 101        Array ID

64:  Real Time (P77)
 1: 1220       Year,Day,Hour/Minute
(midnight = 2400)

65:  Resolution (P78)
 1: 1          High Resolution

66:  Average (P71)
 1: 1          Reps
 2: 1          Loc [ Vbattery    ]

67:  Average (P71)
 1: 4          Reps
 2: 2          Loc [ CNR1_1      ]

68:  Average (P71)
 1: 1          Reps
 2: 6          Loc [ Vtherm      ]

69:  Average (P71)
 1: 1          Reps
 2: 9          Loc [ NRWm2       ]

70:  Average (P71)
 1: 1          Reps
 2: 10         Loc [ AirTc       ]

71:  Sample (P70)
 1: 1          Reps
 2: 11         Loc [ RH          ]

72:  Average (P71)
 1: 1          Reps
 2: 15         Loc [ E_kPa       ]

73:  Wind Vector (P69)
 1: 1          Reps
 2: 0          Samples per Sub-Interval
 3: 0          S, él, & å(él) Polar
 4: 7          Wind Speed/East Loc [
WS_ms2     ]
 5: 8          Wind Direction/North Loc
[ WindDir     ]

74:  Average (P71)
 1: 3          Reps
 2: 17         Loc [ TCsurface ]

75:  Average (P71)
 1: 2          Reps
 2: 21         Loc [ CM283       ]

*Table 2 Program
  01: 30.0000    Execution Interval
(seconds)

1:  Serial Out (P96)
 1: 30         SM192/SM716/CSM1

*Table 3 Subroutines

End Program

-Input Locations-
1 Vbattery   1 1 1
2 CNR1_1     5 2 2
3 CNR1_2     9 1 1
4 CNR1_3     9 1 1
5 CNR1_4     17 1 1
6 Vtherm     1 1 1
7 WS_ms2     1 2 2
8 WindDir    1 2 2
9 NRWm2      1 1 1
10 AirTc      1 3 1
11 RH         1 4 2
12 CSI        1 5 3
13 CSI_R      1 8 8
14 CSI_2      1 3 3
15 E_kPa      1 2 1
16 PaTemp     1 2 1
17 TCsurface  1 1 1
18 IRTbody_1  5 1 1
19 IRTbody_2  17 1 1
20 Timeloca   1 2 1
21 CM283      1 2 2
22 CM297      1 1 1

Program Second CR21X
;{CR21X}-2
;
*Table 1 Program
  01: 30         Execution Interval
```

```
(seconds)

1:  Batt Voltage (P10)
 1: 1        Loc [ Vbattery  ]
;Rain measurement with Rain-o-Matic
resolution 1 mm
;raingauge white P1, black G
2:  Pulse (P3)
 1: 1        Reps
 2: 1        Pulse Input Channel
 3: 2        Switch Closure, All
Counts
 4: 3        Loc [ Rain_mm   ]
 5: 1        Mult
 6: 0.0      Offset
; Latent heat of evaporation
measurement from Etgage at one meter
with Canvas cover #30 and#54
resolution 0.254 mm per tip
 ETgauge-S1 green P2, white G
;ET gauge_S2 green P3, white G

3:  Pulse (P3)
 1: 2        Reps
 2: 2        Pulse Input Channel
 3: 2        Switch Closure, All
Counts
 4: 4        Loc [ ETgauge_1 ]
 5: .254     Mult
 6: 0.0      Offset

;Heated ceramic anemometer
;Red 2EX, black G; blue 2H, yellow 2L

12:  Full Bridge (P6)
 1: 1        Reps
 2: 1        5 mV Slow Range
 3: 2        DIFF Channel
 4: 2        Excite all reps w/Exchan
2
 5: 100      mV Excitation
 6: 8        Loc [ Vbridge   ]
 7: 1.0      Mult
 8: 0.0      Offset

13:  Polynomial (P55)
 1: 1        Reps
 2: 8        X Loc [ Vbridge   ]
 3: 9        F(X) Loc [ Trtd_wnd0 ]
 4: .0333    C0
 5: 2.8089   C1
 6: .0408    C2
 7: 0.0      C3
 8: 0.0      C4
 9: 0.0      C5

14:  Excitation with Delay (P22)
 1: 2        Ex Channel
 2: 500      Delay w/Ex (units = 0.01
sec)
 3: 0        Delay After Ex (units =
0.01 sec)
 4: 2500     mV Excitation

15:  Full Bridge (P6)
 1: 1        Reps
 2: 3        50 mV Slow Range
 3: 2        DIFF Channel
 4: 2        Excite all reps w/Exchan
2
 5: 2500     mV Excitation
 6: 10       Loc [ Vbridgeh_ ]
 7: 1.0      Mult
 8: 0.0      Offset

16:  Polynomial (P55)
 1: 1        Reps
 2: 10       X Loc [ Vbridgeh_ ]
 3: 11       F(X) Loc [ Trtd_wndh ]
 4: .0333    C0
 5: 2.8089   C1
 6: .0408    C2
 7: 0.0      C3
 8: 0.0      C4
 9: 0.0      C5
soil heat flux measurement with Two
soil heat flux plates buried in
undisturbed soil at a depth of 80mm,
;wires to south
17:  Internal Temperature (P17)
 1: 12       Loc [ PaTemp    ]
heat flux plat1
;black 2L, white G

18:  Volt (SE) (P1)
 1: 1        Reps
 2: 2        15 mV Slow Range
 3: 2        SE Channel
 4: 13       Loc [ Fplate1   ]
 5: 40.4     Mult
 6: 0        Offset
heat flux plat2
;black 3H, white G

19:  Volt (SE) (P1)
 1: 1        Reps
 2: 2        15 mV Slow Range
 3: 5        SE Channel
 4: 14       Loc [ Fplate2   ]
 5: 39.4     Mult
 6: 0        Offset
soil thrmocouples(type E)
;blue wire 2L,Red wire G
;buried at a depth of 20 and
60mm,wires to the south
20:  Thermocouple Temp (SE) (P13)
 1: 1        Reps
 2: 3        50 mV Slow Range
 3: 6        SE Channel
 4: 2        Type E (Chromel-
Constantan)
 5: 12       Ref Temp (Deg. C) Loc [
PaTemp    ]
 6: 15       Loc [ Tsoil     ]
 7: 1        Mult
 8: 0        Offset
;Thetaprob ML256/102
;yellow 3H; green G red 12V, Blue G
;bury prob horizontaly with pins in
undisturbed
; soil top pin at a depth of 25mm

21:  Volt (SE) (P1)
 1: 1        Reps
 2: 5        5000 mV Slow Range
 3: 7        SE Channel
 4: 16       Loc [ Vthetha   ]
 5: 0.001    Mult
 6: 0        Offset

out put data program for 15 Minute
44:  If time is (P92)
 1: 0        Minutes into a
 2: 15       Minute Interval
 3: 10       Set Output Flag High

45:  Set Active Storage Area (P80)
 1: 1        Final Storage
 2: 103      Array ID

46:  Resolution (P78)
 1: 1        High Resolution

47:  Real Time (P77)
 1: 1220     Year,Day,Hour/Minute
(midnight = 2400)

48:  Average (P71)
 1: 1        Reps
 2: 1        Loc [ Vbattery  ]

49:  Totalize (P72)
 1: 3        Reps
 2: 3        Loc [ Rain_mm   ]

50:  Wind Vector (P69)
 1: 1        Reps
 2: 0        Samples per Sub-Interval
 3: 0        S, é1, & å(é1) Polar
 4: 6        Wind Speed/East Loc [
WS1m_ms   ]
 5: 7        Wind Direction/North Loc
[ WindDir1  ]

51:  Sample (P70)
 1: 1        Reps
 2: 9        Loc [ Trtd_wnd0 ]

52:  Sample (P70)
 1: 1        Reps
 2: 11       Loc [ Trtd_wndh ]

53:  Average (P71)
 1: 4        Reps
 2: 13       Loc [ Fplate1   ]

54:  Average (P71)
 1: 1        Reps
 2: 17       Loc [ TairTc1   ]

55:  Sample (P70)
 1: 1        Reps
 2: 18       Loc [ RH_1M     ]

56:  Average (P71)
 1: 1        Reps
 2: 22       Loc [ E_KPa     ]

*Table 2 Program
  02: 30         Execution Interval
(seconds)

1:  Serial Out (P96)
 1: 30       Storage Module


*Table 3 Subroutines

End Program

-Input Locations-
1 Vbattery  1 1 1
2 prog_sig  1 0 0
3 Rain_mm   1 1 1
4 ETgauge_1 5 1 1
5 ETgauge_2 17 1 1
6 WS1m_ms   1 2 2
7 WindDir1  1 2 2
8 Vbridge   1 1 1
9 Trtd_wnd0 1 1 1
10 Vbridgeh_ 1 1 1
11 Trtd_wndh 1 1 1
12 PaTemp    1 1 1
13 Fplate1   1 1 1
14 Fplate2   1 1 1
15 Tsoil     1 0 1
16 Vthetha   1 0 1
17 TairTc1   1 3 1
18 RH_1M     1 4 2
19 CSI_1     1 4 3
20 CSI_R     1 8 8
21 csi_2     1 4 3
22 E_KPa     1 2 1
23 airtc1    1 0 0
24 RH        1 0 0
```

Appendix 3.3 The CR7X data logger program for measuring air temperature, relative humidity, water vapour pressure from different radiation shields and using air temperature and relative humidity sensors.

```
Home made Radiation shield from two
Plastic and one Metal used to measure
air temperature
1-using thermocouple Type E,
Location 6,7 and 9 respectively
2- CS500 Probe
Plastic radiation shield
Air temperature Location 21 and 22,
RH Location 33,34
Standard Steven screen, Small
Stevenson screen
(thermocouple type E, CS500 Vaisala)
air temperature location 4,8,19,23
RH location 31,35
 12 Plate Gill radiation shield
Thermocouple type and HMP35c probe
air temperature location 3,18
RH location 30
6-plate Gill radiation shield
thermocouple type E and CS500 probe
air temperature location 5,20
RH 32
 Solar irradiance measurement
CM3 location 12
Wind speed and direction Three Cup
anemometer and vain
Location 16,14
Rain (Rain -o-matic)
Location 17
Evaporation measurement (Etgage)
Location 15
;{CR7}
;Radiation shield *Table 1 Program
  01: 10        Execution Interval
(seconds)

1:  Battery Voltage (P10)
 1: 1          Loc [ Vbattery  ]

2:  Panel Temperature (P17)
 1: 1          In Card
 2: 2          Loc [ Tpanal    ]
Air temperature measurement
;Thermocouple Type E
;Puple H, red L
;CH-1 12RS, CH-2 BSS, CH-3 6RS,CH-4
HBP, CH-4 HSP,CH-5 SSS CH-6 MRS,CH-7
1.5 M
;CH-8 2 m fin thermocouples
3:  Thermocouple Temp (DIFF) (P14)
 1: 9          Reps
 2: 4          50 mV Slow Range
 3: 1          In Card
 4: 1          DIFF Channel
 5: 2          Type E (Chromel-
Constantan)
 6: 2          Ref Temp (Deg. C) Loc [
Tpanal    ]
 7: 3          Loc [ Tc_1      ]
 8: 1.0        Mult
 9: 0.0        Offset
Air temperature, vapour pressure and
RH with HMP35C Temperature and
humidity probe
card no 2
;Red +12V, Yellow  digital control
port1,
;Green 1L (RH),Orange 1H Temperature,
Black switeched exitation port
1(Tempe exitation)
; Clear, white and puple ground

15:  Temp 107 Probe (P11)
 1: 1          Reps
 2: 2          In Card
 3: 1          SE Channel
 4: 1          Ex Card
 5: 2          Ex Channel
 6: 18         Loc [ AirT_12RS ]
 7: 1          Mult
 8: 0          Offset

16:  Do (P86)
 1: 41         Set Port 1 High


17:  Excitation with Delay (P22)
 1: 1          Ex Card
 2: 1          Ex Channel
 3: 0          Delay w/Ex (units = 0.01
sec)
 4: 15         Delay After Ex (units =
0.01 sec)
 5: 0          mV Excitation

18:  Volt (SE) (P1)
 1: 1          Reps
 2: 8          5000 mV Slow Range
 3: 2          In Card
 4: 2          SE Channel
 5: 30         Loc [ RH_12RS   ]
 6: 0.1        Mult
 7: 0          Offset

19:  Do (P86)
 1: 51         Set Port 1 Low

20:  If (X<->F) (P89)
 1: 30         X Loc [ RH_12RS   ]
 2: 4          <
 3: 108        F
 4: 30         Then Do


21:  If (X<=>F) (P89)
 1: 30         X Loc [ RH_12RS   ]
 2: 3          >=
 3: 100        F
 4: 30         Then Do

22:  Z=F (P30)
 1: 100        F
 2: 30         Z LOC [ RH_12RS   ]


23:  End (P95)

24:  End (P95)

25:  Saturation Vapor Pressure (P56)
 1: 18         Temperature Loc [
AirT_12RS ]
 2: 24         Loc [ E_KPA12RS ]


26:  Z=X*F (P37)
 1: 30         X Loc [ RH_12RS   ]
 2: 0.01       F
 3: 36         Z LOC [ CSI_1     ]


27:  Z=X*Y (P36)
 1: 24         X Loc [ E_KPA12RS ]
 2: 36         Y Loc [ CSI_1     ]
 3: 24         Z LOC [ E_KPA12RS ]
 Air temperature, vapour pressure and
RH measurement from 4 CS500
50YC S4650042
;Green ; white Ground, Red +12V,
brown 2H , Black 2L
50YcRO710077 Yellow +12v,Purple
3H,brown 3L,
;green G
Humitter 50YC S5030025, red
+12V,Black 4H,brown 4L,
;green G
Vaisala 50YC R2020010, Yellow
+12V,Black 5H,blue 5L,
;green G
28:  Volt (SE) (P1)
 1: 1          Reps
 2: 8          5000 mV Slow Range
 3: 2          In Card
 4: 3          SE Channel
 5: 19         Loc [ AirTc_BSS ]
 6: 0.1        Mult
 7: -40        Offset


29:  Volt (SE) (P1)
 1: 1          Reps
 2: 8          5000 mV Slow Range
 3: 2          In Card
 4: 4          SE Channel
 5: 31         Loc [ RH_BSS    ]
 6: 0.1        Mult
 7: 0.0        Offset

31:  If (X<=>F) (P89)
 1: 31         X Loc [ RH_BSS    ]
 2: 4          <
 3: 108        F
 4: 30         Then Do

32:  If (X<=>F) (P89)
 1: 31         X Loc [ RH_BSS    ]
 2: 3          >=
 3: 100        F
 4: 30         Then Do

33:  Z=F (P30)
 1: 100        F
 2: 31         Z LOC [ RH_BSS    ]

34:  End (P95)

35:  End (P95)

36:  Saturation Vapor Pressure (P56)
 1: 19         Temperature Loc [
AirTc_BSS ]
 2: 25         Loc [ E_KPABSS  ]

37:  Z=X*F (P37)
 1: 31         X Loc [ RH_BSS    ]
 2: 0.01       F
 3: 36         Z LOC [ CSI_1     ]


38:  Z=X*Y (P36)
 1: 25         X Loc [ E_KPABSS  ]
 2: 36         Y Loc [ CSI_1     ]
 3: 25         Z LOC [ E_KPABSS  ]

Program out put for 15 Minute and 60
Minute data
79:  If time is (P92)
 1: 0          Minutes into a
 2: 15         Minute Interval
 3: 10         Set Output Flag High

80:  Set Active Storage Area (P80)
 1: 1          Final Storage
 2: 101        Array ID

81:  Real Time (P77)
 1: 1220       Year,Day,Hour/Minute
(midnight = 2400)

82:  Resolution (P78)
 1: 1          High Resolution

83:  Average (P71)
 1: 1          Reps
 2: 1          Loc [ Vbattery  ]

84:  Average (P71)
 1: 1          Reps
 2: 12         Loc [ CM3       ]

85:  Totalize (P72)
 1: 1          Reps
 2: 17         Loc [ Rain_mm   ]


86:  Average (P71)
 1: 1          Reps
 2: 20         Loc [ AirTc_6RS ]

87:  Average (P71)
 1: 1          Reps
 2: 26         Loc [ E_KPA6RS  ]

88:  Wind Vector (P69)
 1: 1          Reps
 2: 0          Samples per Sub-Interval
 3: 0          S, é1, & å(é1) Polar
 4: 16         Wind Speed/East Loc [
WS_ms     ]
 5: 14         Wind Direction/North Loc
[ Wind_Dire ]

89:  Totalize (P72)
 1: 1          Reps
 2: 15         Loc [ ETGI      ]
68:  If time is (P92)
 1: 0          Minutes into a
 2: 5          Minute Interval
 3: 10         Set Output Flag High

69:  Set Active Storage Area (P80)
 1: 1          Final Storage
 2: 105        Array ID

70:  Real Time (P77)
 1: 1220       Year,Day,Hour/Minute
(midnight = 2400)

71:  Resolution (P78)
 1: 1          High Resolution

72:  Sample (P70)
 1: 10         Reps
 2: 2          Loc [ T_panal   ]

73:  Sample (P70)
 1: 5          Reps
 2: 18         Loc [ AirT_12RS ]

74:  Sample (P70)
 1: 5          Reps
```

```
 2: 24        Loc [ E_kPa12RS ]

75:  Sample (P70)
 1: 5         Reps
 2: 30        Loc [ RH_12RS   ]

90:  If time is (P92)
 1: 0         Minutes into a
 2: 15        Minute Interval
 3: 10        Set Output Flag High

91:  Set Active Storage Area (P80)
 1: 1         Final Storage
 2: 102       Array ID

92:  Real Time (P77)
 1: 1220      Year,Day,Hour/Minute
(midnight = 2400)

93:  Resolution (P78)
 1: 1         High Resolution

94:  Average (P71)
 1: 10        Reps
 2: 2         Loc [ Tpanal    ]

95:  Average (P71)
 1: 12        Reps
 2: 18        Loc [ AirT_12RS ]

96:  Sample (P70)
 1: 6         Reps
 2: 30        Loc [ RH_12RS   ]

97:  Standard Deviation (P82)
 1: 10        Reps
 2: 2         Sample Loc [ Tpanal    ]


98:  Standard Deviation (P82)
 1: 12        Reps
 2: 18        Sample Loc [ AirT_12RS ]


99:  If time is (P92)
 1: 0         Minutes into a
 2: 60        Minute Interval
 3: 10        Set Output Flag High

100:  Set Active Storage Area (P80)
 1: 2         Final Storage
 2: 103       Array ID

101:  Real Time (P77)
 1: 1220      Year,Day,Hour/Minute
(midnight = 2400)

102:  Resolution (P78)
 1: 1         High Resolution
103:  Average (P71)
 1: 1         Reps
 2: 1         Loc [ Vbattery  ]

104:  Average (P71)
 1: 1         Reps
 2: 12        Loc [ CM3       ]

105:  Totalize (P72)
 1: 1         Reps
 2: 17        Loc [ Rain_mm   ]

106:  Average (P71)
 1: 1         Reps
 2: 20        Loc [ AirTc_6RS ]

107:  Average (P71)
 1: 1         Reps
 2: 26        Loc [ E_KPA6RS  ]


108:  Wind Vector (P69)
 1: 1         Reps
 2: 0         Samples per Sub-Interval
 3: 0         S, él, & â(é1) Polar
 4: 16        Wind Speed/East Loc [
WS_ms     ]
 5: 14        Wind Direction/North Loc
[ Wind_Dire ]

109:  Totalize (P72)
 1: 1         Reps
 2: 15        Loc [ ETG1      ]

110:  If time is (P92)
 1: 0         Minutes into a
 2: 60        Minute Interval
 3: 10        Set Output Flag High

111:  Set Active Storage Area (P80)
 1: 2         Final Storage
 2: 104       Array ID

112:  Real Time (P77)
 1: 1220      Year,Day,Hour/Minute
(midnight = 2400)

113:  Resolution (P78)
 1: 1         High Resolution

114:  Average (P71)
 1: 10        Reps
 2: 2         Loc [ Tpanal    ]

115:  Average (P71)
 1: 12        Reps
 2: 18        Loc [ AirT_12RS ]

116:  Sample (P70)
 1: 6         Reps
 2: 30        Loc [ RH_12RS   ]


*Table 2 Program
  02: 10         Execution Interval
(seconds)

1:  Serial Out (P96)
 1: 30        Storage Module

*Table 3 Subroutines

End Program

-Input Locations-
1 Vbattery  5 2 1
2 Tpanal    5 4 1
3 Tc_1      13 3 1
4 Tc_2      9 3 1
5 Tc_3      9 3 1
6 Tc_4      9 3 1
7 Tc_5      9 3 1
8 Tc_6      9 3 1
9 Tc_7      9 3 1
10 Tc_8      9 3 1
11 Tc_9      17 3 1
12 CM3       1 3 2
13 _________ 0 0 0
14 Wind_Dire 1 3 2
15 ETG1      5 2 1
16 WS_ms     1 2 1
17 Rain_mm   1 2 1
18 AirT_12RS 5 4 1
19 AirTc_BSS 9 4 1
20 AirTc_6RS 9 8 1
21 AirTc_HBP 9 6 1
22 AirTc_HSP 9 6 1
23 AirTC_SSS 17 6 1
24 E_KPA12RS 1 4 2
25 E_KPABSS  1 4 2
26 E_KPA6RS  1 6 2
27 E_KPAHBP  1 4 2
28 E_KPAHSP  1 4 2
29 E_KPASSS  1 4 2
30 RH_12RS   1 5 2
31 RH_BSS    1 5 2
32 RH_6RS    1 7 2
33 RH_HBP    1 7 2
34 RH_HSP    1 7 2
35 RH_SSS    1 7 2
36 CSI_1     1 6 6
```

Appendix 3.4 The 21X data logger program for measuring ETgage surface evaporation from surface temperature energy balance techniques with IRT and thermocouple type E

```
Apogee IRT measuring surface
temperature of Etgage
location
Mininature net radiometer measuring
net irradiance from Etgauge
evaporation surface
 Location
Fine wire Thermocouple Type T
Measuring surface of Etgage , grass
surface, and body temperature
Location
Three-cup wind speed sensors
measuring wind speed and direction
from one and two meters
Location
Vasala CS500 measuring air
temperature and RH at one and Two
meters
Location
Etgage covered with canvas cover #30
and #54 at 1m with 30 cm difference
location
;{21X}
*Table 1 Program
  01: 10.0000    Execution Interval
(seconds)

1:  Batt Voltage (P10)
 1: 1          Loc [ vbattery  ]
;Mini nuture Net radiometer wiring
;black 1H,red 1L
2:  Volt (Diff) (P2)
 1: 1          Reps
 2: 3          50 mV Slow Range
 3: 1          DIFF Channel
 4: 2          Loc [ Min_Net   ]
 5: 1          Mult
 6: 0          Offset

3:  Internal Temperature (P17)
 1: 3          Loc [ Tpanal    ]
;Infrared net radiometer
;yellow with black strip (IRT
thargel)
;yellow 2H, red 2L,shield ground
;Yellow (IRT body)
;yellow 3H,Red 3L,shield ground
4:  Thermocouple Temp (DIFF) (P14)
 1: 2          Reps
 2: 3          50 mV Slow Range
 3: 2          DIFF Channel
 4: 3          Type K (Chromel-Alumel)
 5: 3          Ref Temp (Deg. C) Loc [
Tpanal    ]
 6: 4          Loc [ IRTbody_1 ]
 7: 1          Mult
 8: 0          Offset
;Etg surface temperature
;Purple 4H,Red 4L
5:  Thermocouple Temp (DIFF) (P14)
 1: 1          Reps
 2: 3          50 mV Slow Range
 3: 4          DIFF Channel
 4: 2          Type E (Chromel-
Constantan)
 5: 3          Ref Temp (Deg. C) Loc [
Tpanal    ]
 6: 6          Loc [ ETsurfa   ]
 7: 1          Mult
 8: 0          Offset
;soil surface temperature
;purple 5H,Red ground
6:  Thermocouple Temp (SE) (P13)
 1: 1          Reps
 2: 3          50 mV Slow Range
 3: 9          SE Channel
 4: 2          Type E (Chromel-
Constantan)
 5: 3          Ref Temp (Deg. C) Loc [
Tpanal    ]
 6: 7          Loc [ Tcsurface ]
 7: 1          Mult
 8: 0          Offset
;ETgauge body Temperature
;Purple 5L,Red Ground
7:  Thermocouple Temp (SE) (P13)
 1: 1          Reps
 2: 3          50 mV Slow Range
 3: 10         SE Channel
 4: 2          Type E (Chromel-
Constantan)
 5: 3          Ref Temp (Deg. C) Loc [
Tpanal    ]
 6: 8          Loc [ ET_insid  ]
 7: 1          Mult
 8: 0          Offset
;ETgauge Pulse measurement
;Green pulse port 1,white ground with
;thermocouples and Infrred
thermometer
;Green Pulse port 2,white ground with
;Net radiometer

8:  Pulse (P3)
 1: 2          Reps
 2: 1          Pulse Input Channel
 3: 2          Switch Closure, All
Counts
 4: 9          Loc [ ETgau_1   ]
 5: .254       Mult
 6: 0          Offset
;wind speed sensors
;red pulse port 3,green/black ground
9:  Pulse (P3)
 1: 2          Reps
 2: 3          Pulse Input Channel
 3: 21         Low Level AC, Output Hz
 4: 11         Loc [ Ws1_1     ]
 5: .75        Mult
 6: .2         Offset

10:  If (X<=>F) (P89)
 1: 11         X Loc [ Ws1_1     ]
 2: 4          <
 3: .21        F
 4: 30         Then Do

11:  If (X<=>F) (P89)
 1: 12         X Loc [ Ws1_2     ]
 2: 4          <
 3: .21        F
 4: 30         Then Do

12:  Z=F (P30)
 1: 0          F
 2: 11         Z Loc [ Ws1_1     ]

13:  Z=F (P30)
 1: 0          F
 2: 12         Z Loc [ Ws1_2     ]

14:  End (P95)

15:  End (P95)

16:  Excite Delay Volt (SE) (P4)
 1: 2          Reps
 2: 5          5000 mV Slow Range
 3: 11         SE Channel
 4: 1          Excite all reps w/Exchan
1
 5: 2          Delay (units 0.01 sec)
 6: 5000       mV Excitation
 7: 13         Loc [ windDir_1 ]
 8: .071       Mult
 9: 0          Offset

17:  If (X<=>F) (P89)
 1: 13         X Loc [ windDir_1 ]
 2: 3          >=
 3: 360        F
 4: 30         Then Do

18:  If (X<=>F) (P89)
 1: 14         X Loc [ windDir_2 ]
 2: 3          >=
 3: 360        F
 4: 30         Then Do

19:  Z=F (P30)
 1: 0          F
 2: 13         Z Loc [ windDir_1 ]

20:  Z=F (P30)
 1: 0          F
 2: 14         Z Loc [ windDir_2 ]

21:  End (P95)

22:  End (P95)
;single ended air temperature and
;purple 7H,Green ground,Yellow +12V
for 2m
;black 7L,green/white ground,red +12V
for 1m
23:  Volt (SE) (P1)
 1: 2          Reps
 2: 5          5000 mV Slow Range
 3: 13         SE Channel
 4: 15         Loc [ AirTc_1   ]
 5: .1         Mult
 6: -40        Offset
;RH measurement for 2 and 1m
;Brown 8H,Green ground,yellow +12v
for 2m
;brown 8L,white/yellow ground,red
+12V for 1m
24:  Volt (SE) (P1)
 1: 2          Reps
 2: 5          5000 mV Slow Range
 3: 15         SE Channel
 4: 17         Loc [ RH_1      ]
 5: .1         Mult
 6: 0          Offset

25:  If (X<=>F) (P89)
 1: 17         X Loc [ RH_1      ]
 2: 3          >=
 3: 100        F
 4: 30         Then Do

26:  If (X<=>F) (P89)
 1: 18         X Loc [ RH_2      ]
 2: 3          >=
 3: 100        F
 4: 30         Then Do

27:  If (X<=>F) (P89)
 1: 17         X Loc [ RH_1      ]
 2: 4          <
 3: 108        F
 4: 30         Then Do

28:  If (X<=>F) (P89)
 1: 18         X Loc [ RH_2      ]
 2: 4          <
 3: 108        F
 4: 30         Then Do

29:  Z=F (P30)
 1: 100        F
 2: 17         Z Loc [ RH_1      ]

30:  Z=F (P30)
 1: 100        F
 2: 18         Z Loc [ RH_2      ]

31:  End (P95)

32:  End (P95)

33:  End (P95)

34:  End (P95)

35:  Z=X (P31)
 1: 17         X Loc [ RH_1      ]
 2: 29         Z Loc [ CSI_1     ]

36:  Z=X (P31)
 1: 18         X Loc [ RH_2      ]
 2: 20         Z Loc [ CSI_2     ]

37:  Z=F (P30)
 1: 100        F
 2: 21         Z Loc [ CSI_R     ]

38:  Z=X/Y (P38)
 1: 29         X Loc [ CSI_1     ]
 2: 21         Y Loc [ CSI_R     ]
 3: 29         Z Loc [ CSI_1     ]

39:  Z=X/Y (P38)
 1: 20         X Loc [ CSI_2     ]
 2: 21         Y Loc [ CSI_R     ]
 3: 20         Z Loc [ CSI_2     ]

40:  Z=F (P30)
 1: .6108      F
 2: 21         Z Loc [ CSI_R     ]

41:  Z=X*Y (P36)
 1: 21         X Loc [ CSI_R     ]
 2: 29         Y Loc [ CSI_1     ]
 3: 29         Z Loc [ CSI_1     ]

42:  Z=X*Y (P36)
 1: 21         X Loc [ CSI_R     ]
 2: 20         Y Loc [ CSI_2     ]
 3: 20         Z Loc [ CSI_2     ]

43:  Z=F (P30)
 1: 17         F
 2: 21         Z Loc [ CSI_R     ]

44:  Z=X (P31)
 1: 21         X Loc [ CSI_R     ]
 2: 22         Z Loc [ CSI_0     ]

45:  Z=F (P30)
```

```
 1: .2694     F
 2: 21        Z Loc [ CSI_R     ]

46:  Z=X+Y (P33)
 1: 21        X Loc [ CSI_R     ]
 2: 22        Y Loc [ CSI_0     ]
 3: 22        Z Loc [ CSI_0     ]

47:  Z=X*Y (P36)
 1: 15        X Loc [ AirTc_1   ]
 2: 22        Y Loc [ CSI_0     ]
 3: 23        Z Loc [ CSI_21    ]

48:  Z=X*Y (P36)
 1: 16        X Loc [ AirTc_2   ]
 2: 22        Y Loc [ CSI_0     ]
 3: 24        Z Loc [ CSI_22    ]

49:  Z=F (P30)
 1: 237.3     F
 2: 21        Z Loc [ CSI_R     ]

50:  Z=X+Y (P33)
 1: 15        X Loc [ AirTc_1   ]
 2: 21        Y Loc [ CSI_R     ]
 3: 25        Z Loc [ CSI_R1    ]

51:  Z=X+Y (P33)
 1: 16        X Loc [ AirTc_2   ]
 2: 21        Y Loc [ CSI_R     ]
 3: 26        Z Loc [ CSI_R2    ]

52:  Z=X/Y (P38)
 1: 23        X Loc [ CSI_21    ]
 2: 25        Y Loc [ CSI_R1    ]
 3: 25        Z Loc [ CSI_R1    ]

53:  Z=X/Y (P38)
 1: 24        X Loc [ CSI_22    ]
 2: 26        Y Loc [ CSI_R2    ]
 3: 26        Z Loc [ CSI_R2    ]

54:  Z=EXP(X) (P41)
 1: 25        X Loc [ CSI_R1    ]
 2: 25        Z Loc [ CSI_R1    ]

55:  Z=EXP(X) (P41)
 1: 26        X Loc [ CSI_R2    ]
 2: 26        Z Loc [ CSI_R2    ]

56:  Z=X*Y (P36)
 1: 25        X Loc [ CSI_R1    ]
 2: 29        Y Loc [ CSI_1     ]
 3: 27        Z Loc [ E_KPA1    ]

57:  Z=X*Y (P36)
 1: 26        X Loc [ CSI_R2    ]
 2: 20        Y Loc [ CSI_2     ]
 3: 28        Z Loc [ E_KPA2    ]

58:  If time is (P92)
 1: 0         Minutes into a
 2: 15        Minute Interval
 3: 10        Set Output Flag High

59:  Set Active Storage Area (P80)
 1: 1         Final Storage
 2: 101       Array ID

60:  Real Time (P77)
 1: 1220      Year,Day,Hour/Minute
(midnight = 2400)

61:  Resolution (P78)
 1: 1         High Resolution

62:  Average (P71)
 1: 2         Reps
 2: 1         Loc [ vbattery    ]

63:  Average (P71)
 1: 5         Reps
 2: 4         Loc [ IRTbody_1   ]

64:  Totalize (P72)
 1: 2         Reps
 2: 9         Loc [ ETgau_1     ]

65:  Wind Vector (P69)
 1: 2         Reps
 2: 0         Samples per Sub-Interval
 3: 0         S, ë1, & à(ë1) Polar
 4: 11        Wind Speed/East Loc [
Ws1_1      ]
 5: 13        Wind Direction/North Loc
[ windDir_1 ]

66:  Average (P71)
 1: 2         Reps
 2: 15        Loc [ AirTc_1     ]

67:  Sample (P70)
 1: 2         Reps
 2: 17        Loc [ RH_1        ]

68:  Average (P71)
 1: 2         Reps
 2: 27        Loc [ E_KPA1      ]

*Table 2 Program
  01: 10.0000    Execution Interval
(seconds)

1:  Serial Out (P96)
 1: 30        Storage Module

*Table 3 Subroutines

End Program

-Input Locations-
1 vbattery   1 1 1
2 Min_Net    1 1 1
3 Tpanal     1 4 1
4 IRTbody_1  5 1 1
5 IRTbody_2  17 1 1
6 ETsurfa    1 1 1
7 Tcsurface  1 1 1
8 ET_insid   1 1 1
9 ETgau_1    5 1 1
10 ETgau_2   17 1 1
11 Ws1_1     5 2 2
12 Ws1_2     17 2 2
13 windDir_1 5 2 2
14 windDir_2 17 2 2
15 AirTc_1   5 3 1
16 AirTc_2   17 3 1
17 RH_1      5 4 2
18 RH_2      17 4 2
19 _________ 1 0 0
20 CSI_2     1 4 3
21 CSI_R     1 8 5
22 CSI_0     1 3 2
23 CSI_21    1 2 1
24 CSI_22    1 2 1
25 CSI_R1    1 3 3
26 CSI_R2    1 3 3
27 E_KPA1    1 2 1
28 E_KPA2    1 2 1
29 CSI_1     1 4 3
-Program Security-
0000
0000
0000
Final Storage Label File for:
NET19082.CSI
```

Appendix 4 Calculation procedure for estimating percentage of organic matter content using Walkley A (1947) (taken from Soil Science notes, University of Natal, Pietermaritzburg)

Soil water content determination:

$$\theta(m^3 m^{-3}) = \frac{[1.07 + 6.4V - 6.4V^2 + 4.7V^3] - 8.4}{1.6}$$

where V is measured voltage (mV) with Theta Probe sensor

Preparation				Analysis										
A	B	C	D	E	F	G	H	I	J	K	L	M	N	I
soil sam	mass	K2cr2o7(49.04g	H_2so_4	Deionized water	(85%)H_3PO_4	Na F	Ferroin Indivcato	Ammonium sul	water content	dry mass	conc-left	volume-organim	carbon	carbon%
	g	ml	ml	ml	ml	g	drop	ml	%	g (Soil)	$K_2cr_2o_7$(49.04g/l	$K_2cr_2o_7$(49.04g/l	mg	%
		1N					0.5N				ml(x)	ml(y)		
TW1.1	0.52	10	20	170	10	0.20	10	11.20	4.50	0.50	5.45	4.55	18.14	3.65
TW1.2	0.51	10	20	170	10	0.20	10	13.80	4.50	0.49	6.72	3.28	13.08	2.69
TW2.1	0.56	10	20	170	10	0.20	10	10.90	5.10	0.53	5.31	4.69	18.72	3.53
TW2.2	0.51	10	20	170	10	0.20	10	11.50	5.10	0.49	5.60	4.40	17.55	3.61
TW3.1	0.55	10	20	170	10	0.20	10	16.00	5.20	0.52	7.79	2.21	8.81	1.69
TW3.2	0.58	10	20	170	10	0.20	10	14.10	5.20	0.55	6.87	3.13	12.50	2.28
blank		10	20	170	10	0.20	10	20.55			10.01	-0.01	-0.03	
Calculation										=B-J*B/100			=M*12/4*1.33	
											=0.487*I	=10-L		=N*100/(K*1000)

Organic Matter Analysis

M		N	O	P	Q	R	S	T	U
Location no	Sample No	Air dry sample	Gvm SWC	Oven dry soil	volum titre	Volume not react	Volume .react	Organic Carbon	
		g	g/g g		ml	ml	ml	%	
1.00	1a	0.52	0.02	0.50	11.20	5.60	4.40	35.35	
	1b	0.51	0.02	0.49	13.80	6.90	3.10	25.45	
2.00	2a	0.56	0.03	0.53	10.90	5.45	4.55	34.22	
	2b	0.51	0.03	0.49	11.50	5.75	4.25	34.83	
3.00	3a	0.55	0.03	0.52	16.00	8.00	2.00	15.28	
	3b	0.58	0.03	0.55	14.10	7.05	2.95	21.44	
Average						=(Q29*W$32)/X$32)		27.76	
				=N29-O29			=R$32-Z30	=(S*(12/4)*1.33*100)/(P*100)	

W	X	Y	Z
V.(FAS) Blanl N	$K_2cr_2o_7$ N	(FAS) Bla ml	$V.K_2Cr_2O_7$ ml
0.50	1.00	20.55	10.00

(a)

21X PROMPT SHEET

*MODES

STANDARD SOFTWARE

*0 — Compile/log data
*1, *2, *3 — User program
*4 — Output options:
01:x0 Printer disabled
x1 Printer enabled
0x Tape disabled
1x Tape enabled
02:00 300 baud to printer
01 1200 baud
02 9600 baud
03 76,800 baud

*5 — Set/display time
HH:MM:SS
05:xx Year
05:xxxx Julian day
05:HH:MM: Hours:Minutes
*6 — Display/alter Input Storage, flags
*7 — Display Final Storage
*8, *9 — Dump to tape, Dump to printer
01:xxxxx Current/start F.S. loc
02:xxxxx DSP/end F.S. loc
03:00 Enter any No. to start dump

*A — Memory Allocation
01:xxxx Input Storage loc.
02:xxxx Intermediate Storage loc.
03:xxxxx Final Storage loc.
04:xxxx Remaining program mem. (bytes)
*B — Signatures
01:xxxxx Program memory
02:xxxxx EPROM No. 1
03:xxxxx EPROM No. 2
04:xxxxx EPROM No. 3 (extended software)

NOTE: x represents a digit

EXTENDED SOFTWARE

*C — Security (ESX1 only)
12:0000 Enter password
01:00 Temporarily disable security
01 Set new password
02:xxxx Set password,
0000 disables security
*D — Save/load program
Commands (1 & 2) require baud rate code:
1 — Print program (ASCII)
2 — Load program (ASCII)
3 — Save program on tape
4 — Load program from tape
5 — Save custom PROM (ESX1 only)

21X INSTRUCTION AND *PARAMETER* SUMMARY

INPUT/OUTPUT INSTRUCTIONS

INST. NO. AND DESCRIPTION	*PARAMETERS* 01:	02:	03:	04:	05:	06:	07:	08:	09:
1 VOLT (SE)	*REPS*	*RANGE†*	*IN CHAN*	*LOC*	*MULT.*	*OFFSET*			
2 VOLT (DIFF)	*REPS*	*RANGE†*	*IN CHAN*	*LOC*	*MULT.*	*OFFSET*			
3 PULSE	*REPS*	*IN CHAN*	*CONFIG.†*	*LOC*	*MULT.*	*OFFSET*			
4 EX-DEL-SE	*REPS*	*RANGE†*	*IN CHAN*	*EX CHAN†*	*DEL .01s*	*EXCIT MV*	*LOC*	*MULT.*	*OFFSET*
5 AC HALF BR	*REPS*	*RANGE†*	*IN CHAN*	*EX CHAN†*	*EXCIT MV*	*LOC*	*MULT.*	*OFFSET*	
6 FULL BR	*REPS*	*RANGE†*	*IN CHAN*	*EX CHAN†*	*EXCIT MV*	*LOC*	*MULT.*	*OFFSET*	
7 3W HALF BR	*REPS*	*RANGE†*	*IN CHAN*	*EX CHAN†*	*EXCIT MV*	*LOC*	*MULT.*	*OFFSET*	
8 EX-DEL-DIFF	*REPS*	*RANGE†*	*IN CHAN*	*EX CHAN†*	*DEL .01s*	*EXCIT MV*	*LOC*	*MULT.*	*OFFSET*
9 FULL BR-MEX	*REPS*	*EX RANGE†*	*B RANGE†*	*IN CHAN*	*EX CHAN†*	*EXCIT MV*	*LOC*	*MULT.*	*OFFSET*
10 BATT. VOLT	*LOC*								
11 TEMP-(107)	*REPS*	*IN CHAN*	*EX CHAN†*	*LOC*	*MULT.*	*OFFSET*			
12 RH (207)	*REPS*	*RH CHAN*	*EX CHAN†*	*T LOC*	*RH LOC*	*MULT.*	*OFFSET*		
13 TEMP-TC SE	*REPS*	*RANGE†*	*IN CHAN*	*TC TYPE†*	*REF LOC*	*LOC*	*MULT.*	*OFFSET*	
14 TEMP-TC DIF	*REPS*	*RANGE†*	*IN CHAN*	*TC TYPE†*	*REF LOC*	*LOC*	*MULT.*	*OFFSET*	
16 TEMP-RTD	*REPS*	*R/Ro LOC*	*LOC*	*MULT.*	*OFFSET*				
17 TEMP PANEL	*LOC*								
18 TIME	*OPTION†*	*MODIFY*	*LOC*						
19 SIGNATURE	*LOC*								
20 PORT SET	*OPTION†*	*PORT NO.*							
21 ANALOG OUT	*CAO CHAN*	*MV LOC*							
22 EXCIT-DEL	*EX CHAN*	*DEL W/EX*	*DEL AFTER*	*EXCIT MV (del. unit - 0.01s)*					
26 TIMER	*LOC (to reset and run timer, use this inst. with LOC = 0)*								

PROCESSING INSTRUCTIONS

DESC.	01: 02: 03:	DESC.	01: 02: 03:	DESC.	01: 02: 03:
30 Z = F	F Z	36 Z = X*Y	X Y Z	42 Z = 1/X	X Z
31 Z = X	X Z	37 Z = X*F	X F Z	43 Z = ABS(X)	X Z
32 Z = Z + 1	Z	38 Z = X/Y	X Y Z	44 Z = FRAC(X)	X Z
33 Z = X + Y	X Y Z	39 Z = SQRT(X)	X Z	45 Z = INT(X)	X Z
34 Z = X + F	X F Z	40 Z = LN(X)	X Z	46 Z = X MOD F	X F Z
35 Z = X − Y	X Y Z	41 Z = EXP(X)	X Z	47 Z = X^Y	X Y Z
				48 Z = SIN(X)	X Z

DESCRIPTION	01:	02:	03:	04: 05: 06: 07: 08: 09:
49 SPA. MAX	*SWATH*	*1ST LOC*	*MAX†*	
50 SPA. MIN	*SWATH*	*1ST LOC*	*MIN†*	
51 SPA. AVG	*SWATH*	*1ST LOC*	*AVG*	
52 STD DEV	*REPS*	*X*	*SD*	*N*
53 A*X + B	*STRT LOC*	*A1*	*B1*	*A2 B2 A3 B3 A4 B4*
55 POLYNOMIAL	*REPS*	*X*	*F(X)*	*C0 C1 C2 C3 C4 C5*
56 SAT. VP	*TEMP*	*VP*		
57 WDT-VP	*PRESSURE*	*DB TEMP*	*WB TEMP*	*VP*
58 LP FILTER	*REPS*	*X*	*F(X)*	*W*
59 X/(1-X)	*REPS*	*X*	*MULT.*	

OUTPUT PROCESSING INSTRUCTIONS

DESCRIPTION	01:	02:	03:	04:	05:	06:	07:
70 SAMPLE	*REPS*	*LOC*					
71 AVERAGE	*REPS*	*LOC*					
72 TOTALIZE	*REPS*	*LOC*					
73 MAXIMIZE	*REPS*	*TIME†*	*LOC*				
74 MINIMIZE	*REPS*	*TIME†*	*LOC*				
75 HISTOGRAM	*REPS*	*BINS*	*FORM†*	*BSEL LOC*	*WV LOC†*	*LO LIM*	*HI LIM*
76 W-VECTOR	*REPS*	*SENSOR†*	*WS/WE*	*WD/N*			
77 REAL TIME	*OPTION†*						
78 RESOLUTION	*OPTION†*						
79 SMPL ON MM	*REPS*	*LOC*					
80 YEAR							

PROGRAM CONTROL INSTRUCTIONS

DESCRIPTION	01:	02:	03:	04:
85 LABEL SUBR.	*SUBR #(1-9)*			
86 DO	*COMMAND†*			
87 LOOP	*DELAY*	*COUNT*		
88 IF X <=> Y	*X*	*COMP†*	*Y*	*COMMAND†*
89 IF X <=> F	*X*	*COMP†*	*F*	*COMMAND†*
91 IF FLAG	*FLAG†*	*COMMAND†*		
92 IF TIME	*T into INT*	*INT (min)*	*COMMAND†*	
94 ELSE				
95 END				

† INSTRUCTION OPTION CODES

1-14 *RANGE codes:*
Slow (16.66ms integ. time)
Fast (250μs integ. time)
Full scale range
1 11 5 mV
2 12 15 mV
3 13 50 mV
4 14 500 mV
5 15 5000 mV

3 *CONFIGuration codes:*
To record all counts:
0 High freq.
1 Low level AC
2 Switch Closure
3 High freq. 16 bit
4 Low level AC, 16 bit
To discard counts from excessive intervals:
1x

4-12 *EX CHANnel codes:*
0x Excite all reps with chan x
1x Increment x each rep

13, 14 *TC TYPE — Thermocouple Type Codes:*
1 T (copper-constantan)
2 E (chromel-constantan)
3 K (chromel-alumel)
4 J (iron-constantan)

18 *OPTION code:*
0 0.1 seconds into minute
1 minutes into day
2 hours into year

20 *OPTION code:*
0 Set low
1 Set high
1x Set according to flag x
2x Set opposite of flag x

49, 50 *SMAX/SMIN*
0xxx Store spa. max or min at loc. xxx
1xxx Max or min at loc. xxx and loc of max or min at xxx + 1

73, 74 *TIME of max or min option*
00 Max/min value only
01 With Seconds
10 With Hour-Minute
11 With Hour-Minute, Seconds

75 *FORM code:*
0 Open form (data beyond limits is included)
1 Closed form (data beyond limits is excluded)
WV LOCation:
0 Frequency distribution

76 *SENSOR type code:*
0 Polar (speed & direction)
1 Orthogonal (East & North)

77 *OPTION*
1 Store Seconds
10 Store Hour-Minute
100 Store Julian Day
11 Store Hour-Minute, Sec.
110 Store Day, Hour-Minute
111 Store Day, Hr-Min, Sec.

78 *OPTION*
0 Low resolution
1 High resolution

86-92 *COMMAND codes:*
0 Goto end of Pgm. Table
1-9 Call Subroutine
10-19 Set flag 0-9
20-29 Reset flag 0-9
30 Then Do
31 Exit Loop if true
32 Exit Loop if false

88, 89 *COMParison codes:*
1 X = Y X = F
2 X <> Y X <> F
3 X >= Y X >= F
4 X < Y X < F

91 *FLAG parameter*
1x Do if flag x is set
2x Do if flag x is reset
FLAG DESCRIPTIONS:
0 Output flag
1-8 User flags
9 Intermed. proc. disable flag

CAMPBELL SCIENTIFIC, INC.
P.O. Box 551 • Logan, Utah 84321 • (801) 753-2342 • TLX 453058

ERROR CODES

STANDARD SOFTWARE

3 — Program Table full
4 — Intermediate Storage full
8 — 21X was reset by watch dog timer
11 — Attempt to allocate unavailable storage
20 — Subroutine encountered before necessary END
21 — END without IF, LOOP, or SUBROUTINE
22 — Missing END, Nonexistent SUBROUTINE
24 — ELSE in SUBROUTINE without IF
25 — ELSE without IF
26 — EXIT LOOP without LOOP
30 — IF's and/or LOOPS nested too deep
31 — SUBROUTINES nested too deep
40 — Table 2 Execution Interval too short

EXTENDED SOFTWARE

90 — Inadequate Input Storage
91 — Too short a scan interval
97 — Time out on tape read
98 — Uncorrectable errors on tape read
99 — Wrong tape file type

EXTENDED SOFTWARE INSTRUCTIONS

INPUT/OUTPUT INSTRUCTIONS

INST. NO. AND DESCRIPTION	PARAMETERS 01:	02:	03:	04:	05:	06:	07:	08:	09:	10:	11:	12:
23 BURST MODE**	NO. CHAN	RANGE†	IN CHAN	OPTION†	SCAN(ms)	NO. SCAN	TRIG.OFFSET	TRIG.LIM.MV	EXCIT MV	LOC	MULT.	OFFSET

PROCESSING INSTRUCTIONS

INST. NO. AND DESCRIPTION	PARAMETERS 01:	02:	03:	04:	05:	06:	07:	08:	09:
54 BLOCK MOVE	NO. VALS.	S.LOC	STEP	D.LOC	STEP				
60 FFT**	LOG_2(SAMPLES)	TAPER†	LOG_2(BINS/AVG)	IN LOC	MULT.				
61 INDIR. MOVE	SOURCE	DESTIN.							
62 COV/COR	NO. VALS.	NO.MEANS	NO.VAR.	NO.SD	NO.COV	NO.COR	SAMP/AVG	X	F(X)

PROGRAM CONTROL INSTRUCTIONS

INST. NO. AND DESCRIPTION	PARAMETERS 01:	02:	03:	04:	05:	06:	07:	08:	09:	···	10 + NO.RF	···
90 LOOP INDEX	STEP											
96 SERIAL OUT	OPTION†											
97 INIT.TELE.*	OPTION†	FLAG	LIM.(SEC)	F.DEL.(SEC)	NO.TRYS	S.DEL.(MIN)	TRY LOC	ID	NO.RF	RF STA	NO.DIGIT	PHONE NO.
98 SEND CHAR.*	CHAR VALUE											

*ESX1 only
**ESX2 only

† INSTRUCTION OPTION CODES

23 *RANGE codes:*
Fast (250μs integ. time)
Full scale range
12 15 mV
13 50 mV
14 500 mV
15 5000 mV

23 *OPTION code, 4 digits:*
ABCD
A Trigger
0 — Trigger on 1st analog channel
1 — Digital trigger on channel 1
B Trigger option
0 — Trigger immediately
1 — Trigger if above limit (high)
2 — Trigger if below limit (low)
3 — Trigger on rising edge
4 — Trigger on falling edge
C Destination
0 — Input Storage
1 — Serial port 9,600 baud
2 — Serial port 76,800 baud
D Measurement
0 — Differential measurement
1 — Single-ended measurement

60 *TAPER codes:*
00 No Taper
01 Taper

96 *OPTION codes, 2 digits:*
00 Tape
1x Printer, ASCII
2x Printer, Binary
x Baud Rate Code

97 *OPTION codes, 2 digits:*
0x DC95
1x DC103C
2x Hayes
x Baud Rate Code

BAUD RATE CODES
0 300
1 1200
2 9600
3 76800

JULIAN DAY CALENDAR

	1	2	3	4	5	6	7	8	9	10	11	12	13	14	15	16	17	18	19	20	21	22	23	24	25	26	27	28	29	30	31
JAN	1	2	3	4	5	6	7	8	9	10	11	12	13	14	15	16	17	18	19	20	21	22	23	24	25	26	27	28	29	30	31
FEB	32	33	34	35	36	37	38	39	40	41	42	43	44	45	46	47	48	49	50	51	52	53	54	55	56	57	58	59	60		
MAR	60	61	62	63	64	65	66	67	68	69	70	71	72	73	74	75	76	77	78	79	80	81	82	83	84	85	86	87	88	89	90
APR	91	92	93	94	95	96	97	98	99	100	101	102	103	104	105	106	107	108	109	110	111	112	113	114	115	116	117	118	119	120	
MAY	121	122	123	124	125	126	127	128	129	130	131	132	133	134	135	136	137	138	139	140	141	142	143	144	145	146	147	148	149	150	151
JUN	152	153	154	155	156	157	158	159	160	161	162	163	164	165	166	167	168	169	170	171	172	173	174	175	176	177	178	179	180	181	
JUL	182	183	184	185	186	187	188	189	190	191	192	193	194	195	196	197	198	199	200	201	202	203	204	205	206	207	208	209	210	211	212
AUG	213	214	215	216	217	218	219	220	221	222	223	224	225	226	227	228	229	230	231	232	233	234	235	236	237	238	239	240	241	242	243
SEP	244	245	246	247	248	249	250	251	252	253	254	255	256	257	258	259	260	261	262	263	264	265	266	267	268	269	270	271	272	273	
OCT	274	275	276	277	278	279	280	281	282	283	284	285	286	287	288	289	290	291	292	293	294	295	296	297	298	299	300	301	302	303	304
NOV	305	306	307	308	309	310	311	312	313	314	315	316	317	318	319	320	321	322	323	324	325	326	327	328	329	330	331	332	333	334	
DEC	335	336	337	338	339	340	341	342	343	344	345	346	347	348	349	350	351	352	353	354	355	356	357	358	359	360	361	362	363	364	365

Add 1 to red values during leap years

Reprinted November 1988

(*b*)

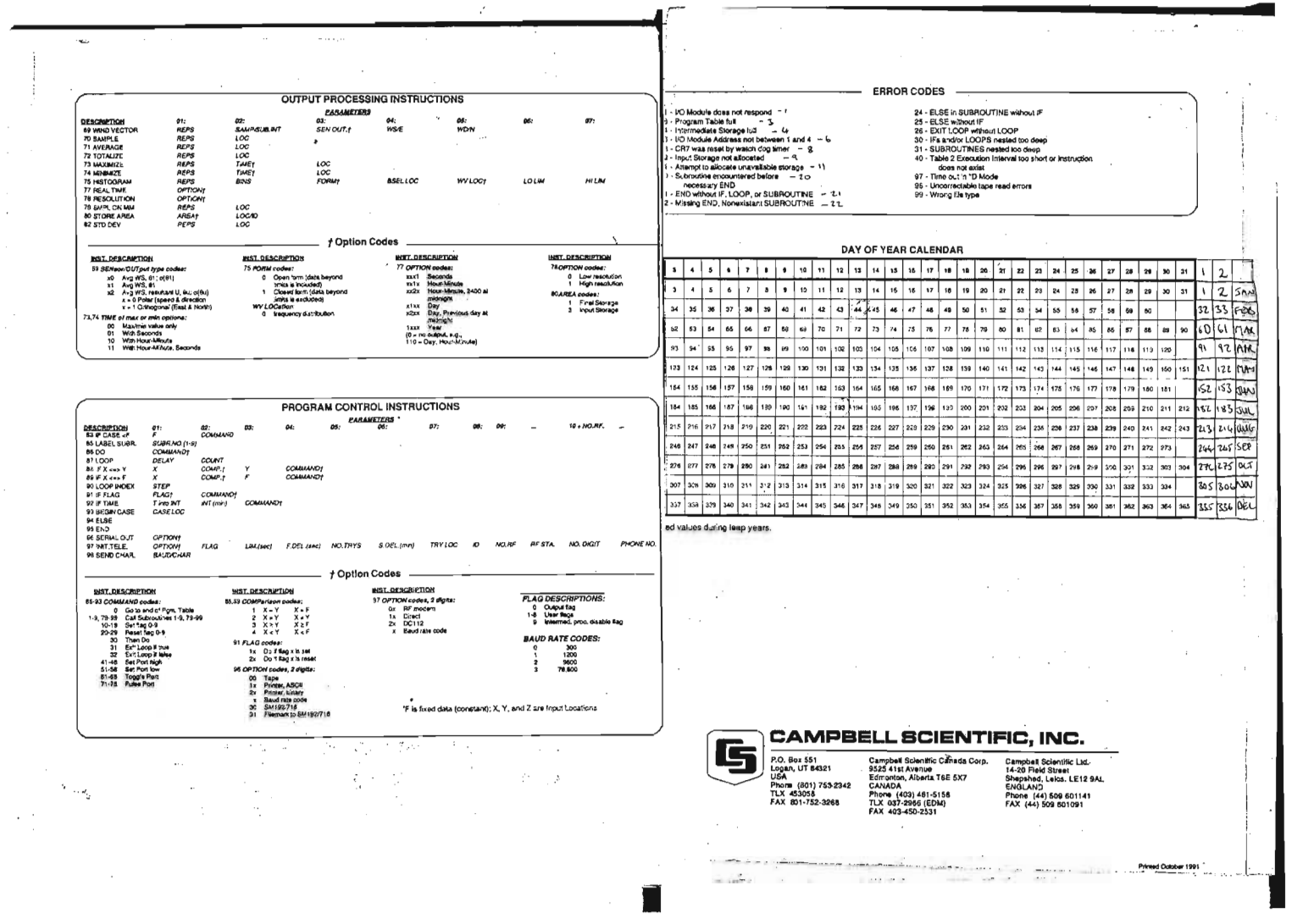

OUTPUT PROCESSING INSTRUCTIONS

PARAMETERS

DESCRIPTION	01:	02:	03:	04:	05:	06:	07:
69 WIND VECTOR	REPS	SAM/PSUB.INT	SEN OUT,†	WS/E	WD/N		
70 SAMPLE	REPS	LOC					
71 AVERAGE	REPS	LOC					
72 TOTALIZE	REPS	LOC					
73 MAXIMIZE	REPS	TIME†	LOC				
74 MINIMIZE	REPS	TIME†	LOC				
75 HISTOGRAM	REPS	BINS	FORM†	BSEL LOC	WV LOC†	LO LIM	HI LIM
77 REAL TIME	OPTION†						
78 RESOLUTION	OPTION†						
79 SAFR, CN, MM	REPS	LOC					
80 STORE AREA	AREA†	LOC/ID					
82 STD DEV	REPS	LOC					

† Option Codes

INST. DESCRIPTION

89 SE/Hex/OUTput type codes:
- x0 Avg WS, 61 ; o(61)
- x1 Avg WS, 81
- x2 Avg WS, resultant U, su, o(9s)
- x + 0 Polar (speed & direction
- x = 1 Orthogonal (East & North)

73,74 TIME of max or min options:
- 00 Max/min value only
- 01 With Seconds
- 10 With Hour-Minute
- 11 With Hour-Minute, Seconds

75 FORM codes:
- 0 Open form (data beyond limits is included)
- 1 Closed form (data beyond limits is excluded)

WV LOCation
- 0 frequency distribution

77 OPTION codes:
- xxx1 Seconds
- xx1x Hour-Minute
- xx2x Hour-Minute, 2400 at midnight
- x1xx Day
- x2xx Day, Previous day at midnight
- 1xxx Year

(0 = no output, e.g., 110 = Day, Hour-Minute)

78 OPTION codes:
- 0 Low resolution
- 1 High resolution

80 AREA codes:
- 1 Final Storage
- 3 Input Storage

PROGRAM CONTROL INSTRUCTIONS

PARAMETERS *

DESCRIPTION	01:	02:	03:	04:	05:	06:	07:	08:	09:	...	10 + NO.RF.	...
83 IF CASE of	F	COMMAND										
85 LABEL SUBR.	SUBR.NO (1-9)											
86 DO	COMMAND†											
87 LOOP	DELAY	COUNT										
88 IF X <=> Y	X	COMP.†	Y	COMMAND†								
89 IF X <=> F	X	COMP.†	F	COMMAND†								
90 LOOP INDEX	STEP											
91 IF FLAG	FLAG†	COMMAND†										
92 IF TIME	T into INT	INT (min)	COMMAND†									
93 BEGIN CASE	CASE LOC											
94 ELSE												
95 END												
96 SERIAL OUT	OPTION†											
97 INIT.TELE.	OPTION†	FLAG	LIM.(sec)	F.DEL (sec)	NO.TRYS	S.DEL (mn)	TRY LOC	ID	NO.RF	RF STA.	NO. DIGIT	PHONE NO.
98 SEND CHAR.	BAUD/CHAR											

† Option Codes

INST. DESCRIPTION

85-93 COMMAND codes:
- 0 Go to end of Prgm. Table
- 1-9, 79-99 Call Subroutines 1-9, 79-99
- 10-19 Set flag 0-9
- 20-29 Reset flag 0-9
- 30 Then Do
- 31 Ex= Loop if true
- 32 Ex= Loop if false
- 41-48 Set Port high
- 51-58 Set Port low
- 61-68 Toggle Port
- 71-78 Pulse Port

85,93 COMPARISON codes:
- 1 X = Y X = F
- 2 X ≠ Y X ≠ Y
- 3 X > Y X ≥ F
- 4 X < Y X < F

91 FLAG codes:
- 1x Do if flag x is set
- 2x Do if flag x is reset

96 OPTION codes, 2 digits:
- 00 Tape
- 1x Printer, ASCII
- 2x Printer, Kinkey
- x Baud rate code
- 30 SM192/716
- 31 Filemark to SM192/716

97 OPTION codes, 3 digits:
- 0x RF modem
- 1x Direct
- 2x DC12
- x Baud rate code

FLAG DESCRIPTIONS:
- 0 Output flag
- 1-8 User flags
- 9 Intermed. proc. disable flag

BAUD RATE CODES:

0	300
1	1200
2	9600
3	76,800

*F is fixed data (constant); X, Y, and Z are Input Locations

ERROR CODES

1 - I/O Module does not respond
3 - Program Table full
4 - Intermediate Storage full
6 - I/O Module Address not between 1 and 4
8 - CR7 was reset by watch dog timer
9 - Input Storage not allocated
11 - Attempt to allocate unavailable storage
20 - Subroutine encountered before necessary END
21 - END without IF, LOOP, or SUBROUTINE
22 - Missing END, Nonexistant SUBROUTINE
24 - ELSE in SUBROUTINE without IF
25 - ELSE without IF
26 - EXIT LOOP without LOOP
30 - IFs and/or LOOPS nested too deep
31 - SUBROUTINES nested too deep
40 - Table 2 Execution Interval too short or Instruction does not exist
97 - Time out in *D Mode
98 - Uncorrectable tape read errors
99 - Wrong Data type

DAY OF YEAR CALENDAR

1	2	3	4	5	6	7	8	9	10	11	12	13	14	15	16	17	18	19	20	21	22	23	24	25	26	27	28	29	30	31	1	2
3	4	5	6	7	8	9	10	11	12	13	14	15	16	17	18	19	20	21	22	23	24	25	26	27	28	29	30	31	1	2	32	33
34	35	36	37	38	39	40	41	42	43	44	45	46	47	48	49	50	51	52	53	54	55	56	57	58	59	60			32	33	60	61
62	63	64	65	66	67	68	69	70	71	72	73	74	75	76	77	78	79	80	81	82	83	84	85	86	87	88	89	90	60	61	91	92
93	94	95	96	97	98	99	100	101	102	103	104	105	106	107	108	109	110	111	112	113	114	115	116	117	118	119	120		91	92	121	122
123	124	125	126	127	128	129	130	131	132	133	134	135	136	137	138	139	140	141	142	143	144	145	146	147	148	149	150	151	121	122	152	153
154	155	156	157	158	159	160	161	162	163	164	165	166	167	168	169	170	171	172	173	174	175	176	177	178	179	180	181		152	153	182	183
184	185	186	187	188	189	190	191	192	193	194	195	196	197	198	199	200	201	202	203	204	205	206	207	208	209	210	211	212	182	183	213	214
215	216	217	218	219	220	221	222	223	224	225	226	227	228	229	230	231	232	233	234	235	236	237	238	239	240	241	242	243	213	214	244	245
246	247	248	249	250	251	252	253	254	255	256	257	258	259	260	261	262	263	264	265	266	267	268	269	270	271	272	273		244	245	274	275
276	277	278	279	280	281	282	283	284	285	286	287	288	289	290	291	292	293	294	295	296	297	298	299	300	301	302	303	304	274	275	305	306
307	308	309	310	311	312	313	314	315	316	317	318	319	320	321	322	323	324	325	326	327	328	329	330	331	332	333	334		305	306	335	336
337	338	339	340	341	342	343	344	345	346	347	348	349	350	351	352	353	354	355	356	357	358	359	360	361	362	363	364	365	335	336		

ed values during leap years.

CAMPBELL SCIENTIFIC, INC.

P.O. Box 551
Logan, UT 84321
USA
Phone (801) 753-2342
TLX 453058
FAX 801-752-3268

Campbell Scientific Canada Corp.
9525 41st Avenue
Edmonton, Alberta T6E 5X7
CANADA
Phone (403) 461-5158
TLX 037-2966 (EDM)
FAX 403-450-2331

Campbell Scientific Ltd.
14-20 Field Street
Shepshed, Leics. LE12 9AL
ENGLAND
Phone (44) 509 601141
FAX (44) 509 601091

Printed October 1991

(*b*)

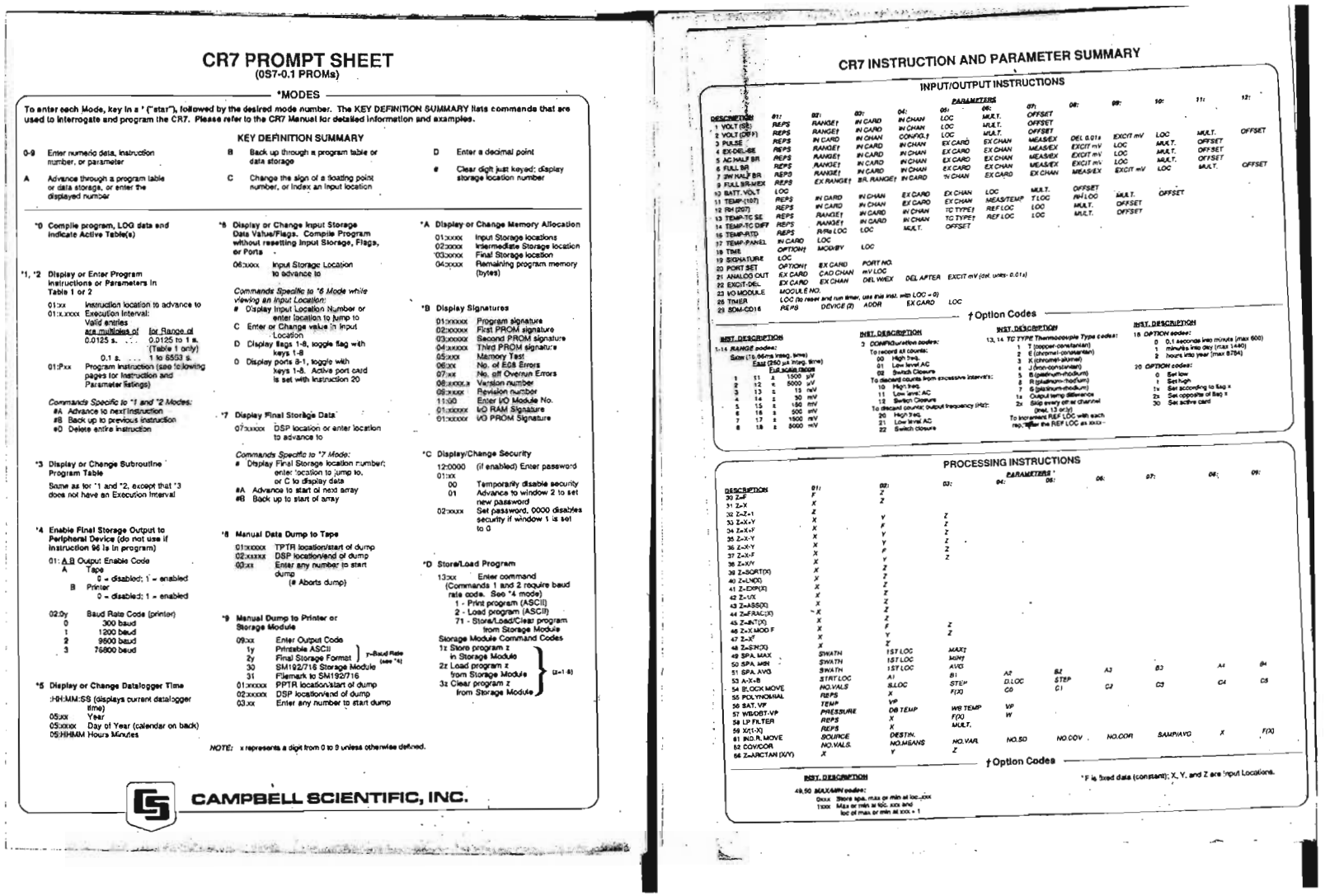

CR7 PROMPT SHEET
(0S7-0.1 PROMs)

*MODES

To enter each Mode, key in a * ("star"), followed by the desired mode number. The KEY DEFINITION SUMMARY lists commands that are used to interrogate and program the CR7. Please refer to the CR7 Manual for detailed information and examples.

KEY DEFINITION SUMMARY

- 0-9 Enter numeric data, instruction number, or parameter
- A Advance through a program table or data storage, or enter the displayed number
- B Back up through a program table or data storage
- C Change the sign of a floating point number, or index an input location
- D Enter a decimal point
- # Clear digit just keyed; display storage location number

***0 Compile program, LOG data and indicate Active Table(s)**

***1, *2 Display or Enter Program Instructions or Parameters in Table 1 or 2**

01:xx Instruction location to advance to
01:x.xxxx Execution Interval:

Valid entries are multiples of	for Range of
0.0125 s.	0.0125 to 1 s. (Table 1 only)
0.1 s.	1 to 6553 s.

01:Pxx Program instruction (see following pages for Instruction and Parameter listings)

*Commands Specific to *1 and *2 Modes:*
#A Advance to next instruction
#B Back up to previous instruction
#0 Delete entire instruction

***3 Display or Change Subroutine Program Table**

Same as for *1 and *2, except that *3 does not have an Execution Interval

***4 Enable Final Storage Output to Peripheral Device (do not use if Instruction 96 is in program)**

01: A B Output Enable Code
A Tape: 0 = disabled; 1 = enabled
B Printer: 0 = disabled; 1 = enabled

02:0y Baud Rate Code (printer)
0 300 baud
1 1200 baud
2 9600 baud
3 76800 baud

***5 Display or Change Datalogger Time**

HH:MM:SS (displays current datalogger time)
05:xx Year
05:xxxx Day of Year (calendar or back)
05:HHMM Hours Minutes

***6 Display or Change Input Storage Data Value/Flags. Compile Program without resetting Input Storage, Flags, or Ports**

06:xxxx Input Storage Location to advance to

*Commands Specific to *6 Mode while viewing an Input Location:*
Display Input Location Number or enter location to jump to
C Enter or Change value in Input Location
D Display flags 1-8, toggle flag with keys 1-8
0 Display ports 8-1, toggle with keys 1-8. Active port card is set with Instruction 20

***7 Display Final Storage Data**

07:xxxx DSP location or enter location to advance to

*Commands Specific to *7 Mode:*
Display Final Storage location number; enter location to jump to, or C to display data
#A Advance to start of next array
#B Back up to start of array

***8 Manual Data Dump to Tape**

01:xxxxx TPTR location/start of dump
02:xxxxx DSP location/end of dump
03:xx Enter any number to start dump (# Aborts dump)

***9 Manual Dump to Printer or Storage Module**

09:xx Enter Output Code
1y Printable ASCII
2y Final Storage Format } y=Baud Rate (see *4)
30 SM192/716 Storage Module
31 Filemark to SM192/716
01:xxxxx PPTR location/start of dump
02:xxxxx DSP location/end of dump
03:xx Enter any number to start dump

***A Display or Change Memory Allocation**

03:xxxx Input Storage locations
02:xxxx Intermediate Storage location
03:xxxx Final Storage location
04:xxxx Remaining program memory (bytes)

***B Display Signatures**

01:xxxxx Program signature
02:xxxxx First PROM signature
03:xxxxx Second PROM signature
04:xxxxx Third PROM signature
05:xxx Memory Test
06:xx No. of E68 Errors
07:xx No. of Overrun Errors
08:xxxx.x Version number
09:xxxx Revision number
11:00 Enter I/O Module No.
01:xxxxx I/O RAM Signature
01:xxxxx I/O PROM Signature

***C Display/Change Security**

12:0000 (if enabled) Enter password
01:xx
00 Temporarily disable security
01 Advance to window 2 to set new password
02:xxxx Set password, 0000 disables security if window 1 is set to 0

***D Store/Load Program**

13:xx Enter command (Commands 1 and 2 require baud rate code. See *4 mode)
1 - Print program (ASCII)
2 - Load program (ASCII)
71 - Store/Load/Clear program from Storage Module

Storage Module Command Codes
1z Store program z in Storage Module
2z Load program z from Storage Module
3z Clear program z from Storage Module
(z=1-8)

NOTE: x represents a digit from 0 to 9 unless otherwise defined.

CAMPBELL SCIENTIFIC, INC.

CR7 INSTRUCTION AND PARAMETER SUMMARY

INPUT/OUTPUT INSTRUCTIONS

DESCRIPTION	01:	02: PARAMETERS	03:	04:	05:	06:	07:	08:	09:	10:	11:	12:
1 VOLT (SE)	REPS	RANGE†	IN CARD	IN CHAN	LOC	MULT.	OFFSET					
2 VOLT (DIFF)	REPS	RANGE†	IN CARD	IN CHAN	LOC	MULT.	OFFSET					
3 PULSE	REPS	IN CARD	IN CHAN	CONFIG.†	LOC	MULT.	OFFSET					
4 EX-DEL-SE	REPS	RANGE†	IN CARD	IN CHAN	EX CARD	EX CHAN	MEAS/EX	DEL 0.01s	EXCIT mV	LOC	MULT.	OFFSET
5 AC HALF BR	REPS	RANGE†	IN CARD	IN CHAN	EX CARD	EX CHAN	MEAS/EX	EXCIT mV	LOC	MULT.	OFFSET	
6 FULL BR	REPS	RANGE†	IN CARD	IN CHAN	EX CARD	EX CHAN	MEAS/EX	EXCIT mV	LOC	MULT.	OFFSET	
7 2W HALF BR	REPS	RANGE†	IN CARD	IN CHAN	EX CARD	EX CHAN	MEAS/EX	EXCIT mV	LOC	MULT.	OFFSET	
8 FULL BR-MEX	REPS	EX RANGE†	BR. RANGE†	IN CARD	IN CHAN	EX CARD	EX CHAN					
10 BATT. VOLT	LOC											
11 TEMP (107)	REPS	IN CARD	IN CHAN	EX CARD	EX CHAN	LOC	MULT.	OFFSET				
12 RH (207)	REPS	IN CARD	IN CHAN	EX CARD	EX CHAN	MEAS/TEMP	T LOC	RH LOC	MULT.	OFFSET		
13 TEMP-TC SE	REPS	RANGE†	IN CARD	IN CHAN	TC TYPE†	REF LOC	LOC	MULT.	OFFSET			
14 TEMP-TC DIFF	REPS	RANGE†	IN CARD	IN CHAN	TC TYPE†	REF LOC	LOC	MULT.	OFFSET			
15 TEMP-RTD	REPS	R/Ro LOC	LOC	MULT.	OFFSET							
17 TEMP-PANEL	IN CARD	LOC										
18 TIME	OPTION†	MOD/BY	LOC									
19 SIGNATURE	LOC											
20 PORT SET	OPTION†	EX CARD	PORT NO.									
21 ANALOG OUT	EX CARD	CAO CHAN	mV LOC									
22 EXCIT-DEL	EX CARD	EX CHAN	DEL W/EX	DEL AFTER	EXCIT mV (del. units= 0.01s)							
23 I/O MODULE	MODULE NO.											
25 TIMER	LOC (to reset and run timer, use this inst. with LOC = 0)											
29 SDM-CD16	REPS	DEVICE (0)	ADDR	EX CARD	LOC							

† Option Codes

INST. DESCRIPTION
1-14 *RANGE codes:*
Scan (16.66ms integ. time)

	Fast (250 µs integ. time)	Full Scan Range	
1	11	± 1500	µV
2	12	± 5000	µV
3	13	± 15	mV
4	14	± 50	mV
5	15	± 150	mV
6	16	± 500	mV
7	17	± 1500	mV
8	18	± 5000	mV

INST. DESCRIPTION
3 *CONFIGuration codes:*
To record all counts:
00 High freq.
01 Low level AC
02 Switch Closure
To discard counts from excessive intervals:
10 High freq.
11 Low level AC
12 Switch Closure
To discard counts/ output frequency (Hz):
20 High freq.
21 Low level AC
22 Switch Closure

INST. DESCRIPTION
13, 14 *TC TYPE Thermocouple Type codes:*
1 T (copper-constantan)
2 E (chromel-constantan)
3 K (chromel-alumel)
4 J (iron-constantan)
5 R (platinum-rhodium)
6 S (platinum-rhodium)
7 B (platinum-rhodium)
1x Output temp difference
2x Skip every nth ac channel (inst. 13 only)
To increment REF LOC with each rep, offset the REF LOC as xxxx

INST. DESCRIPTION
18 *OPTION codes:*
0 0.1 seconds into minute (max 600)
1 minutes into day (max 1440)
2 hours into year (max 8784)
20 *OPTION codes:*
0 Set low
1 Set high
1x Set according to flag x
2x Set opposite of flag x
30 Set active card

PROCESSING INSTRUCTIONS

DESCRIPTION	01:	02: PARAMETERS	03:	04:	05:	06:	07:	08:	09:
30 Z=F	F	Z							
31 Z=X	X	Z							
32 Z=Z+1	X	X	Y	Z					
33 Z=X+Y	X	X	F	Z					
34 Z=X+F	X	X	Y	Z					
35 Z=X-Y	X	X	Y	Z					
36 Z=X*Y	X	X	F	Z					
37 Z=X*F	X	X	Y	Z					
38 Z=X/Y	X	X	Z						
39 Z=SQRT(X)	X	X	Z						
40 Z=LN(X)	X	X	Z						
41 Z=EXP(X)	X	X	Z						
42 Z=1/X	X	X	Z						
43 Z=ABS(X)	X	X	Z						
44 Z=FRAC(X)	X	X	Z						
45 Z=INT(X)	X	X	Z						
46 Z=X MOD F	X	X	F	Z					
47 Z=X^	X	X	Y	Z					
48 Z=SIN(X)	X	X	Z						
49 SPA. MAX	SWATH	1ST LOC	MAX†						
50 SPA. MIN	SWATH	1ST LOC	MIN†						
51 SPA. AVG	SWATH	1ST LOC	AVG						
53 A-X+B	START LOC	A†	B†		A2	B2	A3	B3	A4	B4
54 BLOCK MOVE	NO.VALS	BLOC	STEP		D.LOC	STEP				
55 POLYNOMIAL	REPS	X	F(X)		C0	C1	C2	C3	C4	C5
56 SAT. VP	TEMP	VP								
57 WB/DBT-VP	PRESSURE	DB TEMP	WB TEMP	VP						
58 LP FILTER	REPS	X	F(X)	W						
59 X(1-X)	REPS	X	MULT.							
61 IND.R. MOVE	SOURCE	DESTIN.	NO.VAR		NO.SD	NO.COV	NO.COR	SAMP/AVG	X	F(X)
62 COV/COR	NO.VALS.	NO.MEANS	Z							
66 Z=ARCTAN (X/Y)	X	Y								

† Option Codes

INST. DESCRIPTION
49,50 *MAX/MIN codes:*
0xxx Store spa. max or min at loc.-xxx
1xxx Max or min at loc. xxx and loc of max or min at xxx + 1

*F is fixed data (constant); X, Y, and Z are Input Locations.